Max-Planck-Institut für Metallforschung
Stuttgart

Surfaces for Functional and Patterned Immobilization of Proteins

Petra Stegmaier

Dissertation
an der
Universität Stuttgart

Bericht Nr. 213
Dezember 2007

SURFACES FOR FUNCTIONAL AND PATTERNED IMMOBILIZATION OF PROTEINS

Von der Fakultät für Chemie der Universität Stuttgart
zur Erlangung der Würde eines Doktors der
Naturwissenschaften (Dr. rer. nat.) genehmigte Abhandlung

Vorgelegt von

PETRA STEGMAIER

aus Mainz

Hauptberichter:	Prof. Dr. Herwig Brunner
Mitberichter:	Prof. Dr. Christian G. Bochet
Tag der mündlichen Prüfung:	11. Dezember 2007

Max-Planck-Institut für Metallforschung
und
Institut für Grenzflächenverfahrenstechnik IGVT der Universität Stuttgart

Stuttgart, Oktober 2007

Meinen Eltern

Die Experimente der vorliegenden Arbeit wurden in der Zeit von Dezember 2004 bis Oktober 2007 in der Abteilung von Herrn Prof. Dr. Eduard Arzt am Max-Planck-Institut für Metallforschung in Stuttgart durchgeführt.

Petra Stegmaier

SURFACES FOR FUNCTIONAL AND PATTERNED IMMOBILIZATION OF PROTEINS

Max Planck Institute for Metals Research and
Institute for Interfacial Engineering IGVT, University of Stuttgart, 2007
231 pages, 99 figures, 5 tables

Abstract

Functional and patterned immobilization of proteins onto solid substrates is an important issue in biotechnological processes involving protein purification or detection, or in the study of protein-protein interactions. This thesis presents a new strategy to functional immobilize proteins in selected microregions of a substrate based on photosensitive surface layers containing caged ligands and protein repellent EG chains. Special effort has been paid to the development of surface compositions and architectures that retain protein function in the surface mobilized state.

In the first part of the thesis, branched silanes containing protein repellent OEG arms terminated with one inert -OMe group and one photocleavable, caged amino functionality were synthesized. Silica surfaces were modified with these molecules and the properties of the surface layers were characterized. According to the ellipsometric data, submonolayers with amino surface densities lower than in SAMs of thiols were obtained after optimization of the conditions for the surface reaction. The photolytic properties of the surfaces were analyzed. Irradiation of the surface at 355 nm cleaved the photoremovable cage and liberated the amino functionalities. These were then used to immobilize protein targets from solution after appropriate biofunctionalization. Reflectance Interference Spectroscopy (RIFS) was used to monitor and quantify protein binding. Low non-specific adsorption of proteins onto the surfaces as a consequence of the presence of EG chains was proven. Binding efficiencies were shown to be better than binding onto surface layers containing linear and shorter EG chains. For surface layers with similar architectures (either linear or branched) binding results correlate with the surface density of ligands.

In the second part, silanes possessing different photocleavable groups able to be cleaved individually by using light of different wavelengths (NVoc and DEACM) were synthesized. UV measurements revealed that DEACM can be easily cleaved off upon UV irradiation at 412 nm, without damaging the NVoc group. The NVoc group can be removed at 345 nm. Surface layers containing a mixture of both groups were prepared and used for coupling two different fluorescent dyes to selected microregions of a surface. The expected fluorescence pattern was observed, confirming the possibility of generating complex chemical patterns by using different cages that can be independently addressed.

In a last part of the thesis, magnetite nanoparticles were modified with mixed silane layers containing amino and OH/ OMe terminal groups in different molar ratios and connected to the surface by EG spacers with different lengths. The influence of the amine density and accessibility on the protein loading capacity of the nanoparticles has been analyzed. The optimum silane surface composition for maximum protein loading was identified.

Petra Stegmaier

OBERFLÄCHEN FÜR DIE FUNKTIONALE UND ORTSSELEKTIVE IMMOBILISIERUNG VON PROTEINEN

Max-Planck-Institute für Metallforschung und
Institut für Grenzflächenverfahrenstechnik IGVT, Universität Stuttgart, 2007
231 Seiten, 99 Abbildungen, 5 Tabellen

Kurzzusammenfassung

Die funktionale und ortsselektive Immobilisierung von Proteinen auf festen Oberflächen ist ein wichtiger Aspekt in biotechnologischen Prozessen, der bei der Reinigung von Proteinen, ihrem Nachweis und der Untersuchung von Protein-Protein-Wechselwirkungen eine Rolle spielt. In der vorliegenden Dissertation wurde eine neue Strategie zur funktionalen Immobilisierung von Proteinen in definierten Mikroregionen auf Substraten entwickelt. Diese Methode basiert auf der Herstellung von photosensitiven Oberflächenschichten, in denen geschützte Funktionalitäten und proteinabweisende Ethylenglykol (EG) Ketten eingebaut sind. Ein besonderes Augenmerk wurde dabei auf die Zusammensetzung und Gestaltung der Oberflächenschicht gelegt, um die Funktion des Proteins auch nach der Anbindung an die Oberfläche zu bewahren.

Im ersten Teil der Arbeit wurden Silane synthetisiert, die eine aus protein-abweisenden TEG Armen aufgebaute verzweigte Struktur aufweisen, welche eine inerte Methoxygruppe an einem Ende und eine durch eine photolabile NVoc-Gruppe geschützte Aminofunktionalität am anderen Ende trägt. Siliziumdioxid-Oberflächen wurden mit diesen Silanen modifiziert und die erhaltenen Oberflächenschichten charakterisiert. Auf modifizierten Quarz-Substraten wurde die Abspaltung der photolabilen NVoc-Schutzgruppe durch Bestrahlung im Absorptionsmaximum (bei 355 nm) untersucht. Die bei der Photolyse freigesetzten Aminogruppen wurden nach geeigneter Biofunktionalisierung in der Immobilisierung von Proteinen aus Lösungen getestet. Die selektive Immobilisierung wurde mithilfe von reflektometrischer Interferenzspektroskopie (RIFS) verfolgt und quantifiziert. Aufgrund der vorhandenen OEG Ketten war die unspezifische Adsorption vernachlässigbar klein. Schichten aus verzweigten Silanen wiesen eine höhere Bindungsfähigkeit als die aus linearen und kürzeren EG Ketten aufgebauten Schichten auf. Für Schichten ähnlicher Gestalt (sowohl von linearen als auch von verzweigten Silanen) konnte ein Zusammenhang zwischen Bindungsfähigkeit und der Dichte funktioneller Gruppen auf der Oberfläche gefunden werden.

In einem zweiten Teil wurden Silane mit zwei verschiedenen photosensitiven Gruppen (NVoc und DEACM) synthetisiert, die durch Bestrahlung bei unterschiedlicher Wellenlänge individuell abgespalten werden können. Spektroskopische Untersuchungen der Photolyse beider photolabilen Gruppen zeigten, dass DEACM durch Bestrahlung bei 412 nm fast vollständig abgespalten wird, während NVoc nur wenig beeindrächtigt wird. Eine Abspaltung von NVoc kann bei 345 nm erfolgen. Gemischte Schichten beider Silane wurden hergestellt und in einem zweistufigen Bestrahlungsprozeß nacheinander orts-selektiv entschützt und mit zwei verschiedenen Fluoreszenfarbstoffen gekuppelt. Das erhaltene Fluoreszenz-Muster bestätigt die Möglichkeit, mit diesen beiden Schutzgruppen gezielt chemisch komplex strukturierte Oberflächen zu erzeugen.

Im dritten Teil der Arbeit wurden magnetische Nanopartikel durch Co-Adsorption von verschiedenen Amin- und OH/ OMe-terminierten Silanen mit unterschiedlich langen EG Armen modifiziert. Eine Untersuchung der funktionalen Immobilisierung von Proteinen an diese gemischten Schichten erfolgte im Hinblick auf den Einfluss der Amingruppendichte sowie der Zugänglichkeit dieser funktionellen Gruppen. Somit konnte eine optimale Oberflächenzusammensetzung mit maximaler Bindungsfähigkeit für Proteine ermittelt werden.

Danksagung

Ich möchte mich bei allen Personen bedanken, die zum Gelingen dieser Arbeit beigetragen haben.

Herzlichen Dank an Herrn Prof. Dr. Herwig Brunner für die Übernahme des Hauptberichts. Ich danke ihm für seine Bereitschaft, so kurzfristig einzuspringen, seine unkomplizierte und überaus freundliche Art und das Interesse an meiner Arbeit.

Herrn Prof. Dr. Eduard Arzt danke ich für die Möglichkeit, diese interessante Arbeit in seinem Arbeitskreis durchzuführen und die umfangreiche finanzielle Unterstützung. Ich habe es sehr geschätzt, in einem interdisziplinären Umfeld mit toller Ausstattung und idyllischer Umgebung arbeiten zu dürfen.

Bei Herrn Prof. Dr. Christian Bochet möchte ich mich für die freundliche Übernahme des Mitberichts bedanken.

Ein großer Dank geht an meine Betreuerin, Frau Dr. Aránzazu del Campo, ohne die diese Arbeit niemals entstanden wäre. Ich danke ihr für das spannende und herausfordernde Thema und die wundervolle Betreuung während der gesamten Doktorarbeit, ausserdem für die viele Energie, die sie in diese Arbeit gesteckt hat, ihre Ideen und für alles, was ich durch sie lernen durfte. Als ihre erste Doktorandin habe ich ihre Begeisterung für die Wissenschaft miterlebt, mit der sie es immer wieder geschafft hat, mich anzustecken und zu ermutigen. Am Ende hat es sich gelohnt, und auch die Partikel, mit denen in Italien alles angefangen hat, haben ihren Weg in diese Arbeit gefunden…

Danke an die Max-Planck-Gesellschaft für die finanzielle Unterstützung.

Bei meiner Ankunft in Stuttgart gab es noch kein Chemielabor… die ersten eineinhalb Jahre meiner Doktorarbeit waren nicht leicht und haben an vielen Stellen Einschränkungen und Kompromisse erfordert. Danke an alle Personen, die mit ihrer Hilfsbereitschaft und Flexibilität dazu beigetragen haben, dass ich mich in diesem Chaos dennoch wohlfühlen und einen Weg zum Arbeiten finden konnte. Besonders möchte ich die Hilfe von Dr. Ralf Kemkemer und Simon Jungbauer erwähnen.

Danke an alle Abteilungen, deren Geräte ich benutzen durfte.

Organische Synthese hat den Hauptteil meiner Arbeit ausgemacht und wäre ohne Charakterisierung mittels NMR nicht möglich gewesen. Herzlichen Dank an die Abteilungen Jansen und Aldinger, dass ich ihre Spektrometer mitbenutzen durfte und für die Hilfsbereitschaft, die ich stets bekam, wenn etwas nicht richtig funktionierte. Besonders möchte ich dabei Herrn Carsten Schmitt und Herrn Dr. Peter Gerstel für die nette Einführung in die Geräte danken, sowie Herrn Dr. Thomas Jaeschke für die Hilfe beim Exportieren der Daten.

Herzlichen Dank an die Abteilung Spatz, dass ich die UV-Spektrometer, Fluoreszenzmikroskope und Lichtmikroskope benutzen durfte.

Mein Dank gilt ebenfalls der Abteilung Kern für die Möglichkeit, das Ellipsometer zu benutzen und Herrn Dr. Alexander Bittner für die kompetente Einführung in das Gerät.

Ich möchte mich bei allen Serviceeinrichtungen des Hauses für ihre Hilfsbereitschaft bedanken. Besonderer Dank gilt dabei Herrn Kammerländer und seinem Glasbläser-Team für die prompte Ausführung meiner Aufträge und die Erfüllung vieler Sonderwünsche sowie Herrn Konrad vom Forscherbedarfslager für seinen Einsatz rund um die Chemikalien. Gedankt sei auch der Feinmechanischen Werkstatt, dem Tieftemperaturservice, der Elektronik, unseren fürsorglichen Betriebskrankenschwestern, den Reinigungskräften und nicht zuletzt dem Sicherheitsdienst für seinen Einsatz rund um die Uhr.

Danke an Herrn Dr. José Maria Alonso für die Herstellung der EG-NVoc- und Bnz-CPTS-Schichten, seine Hilfsbereitschaft bei chemischen Fragen und das offene Ohr für wissenschaftliche Diskussionen.

Desweitern möchte ich Herrn Prof. Dr. M. Goeldner für die Bereitstellung des geschützten Peptids bedanken und Herrn Prof. Dr. C. Eisenbach für hilfreiche Diskussionen in der Anfangszeit dieser Arbeit.

Ich danke allen Personen, die mir im Labor tatkräftig zur Seite gestanden haben: Frau Svea Petersen und Frau Melanie Wirkner für die Unterstützung bei den Partikelexperimenten sowie Frau Uta Pawelzik für ihren eifrigen Einsatz beim Nachziehen der ersten Stufe. Besonders möchte ich Melanie Wirkner für die gute Organisation des Labors danken und die unendlich vielen kleinen Handgriffe, die sie mir im Laboralltag abgenommen hat.

Frau Henriette Ries und Frau Alexandra Goldyn haben die Zellexperimente mit mir zusammen durchgeführt. Die schönen Fluoreszenzmikroskopbilder entstanden dank guter Augen von Simon Jungbauer, Alexandra Goldyn und Sarah Biela. Danke für Eure Nettigkeit, die vielen Erklärungen und dass ich mich bei Euch in der Gruppe immer willkommen gefühlt habe!

Ich möchte mich bei allen Mitgliedern des Arbeitskreises Arzt (ehemalige und aktuelle) für die nette und sehr angenehme Arbeitsatmosphäre bedanken. Besonders geschätzt habe die lustigen Kaffeepausen nach dem Essen und die Unterstützung und Aufmunterung, die ich in der „heißen Phase“ des Zusammenschreibens bekommen habe.

Herzlichen Dank an Dagmar Voigt für das Korrekturlesen der Zusammenfassungen und dass sie dazu beigetragen hat, dass die unverzichtbaren Nacht- und Wochenendschichten nicht ganz so einsam waren.

Danke an Frau Hess, die gute Seele unserer Abteilung, für ihr offenes Ohr und die Meisterung aller bürokratischen Probleme.

Den größten Teil meiner Doktorarbeit habe ich im Labor verbracht und ich bin froh, dass ich solche tollen Laborkolleginnen wie Melanie, Svea und Ute hatte! Ich möchte mich bei Euch für die super Atmosphäre bedanken, die Singeinlagen, den Spaß, den wir mit der deutschen Sprache hatten und die imaginären Kochstunden. Ich will nicht wissen, wie die letzten zwei Jahre ohne Euch gewesen wären!

Ich habe in den vergangenen drei Jahren nicht nur gelernt, wie man erfolgreich Oberflächen modifiziert, sondern auch viel über mich selbst, meine Grenzen und das Leben. Ich danke allen Personen, die mit positiven und negativen Erfahrungen dazu beigetragen haben.

Ich danke allen meinen Freunden, die auf unterschiedlichste Weise zum Gelingen dieser Arbeit beigetragen haben, nicht nur meinen langjährigen Freunden, sondern auch all den wunderbaren Freunden, die hier in Stuttgart dazugekommen sind!

Grazie a Carmine per tutto il suo aiuto e la forza che mi ha dato durante il tempo che abbiamo camminato insieme sulla stessa strada e che mi portano avanti ancora adesso che le nostre strade si sono divise. Un po' d'Italia resterà nel mio cuore per sempre.

Danke, Guillaume, dass Du die Zeit hier in Stuttgart zu etwas Besonderem für mich gemacht hast!

Zuletzt möchte ich mich bei meinen Eltern für ihre bedingungslose und großartige Unterstützung bedanken, mit denen sie mich durch mein Studium und die Doktorarbeit begleitet haben und ihnen als Dankeschön diese Arbeit widmen.

Symbols and Abbreviations

SYMBOLS

δ	chemical shift
ε	molar extinction coefficient
ρ	density
γ	surface tension
γ_l	surface tension of the liquid
γ_{ls}	interfacial energie between solid and liquid
γ_s	surface tension of the flat surface
λ	wavelength
λ_{abs}	absorbance wavelength
λ_{em}	emission wavelength
λ_{max}	wavelength of the absorbance maximum
$\lambda_{max, abs}$	wavelength of the absorbance maximum
$\lambda_{max, em}$	wavelength of the emission maximum in the fluorescence spectrum
ν	frequency
θ	contact angle
$\Delta\Gamma$	surface loading
$\Delta\varphi$	phase difference
c	concentration
h	Planck constant
J	coupling constant in Hz (NMR)
n	refractive index
R	reflectance

V	volume
V/ V	volume-volume ratio
w	weight
w/ V	weight per volume

UNITS

Å	ångström or angstrom = 10^{-10} m
°C	degree Celsius
g	gram
mg	milligram (10^{-3} g)
h	hour
Hz	Hertz
J	Joule
l	liter
m	meter
M	molar
min	minute
ml	milliliter
mm	millimeter
mM	millimolar
mmol	millimol
µg	microgram (10^{-6} g)
µl	microliter (10^{-6} l)
µm	micrometer (10^{-6} m)
N	normal
ng	nanogram
nm	nanometer
nM	nanomolar
Ω	ohm
ppm	parts per million
s	second

ABBREVIATIONS

A	adenine
APTS	aminopropyltriethoxysilane
aq.	aqueous
BCA	bicinchoninic acid
Bhc-OH	(6-bromo-7-hydroxycoumarin-4-yl)methanol
Bnz-CPTS	12,12,12-triethoxysilyl-dodecanoic acid-1-(3,5-dimethoxy-phenyl)-2-oxo-2-phenylethyl ester
BSA	bovine serum albumina
C6	six methylene units
CA	contact angle
CM	coumarin-4-ylmethanol
conc.	concentrated
cyclo[RGDfK]	cyclic (Arginine-Glycine-Aspartate-Phenylalanine-Lysine)
cyclo[RG(DMNPB)-DfK]	cyclic (RGDfK) caged with 3-(4,5-dimethoxy-2-nitro-phenyl)-2-butyl ester at the carboxylic side chain of the aspartic acid
dA_{25}	25-mer adenine
DEACM-OH	(7-diethylaminocoumarin-4-yl)methanol
DMACM	7-dimethylaminocoumarin-4-yl
DMAP	4-dimethylaminopyridine
DMCM-OH	(7-dimthylaminocoumarin-4-yl)methanol
DMF	dimethylformamide
DMNPB	3-(4,5-dimethoxy-2-nitrophenyl)-2 butyl
DMSO	dimethylsulfoxid
DNA	deoxyribonucleic acid
dT_{25}	25-mer thymine
EDTA	ethylenedinitrilotetraacetic acid
EG	ethyleneglycol
equ.	equivalent
Et	ethyl-
EtOH	ethanol
f	fluorescein
FBS	fetal bovine serum
FITC	fluorescein isothiocyanate

GC-MS	gas chromatography-mass spectrometry
Hal	halogene
His	histidine
HMDS	hexamethyldisilazane
M	molarity
IgG	immunoglobulin G
i-PrOH	isopropanol, isopropyl alcohol, propan-2-ol
ITO	indium tin oxide
MCM-OH	(7-methoxycoumarin-4-yl)methanol
Me	methyl-
Milli-Q	deonized, filtered ultrapure water
MeOH	methanol
molecs	molecules
M_w	molecular weight
NHS	N-hydroxysuccinimide
NH2	amino group
NIH/ 3T3	fibroblasts (from the standard fibroblast cell line 3T3)
NMR	nuclear magnetic resonance
NTA	nitrilo-triacetic acid
NVo	nitroveratryl
NVoc	nitroveratryloxycarbonyl
NVocCl	nitroveratryloxycarbonyl chloride
OEG	oligoethyleneglycol
OH	hydroxyl
OMe	methoxy
OND	oligonucleotide
p	para
PBS	phosphate-buffered saline
PDMS	polydimethylsiloxane
PEG	polyethylene glycol
piranha	solution of conc. H_2SO_4/ 30% H_2O_2 (5:1 V/V)
PT	phase transfer
PTFE	poly(tetrafluoroethylene)
RGD	arginine-glycine-aspartic acid
RIFS	reflectance interference spectroscopy
R	organic rest

R_f	retardation factor (chromatography)
RT	room temperature
SAM	self assembled monolayer
SPION	superparamagnetic iron oxide nanoparticle
ss	single-stranded
SSC	sodium citrate buffer
T	thymine
TEG	tetraethylene glycol
THF	tetrahydrofurane
TLC	thin layer chromatography
Tris base	2-amino-2-hydroxymethyl-1,3-propanediol
Ts	p-toluenesulfonyl
TsOH	p-toluene sulfonic acid
UV	ultraviolet
UV/vis	ultraviolet-visible
X	leaving group
^{1}H NMR	proton NMR spectroscopy
^{13}C NMR	carbon NMR spectroscopy
$\alpha v\beta_3$	membrane protein integrin
3’	three prime end of an OND strand
5’	five prime end of an OND strand

Symbol suffixes for surface layers (Chapter 3)

Y-alkyl-	branched silane with alkyl spacer chain
Y-EG-	branched silane with only EG spacer chains
-NH2	free head group functionality (irradiated sample)
-NVoc	protected head group functionality
-OMe	methoxy termination
EG-	linear silane

Index

Introduction

Solid supports modified with organic surface layers containing bioactive ligands are today well established tools in the biotechnology lab. Relevant examples are surface activated nanoparticles for isolation and detection of biomolecular species (eg. stationary phase in affinity chromatography or magnetic separation processes), or multidetection systems in array format ("microarrays") for the investigation of biological interactions at the molecular level. The through-put of the separation process and the sensitivity and specificity of such detection systems strongly depend on the ability of the surface layer to permit natural biological interactions to occur in such a way that the results can be interpreted clearly and related to biology *in vivo*. Moreover, bioprocesses often involve the interplay of more than one molecular entity and, therefore, coexistence of different ligands on the surface may be required. In same cases the spatial localization of the immobilized species needs to be realized, or precise temporal control of the biomolecular interaction under investigation needs to be provided. This requires the development of surface layers whose bioactivity changes upon application of an external trigger.

The activity of a molecule can be inhibited by attaching a photoremovable protecting group to its reactive site. Subsequent light irradiation releases the cage and restores function. It has recently been demonstrated that different cages can be used to protect individual functionalities which can be then independently activated by using light of different wavelengths. When attached to bioactive ligands on a surface, such strategy

can be exploited to generate surfaces with triggerable affinity for more than one target. However, this requires the selection of cages with sensitivity to wavelengths above 320 nm, so that chromophores included in the biomolecular species do not interfere with the photoactivation process.

In order to achieve effective and stable binding of biomolecular targets, appropriate density and accessibility of the ligands at the surface need to be provided since crowding of receptors or hindered exposure difficulties the binding event. In addition, non-specific interactions between the molecules and the solid surface, which could interfere with the binding event and mask the obtained results, should be prevented. The target should also retain its activity in the surface immobilized state. If the target is a protein, these requirements are typically achieved by including oligoethyleneglycol (OEG) chains in the surface layer. The length, density and branching of the OEG, and the distribution and density of anchored ligands in the surface determine the final immobilization performance. Optimum surface architectures for maximum binding have been established for self-assembled monolayers of thiols on gold. However, these do not necessarily apply to more complex systems, like alkoxysilanes on metal oxide surfaces (eg. silica), of wider application in biotechnological fields.

In this context, this work combines photoresponsive molecules with well-defined OEG architectures (linear and branched) to generate bioactive and photoresponsive silica surfaces with up to three wavelength-selective functional levels. The synthesis of the surface modification agents was achieved, and the properties of the resulting surface layers were characterized. The performance of these layers in functional and selective capture of target proteins from solution was tested and analyzed with respect to surface architecture (ligand density, branching and surface exposure). The ability of the surfaces to generate complex protein patterns after light exposure through a mask has also been demonstrated.

The thesis is organized as follows. *Chapter 1* reviews reported literature and describes the state-of-the-art of the methods for the immobilization and patterning of proteins onto surfaces. *Chapter 2* describes some of the surface techniques employed for characterizing the surface layers and detecting and quantifying the protein binding events. *Chapter 3* presents the synthesis of two branched silanes containing photoresponsive ligands for protein anchoring and OEG-based inert arms. The influence of the length and branching of the OEG chain on the physical properties of the resulting layers, as well as on the protein binding efficiency is described. *Chapter 4* presents the synthesis and photolytic properties of two wavelength sensitive silanes which can be independently removed using light > 320 nm. The possibility of generating complex patterns with different proteins immobilized on selected microregions of a substrate after a two-step irradiation process is demonstrated. *Chapter 5* studies the influence of the ligand density and accessibility in the protein binding capacity of mixed silane layers. The optimum silane layer composition for maximum binding is identified and applied to the generation of bioactive magnetic nanoparticles with high binding efficiency.

Chapter 1

Background and Literature Review

1.1 Surfaces in biotechnology

Many processes in modern biotechnology rely on the ability to immobilize target biomolecules onto surfaces. Isolation and purification of costly biomolecular species using surface activated nanoparticles (eg. affinity chromatography, magnetic separation[1-3]), or multidetection systems based on biosensors in array format ('biochips')[4] are examples of technological relevance.

The success of any biomolecular immobilization process relies on a careful balance of the intermolecular forces driving the interaction between the biomolecule and the outmost layer of the substrate surface (Figure 1.1). In general biomolecules are long and sometimes branched chains composed of multiple fragments (aminoacids in proteins, oligonucleotides (ONDs) in DNA, sugars in carbohydrates) with different chemical constitution. A single biomolecule may posses charged, polar and hydrophobic units ordered in a characteristic sequence which determines their function. In addition, the 3D arrangement of these groups (the molecular conformation) is mostly maintained through non-covalent and reversible interactions which may change with the external conditions (pH, temperature, ionic strength etc.). This structural complexity makes the

immobilization of biomolecules onto solid surfaces a complicated task. On the one hand, biomolecules usually show great affinity for almost any kind of surfaces, since their chemical diversity allows them to interact by any type of intermolecular forces. However, this strong interaction usually leads to unwanted non-specific adsorption, wrong orientation of the active site for subsequent binding, or denaturing effects (Figure 1.2). These issues strongly limit the efficiency and sensitivity of many bio-purification processes and detection of the biomolecules in their immobilized state.

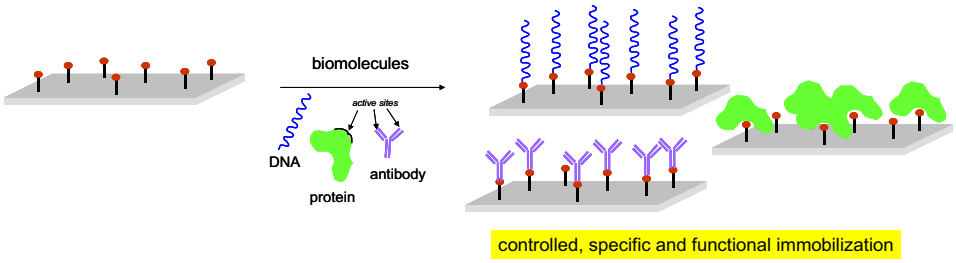

Figure 1.1: Schematic representation of an ideal performed immobilization of biomolecules onto surfaces.

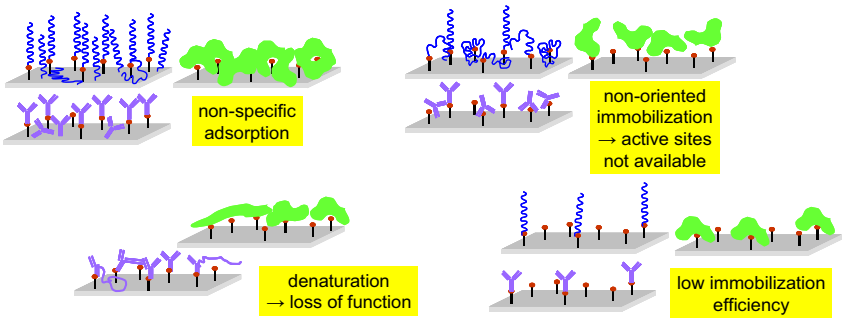

Figure 1.2: Schematic representation of the limitations of most immobilization strategies.

The affinity between a target biomolecule and a substrate is usually controlled by surface modification of the substrate with active groups able to interact selectively with the target. Alternatively, the biomolecule itself may also be engineered as to possess particular reactive sites capable of binding with surfaces. The selection of the best immobilization method for any particular application depends on the type, cost and availability of the biomolecule involved and the experimental conditions and immobilization efficiency required.

1.1.1 Bioarrays

Microarrays or *biochips* are assemblies of different biomolecules (DNA, proteins, carbohydrates or cells) on a solid surface forming a microscopic array (Figure 1.3). These high-throughput screening tools permit scientists and clinicians the possibility of studying the function of many biomolecules in parallel.[5]

The fabrication of microarrays requires the development of patterning techniques able to deliver small quantities of biomaterial onto selected positions. This has been achieved by spotting, ink-jetting or printing small volumes from a solution of the arrayed materials. Alternatively, photochemical methods have been applied to generate chemical patterns with reactive sites that can capture the arrayed material from solutions or even allow direct synthesis of the arrayed material onto the surface. Some of these methods will be described in section 1.5.

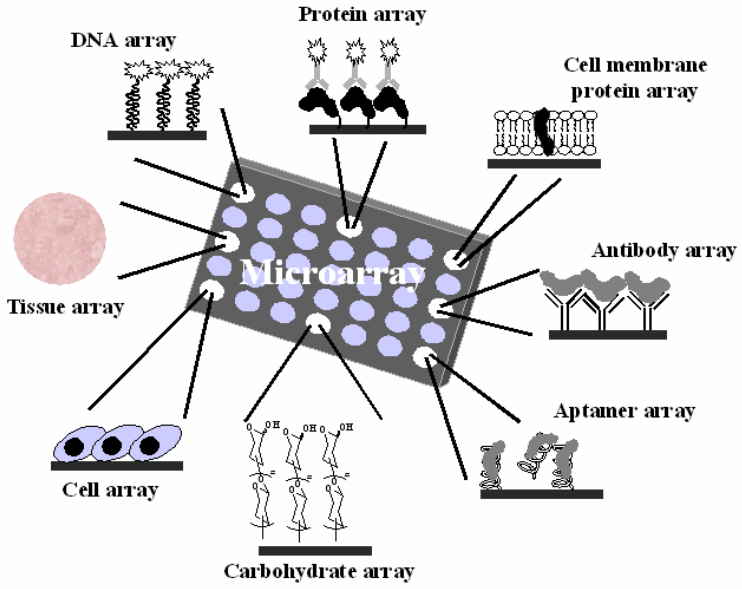

Figure 1.3: Schematic representation of different types of microarrays by arrayed material, reprinted from ref[6] with permission of Dr. A. del Campo.

1.1.2 Magnetic nanoparticles for magnetic separation processes

Nanoparticles with their large surface area represent a convenient system to isolate and analyze the interaction of biomolecules with surfaces. The quantification of the surface loading does not require sensitive surface characterization techniques, but can be performed indirectly by analysis of the presence or absence of reactants in the supernatant, such as determination of the DNA or protein content by UV spectroscopy (due to their absorbance at 260 and 280 nm, respectively).

UV analysis of the supernatant requires previous separation of the particles from the liquid. In the case of silica or polymeric particles, separation is performed by sedimentation or centrifugation of the particle suspension. Alternatively, superparamagnetic nanoparticles can be removed from the supernatant by application of a magnetic field. This method is easier and quicker than centrifugation, especially for much diluted suspensions. The working principle of magnetic separation (as illustrated in Figure 1.4) relies on the separation of magnetic components from non-magnetic components and thus can be performed directly in crude samples containing suspended solid material which complicates particle separation by centrifugation. Magnetic carriers with appropriate surface modification bearing particular affinity for the biomolecule to be isolated are mixed with the target containing sample (i). The target specifically binds to the particle surface (ii), and this particle-target complex is then easily removed from the supernatant by applying a magnetic field and removing the supernatant (iii). Contaminates are removed by washing the particles by repeated suspension and separation. The target molecule can then be eluted from the particles (iv) by changing the medium (pH change, change in temperature). After applying a magnetic field, the supernatant can be removed and analyzed for its target content. In case of complete recovery, the magnetic particles can be used for further purifications.

Magnetic separation technique is already implemented in purification systems for nucleic acids or detection of food contamination (i.e. *brucella* and *listeria* in milk[7] or toxic *algae* in shellfish samples[8]). Application of magnetic carriers in diagnostics and therapeutics was already proposed in the late 1970s[9, 10] and recently implemented. They function as drug carriers targeting specific sites *in vivo* within the body, generally cancerous tumors. Their magnetic properties enable, once they have entered the

bloodstream, concentration of the particles in the desired region by applying an external high-gradient magnetic field. Drug release from the drug/ carrier complex in the defected part of the body occurs either by enzymatic activity or changes in physiological conditions (pH, temperature).[11] As required for such a magnetic guiding, the magnetic force has to exceed the hydrodynamic drag force acting on the magnetic particle in the flowing solution (blood).[12] A site-selective particle concentration and thus drug release in the concerned areas reduces the poisoning side-effect associated to non-specific chemotherapies.

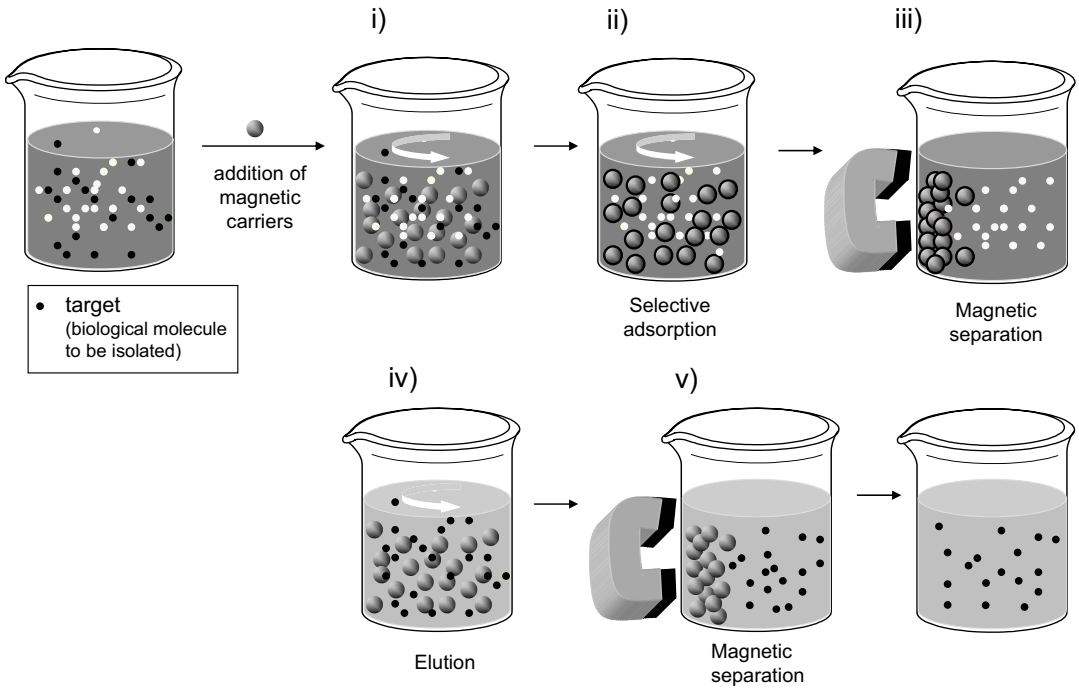

Figure 1.4: Working principle of magnetic separation: (i) addition of surface activated magnetic particles (with particular affinity for the target) to the target solution, (ii) adsorption of the target biomolecules onto the particle surface (appropriate incubation time needed, depends on kind of interaction), (iii) magnetic separation of the particles from the solution and removal of supernatant, (iv) elution of the biomolecules in a different medium, (v) magnetic separation of the particles from the supernatant to yield the target molecules in solution.

1.2 Strategies for immobilization of proteins onto surfaces

Proteins are complex structures built up by at least 20 different amino acids with different chemical and physical properties like charge, hydrophobicity or polarity. The polypeptide chain is folded and builds a functional three dimensional structure with different levels of structural and functional organization:

- the primary structure that describes the linear order of amino acid residues along the peptide chain
- the secondary structure that describes the spatial arrangement of residues that are close together in the primary sequence forming either an α helix or a β strand, and
- the tertiary structure that describes further organization in more complex topology or folds by interaction between residues that are often widely separated in the primary sequence. Interactions between residues may be covalent (eg. two thiol side chains forming a disulfide bridge) or non-covalent (hydophobic forces, van der Waals interactions, hydrogen bonding)

Proteins which are built up by more than one polypeptide chain present also a quarternary structure which describes the interaction of two or more polypeptide chains forming dimers or trimers.[13]

The ways in which proteins can be immobilized on solid surfaces are many and varied. The simplest way is by **physisorption** driven by van der Waals interactions, hydrogen bonding or electrostatic interactions between the functional groups at the protein surface and at the solid surface. Examples of this kind of immobilization are adsorption onto glass slides covered with hydrophobic nitrocellulose-based polymers, or adsorption onto negatively charged polylysine modified surfaces. In spite of their advantageous general validity, immobilization processes based on these interactions suffer from high levels of non-specificity and instability against certain working media.

More stable attachment of the protein to the surface can be achieved by covalent bonding (**chemisorption**). Substrates modified with amine, aldehyde or epoxy groups can be used for such purpose and attachment occurs by reaction of those with the free amino, carboxylic, thiol or hydroxyl groups of the peptide chains. In these cases, the protein is immobilized to the surface in a random, non-oriented fashion. Some chemical strategies for this kind of immobilization are (i) glutaraldehyde coupling between amino modified substrates and protein free amino groups,[14] (ii) Michael addition between maleimidyl activated surface and protein thiol groups, (iii) succimidyl/ amine or epoxy/ amine couplings, or (iv) Diels-Alder reaction between a peptide-cyclopentadiene conjugate to a self-assembled monolayer (SAM) of benzoquinone,[15] as represented in Figure 1.5.

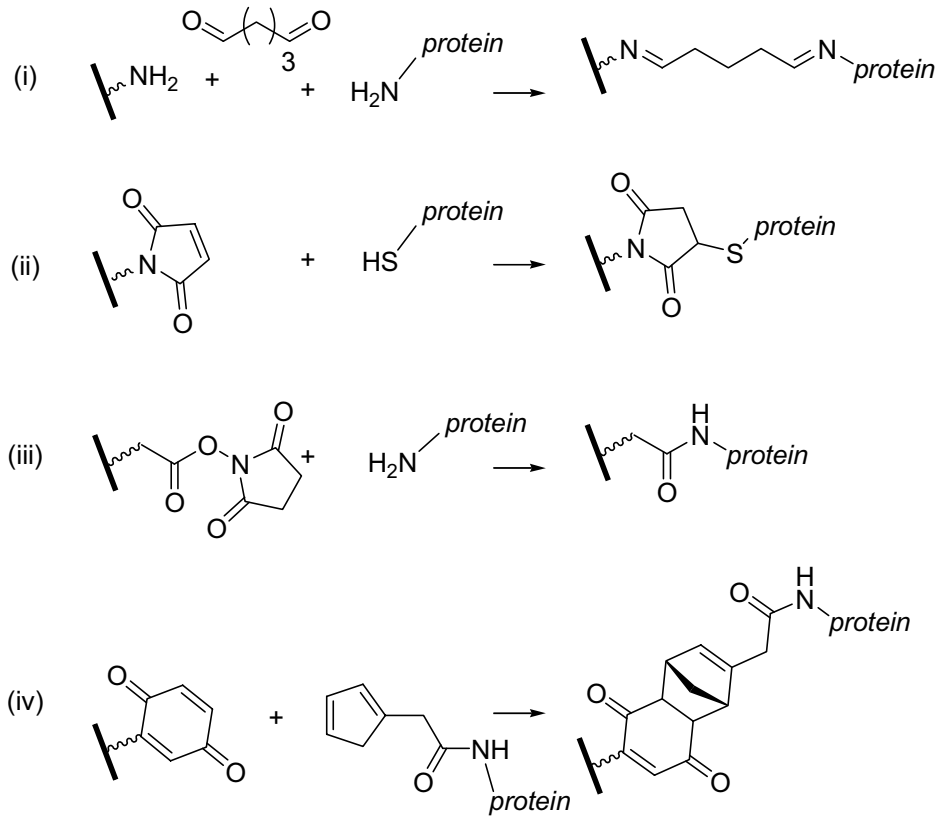

Figure 1.5: Strategies for covalent immobilization of proteins. Glutaraldehyde coupling (i), Michael addition reaction (ii), succinimidyl ester/ amine coupling (iii), Diels-Alder reaction (iv).

More specific immobilization strategies can be applied using affinity capture reagents which address only specific sites of a protein *via* **molecular recognition**. Exploited examples are the conjugation of biotin-tagged proteins to streptavidin modified surfaces,[14] and the recognition of proteins by immobilized antibodies or aptamers,[14] small, specific molecular ligands[16-18] or peptide sequences[19-22] etc. This immobilization method provides a better control over accessibility of target molecules to the protein's 'active sites' (epitope).

An interesting method for oriented and reversible immobilization of proteins is the surface functionalization with nitrilotriacetic acid (NTA) for immobilization of histidine-tagged proteins in the presence of Ni^{2+} (or other bivalent ions, eg. Cu^{2+}). A complex is formed between the NTA at the surface, the His residues and the Ni^{2+} cation,[19, 20, 23-28] as illustrated in Figure 1.6. This complex can be destroyed by addition of imidazole in solution and the protein can then be removed from the surface.

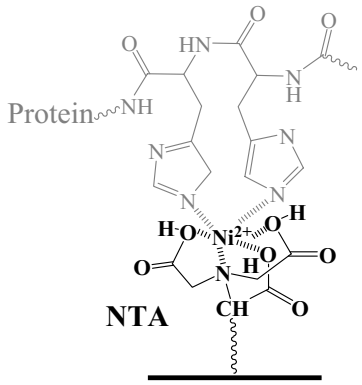

NTA-His complex

Figure 1.6: Oriented immobilization of His-tagged proteins onto NTA modified surfaces.

1.3 Protein resistant surfaces

Beside stable attachment, in certain cases a reduction of the protein-surface interactions is required to avoid non-specific adsorption and denaturing effects of the protein in the surface immobilized state. The following methods can be used to reduce protein-surface interactions: (i) the use of 'blocking agents' in the coupling and washing solutions along the immobilization protocol, (ii) attachment of protein-repellent chains to the protein (eg. PEGylation), or (iii) incorporation of protein-repellent molecules (eg. PEG or carbohydrate chains) in the reactive surface layer.[29]

Blocking agents are molecules that show high affinity for almost any kind of surfaces (such as also bovine serum albumina (BSA), casein or milk powder) and are often used in combination with surfactants (Tween, EDTA…). When incorporated to the protein solution in relatively high concentrations, they reduce non-specific adsorption by effective saturation of the positions of the surface with which the protein may interact non-specifically. Steric hindrance caused by the blocking agents may also reduce the final amount of protein that is immobilized specifically, as a negative consequence.

Proteins can be *PEGylated* by protein engineering by attaching PEG chains covalently as side chains at the protein surface. Since PEGylation occurs at any position of the peptide chain, alteration of the protein function constitutes a significant drawback of this method.

Protein-resistant surface modifications can either be prepared by physical adsorption or by covalent immobilization (grafting or chemical coupling) of PEG or carbohydrate derivatives to the reactive surfaces.[30-42] The protein-repellent chains can be incorporated (a) as linker between surface and reactive surface functionality [e.g.[43]], (b) as additional surface modification agent *via* coadsorption with a reactive moiety, or (c) as part of the reactive modification agent forming a branched structure[44] (Figure 1.7).

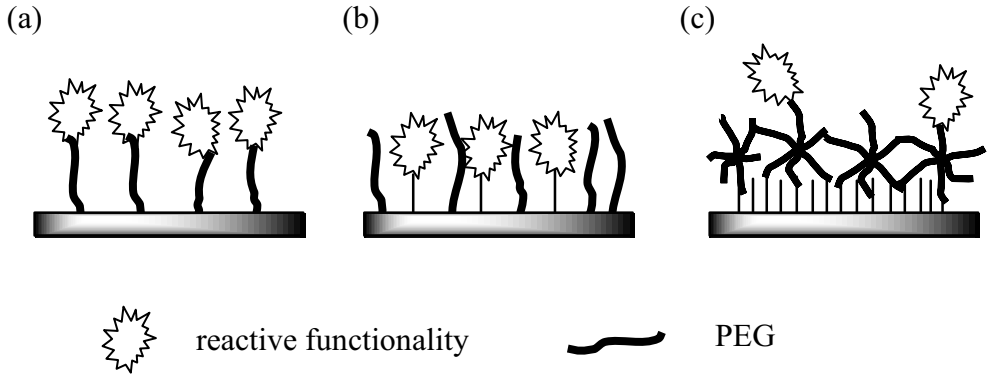

Figure 1.7: Schematic representation of incorporation of protein repellent chains into the reactive surface layer: (a) as spacers, (b) as extra component in the surface modification mixture, (c) as arm in a branched molecule.

There are two schools of thought on the physicochemical basis of fouling resistance of PEG chains.[45, 46] The "physical view" stems from the de Gennes-Alexander theory of polymer interfaces[47-49] and attributes the fouling-resistant characteristics of PEG to solely entropic effects.[50-55] The picture of a tethered and freely fluctuating chain of PEG that is resistant to adsorption and adhesion because of its large conformational freedom, however, does not take into account its molecular structure and its interaction with aqueous media. The "chemical view" recognizes these interactions, for example, hydrogen bonding (between water molecules in the media and specific chemical functional groups on the surface-tethered molecules) cause perturbation of the water's three-dimensional structure and increase the free energy of the system, which may lead to protein adsorption from the media. Such an interaction between surface functional groups and surrounding water is dictated by the electron-donor/ electron-acceptor characteristics of the species involved.[56-59] Even though the more recent studies have been biased toward the chemical view of nonfouling, it is a complicated phenomenon, and one should have an open mind in evaluating the various factors at play, whether it is entropy, interaction, or both (one being more critical than the other or being equally important).

Besides hydrophilicity, a high surface coverage is the most important parameter in determining the ability of a polymer layer to prevent protein adsorption.[55, 60-62] It has also been predicted that branched polymer architectures should be superior for

prevention of unspecific protein adsorption.[63, 64] Thus, branched shaped molecules are interesting and promising alternatives to linear systems. Some examples of star shaped hydroxyl terminated PEG molecules have been tethered to silicon surfaces and tested for their ability to suppress protein adsorption in comparison to grafted linear PEG.[44, 64-69]

1.4 Biofunctionalization of silica surfaces

1.4.1 Surface properties of silica

Silica surfaces are present in a wide range of morphologies and formats, as flat substrates (such as glass and quartz slides, oxidized silicon wafers) or in form of particles (colloidal silica, silica gel, mesoporous silica, silica-coated nanoparticles). In a biotechnology context, the low cost of glass slides and silica particles makes them very attractive for application in array production and separation technologies.[70]

The reactivity of the silica surface is intrinsically linked to the presence of surface silanol groups (Si-OH), as illustrated in Figure 1.8. These groups can be classified according to their hydrogen bonding (either free or bound silanols; the latter divided into silanols bridged to other silanols and silanols hydrogen-bonded to physisorbed water), their coordination to silicon (single and geminal silanols) and their communication or accessibility to water (internal or external silanols). The charge, acidity, solubility and hydrophilicity of a particular silica surface depend on the ratio at which each silanol type is present. At neutral pH, the silica surface is negatively charged as a consequence of dissociation of the terminal silanols (pK_a (SiOH) $\approx$ 7.5), see Figure 1.9.[71]

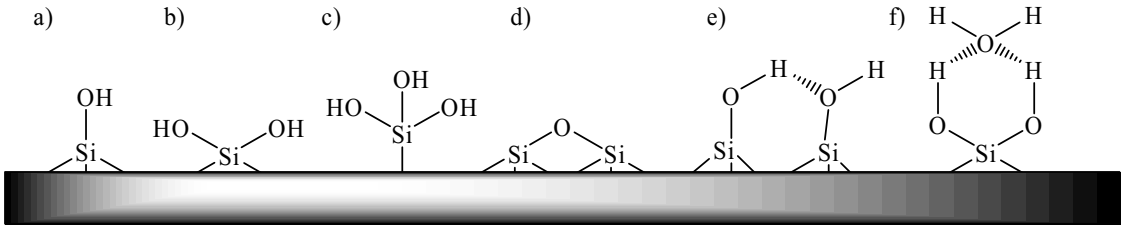

Figure 1.8: Functional groups located on silica surfaces. The silanols can be either free (a, b, c) or bound (d, e, f). In detail: single silanols (a), geminal silanols (silanediols, b), triple terminated silanols (c), siloxane bridged silanols (d), hydrogen-bonded silanols (e, f).

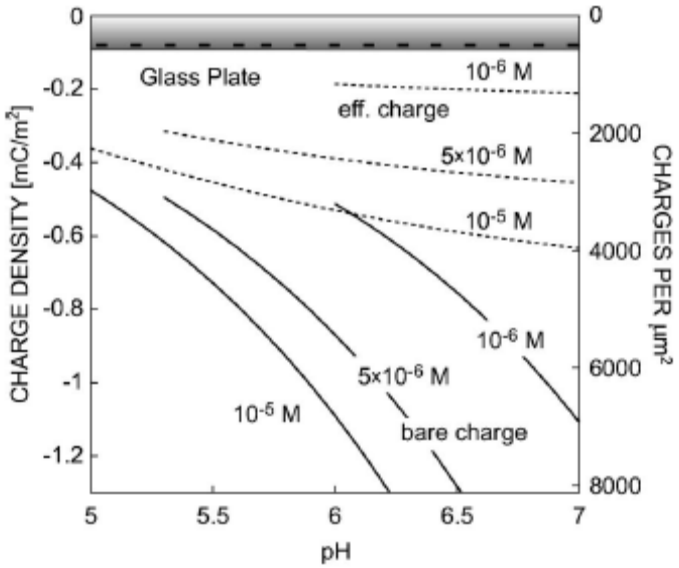

Figure 1.9: Charge density of silica versus pH. Reused from reference[71] with permission from Sven H. Behrens and David G. Grier, Journal of Chemical Physics, 115, 6716 (2001). Copyright 2001, American Institute of Physics.

Treatment with strong acids and oxidizing agents, such as piranha solution (a 5:1 V/V mixture of conc. H_2SO_4 and 30% H_2O_2), results in the generation of more free silanol-groups on the silica surface and is therefore used as cleaning and activation procedure prior surface modification.[26, 35, 72]

1.4.2 Activation of silica surfaces with organosilanes

Organosilanes can covalently react with silica surfaces and build thin organic layers on the top of the inorganic Si-OH surface. This reaction is not exclusive to silica and other oxide surfaces like ITO, ZrO_2, Fe_3O_4, or TiO_2. Even plasma treated PDMS polymers also show the same kind of reactivity towards organosilanes.[73-75]

Organosilanes used for silica modification are generally composed of three different parts: (i) an anchoring group (mono, di or trichloro or alkoxy groups) to attach to the surface, (ii) a reactive head group which determines the final chemical properties of the modified surface, and (iii) a flexible spacer which connects the functional head group to the surface (Figure 1.10).

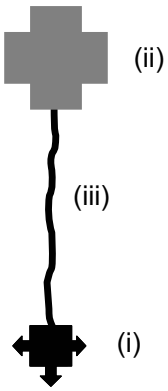

Figure 1.10: Schematic representation of surface modification agents, exhibiting three different parts: an anchoring group (i), a head group (ii) and a flexible spacer (iii).

Alkoxysilanes are less reactive than chlorosilanes and therefore preferred due to easier handling in the laboratory. In theory, the mechanism of silanization of surfaces with alkoxysilanes (either as one or multicomponent mixtures) is relatively simple: hydrolysis of the silane alkoxy groups yields hydroxyl groups that can covalently interact with the silanol surface. This process can be either performed in solution or in gas phase. Subsequent thermal curing of the film cross-links the free silanol groups and improves the stability of the silane films (Figure 1.11).

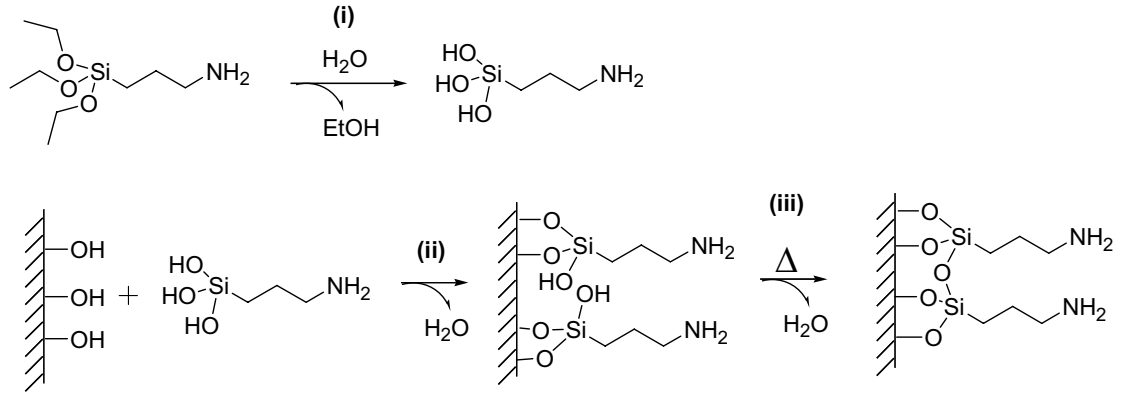

Figure 1.11: Silanization of silica surfaces with aminopropyltriethoxysilane (APTS): (i) hydrolysis of the alkoxy groups, (ii) condensation with the surface silanol groups, (iii) thermal curing to cross-link the free silanol groups.

In reality, the situation is much more complicated. The hydrolyzed silanol groups can not only condense with the surface residues to form siloxane linkages, but also condensate with each other and build oligomers in solution prior to condensation with the solid substrate (Figure 1.12). In multicomponent mixtures, additional problems in terms of phase separations due to different hydrolysis kinetics of the components may occur.

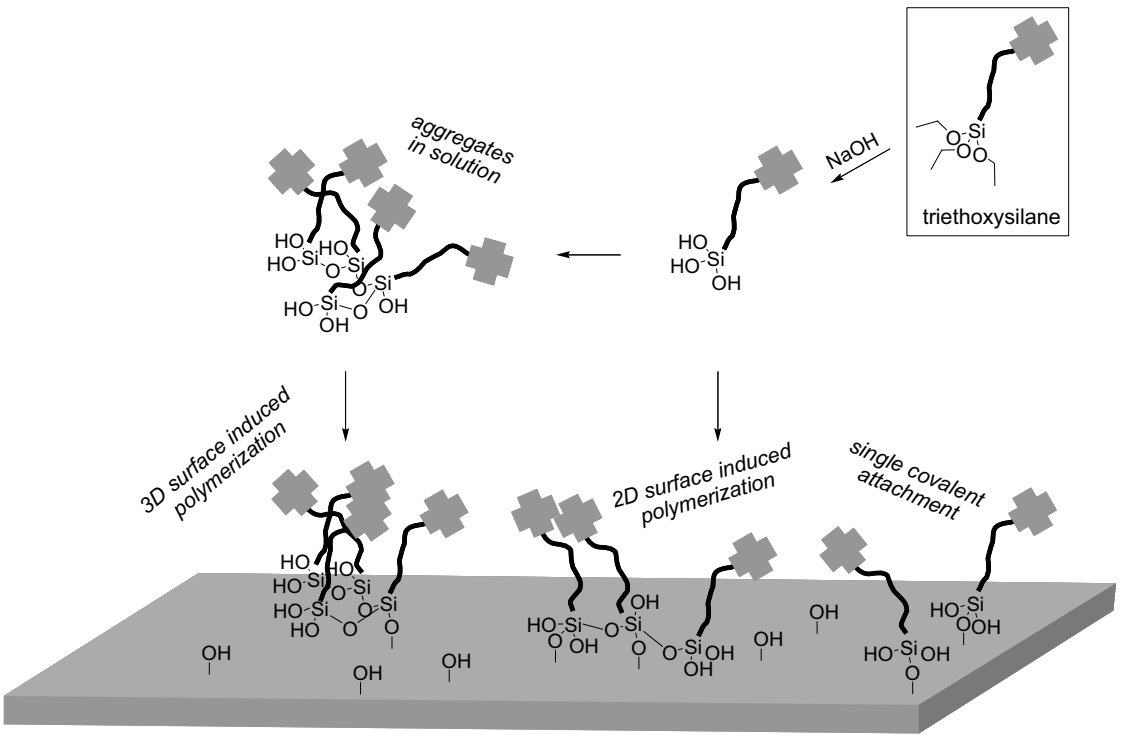

Figure 1.12: Surface modification of silica with trialkoxysilanes.

1.5 Photochemical methods for surface patterning

Chemical patterned surfaces can be used to site-selectively immobilize molecular targets like proteins. Several patterning methods are available and have been exploited to generate protein patterns (protein microarrays): photolithography and subsequent chemical activation and protein attachment at the photoresist-free regions,[76, 77] microcontact printing of proteins using flexible PDMS stamps,[78-83] or microspotting or ink-jetting protein solutions using positioning robots.[84-86]

Alternatively, chemical patterns have also been accomplished by modifying a substrate with photosensitive molecules and using light irradiation through a mask to generate regions with different chemistries. Different strategies based on different photochemical processes can be used[87]:

1) Irradiation of alkyl and arylsilanes layers at very short wavelengths (< 250 nm, high UV energy) in the presence of oxygen removes the organosilane layer from the irradiated regions.[88] Masked irradiation in these conditions generates silica surfaces with a pattern of organosilane modified and unmodified (photochemically etched) regions.

2) Irradiation of thiol layers on gold induces oxidation of the thiol group to a sulfonate and removes the organic layer from the irradiated regions.[89]

3) Light-induced attachment of aldehydes or 1-alkenes to hydrogenated silicon surfaces.[90]

4) Photografting molecules after irradiation of benzophenone-modified silane layers.[91]

5) Irradiation of organic surface layers bearing photoremovable cages. Irradiation removes the cage and liberates a reactive organic group. Patterns of reactive (irradiated) and caged regions can be created and can be used for further chemical synthesis at the surface,[92, 93] or for subsequent attachment of targets from solution.[87]

1.6 Surface patterns with caged coupling agents

Caged surfaces can be prepared either by attaching the photoremovable groups to previously modified surfaces containing the reactive groups,[93-96] or by modifying the bare surface with a previously prepared caged coupling agent.[97-100] The first method typically occurs in a two-step procedure. First, surface-active molecules with unprotected functional groups are coupled to the substrate. These functional groups determine the properties of the newly formed surface, like reactivity, polarity, and charge. In the second step, the photosensitive moieties are introduced into the monolayer by reaction with the functional surface groups. This is the limiting step of the process, since surface reactions are rarely quantitative and protected and unprotected molecules always coexist within the layer. Patterning is performed by masked irradiation and deprotection of the caged layer through a mask. This method has been already implemented in the industry for the synthesis of customized OND-microarrays[93, 95, 101-106] (Figure 1.13).

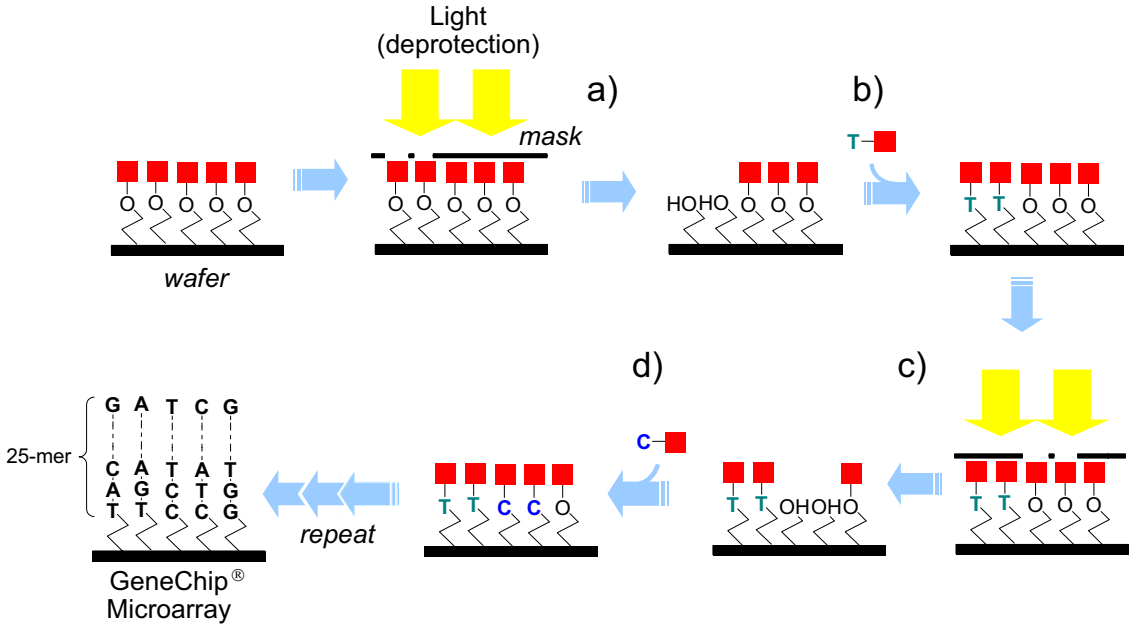

Figure 1.13: Preparation of GeneChip® Arrays by combination of photolithography and combinatorial chemistry (adapted from a figure of Affymetrix Company): A photo-protected quartz substrate is treated in four steps: (a) selective irradiation through a mask, releasing free hydroxyl groups, (b) chemical coupling of nucleotides at the activated positions, (c) selective irradiation with a new mask, (d) chemical coupling of nucleotide. Repetition of all steps until the desired set of probes (number of repetitions depends on the length of oligonucleotides to be immobilized).

Alternatively, caged surface coupling agents with their reactive groups protected with the photoremovable group can be synthesized prior to monolayer preparation and used in a one-step surface process for preparing the caged surfaces.[87, 97, 107] Subsequently, the desired functionality can be activated by light irradiation on selected positions of the substrate after surface modification (see schematic representation in Figure 1.14). This method allows higher selectivity and better control over the layer composition than the previous one.

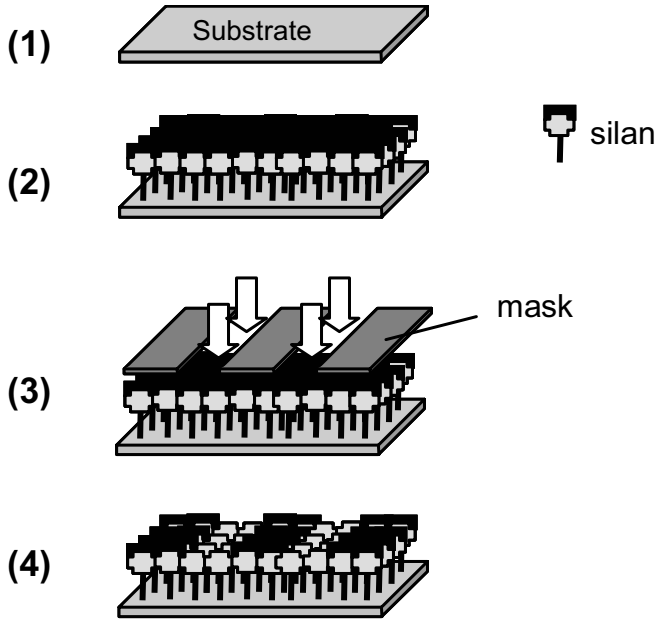

Figure 1.14: Schematic representation of surface patterning using photoactivable silanes.

As an additional advantage, the last strategy allows the generation of more complex patterns with different functionalities using organosilanes functionalized with different protecting groups that can be independently addressed using different wavelengths. Previous results have been achieved by simultaneous coadsorption of two different silanes with different head-group functionalities, amine and carboxyl, caged by two different photoremovable protecting groups, NVoc for the amine group and Bnz for the carboxylic group which can be selectively cleaved upon irradiation at 411 nm and 254 nm, respectively. The resulting complex photopatterned mixed layers have been successfully implemented in the site-selective immobilization of small molecules, colloidal particles or OND.[87, 108] See section 4.1 for further information.

Chapter 2

Characterization methods

Different characterization methods have been used during this PhD work in order to analyze the structure and properties of the synthesized molecules and derived surface layers. The molecular structure of the silanes was characterized by ^{1}H and ^{13}C NMR spectroscopy. The surface composition, surface hydrophobicity and layer thickness were characterized by UV spectroscopy on modified quartz substrates, contact angle measurement and ellipsometry and reflectance interference spectroscopy, respectively. Some of these methods will be described in this chapter.

2.1 Contact angle measurement

The contact angle (CA) of water on a substrate in air is measured to give idea about surface/ interface energies and therefore determination of the hydrophilicity or hydrophobicity of a surface. In the sessile drop method the angle between the baseline of the drop and the tangent at the drop boundary is measured by optical microscopy (Figure 2.1).

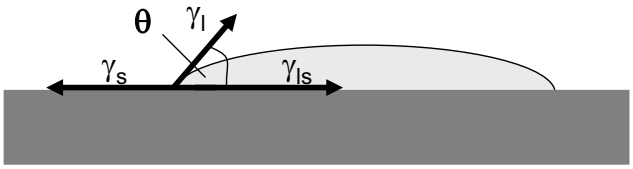

Figure 2.1: Determination of contact angle θ by sessile drop method.

The macroscopic description of the contact angle θ is given by Young's equation (Equation 2-1) as dependence of surface tension of the liquid, γ_l, the surface energy of the flat solid surface, γ_s, and the interfacial energy between solid and liquid, γ_{ls}.

$$\gamma_l \cdot \cos\theta = \gamma_s - \gamma_{sl} \qquad \text{(Equation 2-1)}$$

The contact angle is influenced by surface roughness, surface inhomogeneities and restructuring of surface upon contact with water. Pure silica surfaces are hydrophilic and the water droplet spreads to give small contact angles. By surface modification, the hydrophilicity of pure silica is reduced and can be observed by the detection of a higher water contact angle.

2.2 Ellipsometry

An ellipsometer as measurement tool permits the determination of the thickness of a molecular monolayers on solid substrates with Angstrom resolution. The technique is based on the measurement of changes in the polarization state of light, when it is reflected from a sample. In an ellipsometer, as schematically illustrated in Figure 2.2, linear polarized monochromatic light with equal polarization components parallel and perpendicular to the surface is generated from a laser beam by passing first through a polarizer and then through a compensator in ± 45° orientation. Different interactions of the parallel and the perpendicular components of the incident beam with the surface layer lead to optical retardation and thus elliptical polarization of the light reflected at the dielectric interfaces from the sample. The analyzer is equipped with an optical retardation that compensates for the retardation caused by this polarization dependent reflection at the interfaces. Knowing the refractive index of the film, the layer thickness

can be calculated from the relative phase change and the relative amplitude change.

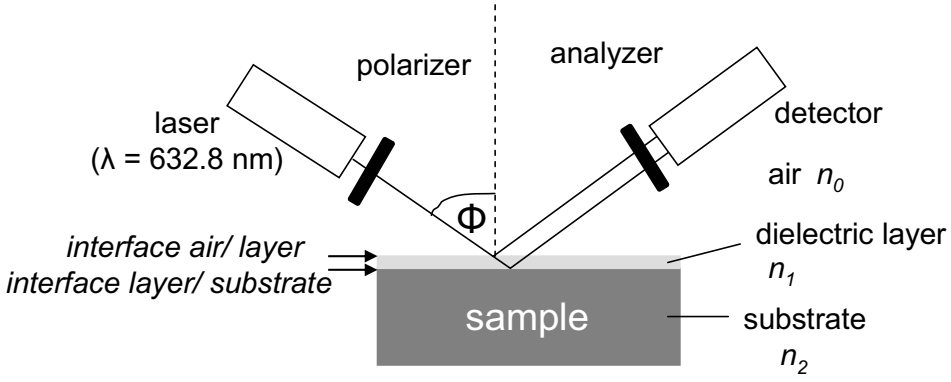

Figure 2.2: Schematic assembly of an ellipsometer.

2.3 Reflectance Interference Spectroscopy

White light that passes through a thin film is reflected at the interfaces, thus generating two reflected partial beams which can superimpose (Figure 2.3a). The interferometric pattern which results from the phase difference $\Delta\varphi$ for films in the micron range can be used to estimate the thickness of the interfering layer[109] (Figure 2.3b). This principle is used in Reflectance Interference Spectroscopy (RIFS) to monitor and quantify adsorption or desorption of proteins onto or from substrates.

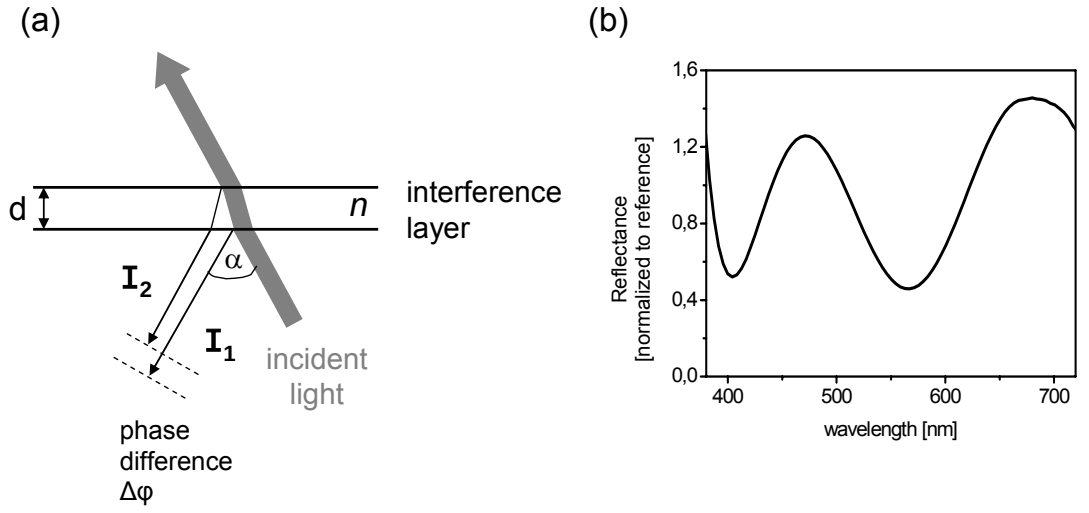

Figure 2.3: Reflectance Interference Spectroscopy: (a) schematic light path in the transducer, (b) reflectance pattern of a thin film with modulation with cos(1/λ) analogues (Equation 2-2), adapted from ref[110].

The reflectance for a transparent (non-absorbing) and weakly reflecting (in the lower percent range) film for perpendicular incidence (α = 90) is given by Equation 2-2.[110]

$$R = R_1 + R_2 + 2\sqrt{R_1 \cdot R_2}\cos\left(\frac{4 \cdot \pi \cdot n \cdot d}{\lambda}\right) \qquad \text{(Equation 2-2)}$$

with R_1 and R_2, the Fresnels reflectances of the boundaries, d the film thickness and λ the wavelength of incident light. The thickness of the monitored layer can be estimated from the postion of the maximum with a given order value m from Equation 2-3.

$$n \cdot d = \frac{m \cdot \lambda}{2} \qquad \text{(Equation 2-3)}$$

Binding or adsorption of any organic molecules onto the interference layer (silica) causes a shift in the interference pattern which can be monitored by a simultaneous spectrometer (which detects the complete spectrum) and allows real-time *in-situ* determination of the optical layer thickness and thus of the amount of adsorbed molecules.

Chapter 3

Photoactive branched silanes for functional and patterned immobilization of proteins

3.1 Introduction

The compositional complexity and dynamic nature of biological processes make it difficult to study certain fundamental aspects of biological systems in detail. Model surfaces with well-defined compositions are today well established tools for *in-vitro* investigating single recognition processes at the molecular level, or for determining the effect of individual recognition events on the functional behavior of cells. One primary challenge in developing model surfaces *ex vivo* is the precise control of the composition and structure of the surface which permits natural biological interactions to occur in such a way that the results can be interpreted clearly and related to biology *in vivo*. Non-specific interactions of the intervening biomolecules and the artificial surface need to be abolished so that the obtained results can be solely attributed to the biological process under investigation. In addition, bioprocesses *in vivo* often involve the interplay of more than one molecular species. *In vitro* modelling of this scenario requires the performance

of numerous experiments under different influencing factors, and positive and negative controls to ensure the validity of the obtained results. Practical realization of such a number of experiments requires surfaces patterned with multiple and independent reactive sites where the different conditions can be tested and analyzed in parallel (eg. DNA, protein or cell arrays).

Different techniques have been developed to pattern surfaces with multiple and independent bioactive sites. Local delivery of the biological species from a reservoir can be performed by spotting, ink-jetting, or dip-pen deposition.[84, 85] Alternatively, the biological material can be patterned by contact printing using loaded poly(dimethylsiloxane) stamps.[78, 80] Direct immobilization of the biological material to desired places on a substrate from a solution can also be mediated by surface layers containing patterned complementary functionalities that can be recognized by the target.[87, 93, 96, 97, 100, 101, 111-116] These are initially protected with a photocleavable group and can be site-selectively activated by light irradiation through a mask. Using this principle, patterns of oligonucleotides have been prepared on silica surfaces which were previously modified with photosensitive organosilanes.[87] However, results have shown very limited selectivity in the assembly as a consequence of high non-specific interactions of the ONDs with the surface.

This demonstrates that functional surface coupling of the biomolecular species requires the photoactive sites to be biocompatible in order to prevent non-specific adsorption or loss of function of the arrayed material, and to permit the maximum selectivity and sensitivity of the test. In the case of proteins, surfaces containing ethyleneglycol (EG) units into the surface layer are well known to present nonfouling properties.[46, 117] The length, packing density[68, 118-120] and branching[67, 121-124] of the OEG chains seem to strongly determine the protein repellence performance. Accordingly, different strategies have been followed to incorporate OEG units to a functional surface: direct coupling of surface active functionality through OEG linkers, coadsorption from solution of OEG and functional molecules (either in parallel[125-127] or sequential[128] surface reactions), or the use of branched surface coupling agents containing protein repellent and protein attractive arms.[67, 121-124] Branched molecules like star-shaped PEG have been demonstrated to be superior for prevention of unspecific protein adsorption than linear

structures provided that they can be attached to the surface and form dense layers.[65, 67, 29]

3.2 Objectives

This chapter describes the design and synthesis of functional organosilanes with a branched structure capable of pattern and couple proteins to surfaces while maintaining their biofunctional state. Their molecular structure exhibits the following domains (Figure 3.1):

- A chloro- or alkoxysilane group for the covalent attachment to silica surfaces
- A functional group capable to react with proteins and capped by
- A photoremovable protecting group as built-in patterning tool
- A protein-repellent arm
- A trifunctional linker connecting the three domains via flexible OEG or alkyl spacers

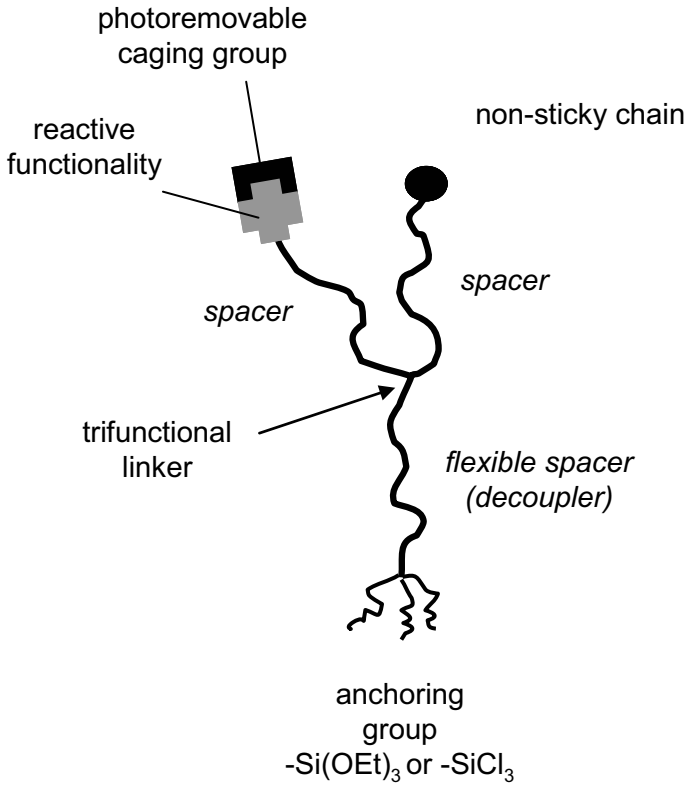

Figure 3.1: Schematic representation of the new type of multifunctional branched organosilane presented in this Chapter.

In their initial, protected state, surfaces modified with these molecules should not show any affinity for proteins. Only after cleavage of the photoprotecting group by light exposure surfaces should be able to immobilize proteins at the irradiated regions (Figure 3.2).

Two different variants of this structure were synthesized and used to modify silica surfaces onto which proteins were patterned: one containing only EG spacers and one containing one alkyl spacer connected to the anchoring groups which is expected to help in the formation of more dense surface layers due to lateral hydrophobic interactions between neighboring molecules at the surface.

The bioactivity of layers made of these silanes will be tested, as well as their ability to site-selectively immobilize biomolecular species and cells building surface micropatterns.

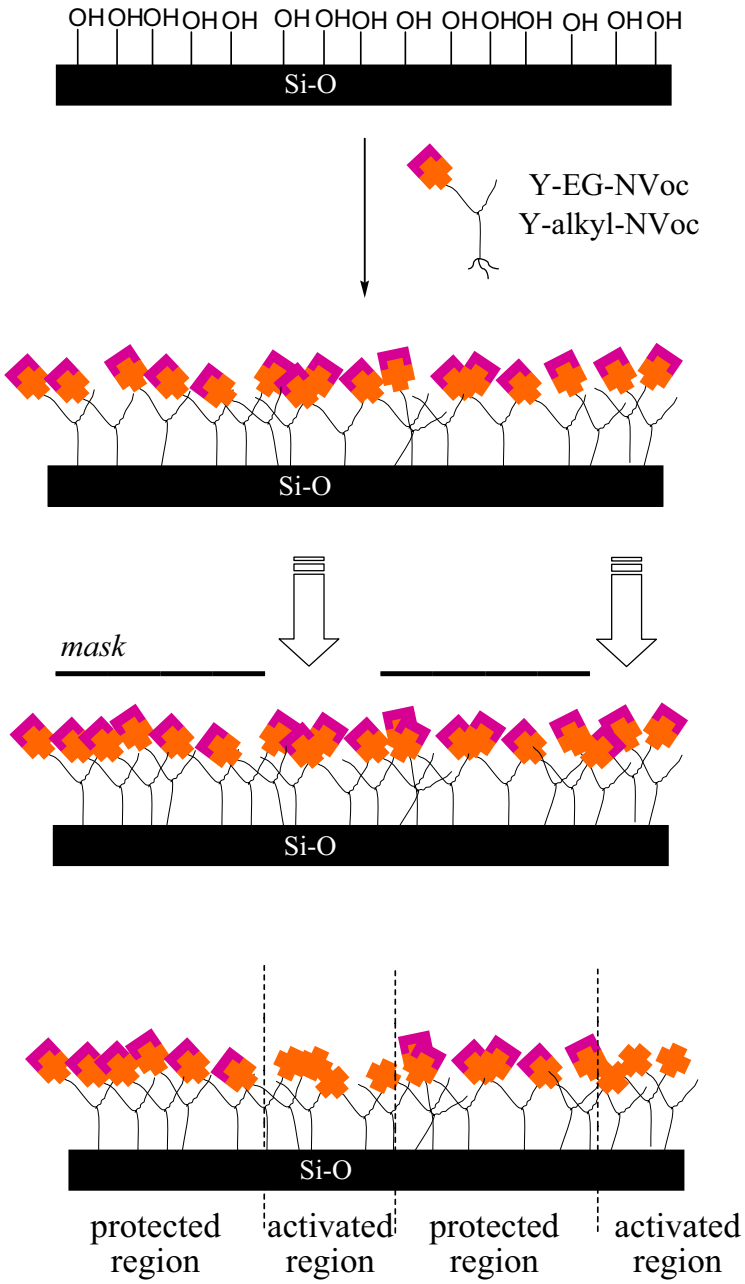

Figure 3.2: Schematic representation of surface pattern by irradiation through a mask. A pattern of activated (irradiated) and non activated areas is generated.

3.3 Synthetic strategy

3.3.1 Considerations to molecular design

Initially, functional considerations and synthetic limitations were taken into account in order to define the specific chemical structure and synthetic path to our key molecule. Functional considerations include:

- The molecule should not show any affinity for proteins in its initial, protected state. This means that the structure should contain EG units long enough to prevent protein adsorption. For the same reason, charged or strong hydrophobic groups should be avoided in the chemical structure and the different functional groups should be preferentially linked to the EG spacers *via* ether bonds. Ethers have also the advantage of being stable against most basic or acidic conditions used in organic synthesis.

- The reactive functionality after deprotection should be able to couple to proteins *via* common coupling methods (see section 1.2 in Chapter 1 for examples).

- The molecule and its synthetic route should be built in a modular manner. In this way future access to more sophisticated molecules is provided by changing the starting products but keeping a similar synthetic path. Such structural variations could be longer or asymmetric arms, a different functional group for protein attachment or a different photo-caging group.

- Activation of the molecule by irradiation should not affect the rest of the structural units (photostability).

- The presence of chromophores other than the photoremovable group in the molecular structure should be avoided because their UV absorption would interfere and reduce the yield of the light deprotection process.

- The molecule should be stable against physiological conditions which will be used in the application. Water hydrolysis resistance means that ether, amine or carbamate linking groups will be preferred against carbonate, ester or amide

groups.

- Chloro- or alkoxysilane groups are required for binding to silica surfaces.

- Chloro- or alkoxysilanes can be mono, di or trivalent. Trivalent silanes give more stable surface layers due to lateral crosslinking of the silanol groups.

The following chemical constraints need also to be considered when planning the synthetic path:

- Chlorosilanes are very reactive species and therefore more difficult to purify than alkoxysilanes.

- Chloro- or alkoxysilane groups hydrolyze easily in the presence of catalytic amounts of water. Therefore, introduction of this functional group should take place at the last step of the synthetic route.

- Functional groups with acid or basic character (hydroxyl, carboxylic, amine…) cannot be present in the molecule without being previously caged in order to avoid hydrolysis of the chloro or alkoxysilane group.

- Chloro- or alkoxysilane groups are usually introduced by hydrosilylation of olefins under Lewis acids catalysis using transition metal complexes. Hydrosilylation does not work in the presence of basic groups (such as amines) because they can neutralize the catalyst. Because of complexation of the catalyst's metal center, sulfur containing groups may also inhibit hydrosilylation.

- Etherification reactions require strong basic media which may affect other functional groups. Amines interfere as nucleophiles under Williamson etherification conditions.

- The purification of reaction products containing long ethyleneglycol chains and differing only in the terminal functionality can be difficult if the polarity of the end-groups does not differ considerably.

Taking these issues in mind, the design of the synthetic route started by selecting an appropriate trifunctional linker to which the three different arms could be attached. A range of commercially available trifunctional molecules are potential candidates (Figure 3.3): tertiary amines (a), tertiary carbons (b), trisubstituted aryl compounds (c), malonate derivatives (d), or triols (e).

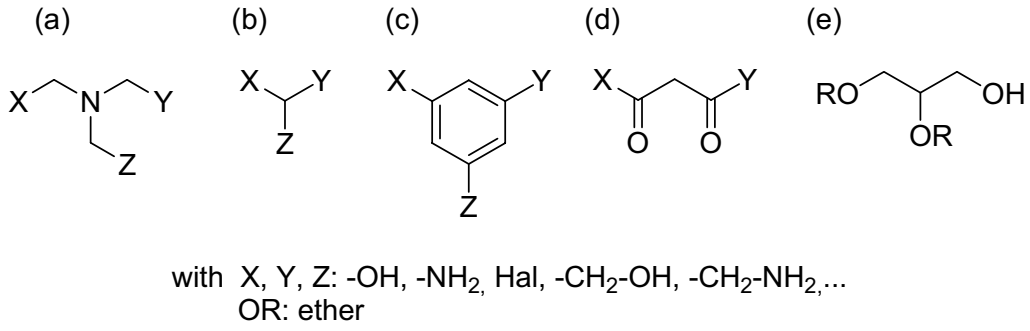

Figure 3.3: Commercial trifunctional molecular structures: tertiary amines (a), tertiary carbons (b), 1,3,5 substituted aryl compounds (c), malonate derivatives (d), triols (e).

Amines were discharged because of their basic character which could interfere with the hydrosilylation reaction. Trisubstituted aryl compounds may show UV absorption bands at the irradiation wavelength required for cleavage of the protecting group and this would diminish the photolytic efficiency of the irradiation step. Malonate derivatives would connect the different arms through ester or amide bonds, with less stability than ether units. Triols with three hydroxyl groups with different reactivity are of special interest because they can be reacted separately to form stable ether bonds. Three different commercial available variants of glycerol were considered as potential candidates for the synthesis: (+/-)-3-benzyloxa-1,2-propanediol, 1,2-iso-propylidene-rac-glycerol (*solketal*), and (+/-) glycidol (Figure 3.4).

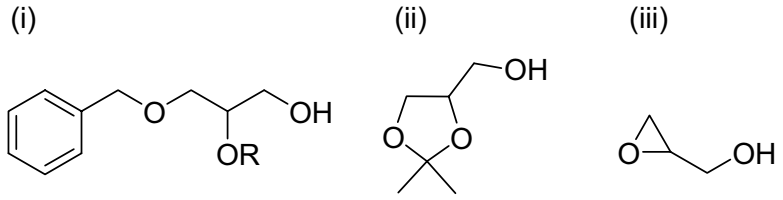

Figure 3.4: Structures of commercial available triol derivatives: (+/-)-3-benzyloxa-1,2-propanediol (i), 1,2-iso-propylidene-rac-glycerol (*solketal*, ii), and (+/-) glycidol (iii).

Heterofunctional ethyleneglycol spacers are then required to couple the different end-groups of the branched molecule to the selected linker. The length of the ethyleneglycol spacers was set to four units. According to published results on SAMs of thiols, this length seems to be enough for inhibiting protein adsorption.[130] In addition, the starting compound TEG is cheap and some mono- and disubstituted variants are commercially available. Longer spacers may give a better performance, but they would increase the number of synthetic steps and the price of the molecule.

A synthetic variant was conceived using an alkyl chain instead of a TEG spacer for surface anchoring. The length of this spacer was selected to be almost the same as TEG for allowing meaningful comparison.

The three different arms of the branched molecule will be then composed of heterofunctional spacers (TEG or alkyl) activated on one end with a good leaving group for coupling to the linker (eg. halogene, sulphate or *p*-toluenesulfonate), and on the other end with the required functionality. Heterofunctional TEG derivatives can be synthesized by asymmetric derivatization of TEG, as well as by chain length extension reactions starting from commercial available functionalized di- or triethylene glycols.[131] Reactions involving mono- and heterofunctionalization of symmetric molecules have to deal with difunctionalized byproducts and therefore purification processes will always be necessary.[132]

The TEG arm for surface anchoring can carry a double bond as precursor for the triethoxysilyl group. A double bond is a stable functional group which is expected to resist the reaction conditions of the whole synthetic route before it gets hydrosilylated. The protein repelling arm can be a OH or OMe terminated TEG, since both groups have been demonstrated to work well against protein adsorption. A hydroxyl group can also react under Williamson ether synthesis conditions and needs to be protected (eg. as tetrahydropyranyl ether which are stable under strong basic conditions).

An amine was selected as functional group for later coupling of proteins. This group needs to be protected with the photoremovable cage. We selected the 6-nitroveratryloxycarbonyl (NVoc) group. NVoc protected amines have been uncaged by irradiation with wavelengths longer than 320 nm.[133] Beside the desired free amine,

carbon dioxide and an ortho-nitrosobenzaldehyde are liberated as well in this intramolecular redox reaction (Figure 3.5).

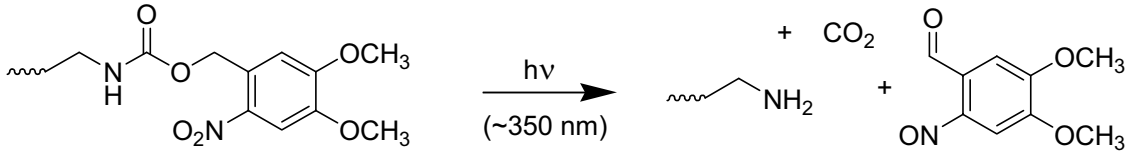

Figure 3.5: Photocleavage of NVoc protected amines upon UV irradiation.

The chemical structures of two key molecules synthesized during this thesis are given in Figure 3.6. These silanes, **22** and **33**, will be abbreviated Y-EG-NVoc and Y-alkyl-NVoc in the following.

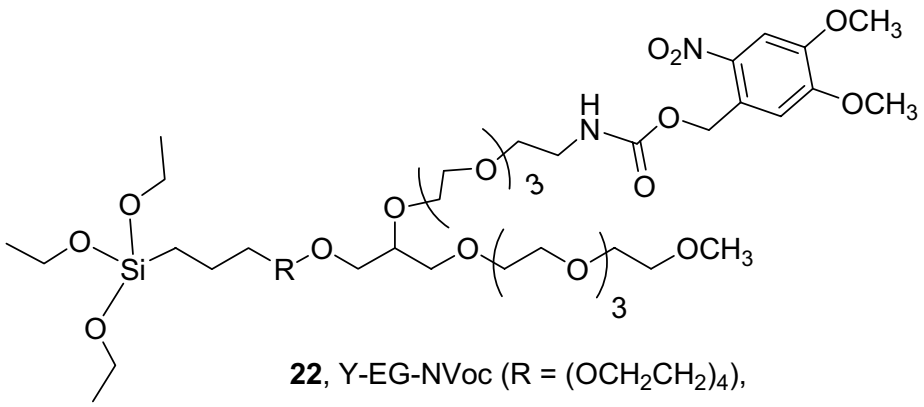

Figure 3.6: Structures of the two silanes, **22** and **33**, synthesized during this thesis. They are abbreviated in the following with Y-EG-NVoc and Y-alkyl-NVoc, respectively.

3.3.2 Proposed synthetic routes

Considering the issues mentioned in the previous paragraphs, three different synthetic alternatives based on different linker molecules and small variations in the overall structure of the attached arms were conceived. Not all of the proposed paths lead in praxis to the desired molecule. The achieved compounds and difficulties occurred during the implementation, in terms of unsuccessful reactions or isolation processes, will be described in following sections.

Route I (via 3-Benzyloxy-1,2-propanediol)

(+/-)-3-Benzyloxy-1,2-propanediol possesses three hydroxyl groups with marked difference in reactivity to which the three arms of the branched molecule can be attached in successive Williamson etherification reactions, starting with the primary and followed by the secondary and benzyl protected one (after previous deprotection).[134, 135] In this synthetic variant, a hydroxyl group was selected as terminal functionality of the protein repellent arm, which needs to be protected as pyranyl ether in order to resist the etherification conditions. A N-phthalimide group is used as precursor for the amine functionality (Figure 3.7).

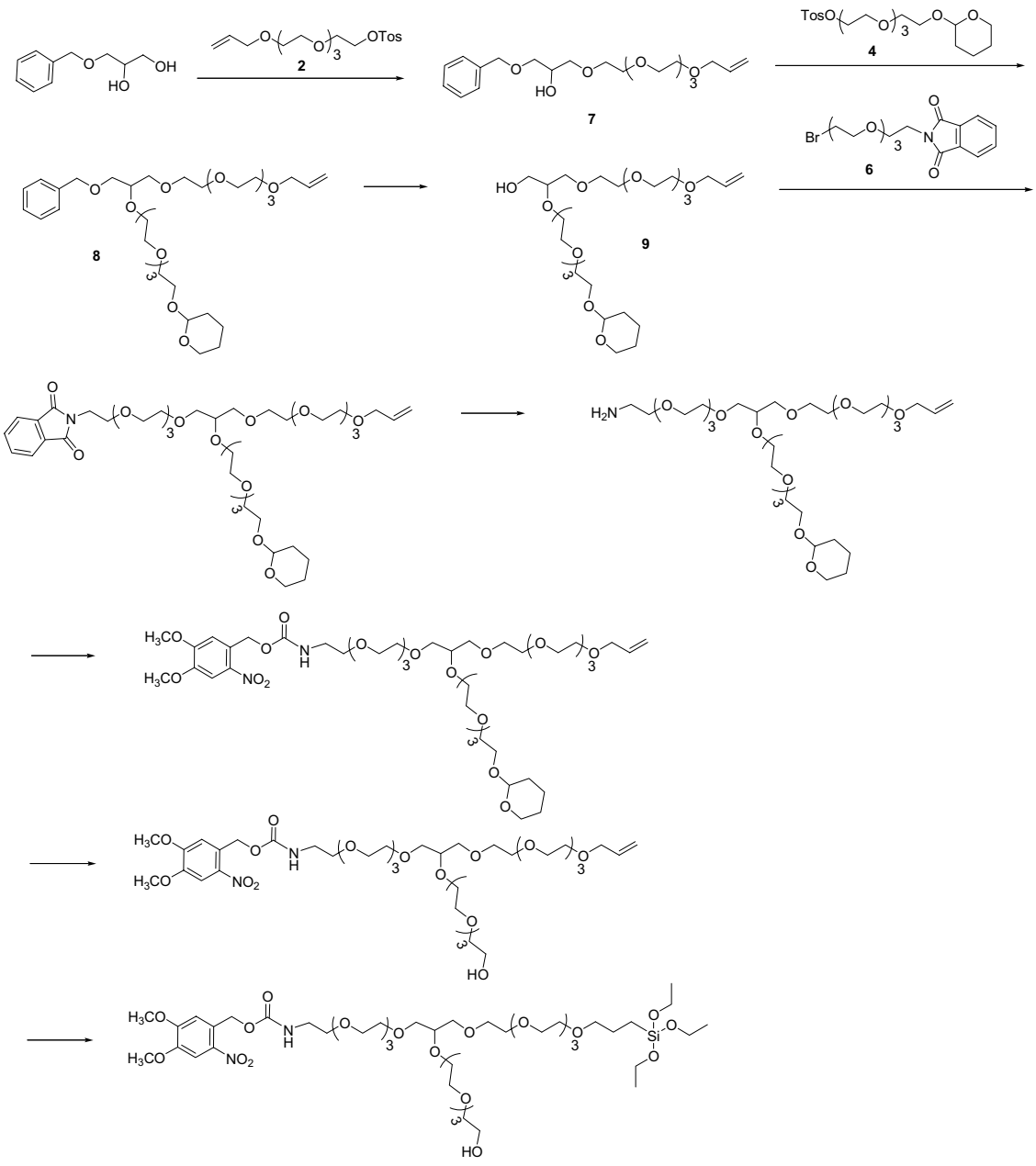

Figure 3.7: Proposed Route I using (+/-)-3-Benzyloxy-1,2-propanediol as linker.

The synthesis of the arms **2**, **4** and **6** required in the process is represented in Figure 3.8. TEG is first converted to the allylether **1**, or to the tetrahydropyranylether **3**, and then transformed into the respective *p*-toluenesulfonyl derivatives **2** and **4**, respectively to be anchored to the OH groups of the linker. The heterofunctionalization of **6** requires first a bromation step followed by conversion of only one bromine end group to the phthalimide derivative **6**.

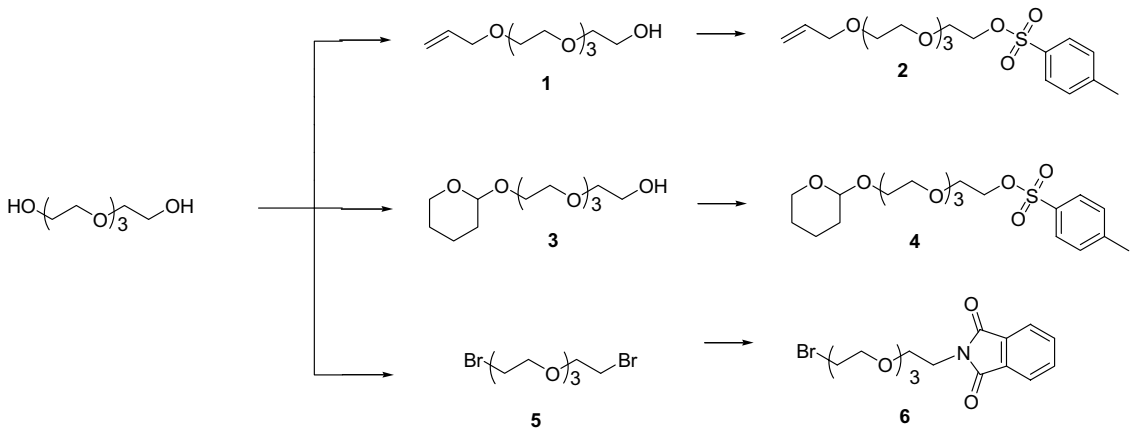

Figure 3.8: Route for synthesis of **2**, **4** and **6**. These heterofunctional TEG precursors possess a good leaving group (-Br or –OTs) on one end and the required functionality on the other end: a double bond as precursor for the triethoxysilyl functionality (**2**), a hydroxyl group as THP-ether as non-sticky end (**4**), and a phthalimide as amine precursor (**6**).

Once the three arms are connected, the photoprotecting group is introduced in order to minimize consumption of the expensive NVoc moiety in following synthetic steps. This occurs after conversion of the N-phthalimide to a primary amine[136] which can be coupled to commercial 6-nitroveratryloxycarbonyl chloride in a further reaction step to form the carbamate. Deprotection of the pyranyl ether and hydrosilylation of the allylic double bond yield the functional branched silane.

Route II (via solketal)

The reaction path using solketal as linker molecule is illustrated in Figure 3.9. The first arm can be attached to the primary hydroxyl group.[134] Opening of the acetal ring generates one primary and one secondary hydroxyl group from which marked reactivity difference in a Williamson etherification process is expected.[134, 135, 137] Two similar but not identical molecules can be obtained through this path depending on the selected sequence of attachment of the arms. The path to molecule **22** was preferred because it attaches first the arm **10** which is easier to obtain.

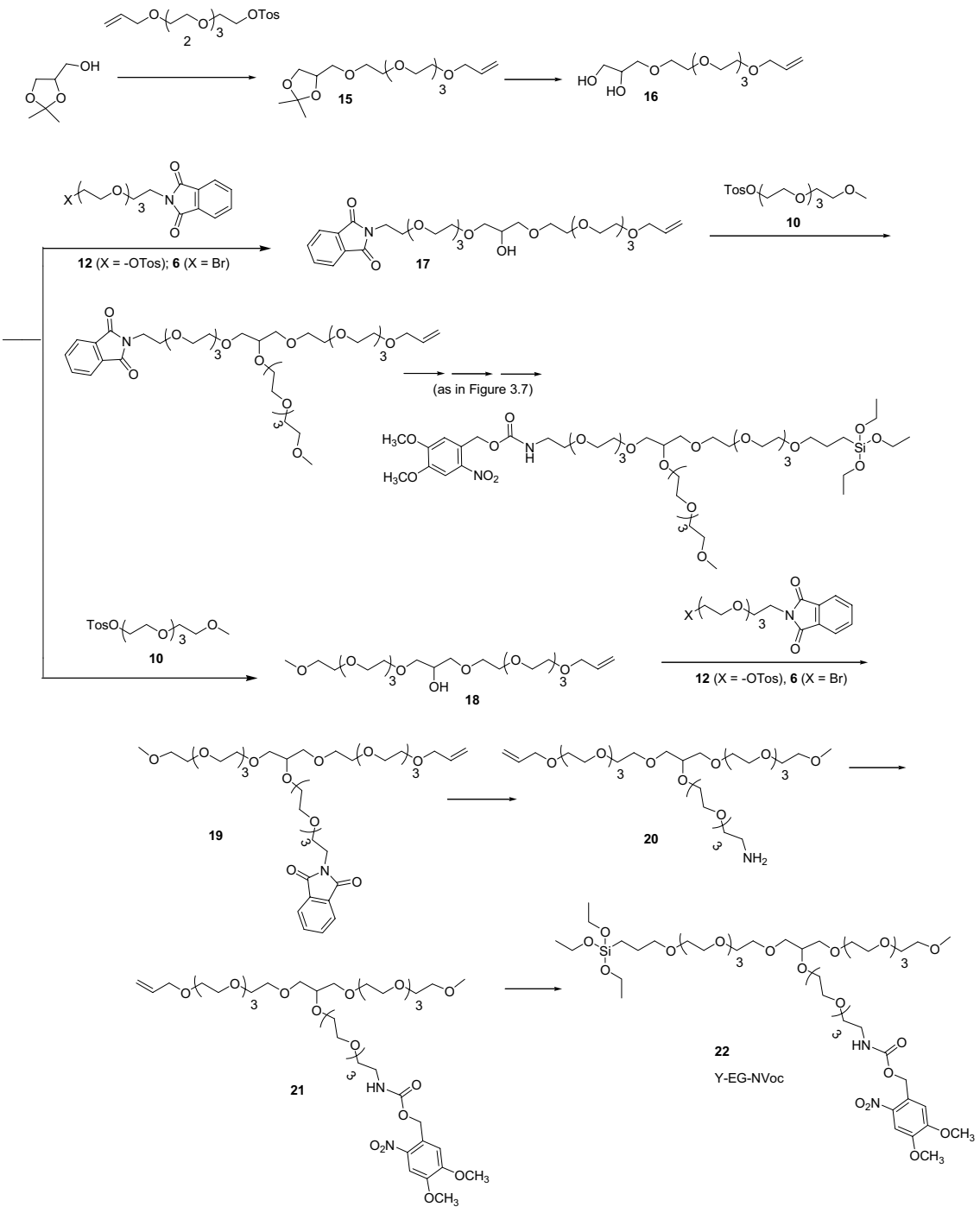

Figure 3.9: Proposed synthetic routes *via* solketal as linker molecule.

A methoxy terminated protein-repellent arm was selected which simplifies the overall synthetic route because no protection/cleavage steps are required, as in the case of OH terminated arms. The heterofunctional TEG derivatives **10** and **12** can be obtained through similar reaction steps as in molecules **2** and **6**.

Route III (via epichlorhydrin)

This route allows sequential generation of hydroxyl groups at the linker molecule so that linking of the three arms through etherification reactions occurs selectively (Figure 3.10). Consequently, product mixtures are avoided and purification processes are expected to be easier. After linking the first arm to the epichlorhydrin molecule *via* alkoxylation of the $-CH_2Cl$ group, a nucleophilic ring opening reaction under basic conditions allows binding of the second arm and liberation of a secondary hydroxyl group for subsequent linking of the third arm.[138] The rest of the synthetic path is analogous to that described in Route I. The same synthetic route can be used to obtain the branched silane with alkyl chain for surface anchoring **33** starting from commercial available 9-decen-1-ol.

Alternatively the NVoc group can be coupled to the arm before attachment to the linker (Figure 3.11). This synthetic variant reduces the number of reaction steps performed with the large molecule **19** and may be advantageous if purification processes at that stage turn out to be difficult. The synthetic route for the NVoc-containing arm required in this variant is presented in Figure 3.12.

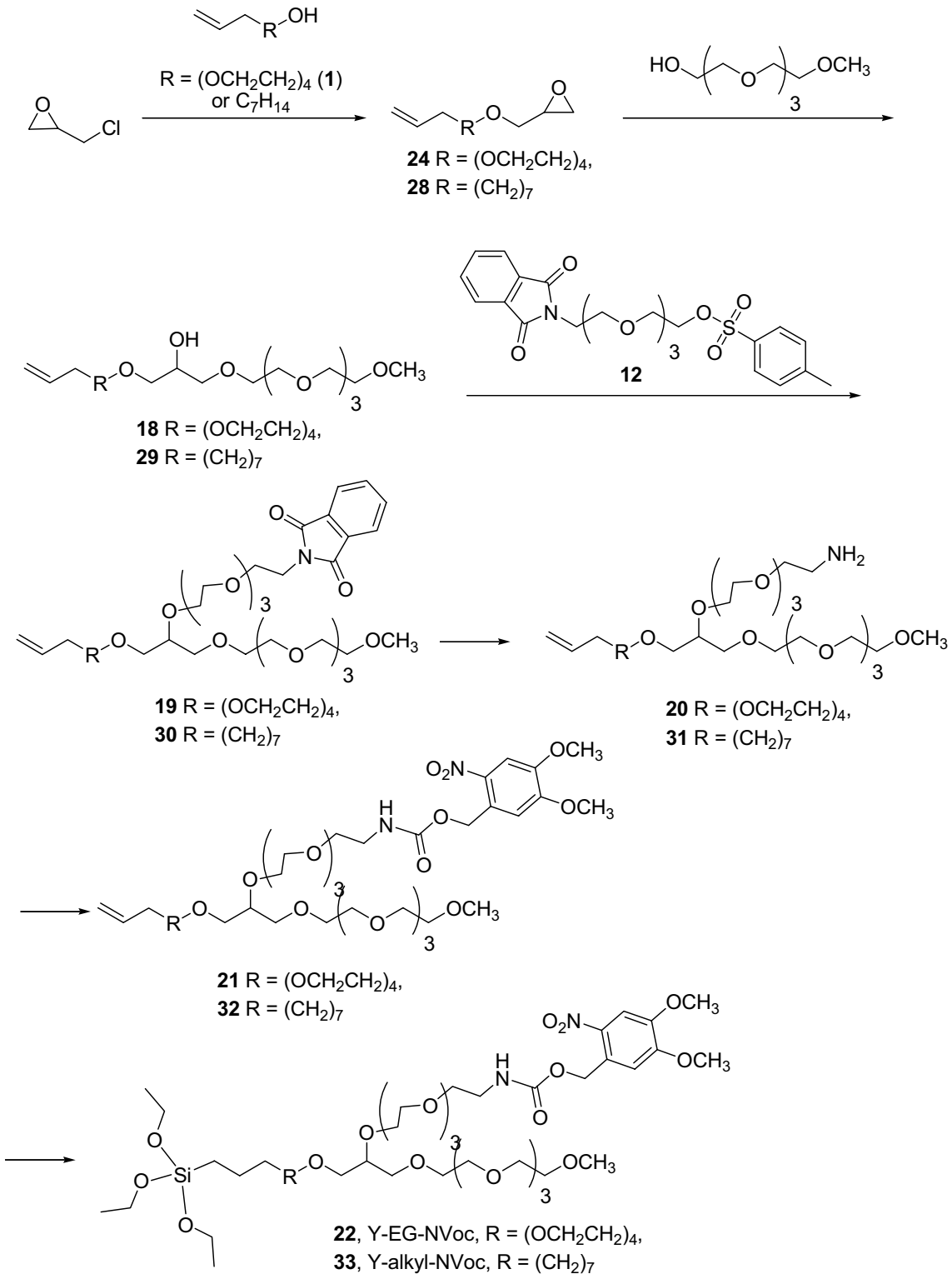

Figure 3.10: Synthetic route using epichlorhydrin as linker molecule.

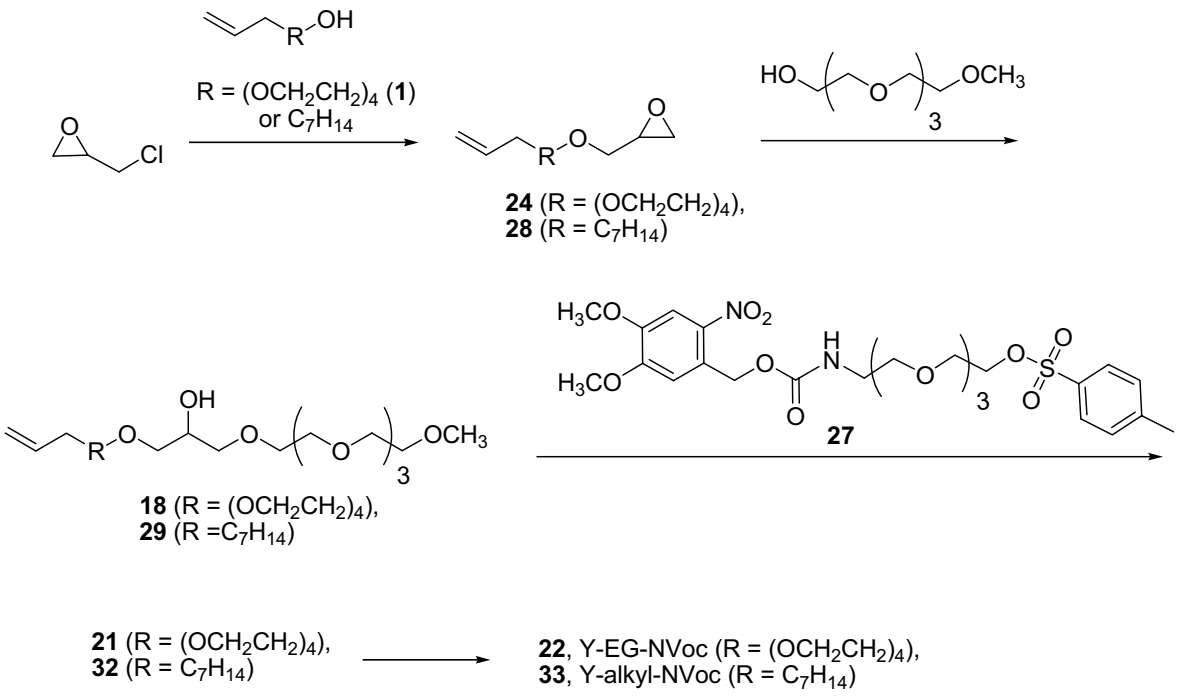

Figure 3.11: Synthetic path with NVoc-containing arm coupled to the linker.

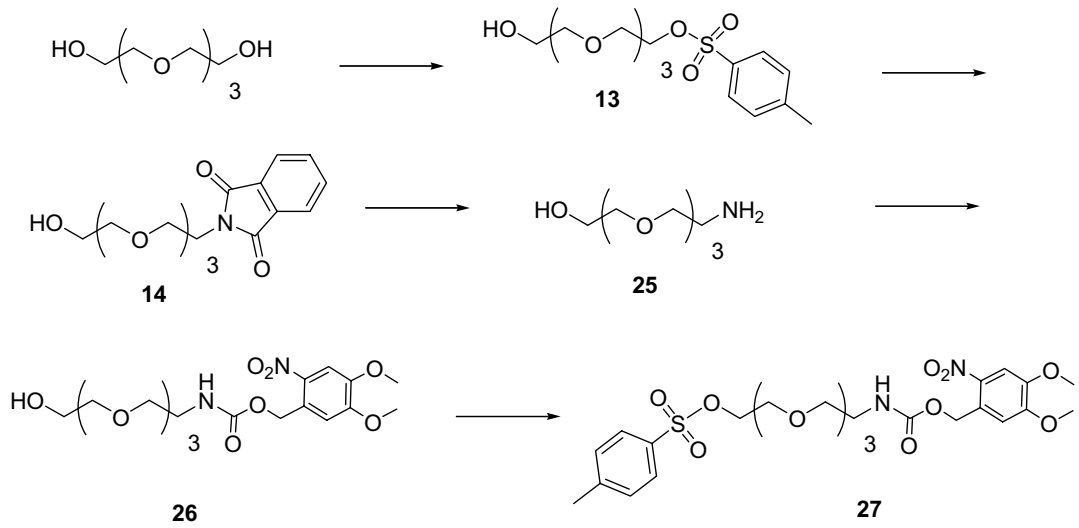

Figure 3.12: Synthesis of NVoc-containing arm.

3.4 Experimental

Synthesis

The detailed synthetic procedure of compounds **1** to **33** following Routes I to III is described in Appendix A.2.1.

Surface modification of silica surfaces

Silanization of the substrates with silanes Y-EG-NVoc and Y-alkyl-NVoc was performed in THF solution using catalytic amounts of 1N NaOH and 1% (w/V) silane concentration. After a certain prehydrolysis time during which triethoxysilanes hydrolyse to silanols, Piranha-cleaned substrates were immersed in the silane solution for a given time. Silanization conditions (reaction time and catalyst concentration) were optimized in order to obtain maximum and homogeneous surface coverage. Once the surface reaction is completed, the substrates were rinsed to remove physisorbed molecules and baked in an oven for increasing the crosslinking degree with the surface and improving the stability of the layer.

Characterization of the surface layers

The surface modification process was monitored by UV spectroscopy on quartz substrates by detecting the absorption bands of the chromophore. With this method, it was possible to identify the optimal silanization time (maximum absorption) for each silane. Static water contact angles were used to determine the changes in the hydrophilicity of the surface reflecting the presence of the silanes. The layer thickness was determined by ellipsometry (the refractive index was assumed to be 1.4571 in the deposited layers in a three phase model silicon substrate/ silica+organic layer/ air). Surface loadings $\Delta\Gamma$, in terms of molecs mm^{-2} were estimated from the ellipsometric thickness assuming a refractive index of 1.4571 for the silane layer, a typical density ρ of 1.0 g cm^{-3} for an organic layer with a refractive index *n* of 1.43, and an increment $dn/d\rho$ of 0.24 g cm^{-3}.[43, 139]

Irradiation of the substrates for photodeprotection

Activation of the surface functionality by photocleavage of the NVoc group was carried out using a Xe-lamp coupled to a monochromator. The deprotection was monitored by the decay in the UV-vis spectrum (as a consequence of the cleavage of the chromophore). The minimum irradiation time for full deprotection was obtained from different experiments at various irradiation times.

For laterally structured deprotection, quartz slides with chrome patterned fields containing 10 μm micrometric stripes spaced by 50 μm were placed on top of the substrate during irradiation. Additional details are given in the Appendix sections A.2.3 and A.2.4.

Protein binding studies

Protected and irradiated surface layers were tested in their ability to immobilize proteins. For this purpose, two different protein binding experiments were performed: (i) Bovine serum albumina (BSA) was covalently immobilized onto amine surfaces *via* glutaraldehyde coupling, (ii) Streptavidin was immobilized onto amine surfaces *via* molecular recognition of biotin units previously coupled to the surface *via* (+)-biotinyl N-hydroxysuccinimidyl ester. Protein immobilization was label-free monitored and quantified in real time using reflectance interference spectroscopy (RIFS). This technique detects binding on the surface of a thin silica interference layer (see section 2.3 in Chapter 2).[140] Control experiments to test the specificity of the binding event were performed in parallel.

Fluorescent labelling with dyes

The presence of free surface amine groups generated in the photolytic process was verified by fluorescence staining of patterned substrates using Alexa Fluor® 647 carboxylic acid succinimidyl ester. Amine coupling with the succinimidyl ester results in the formation of an amide bond between the fluorophore and the surface. Coupling conditions can be found in A.2.4.

Oligonucleotide, protein, antibody and cell patterns

The ability of masked irradiated surfaces for effective site-selective and functional immobilization of biomolecules and cells was tested in four different experiments:

(i) ONDs patterns were obtained by first covalently immobilizing an amino-terminated single stranded OND with 25 thymine units (NH_2-C6-5'-dT_{25}-3') *via* glutaraldehyde coupling, and subsequent hybrid capture of its fluorescein labeled complementary strand (f-5'-dA_{25}-3'). The resultant fluorescent pattern was visualized under the fluorescent microscope.

(ii) Antibody patterns were obtained by covalently immobilizing IgGs *via* glutaraldehyde coupling to masked irradiated substrates. Incubation of these patterns with the fluorescent antibody allows visualization of the pattern if the recognition process takes place selectively.

(iii) Streptavidin patterns were obtained by incubating substrates with streptavidin after masked irradiation and biotinylation. The streptavidin pattern was visualized by fluorescence microscopy after capturing fluorescein labeled biotin to unoccupied biotin binding sites of the immobilized streptavidin.

(iv) Cell patterns were obtained by coupling RGD motifs to the activated amine groups via glutaraldehyde linker, and subsequent incubating the RGD patterned substrates with NIH/ 3T3 fibroblasts.

3.5 Results

3.5.1 Synthesis

Route I

Initially, the synthesis of the three different arms **2**, **4** and **6** was attempted. The synthesis of **2** starts with the reaction of TEG with allyl chloride in basic medium to obtain compound **1**. This compound is common for all the formulated routes and was obtained using two different experimental conditions. In a phase transfer (PT) reaction with equimolar amounts of TEG and allyl chloride (Figure 3.13, way A), a mixture of non reacted TEG, monoallyl ether **1** in 39% yield, and diallyl ether in 19% yield was obtained. In an attempt to reduce the amount of disubstituted product, the etherification reaction was carried out in TEG as solvent (Figure 3.13, way B).[131] In these conditions, the yield of **1** was increased up to 65%. However, separation of **1** from the large excess of TEG appeared to be an important drawback of this method. Purification by distillation failed due to the formation of azeotropic mixtures. Chromatographic purification worked but required large columns due to the large amount of TEG present in the reaction crude. Consequently, method A was preferred. Tosylation of **1** afforded pure tetraethyleneglycol monoallylether *p*-toluene sulfonate **(2)** in 90% yield.

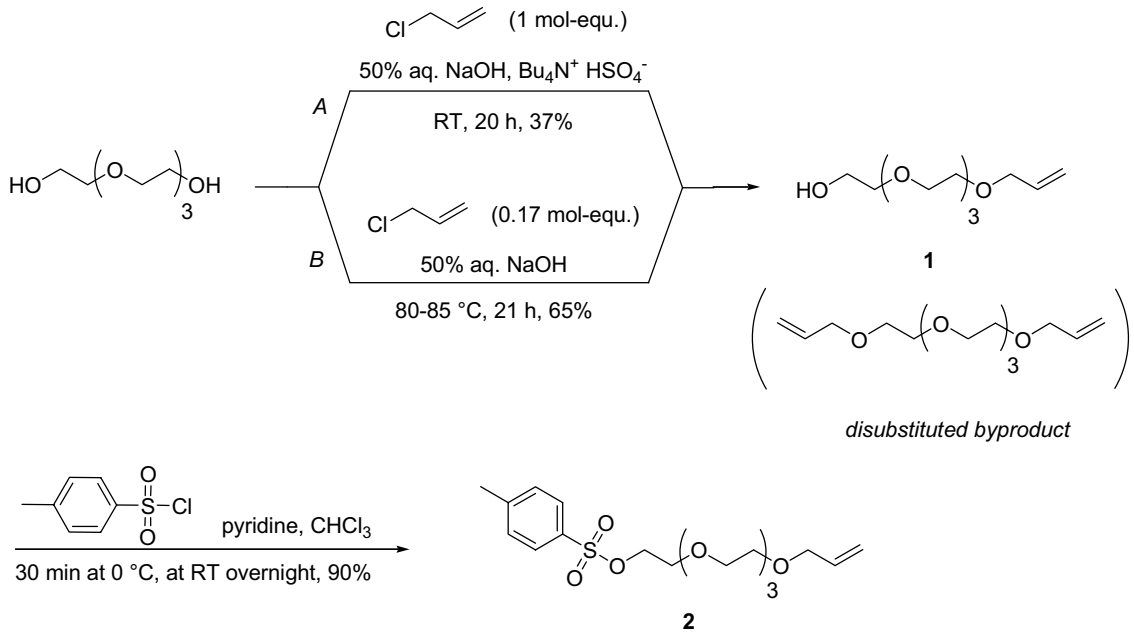

Figure 3.13: Synthesis of tetraethyleneglycol monoallylether *p*-toluene sulfonate (**2**).

The synthesis of the arm **4** (Figure 3.14) starts by protecting one TEG hydroxyl group as tetrahydropyranyl (THP) ether using a strongly acidic cationic exchanger resin as catalyst (Amberlist H-15). Compound **3** could be isolated in a yield of 26% from a mixture of unreacted TEG and di-THP ether. In an effort to reduce the amount of disubstituted product and improve the yield of the reaction, an alternative procedure using TsOH-H_2O as catalyst and large excess of TEG was tested but did not proved to be any better.[141] Tosylation of **3** afforded tetraethylene glycol monotetrahydropyranyl ether *p*-toluene sulfonate (**4**) in a yield of 57% after purification.[131]

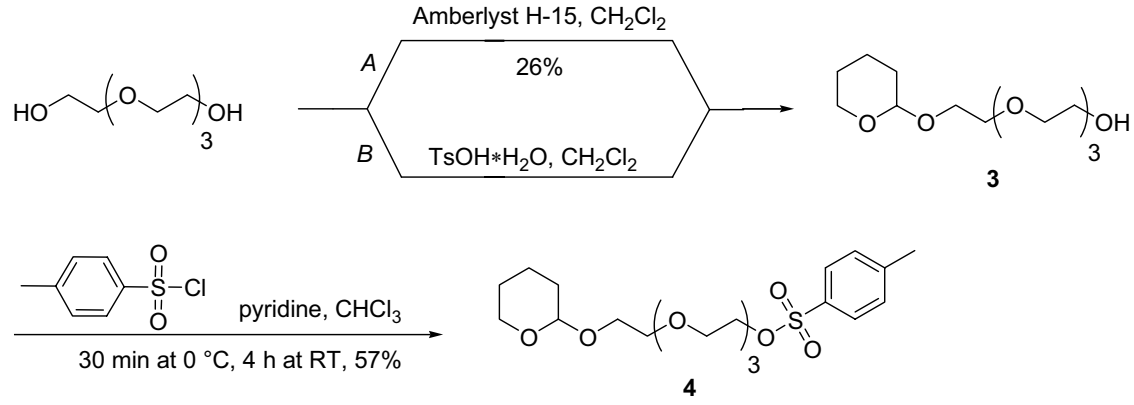

Figure 3.14: Synthesis of **4**.

The synthesis of the third arm (**6)** was performed as described in literature (Figure 3.15). Dibromated TEG, **5**, was first obtained in a yield of 54% and converted to the monophthalimide derivative **6** in a Gabriel reaction.[142] Following the published synthetic protocol,[143] the reaction was performed in DMSO at room temperature for 10 days using 0.5 mol equivalents of phthalimide and potassium carbonate. Despite the long reaction times, the reaction does not proceed to completion and compound **6** could only be obtained purified in a yield of 54%. In an effort to reduce the reaction time and to improve the reaction yield, other reaction conditions were tested. Higher reaction temperatures in either DMF or DMSO resulted in a loss of the tosyl group, and **6** could be obtained purified only in yields varying from 0% to 37%. The use of potassium phthalimide instead of its *in-situ* preparation from phthalimide and potassium carbonate did not affect the reaction yield either. ^{1}H NMR analysis of the reaction mixture revealed loss of the reactants. Intramolecular cyclation reactions may occur.

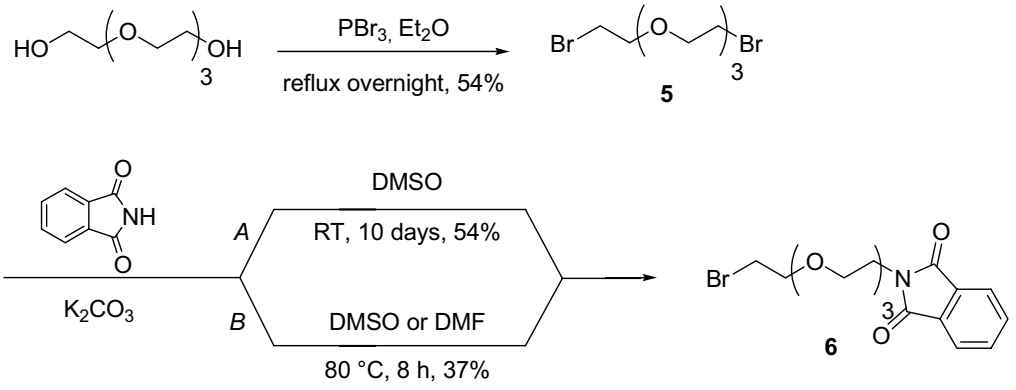

Figure 3.15: Preparation of Brom-tetraethyleneglycol phthalimide (**6**)**.**

Once the three arms were synthesized, the attachment to the linker was attempted. Reaction of **2** with benzyloxy-propanediol under Williamson etherification conditions using sodium hydride as deprotonating agent afforded **7** (Figure 3.16). ^{1}H NMR analysis indicated complete consumption of **2**. Twofold column chromatography was required to isolate **7** in a yield of 31% from the starting material benzyloxy-propanediol also present in the reaction mixture. ^{1}H NMR analysis proves selective attachment to the primary alcohol (position of the signals attributed to the tertiary carbon at 3.81-3.91 ppm). Attachment of the second arm, **4**, to the secondary hydroxyl group of the linker **7** was performed under similar conditions. The reaction did not proceed to

completion, presumably due to the lower reactivity of the secondary hydroxyl group. Reactants and products appeared to have similar and rather low R_f values, even when using very polar eluents, presumably because of the strong interaction of TEG and hydroxyl groups with the silica surface masking the polarity differences due to the different chain lengths or terminal groups. In fact, only a 1:1 mixture of **8** and starting compound **7** could be gained after chromatographic separation.

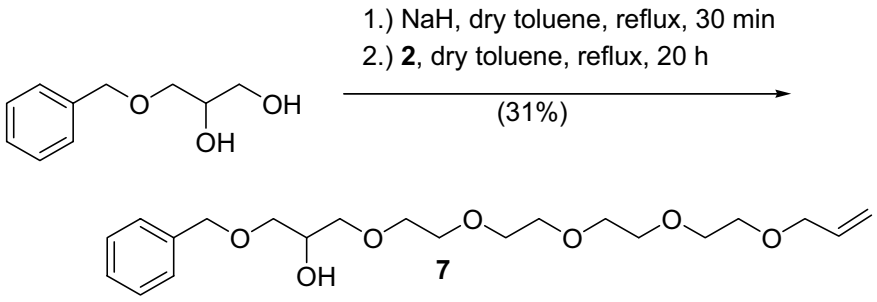

Figure 3.16: Synthesis of **7**.

The 1:1 mixture of **7** and **8** was used to test the deprotection of the benzyl ether (Figure 3.17).[144] ^{1}H NMR analysis of the reaction mixture indicated formation of a new product, but the signals corresponding to the benzyl ether were still visible. The signals corresponding to the THP-ether could not be found in the spectrum, indicating undesired deprotection of the primary end-group. Several products were visible on the TLC plate and were chromatographic isolated and characterized by ^{1}H NMR. None of them corresponded to the expected compound **9**.

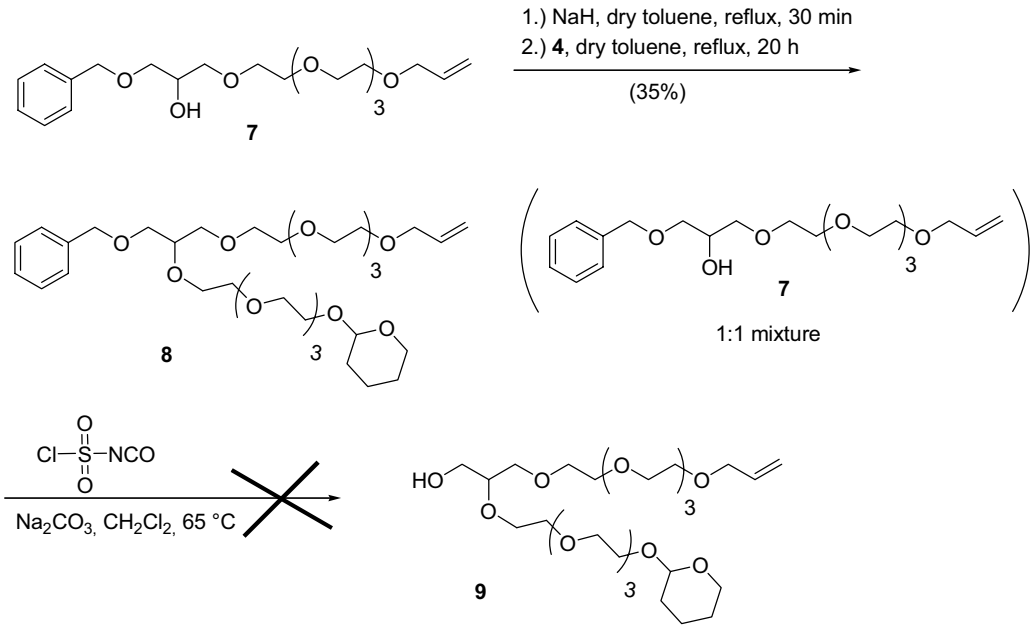

Figure 3.17: Attempted synthesis of **9**.

In view of the difficulties associated with the separation and deprotection steps, this route was not further prosecuted.

Route II

Two new arms, **10** and **12**, were previously prepared to be attached to the solketal linker. The synthesis of **10** only requires tosylation of the commercial TEG monomethyl ether (Figure 3.18) which could be obtained pure in a yield of 92%.

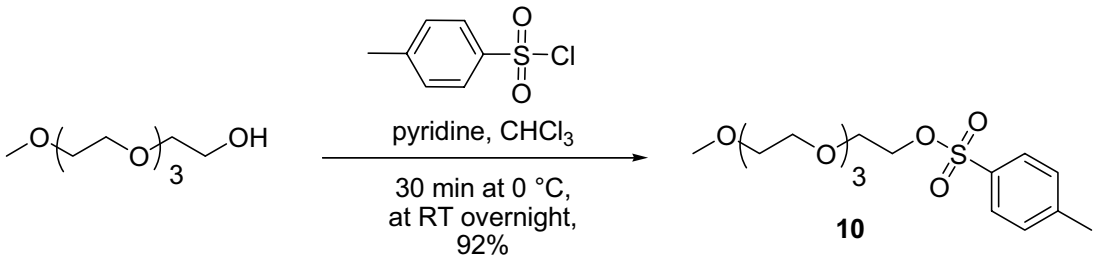

Figure 3.18: Synthesis of tetraethyleneglycol monomethylether *p*-toluene sulfonate (**11**)**.**

Compound **12** (tosyl derivative) is analogous to compound **6** (bromine derivative), and was first obtained using a similar synthetic path (Figure 3.19, way A). The hydroxyl groups of TEG were tosylated to obtain **11** in 63% yield. Conversion to the

monophthalimide **12** only succeeded when using mild reaction conditions and long reaction times, as already observed in the synthesis of compound **6**. Higher reaction temperature to speed up the reaction always caused a complete loss of the tosyl group, supposedly through internal cyclization.

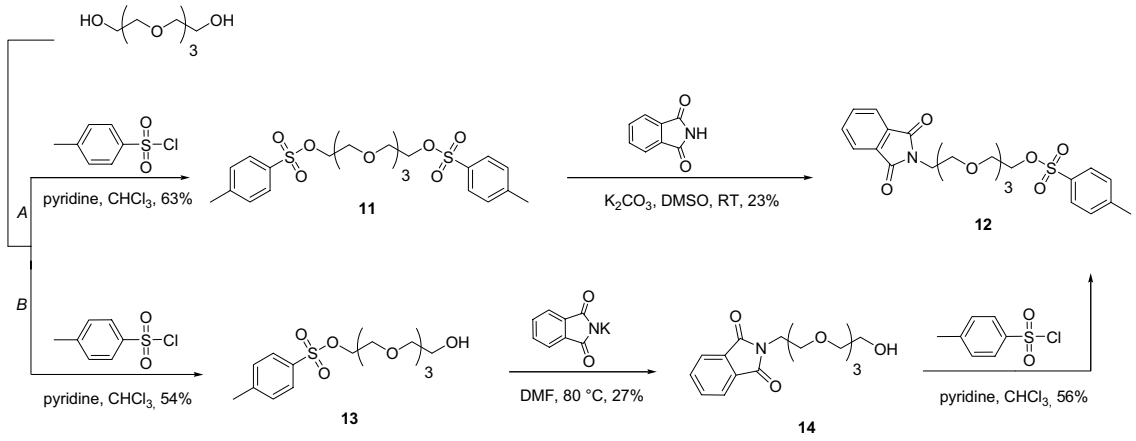

Figure 3.19: Synthesis of **12** in two different ways.

A second method was attempted in order to reduce the reaction times and increase the yield (Figure 3.19, way B). It starts with the heterofunctionalization of TEG to form the mono-tosyl derivative **13** which could be obtained purified in a yield of 54%.[145] Conversion of **13** to the respective phthalimide derivative **14** could be performed at higher temperatures and shorter reaction times than the conversion of **11** to **12** and a yield of 27% was obtained. Tosylation of the remaining hydroxyl group afforded **12** in 56% yield. Overall, this reaction path does not entail significant improvement over the previous one in terms of actual yield, time, consumption of solvents and costs. Thus, there is no preference regarding the two alternative ways. Method A was followed.

Attachment of the different arms to the linker starts by reaction of the arm **2** with solketal under Williamson etherification conditions using KOH in boiling toluene, analogues a similar reaction described in literature[134] (Figure 3.20). The desired product **15** was obtained only in traces. Better yields, up to 63%, were obtained using sodium as deprotonation agent and solketal as solvent.

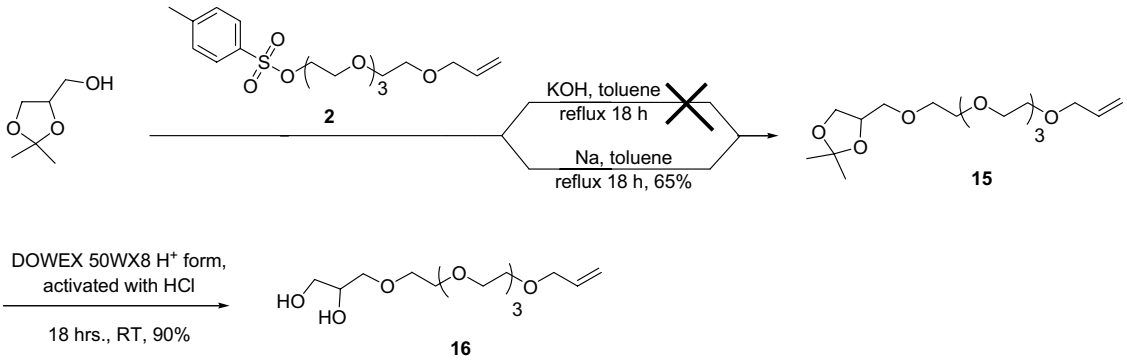

Figure 3.20: Synthesis of **16**.

In order to identify the best conditions for opening the ketal group in **15**, the reactivity of solketal in different acidic media was previously tested. The conditions used and obtained results in terms of glycerol formation are presented in Table 3-1. Complete cleavage of the isoproyliden group could be observed when using *p*-toluenesulfonylic acid[137] and acidified DOWEX 50WX8 (either in H^+ or Na^+ form previously activated with sodium hydrochloride).[146] The latter method was selected for the synthesis of **16**. The reaction occurred cleanly and in a yield of 90%. Purification by column chromatography yielded the diol **16** in 73% yield.

Table 3-1: Summarized results for the removal of the isopropyliden protecting group of soleketal under different conditions.

	catalyst	solvent	temperature	pH	crude product	
					solketal	glycerol
A	$TosOH \cdot H_2O$	MeOH	RT	2-3		✓
B	Amberlyst H-15	THF	RT	7	✓	✓
C	DOWEX 50WX8 Na^+ form	THF/ H_2O (5:3)	35 °C	7	✓	
D	DOWEX 50WX8 H^+ form	THF/ H_2O (5:3)	35 °C	6		✓
E	DOWEX 50WX8 Na^+ form, previously activated by washing with 1N HCl	THF/ H_2O (5:3)	35 °C	3		✓

RT: Room Temperature

The attachment of a second arm to **16** is expected to occur preferentially through the primary hydroxyl group. First, attachment of compound **6** was tried using sodium as deprotonating agent. TLC analysis of the crude product showed disappearance of the reagents and the formation of many side products. An attempted isolation of the products by column chromatography was not successful. Identification of the desired product **17** by integration of the ^{1}H NMR signals of the reaction crude was not possible because of overlapping of the significant signals with other molecular peaks (Figure 3.21a).

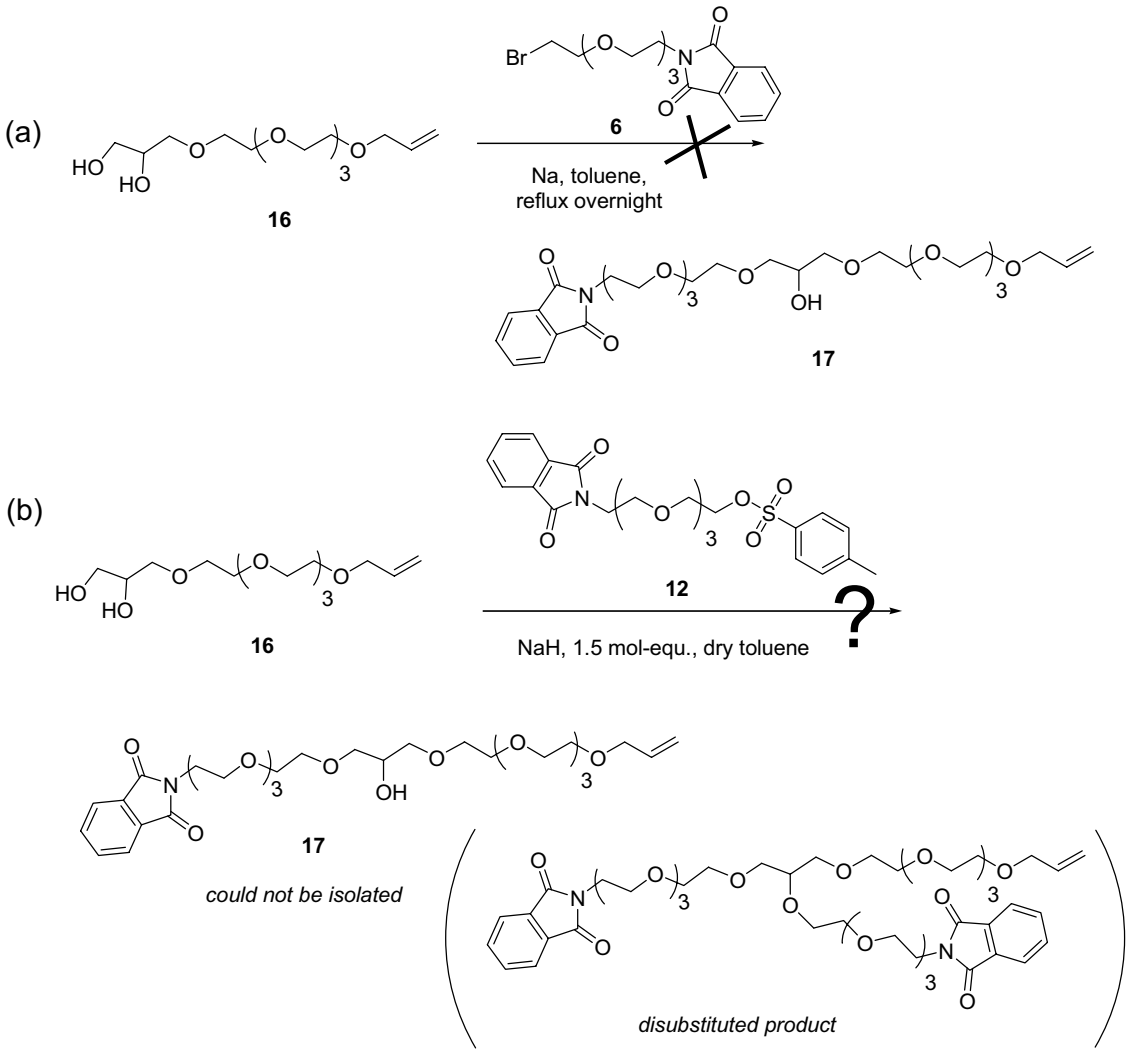

Figure 3.21: Attempted conversions of **16** to **17**.

Attachment of the arm **12** to the diol **16** using sodium hydride rendered a mixture of the two reactants and two new products, according to TLC analysis (Figure 3.21b). Isolation of the two new products by column chromatography on silica was not successful due to strong tallowing of both compounds. ^{1}H NMR spectroscopic analysis of the mixed fractions proved the presence of the mono- and di-substituted compounds**.**

Finally, the arm **10** was reacted with the diol **16** in order to see if the separation of the possible reaction products is easier than with the arm **12** (Figure 3.22). Analysis of the reaction mixture by TLC indicated the presence of more than one reaction product. ^{1}H NMR spectroscopy did not give clear information about the chemical nature of the products and chromatographic separation did not succeed either. In view of these results, this route was not followed any further.

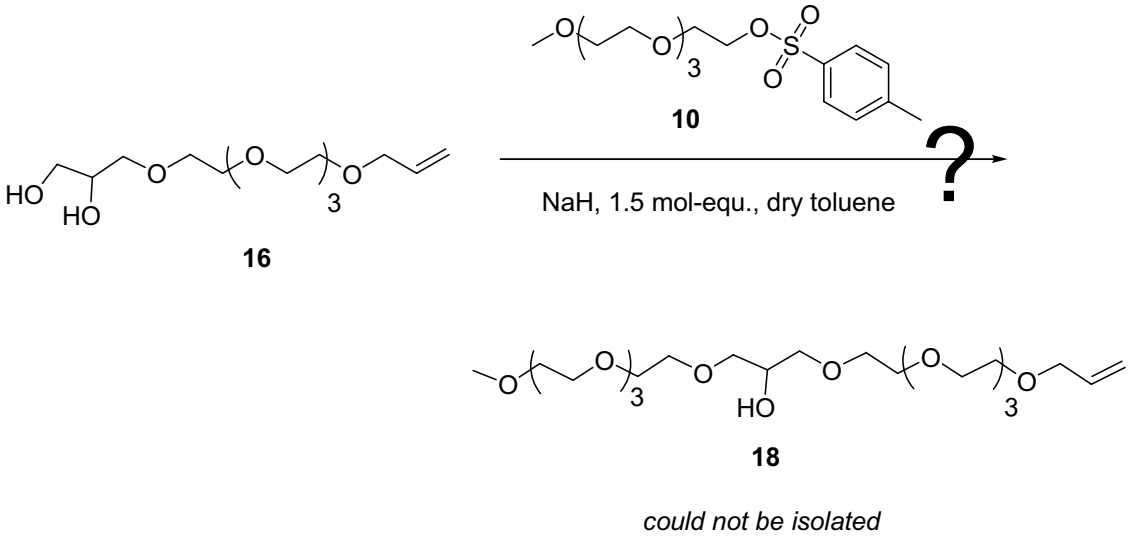

Figure 3.22: Attempted conversion of **16** to **18** in a Williamson ether synthesis with **10**.

Route III

The arms **1** and **12** were obtained as described before and tetraethylenglycol monomethoxyether is commercially available. Attachment of **1** to epichlorhydrin in basic medium worked in ~60% yield (Figure 3.23).[147] Purification of **24** from the remaining mixture of **1** and epichlorhydrin could be done by distillation, but long times and several passages were required to isolate **24** in 30 % yield. Alternatively, purification was performed by column chromatography and **24** was obtained purified in a yield of 29%. The best results could be obtained by a combination of both methods. Removal of first epichlorhydrin by distillation (70-100 °C, 3×10^{-3} mbar) and then **1** by column chromatography yielded pure **24** in a yield of 54%.

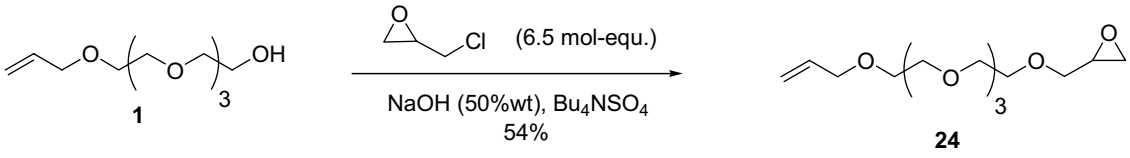

Figure 3.23: Synthesis of **24**.

Coupling tetraethylenglycol monomethoxy ether to **24** by nucleophilic ring opening of the epoxy group was done in the presence of catalytic amounts of NaH in THF and excess of the alcohol (Figure 3.24).[138] The reaction was followed by ^{1}H NMR spectroscopy. After complete disappearance of **24**, the excess of tetraethyleneglycol monomethoxy ether was removed by distillation. ^{1}H and ^{13}C NMR spectroscopic analysis of the remaining crude confirmed that only the desired product **18** was present. The absence of **16** was confirmed by GC-MS spectrometry. Compound **18** was then used in the next reaction without further purification in order to avoid unnecessary loss of product.

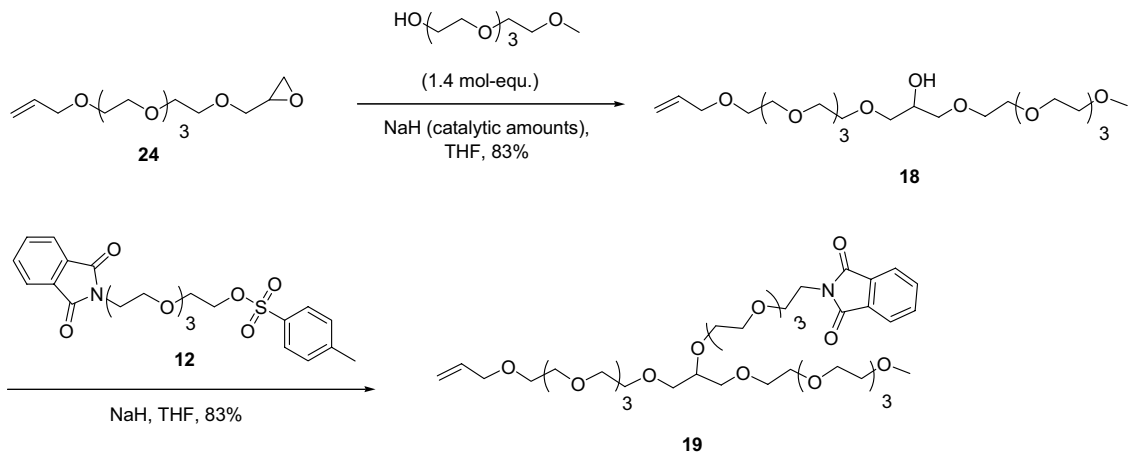

Figure 3.24: Synthesis of **19** by nucleophilic ring opening of the epoxy group in **24** to **18**, followed by attachment of **12**.

Attachment of the third arm (**12**) to the secondary hydroxyl group of **18** was performed using equimolar amounts of the reactants and sodium hydride in THF under reflux (Figure 3.24). The use of NaH in excess is detrimental and leads to loss of the phthalimide groups in this process. After work-up in aqueous medium and removal of short chain molecules (hydrolyzed **12**) by distillation, the crude product was identified as **19** in a yield of 83% by ^{1}H and ^{13}C spectroscopy and used without further purification in the next step.

Conversion of the phthalimide group in **19** to the free amine in **20** by hydrazinolyzation (Ing-Manske procedure) worked quantitatively according to NMR analysis of the reaction mixture (Figure 3.25). The excess of hydrazine was removed by distillation and **20** was used in the next step without further purification. In some cases the reduced compound was also formed (in yields up to 25%). Attachment of the NVoc group to the free amine in **20** was achieved by reaction of **20** with commercial 6-nitroveratryloxycarbonyl chloride under Schotten-Baumann conditions. Chromatographic purification of the reaction mixture afforded the desired carbamate **21** in 69% yield. A small fraction (< 10%) of the reduced compound **23** was also present after purification.

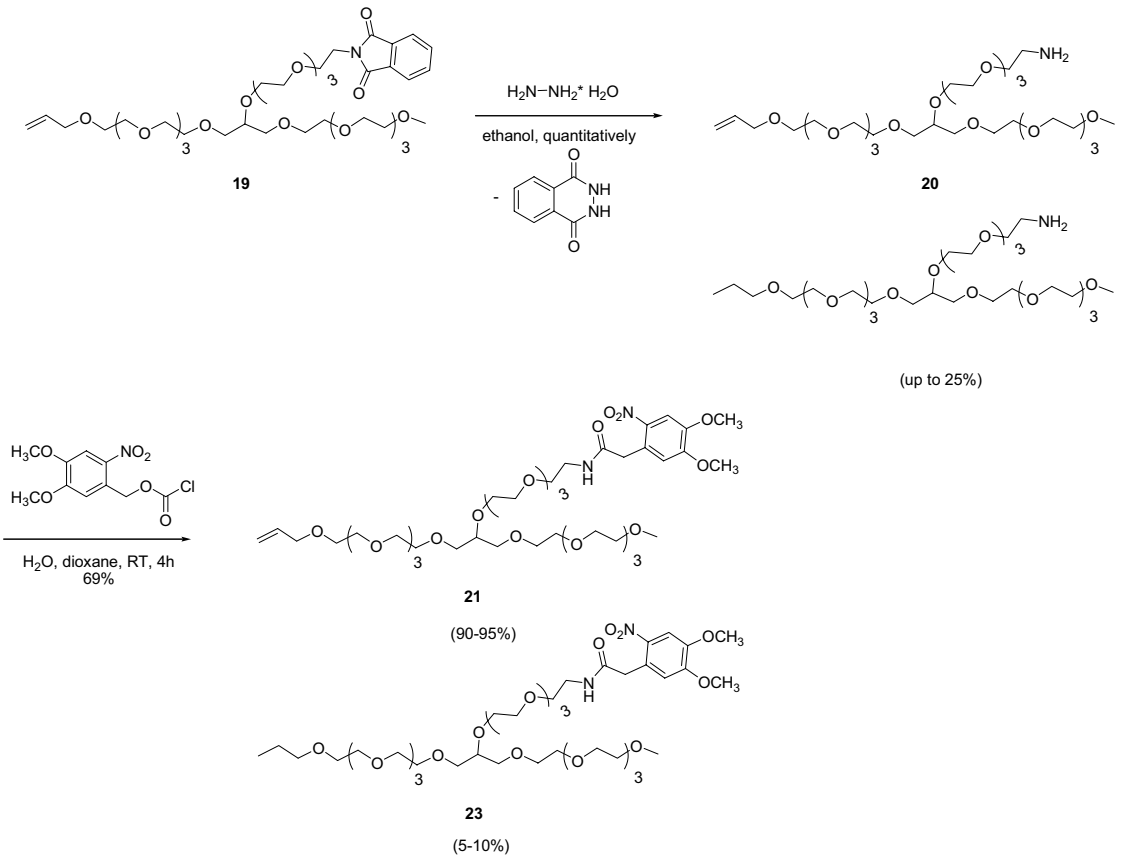

Figure 3.25: Conversion of **19** to **21** by reaction with hydrazine monohydrate (Ing-Manske procedure), followed by reaction with 6-nitroveratryloxycarbonyl chloride to a 95:5 mixture of **21** and the reduced compound **23**.

The last step of this synthetic route was the hydrosilylation of the double bond in **21** to obtain the triethoxysilane derivative **22**. The progress of the reaction was followed by performing ^{1}H NMR spectroscopic analysis of aliquots extracted after different reaction times. After 4 hours reaction at 80 °C, **21** was consumed completely, acccording to the disappearance of the ^{1}H NMR signals attributed to the allylic bond (around 5.50 ppm and 5.22 ppm) and the appearance of two new multiplets around 0.62 and 1.70 ppm, attributed to the methylene groups attached to the Si atom of **22**. The intensity of the signals at 0.9 ppm and 1.59 ppm, already present in the previous reaction step and attributed to the methyl group and the neighboring methylene group of the reduced side-product **23**, increased. The crude product was purified by column chromatography on passivated silica gel in order to avoid severe loss of the triethoxysilane derivative **22** in the column by reaction with the free silanol groups at the surface of the silica gel. Passivation of the silica gel was performed by reaction with hexamethyldisilazane

(HMDS), prior to packing of the column.[148] The hydroxyl groups are thus partially converted to hydrophobic methyl groups which are not longer able to react with **22**. Compound **22** was obtained in a mixture with the reduced compound **23** in a molar ratio of 0.7 as determined by ^{1}H NMR spectroscopy (Figure 3.26).

The purity of the starting allylic compound **21** is an important prerequisite for a successful hydrosilylation reaction. Traces of unreacted amine **20**, or of NVoc-OH coming from the hydrolysis of the NVoc carbamate may lead to catalyst contamination and inhibit the hydrosilylation reaction. The amount of Speier catalyst used and the reaction time and temperature need also to be optimized in order to reduce the amount of side-product **23**.

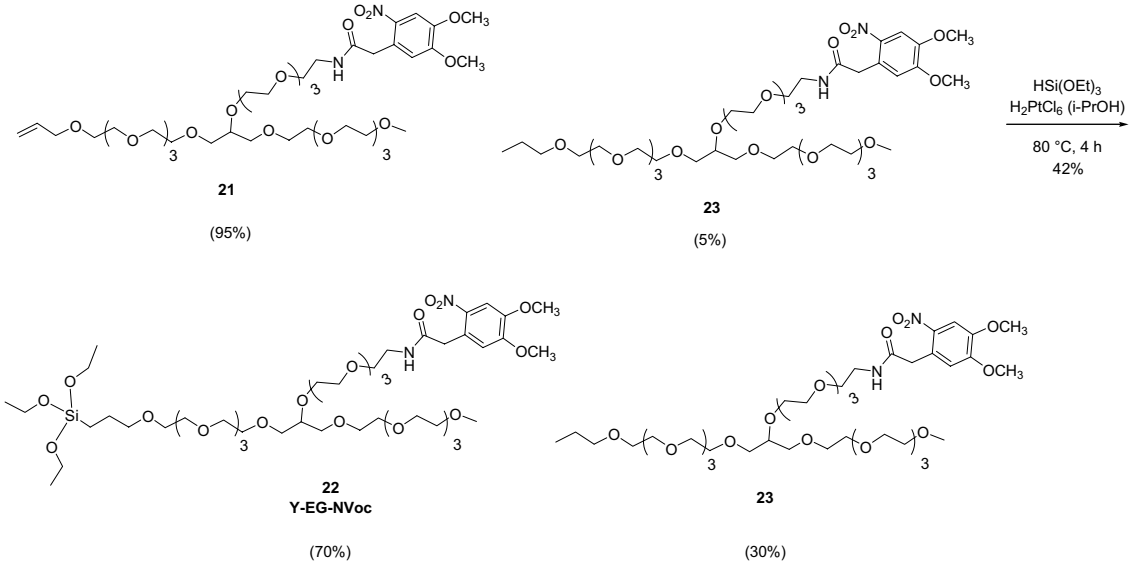

Figure 3.26: Hydrosilylation of **23** with triethoxysilane, catalyzed by hexachlorplatinic acid (Speier's catalysator).

An alternative approach to obtain **20** was tried in which the NVoc group was attached to the arm **18** before linking it to the rest of the molecule. The synthesis of the new arm **27** involved quantitative hydrazinolyzation of the phthalimide derivative **14** to the free amine **25**, followed by reaction with 6-nitroveratryloxycarbonyl chloride to give the desired carbamate **26** purified in a yield of 79%. Tosylation of the second hydroxyl group gave **27** purified in a yield of 88% (Figure 3.27). Attachment of **27** to **19** under Williamson etherification conditions failed because of hydrolysis of the carbamate bond

and consequent loss of the NVoc group. This synthetic path was therefore neglected.

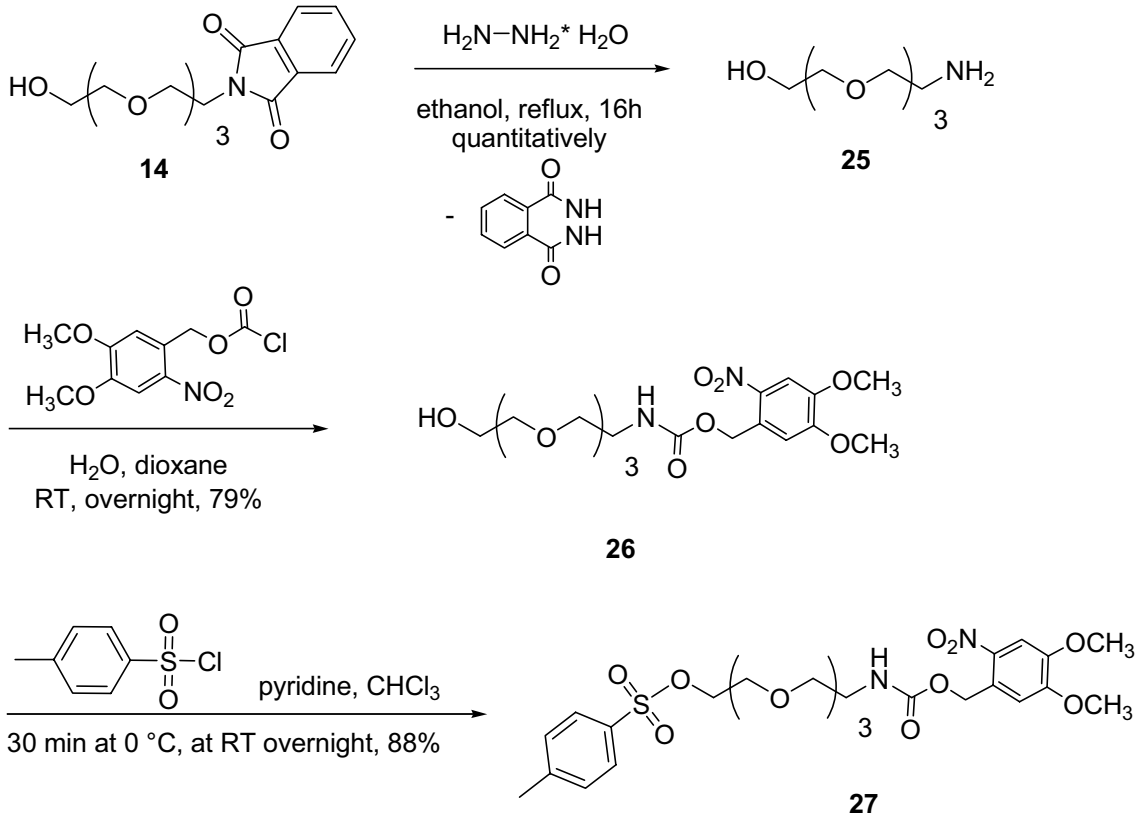

Figure 3.27: Synthesis of **27**.

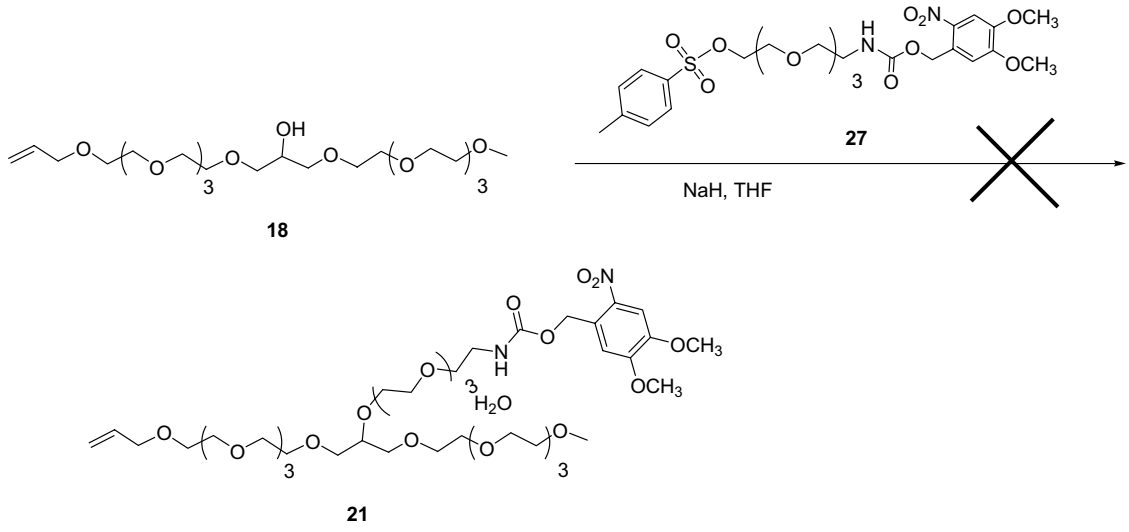

Figure 3.28: Attempted conversion of **18** to **21** by reaction with the directly NVoc-functionalized compound **27** in a Williamson ether synthesis.

Finally, the synthesis of Y-alkyl-NVoc (**33**) was achieved following a similar synthetic path for the successful synthesis of **22**, as illustrated in Figure 3.29. Commercial 9-decen-1-ol was used as alkyl arm which was attached to epichlorhydrin to yield **28** in 68%. The second arm, commercial tetraethyleneglycol monomethylether, was attached and the product **29** was isolated by distillation in 50% yield. Attachment of the third arm, **12**, yielded **30** in 80%. Reduction to the free amine **31** occurred quantitatively and further reaction with 6-nitroveratryloxycarbonyl chloride yielded the carbamate **32** chromatographically purified in a yield of 48% (as 70% mixture with **33**). Hydrosilylation yielded a mixture of desired silane **33** and reduced compound **34** in 0.6 molar ratio. As observed in the synthesis of **22**, chromatographic separation of **33** from **34** was not possible and only a filtration step through Celite 500 was carried out in order to remove catalyst residues.

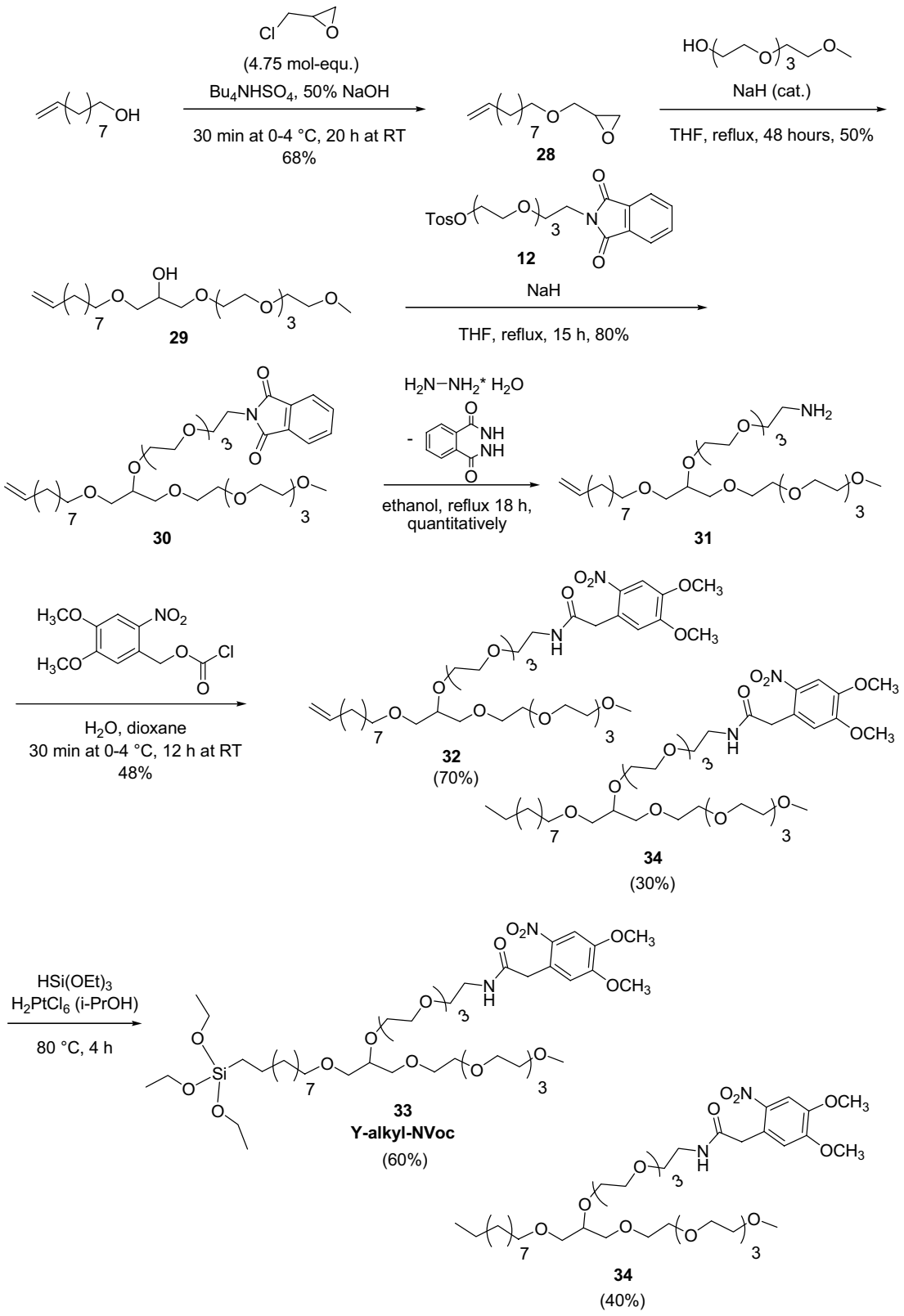

Figure 3.29: Synthesis of **33**.

3.5.2 Surface modification and characterization

Surface layers of Y-EG-NVoc and Y-alkyl-NVoc were obtained on silica surfaces by silanization in solution. Anchoring to the silica surface requires previous hydrolysis of the alkoxy groups to generate the reactive silanol species which will then bind covalenty to the silanols at the surface. The conditions for the prehydrolysis need to be carefully selected in order to avoid extensive crosslinking reactions of the tri-silanols in solution, which can lead to the formation of aggregates in solution and end in substantial surface roughness. The progression of these reactions and consequently the characteristics of the final surface layer critically depend on experimental variables such as type of solvent, temperature, and reaction time, as well as on the catalyst and the concentration of the organosilane.[149-153] According to literatue silanization in THF catalytic amounts of NaOH affords dense and smooth surface layer. Similar conditions were used and further optimized for our compounds. For this purpose, the course and extent of the surface modification reaction was followed by ellipsometry and UV/vis spectroscopy and the silanization conditions were varied to maximize the layer thickness and UV/vis absorption values.

The UV spectra of substrates modified with the photosensitive silanes Y-EG-NVoc and Y-alkyl-NVoc are shown in Figure 3.30. The spectra agree with those obtained in solution and show absorption maxima, λ_{max}, at 355 nm.

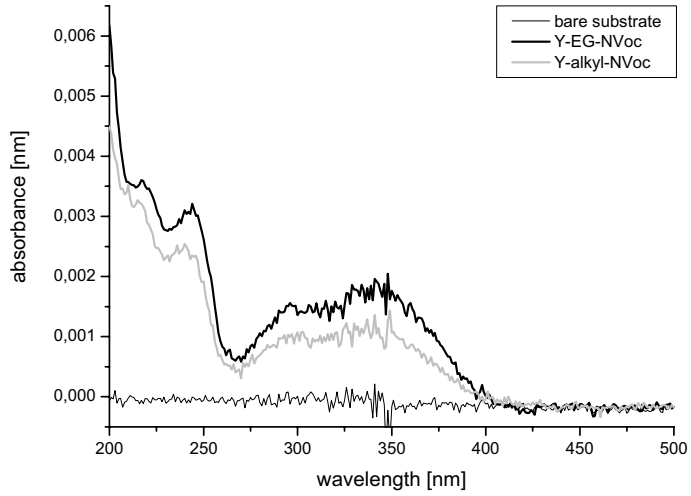

Figure 3.30: UV absorbance spectra of a quartz substrate modified with Y-EG-NVoc (▬) or Y-alkyl-NVoc (▬).

Substrates obtained in the optimized conditions revealed formation of layers with a maximum thickness of 2.2 and 1.2 nm and static water contact angles of 51 and 63° for silanes Y-EG-NVoc and Y-alkyl-NVoc respectively (Table 3-2). Under the same surface modification conditions, the reaction time for maximizing the layer thickness was longer for Y-EG-NVoc than for Y-alkyl-NVoc. This means that Y-alkyl-NVoc shows higher affinity for the surface than Y-EG-NVoc. However, the maximum thickness achieved in Y-alkyl-NVoc layers is significantly smaller than the maximum thickness of Y-EG-NVoc layers. In both cases, the layer thickness is smaller than the molecular length (4.8 and 4.2 nm respectively) and corresponds to the formation of submonolayers. Assuming a refractive index of 1.4571 for the silane layer, the layer density can be estimated[43, 139] (a typical density ρ of 1.0 g cm^{-3} is assumed for an organic layer with a refractive index n of 1.43, and an increment $dn/d\rho$ of 0.24 g cm^{-3}). From a layer density value of 1.113 g cm^{-3} and the experimental layer thickness, the molar surface loading $\Delta\Gamma$ and surface coverage were estimated. Notably higher surface density was obtained from Y-EG-NVoc layers than from Y-alkyl-NVoc, in agreement with the UV spectra and measured layer thicknesses (Table 3-2).

Table 3-2: Data from UV spectroscopy, ellipsometry and contact angle measurement for substrates obtained under optimized silanization conditions. The molar surface loading and surface coverage were calculated from the experimental layer thickness. All given errors correspond to the standard deviation obtained from measurements of different samples obtained under the same conditions.

Surface modification	Layer thickness, [nm]	Water contact angle, [°]	molar surface loading ΔΓ, [ng mm^{-2}]	Surface coverage, [molecs mm^{-2}]
Y-EG-NVoc	2.2±0.8	51±5	2.4±1	1.6×10^{12}
Y-alkyl-NVoc	1.4±0.3	63±5	1.6±0.5	1.1×10^{12}
EG-NVoc*	2.65±0.11	57±2	2.95	3.2×10^{12}
Mixed layers EG-NVoc and EG-OMe (1:1)*	2.00±0.95	52±2	2.26	3.3×10^{12} (only half are NH_2)

*Data from[154]

These data can be compared with those published for layers obtained with the linear silane EG-NVoc and for a 1:1 molar ratio mixture of silanes EG-NVoc and EG-OMe (Figure 3.31). It seems that the shorter and linear TEG spacer allows the formation of more compact layers.

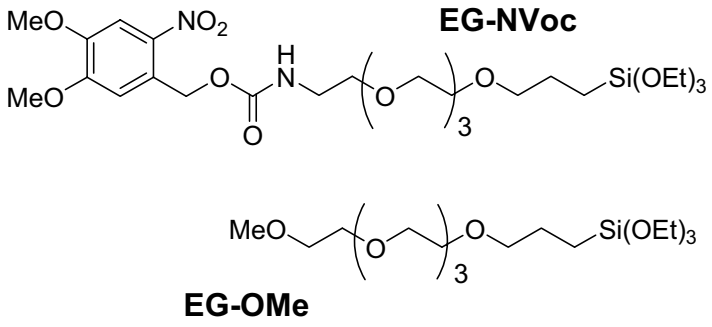

Figure 3.31: Silanes EG-NVoc and EG-OMe.

3.5.3 Photolytic experiments

Light of a wavelength equal to λ_{max} was used in the irradiation experiments for cleaving the NVoc group in order to have maximum sensitivity and minimum irradiation time. Light cleaves the NVoc group *via* an intramolecular redox reaction and liberates the reactive amine group at the surface (Figure 3.32).

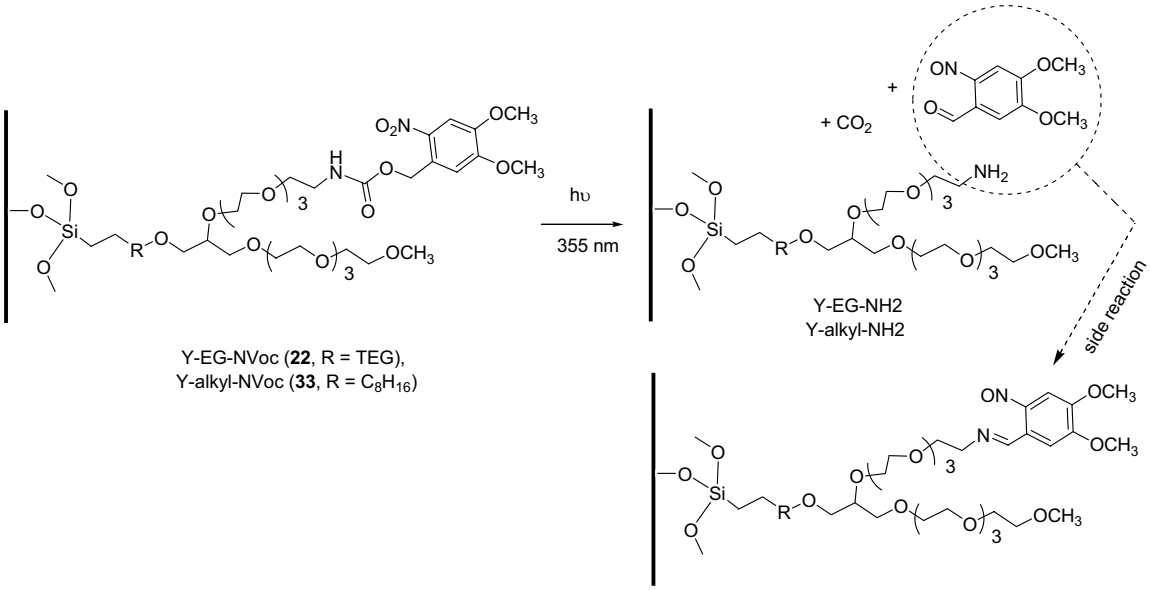

Figure 3.32: Photochemical deprotection reaction on the surface yielding free amine groups. A possible side reaction after photodeprotection is the reaction between the benzaldehyde-photofragment and the generated primary amino group at the surface, yielding an imine.

The photolytic reaction can be followed by the decay of the UV absorbance of the substrate after washing because the chromophore is lost. Figure 3.33a shows the UV spectra of a substrate modified with Y-EG-NVoc after different irradiation times. The absorbance dropped 50–60 % after irradiation for 10 minutes, but it did not decrease further with longer irradiation times (Figure 3.33b). This is presumably due to imine formation between the benzaldehyde photofragment and the primary amino group at the surface (Figure 3.32). This side reaction reattaches the chromophore to the surface, causing a residual absorbance and decreasing the final density of amine groups.[87] The photolytic reaction also reduces the water contact angle of the surface by ca. 2°, indicating the liberation of the more polar amine group. The ellipsometric thickness also decreased in > 0.5 nm after irradiation as a consequence of the loss of the chromophore from the surface.

No significant differences in sensitivity are expected between silanes Y-EG-NVoc and Y-alkyl-NVoc. Therefore, substrates modified with these silanes were always irradiated at 355 nm for 10 min to achieve maximum deprotection.

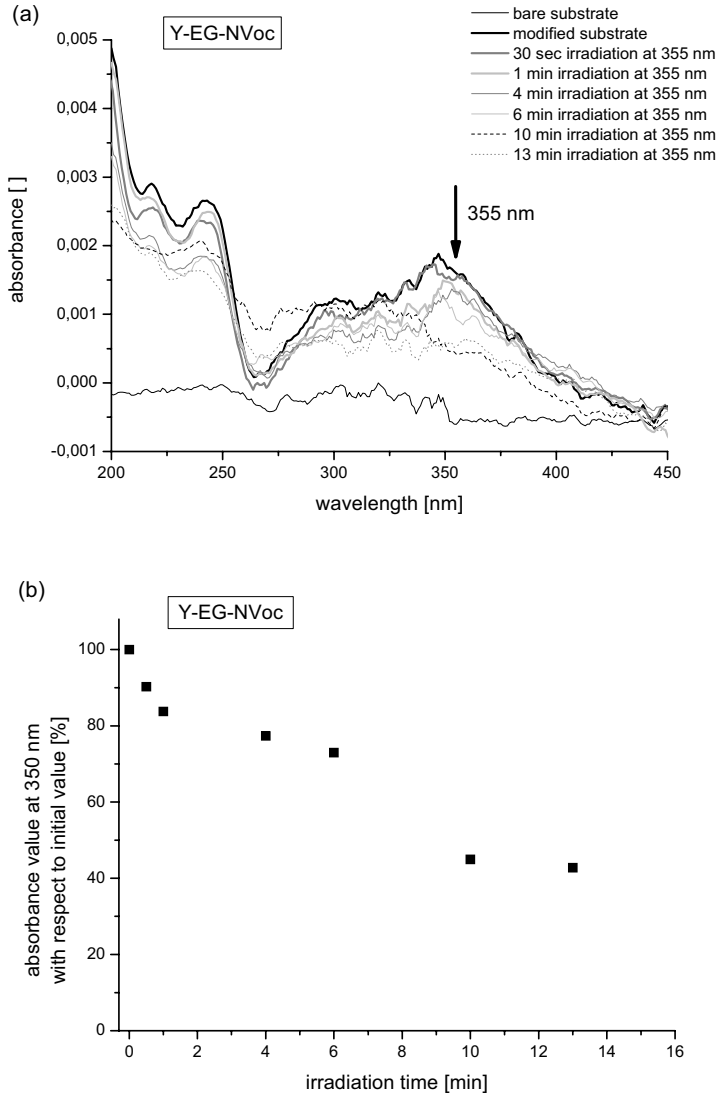

Figure 3.33: Irradiation of Y-EG-NVoc at 355 nm. (a) UV/ vis spectra of Y-EG-NVoc modified quartz substrates, taken after different irradiation times, (b) relative absorbance in the maximum versus irradiation time.

3.5.4 Protein binding to functional surfaces

Substrates modified with silanes Y-EG-NVoc and Y-alkyl-NVoc were tested in their ability to selective and functional immobilize proteins. Protein binding events were monitored in real time using label-free detection by reflectance interference spectroscopy (RIFS).[155] This technique detects binding on the surface of a thin silica interference layer. Binding curves were obtained from the shift of the interference spectrum.

Initially, experiments were performed to determine and quantify the degree of non-specific interaction between the branched silanes and a model protein. For this purpose, the adsorption of Bovine Serum Albumin (BSA) to substrates modified with Y-EG-NVoc and Y-alkyl-NVoc before and after irradiation was monitored by RIFS.

Figure 3.34 shows the results of the experiment. For comparison, data corresponding to adsorption of BSA onto bare silica surfaces, silica modified with aminopropylsilane, and silica modified with the linear silane EG-NH2 are also shown. Upon injection of the BSA solution, a clear increase in the optical layer thickness is observed onto all surfaces due to the adsorption of BSA onto the surface, until saturation is achieved. The bare silica surface shows the maximum adsorption of BSA, followed by surfaces modified with the silane EG-NVoc, aminopropylsilane and Y-alkyl-NVoc. Y-EG-NVoc shows the best results in terms of protein repellence (lowest adsorption) as a consequence of its longer EG chain and the absence of hydrophobic alkyl spacer. The linear and shorter silane EG-NVoc behaves significantly worse in avoiding protein sticking than the longer and branched analogues. Removal of the hydrophobic NVoc group by irradiation of the layer causes a general decrease in the adsorption values.

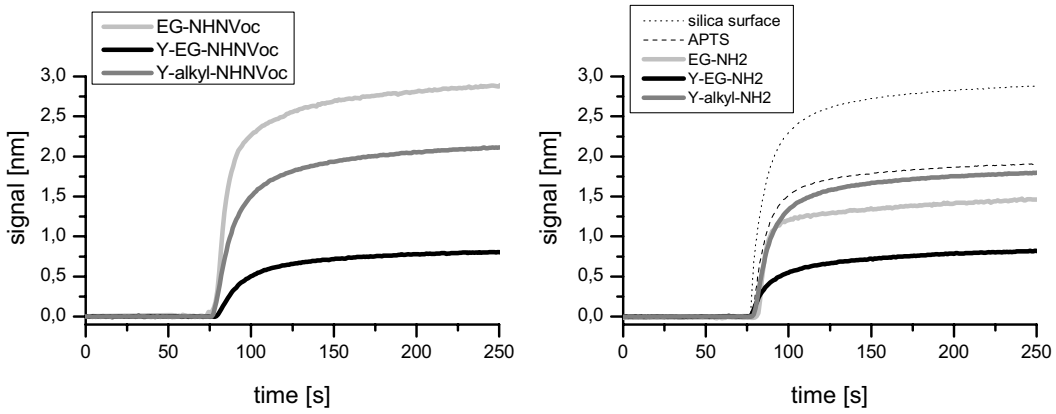

Figure 3.34: Adsorption of BSA onto different substrates as monitored by RIFS.

In a second experiment, we checked the ability of the substrates to specifically bind proteins through molecular recognition of immobilized receptors. Surfaces modified with the branched silanes Y-alkyl-NVoc and Y-EG-NVoc before and after irradiation were incubated with (+)-Biotin N-hydroxysuccinimidyl ester. The biotin units are expected to attach selectively to the free amine groups of the irradiated substrates (Figure 3.35) and capture streptavidin from solution in a subsequent step.

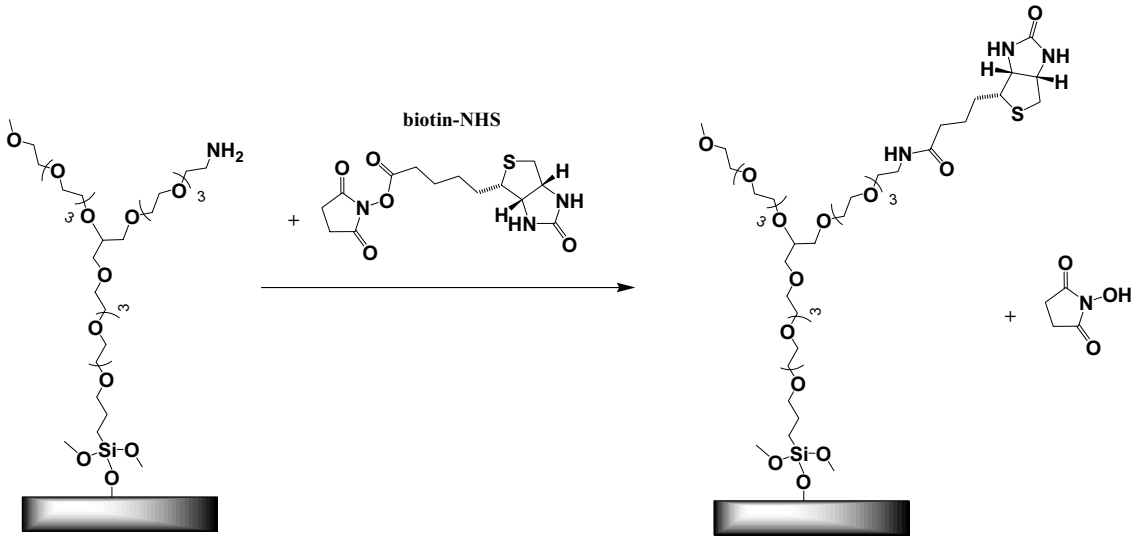

Figure 3.35: Immobilization of NHS-biotin onto irradiated surfaces (previously modified with Y-EG-NVoc).

Figure 3.36 shows the binding of streptavidin to the biotinylated surfaces. Negligible binding was observed onto the NVoc terminated silanes, indicating that the EG chains are able to hinder completely non-specific binding of the streptavidin protein to the surfaces. High degree of specific binding was observed onto Y-EG-NH2 layers and less binding onto the Y-alkyl-NH2 surface. This can be attributed to the larger density of functional groups obtained for Y-EG-NH2 layers (1.6×10^{12} *vs.* 1.1×10^{12} molecs mm^{-2} for Y-EG-NVoc and Y-alkyl-NVoc respectively, see Table 3-2) which allows coupling of a larger number of biotin units. For comparison, binding onto layers of the linear EG-NVoc and EG-NH2 silane are also shown. The amount of immobilized streptavidin onto EG-NH2 layers is less than onto Y-EG-NH2 surfaces, in spite of the higher packing density of Y-EG-NH2 layers, suggesting that the longer and branched EG chains afford better accessibility of the biotin groups for binding. This result is corroborated by comparing the higher binding values of Y-EG-NH2 with respect to mixed EG-NH2/ EG-OMe layers, with similar densities of active groups.

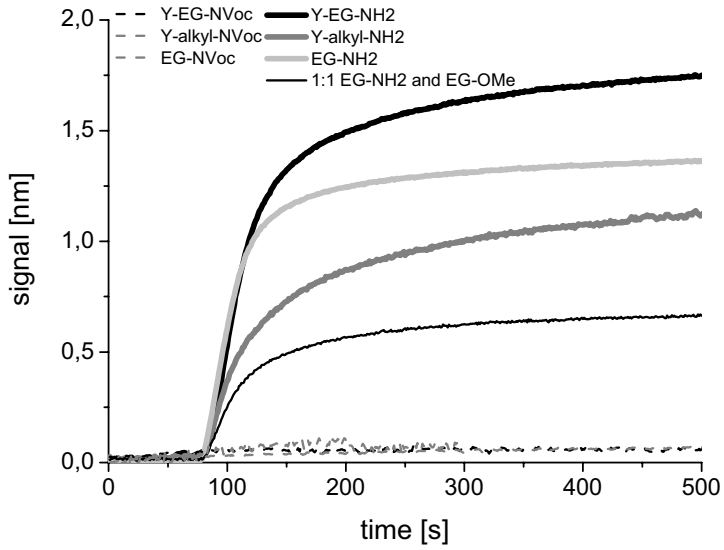

Figure 3.36: Immobilization of streptavidin on biotynilated surfaces.

3.5.5 OND and protein patterns

The capability to implement laterally patterned protein immobilization was tested by irradiating the substrates through a mask containing micrometric stripes. This process generates activated areas (those uncaged by irradiation), with the shape of the mask, which were subsequently reacted with different compounds.

First, the existence of free amine groups after deprotection was tested by reacting Alexa Fluor® 647 succinimidyl ester with the masked irradiated surfaces (50 µm chrome lines on quartz, separated by 10 µm). A clear pattern of fluorescent lines (10 µm) on a non-fluorescent background was visualized by fluorescence microscopy (Figure 3.37a) proving the success of the irradiation process and the presence of free amine groups on the irradiated regions.

In the second step, site selective immobilization of single-stranded (ss) ONDs and their ability to capture fluorescently labeled complementary strands was investigated. After masked irradiation (through quartz with deposited 50 µm wide chrome stripes, separated by 10 µm), the surface amino groups were reacted with ss-5'-$NH_2(CH_2)_6$-$_d$T25-3' *via* glutaraldehyde coupling. The resulting imine is reduced to an amine bond by reductive amination with $NaBH_3CN$. The surfaces are then used for hybrid capturing of the fluorescent-labeled complementary strand 5'-f_dA_{25}-3'. Under the fluorescence microscope, clear lines were observed in the expected pattern (10 µm wide lines, separated by 50 µm, Figure 3.37b), indicating successful hybridization. The low non-specific adsorption of the ONDs onto the non-irradiated areas of the substrates shows only week unwanted interactions between the ONDs as polyanionic chains and the protected surface.

The ability in spatial and functional protein immobilization was investigated by coupling of goat IgG to the masked irradiated surface, followed by uptake of the corresponding fluorescently labeled antigen, anti-goat IgG (developed in rabbit). Fluorescence microscopic analysis indicated the presence of anti-goat IgG in the irradiated regions (Figure 3.37c), thus verifying preservation of the biological functionality of goat IgG during immobilization to these regions.

In a last experiment, site selective immobilization of proteins was investigated by coupling NHS-biotin ester to the masked irradiated surface, followed by immobilization of streptavidin. The streptavidin pattern was visualized by fluorescence microscopy after capturing fluorescently labeled biotin to unoccupied biotin binding sites of the immobilized streptavidin (Figure 3.37d). Bright fluorescent stripes with a width of 10 µm were observed, confirming selective binding of fluorescent biotin to the irradiated (active) regions.

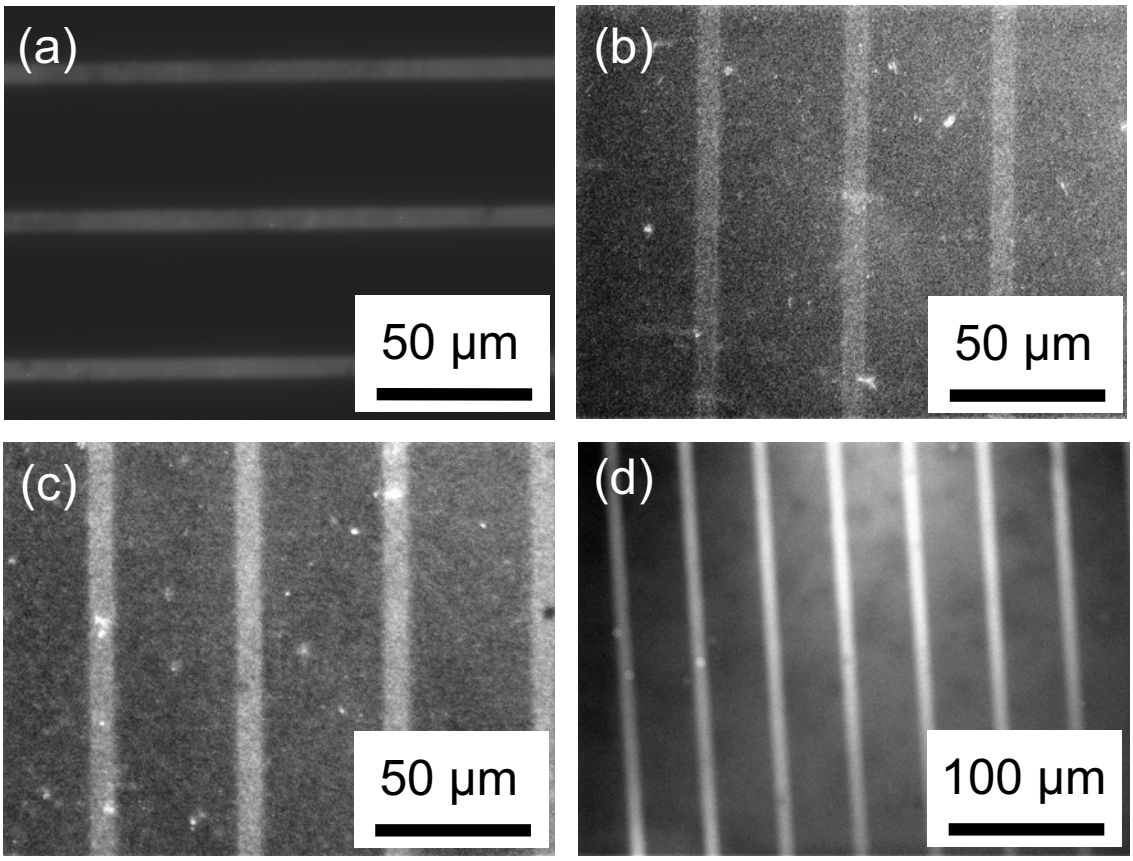

Figure 3.37: Fluorescence microscope images of Y-EG-NVoc modified substrates onto which different fluorescent-labeled dyes or biomolecules have been patterned. (a) Alexa Fluor® 647 (b) f-5'-dA_{25}-3' by hybrid capturing of previously immobilized ss-5'-$NH_2(CH_2)_6$-$_dT_{25}$-3', (c) FITC-labeled rabbit anit-goat IgG by specific interaction with previously immobilized goat IgG, (d) biotin-4-fluorescein by specific interaction with free binding sites of streptavidin previously immobilized by specific biotin-coupling.

3.5.6 Cell patterns

In view of the low non-specific absorption of proteins on Y-EG-NVoc layers, and the demonstrated possibility of selective and functional immobilize protein targets when functionalized with appropriate receptors, we tested the performance of these layers to specific recognize adhesion proteins at the cell membrane (integrins) via surface bound receptors (RGD peptide). If successful, this method could be used to generate micropatterns of cells at surfaces after masked irradiation and activation.

The cyclic peptide cyclo[RGDfK] is well known to promote cell adhesion *via* recognition of the binding site at the membrane protein integrin $\alpha v\beta_3$.[156, 157] A modification of this peptide that includes a 3-(4,5-dimethoxy-2-nitrophenyl)-2-butyl (DMNPB) photoremovable cage at the carboxylic group of the aspartic acid, cyclo[RG(DMNPB)-DfK], has been recently developed.[158] Figure 3.38 shows the chemical structure. Upon irradiation, the DMNPB group is removed and liberates active cyclo[RGDfK]. In its protected form, the caged peptide is not recognized by $\alpha v\beta_3$ integrins but, after light induced uncaging, integrins can bind and mediate cell adhesion.[158] We have used this peptide for our cell studies.*

* Access to cyclo[RG(DMNPB)-DfK] was possible *via* an on-going collaboration between the groups of Prof. Maurice Goeldner (University Strasbourg, France) and Dr. A. del Campo (MPI für Metallforschung, Stuttgart, Germany).

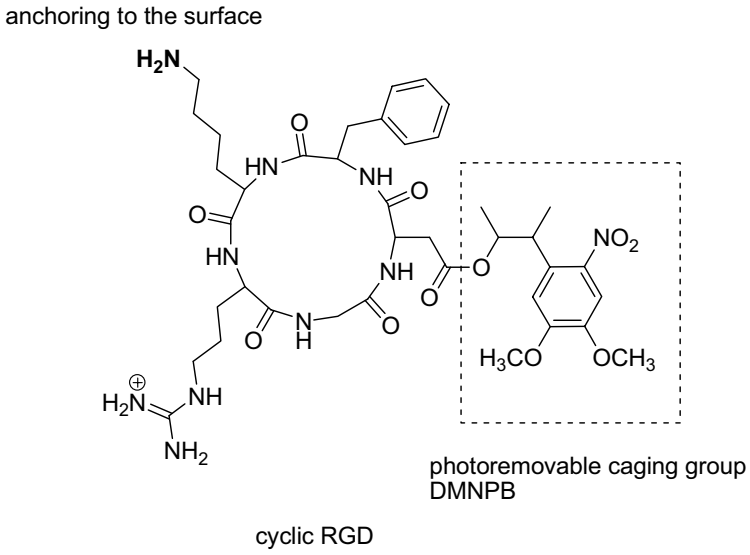

Figure 3.38: Structure of cyclo[RG(DMNPB)-DfK].[158] UV irradiation induces photochemical cleavage of the DMNPB group liberating cyclo[RGDfK].

We first tested the activity of the caged and uncaged cyclo[RG(DMNPB)-DfK] onto Y-EG-NVoc surfaces. For this purpose, we first coupled cyclo[RG(DMNPB)-DfK] to fully irradiated Y-EG-NH2 surfaces *via* a glutaraldehyde linker. Attachment of the peptide to the surface is expected to occur via the NH_2 side group of the Lys residue, although the guanidinium group of the arginine may also interfere. Masked irradiation of the cyclo[RG(DMNPB)-DfK] modified surfaces generated a pattern of free RGD and caged RGD areas. Fibroblasts were then platted onto the irradiated substrates and their attachment was followed by optical microscopy at different times (4 and 19 hours) after plating. The corresponding images are provided in Figure 3.39. Preferential adhesion of cells to the irradiated regions, where uncaged cyclo[RGDfK] was exposed, can be already observed after 4 hours. Longer incubation times increased the selectivity of the attachment, as seen in the images after 19 hours incubation. In fact, the ratio between cells adhered to cylco[RGDfK] containing regions and regions without active RGD was 3:1 after 4 hours after plating and increased to 18:1 after 19 hours plating. The absolute number of attached cells decreased, because the substrate was covered with medium after 4 hours, thus diluting the number of not adhered cells in solution.

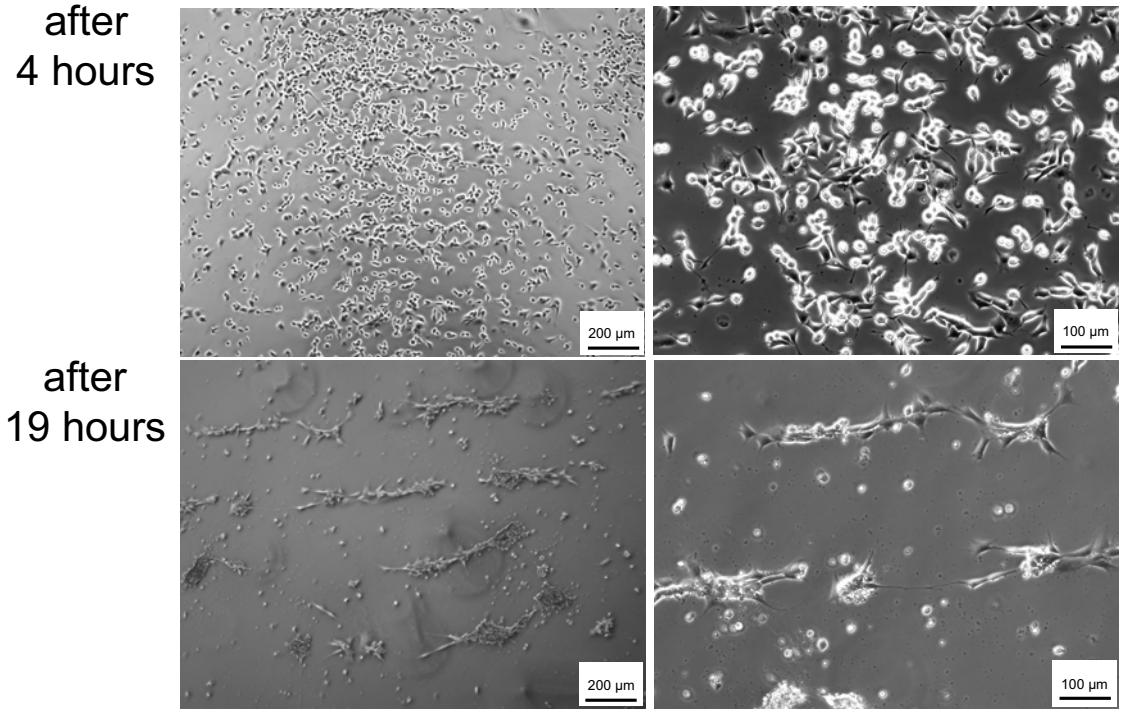

Figure 3.39: Microscopic image of fibroblasts plated on substrates modified with caged cyclo[RG(DMNPB)-DfK] and uncaged cyclo[RGDfK]. The mask consisted of 200 µm chrome stripes separated by 100 µm quartz stripes. Initial concentration of fibroblasts was 500 cells/ mm^2. Cells adhere and spread on the cyclo[RGDfK] areas and can be easily distinguished from those which are not attached (bright round vesicles).

In a second experiment, the non-specific attachment of cells onto Y-EG-NVoc and Y-EG-NH2 surfaces (without modification with the RGD peptide) was analyzed and results are shown in Figure 3.39, right side. Almost no cells adhered to the substrates, even after 21 hours of incubation time. No pattern was visible, indicating that the NVoc and NH2 terminated surface behave analogously with respect to cell attachment. The EG layer seems to maintain its protein repellence properties during the whole incubation time.

More complex patterns with coexisting regions with the four different chemistries were then created in a two-step irradiation process. Y-EG-NVoc modified substrates were first irradiated at 355 nm through a mask patterned with horizontal 200 µm wide chrome stripes separated by 100 µm gaps. Cyclo[RG(DMNPB)-DfK] was then coupled to the free amine groups generated at the irradiated regions. In a second irradiation step at 351 nm using a mask with vertical 200 µm wide chrome stripes, the DMNPB group of

the RGD motif is removed at the exposed regions. Since both caging groups, NVoc and DMNPB, are photolytically cleaved off upon irradiation at around 350 nm, the NVoc groups present in the exposed areas during the second irradiation step are also removed. After the second irradiation process, four microregions with different terminal chemistries are generated on the substrate (Figure 3.40): (I) Y-EG-NVoc; (II) Y-EG-NH2; (III) cyclo[RG(DMNPB)-DfK, and (IV) cyclo[RGDfK].

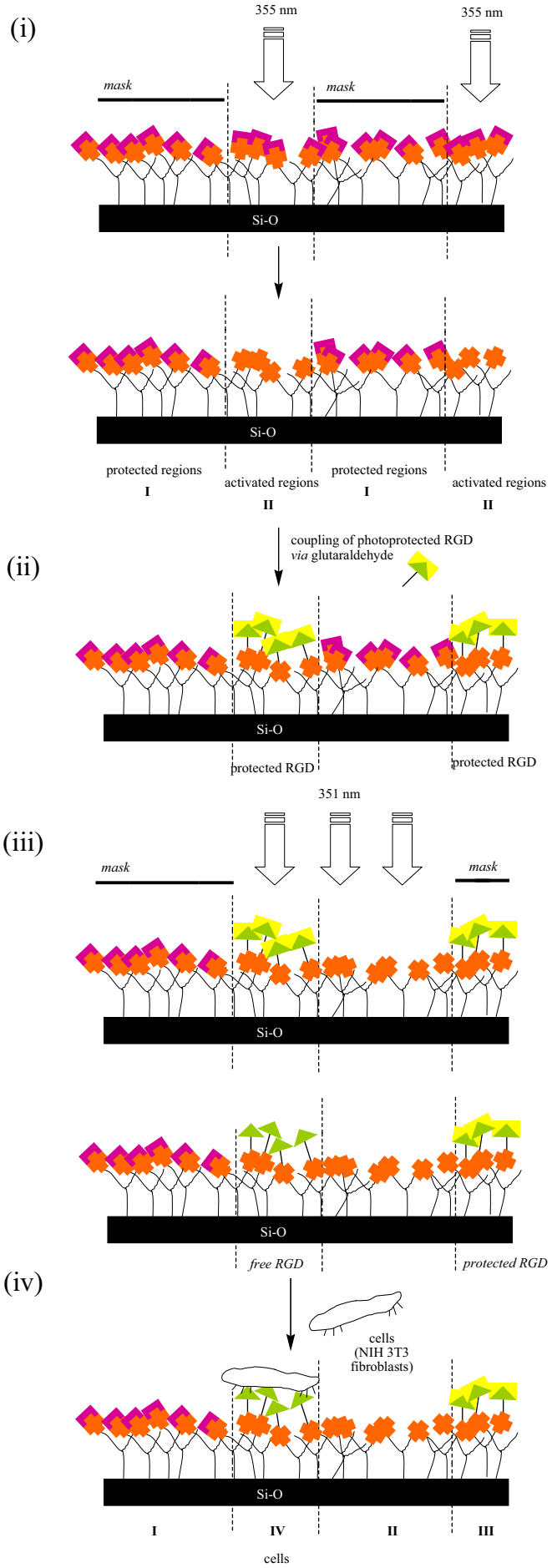

Figure 3.40 Schematic representation of cell adherence experiments. Surface patterning after two-step masked irradiation of Y-EG-NVoc modified substraes. (i) Masked deprotection of Y-EG-NVoc at 355 nm, (ii) Coupling of DMNPB-protected cyclo[RGDfK] to released amine groups, (iii) Masked deprotection of DMNPB at 351 nm, (iv) Attachment of cells. After this process, four regions with different chemistries have been defined at the surface.

Figure 3.41, left side, shows the adhesion of fibroblasts platted onto such substrates after incubation for 3, 6 and 21 hours. Cell attachment is only significant onto the 100 µm × 100 µm squares exposing uncaged cyclo[RGDfK] (IV), as expected. Images recorded 21 hours after plating revealed the highest selectivity (Figure 3.42). The density of attached cells agrees with the results obtained in the previous experiments.

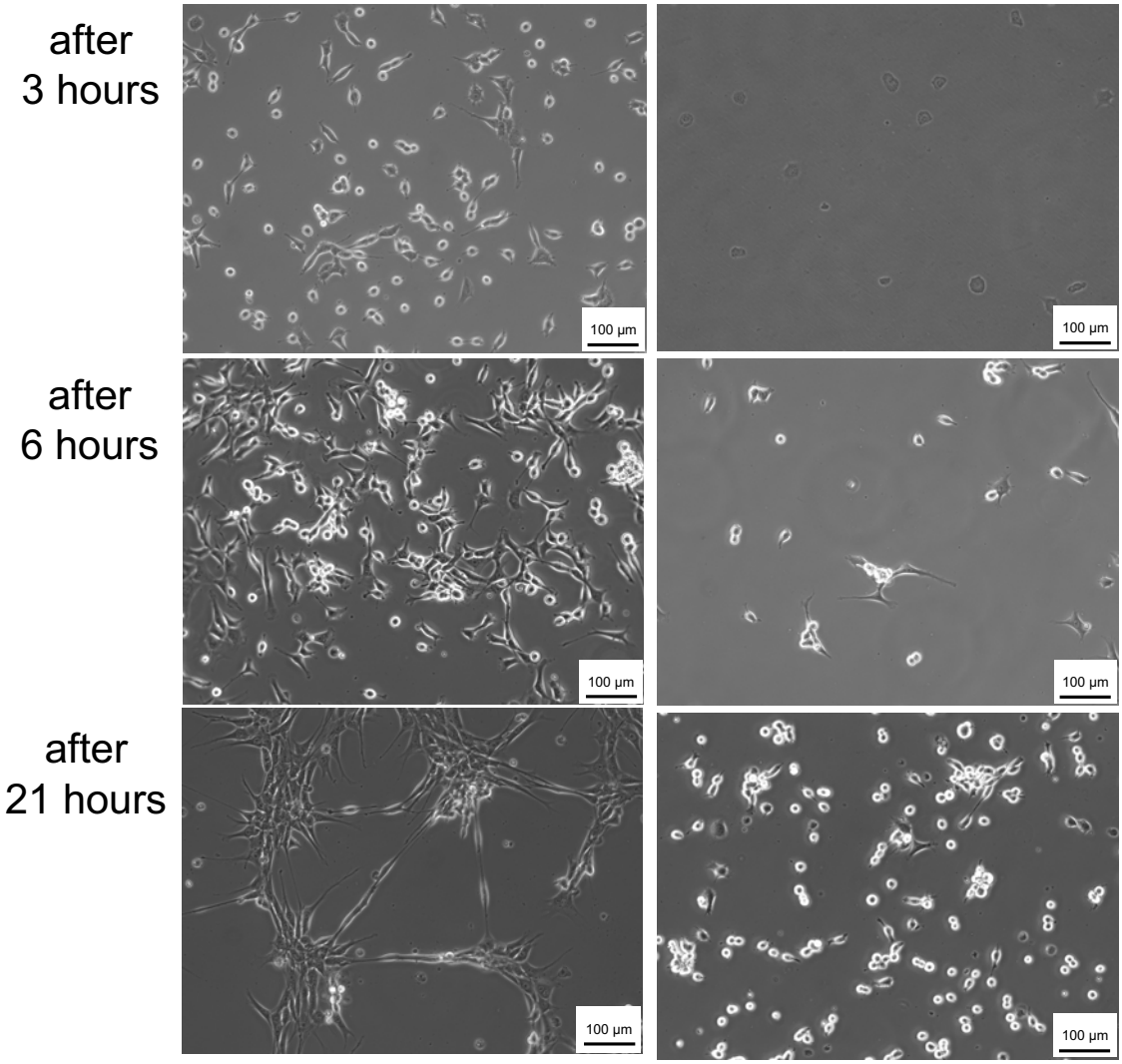

Figure 3.41: Microscope images of fibroblasts plated on substrates treated analogues Figure 4.40, taken after 3, 6 and 21 hours after plating. Deprotection of Y-EG-NVoc occurred in 100 µm wide horizontal lines (separated by 200 µm, activation of cyclo[RGDfK] in vertical lines (100 µm wide, separated by 200 µm). Images on the **right** are from substrates without coupling of cyclo[RGDfK].

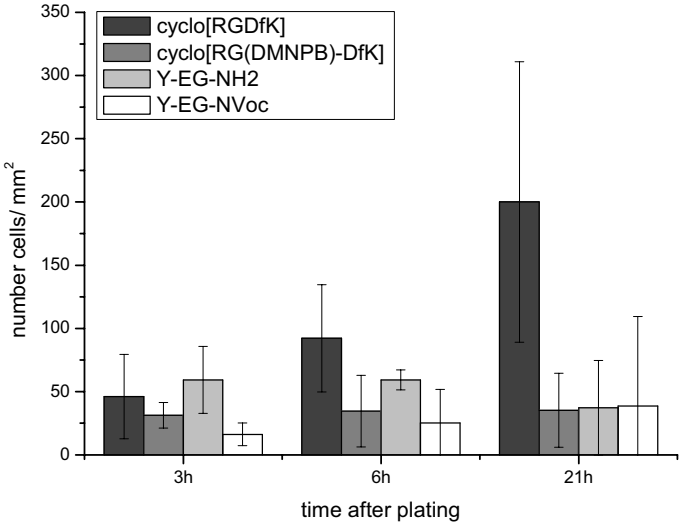

Figure 3.42: Representation of number of adhered cells per area [mm^2] after 3, 6 and 21 hours after plating, respectively. The numbers were obtained by overlaying a lattice on the microscope images from Figure 3.39 (left images) and counting the number of adhered cells.

The cell experiments presented were performed in serum-free medium (protein concentration less than 1%) with a plated concentration of 300 to 600 cells/ mm^2. Higher initial concentrations of cells afforded complete coverage of the substrate and no selectivity (Figure 3.43).

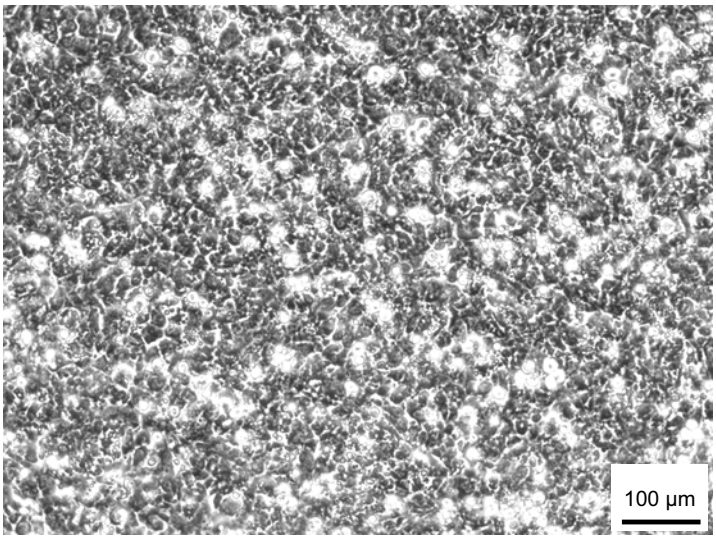

Figure 3.43: Microscope image of fibroblasts plated on a RGD patterned substrate after 15 hours plating. Initial concentration of fibroblasts: 3.000 cells/ mm^2.

3.6 Discussion

In previous works, it has been demonstrated that photocleavable, caged silanes can be used as surface coupling agents to site-selectively immobilize small molecules and colloidal particles at predefined positions on a surface.[87, 97] The immobilization is based on surface groups which get activated in selected regions of the substrate upon masked UV irradiation, and can then selectively interact with complementary targets from a surrounding solution. The selectivity of this interaction requires a careful design of the surface agent in order to avoid non-specific interactions with the caged regions, which would diminish the selectivity of the assembly. In this work, we have extended this principle to the site-selective and functional immobilization of proteins. For this purpose, silanes with a branched structure containing protein repellent TEG arms and protein-specific terminal functionalities have been designed and synthesized. Three different routes have been proposed for the preparation of branched silanes, but only the route *via* epichlorhydrin as linker attaching TEG based arms afforded the desired target molecule. Isolation of TEG containing precursors in the synthetic route constitutes the main difficulty along the synthetic path. The polar TEG chain seems to dominate the interaction of the compounds to be separated with the silica support, independently of the nature of the end groups. Significant loss of product during chromatographic separation occurred due to the closeness of the R_f of the different products and strong tailing of the TEG derivatives. The presence of free hydroxyl groups in many precursors hampered the purification by distillation due to their tendency to form azeotropic mixtures. If the molecules to be separated differ notably in chain length (eg. in reactions involving addition of the second or third arm to the linker molecule), distillation could be used for purification, but azeotropic mixtures were obtained in case of similar chain length. Preparative GPC could constitute an alternative in the separation of TEGs with different chain length but it was not used in this work.

An additional difficulty arised in the purification of the final silanes Y-EG-NVoc and Y-alkyl-NVoc. Chromatographic separation with silica gel led to low yields of purified substance (< 10%) as a consequence of the condensation reaction of the alkoxysilane groups of the molecule with the Si-OH groups at the surface of the silica gel. This

causes irreversible retention of the product in the chromatographic column. Better results were achieved by using silica gel that was previously passivated with hexamethyldisilazane (HMDS). This reagent converts the reactive free hydroxylic groups at the surface of the silica gel into inert -Si(OCH_3)$_3$. The passivation slightly modifies the polarity of the chromatographic support and, consequently, the final separation process. In general shorter elution times were detected. Parallel experiments using thin-layer chromatography plates after similar treatment with HMDS helped for assessing the adequate solvent mixture for the separation.

Silanes Y-EG-NVoc and Y-alkyl-NVoc could not be isolated from their reduced analogues (byproduct in the silanization reaction). Since no interference of the reduced compound with the silica surface is expected, the mixture was used for surface modification. Complete removal of triethoxysilane from the last reaction step was ensured, since this reactant would interfere during the surface reaction.

Surface layers of silanes Y-EG-NVoc and Y-alkyl-NVoc show higher hydrophobicity than layers obtained from linear grafted PEG (CA ~30°) or star PEG (CA ~45-37°),[67] as a consequence of the presence of the NVoc groups. The presence of the alkyl chain in Y-alkyl-NVoc also increases the hydrophobic character of the surface layer.

Contrary to expectations, hydrophobic interactions between the alkyl spacer do not promote more dense packing of the Y-alkyl-NVoc layers, as it can be usually seen for SAMs of long chain alkyl thiols. Overall, the obtained surface loading (1.6×10^{12} and 1.1×10^{12} molecs mm^{-2} for Y-EG-NVoc and Y-alkyl-NVoc respectively) is 3 to 4 times smaller than the typical surface density of a SAM of thiols on gold with maximum coverage (4.5×10^{12} molecs mm^{-2}). Surface loading is about 2 times lower than in layers obtained from the shorter and linear silane EG-NVoc. Branched and longer EG spacers seem to sterically hinder the surface reaction.

The differences in the layer properties get reflected in the results of the protein binding experiments. Non-specific adsorption of the protein BSA onto the surfaces is higher if alkyl spacers or shorter EG spacers are used, as a consequence of stronger hydrophobic interactions between the protein and the layer. The surface loading of active groups strongly correlates with the amount of streptavidin which gets immobilized on the

surface when comparing the results obtained from the branched silanes Y-EG-NVoc and Y-alkyl-NVoc. However, higher surface loadings obtained from the short EG-NH2 layers or EG-NH2/ EG-OMe layers do not improve the binding performance, presumably as a consequence of crowding of the receptors at the surface. Clearly the right balance between spacer length and branching is necessary to maximize selective binding performance and minimize non-specific interactions with proteins.

Patterned OND, protein, antibody and cell substrates were successfully generated after appropriate biofunctionalization of the substrate with the corresponding receptors. It is important to note that the binding selectivity was maintained over different surface coupling steps to form the final complex. In the case of cell patterns, selectivity was maintained over 20 hours of incubation. Attached cells secrete their own extracellular matrix, and that this protein layer may change the properties of the substrate. Under these conditions, the Y-EG-NVoc layers demonstrate to maintain their stability against non-specific protein and cell binding over at least 20 hours. Experiments at higher serum containing media are in progress in order to test the applicability of the substrates at serum concentrations closer to *in-vivo* conditions.

Chapter 4

New Coumarin-4-ylmethyl protected silanes for wavelength-selective photoactivation

4.1 Introduction

Miniaturized and high-throughput chemical and biological analysis systems in microarray format have moved to the forefront of the bioanalytical science area. They only require small amounts of analytes and reagents for accurate detection and allow analysis of a variety of samples in parallel.[6] The fabrication of these analytical platforms requires the development of surface patterning strategies able to create a high density of individual and isolated reactive sites on a substrate, onto which the biomolecular species will be immobilized for detection.[29, 159] Among them, photoreactive surface layers which can be site-selectively activated upon masked irradiation constitute an interesting patterning alternative with many possible variants. Light can be used (i) to destroy or remove molecular layers at selected positions to render the bare, inactive substrate,[88, 89] (ii) to graft molecular species to irradiated regions *via* photogenerated radical cross-reactions occurring between a photosensitive

surface layer and the biological molecule (photoaffinity),[160-164] or (iii) to direct synthesis of small molecules on the surface (peptides,[93, 165] oligocarbamates,[166] oligonucleotides,[18, 167-169] peptoids[170]) through iterative unmasking of photoreactive groups and monomer coupling cycles. Alternatively, surface layers containing the reactive functionalities protected with a photocleavable[101, 111, 112] group can be used for site-specific coupling of complementary functionalities after light-deprotection.[87, 93,96, 97, 100, 113-116] The latter is a particularly flexible approach, since a good number of photoremovable groups are known that can be combined with many different reactive species. Moreover, it has been recently demonstrated that different protecting groups may be independently cleaved using light of different wavelengths and intensities[171, 172] and that this approach can be very useful in solid phase peptide synthesis[173] or in generating complex chemical patterns with more than one single functionality.[87, 97]

Up to now, only two pairs of photoremovable groups have shown wavelength selective cleavage (Figure 4.1). Nitroveratryl esters (**NVo**) have been selectively cleaved at 350 nm in a 87% yield in the presence of the pivaloylpropanediol group (**Piv**), with virtually no absorbance at this wavelength, and which can be subsequently cleaved at 300 nm.[174] The wavelength selective cleavage only works when **NVo** is removed before **Piv**, because compound **NVo** also shows appreciable photosensitivity at 300 nm. A more interesting combination was demonstrated with 3,5-dimethoxybenzoin esters (**Bnz**), which were effectively cleaved by low intensity irradiation at wavelengths below 300 nm, while nitroveratryl esters (**NVo**), being less reactive, were cleaved at much longer wavelengths (up to 420 nm) and higher irradiation intensities.[87, 173] These two protecting groups are orthogonal (the group **Bnz** does not show any absorbance at $\lambda > 380$ nm and group **NVo** requires much higher intensities for cleavage) and can be individually addressed in any chronological sequence.

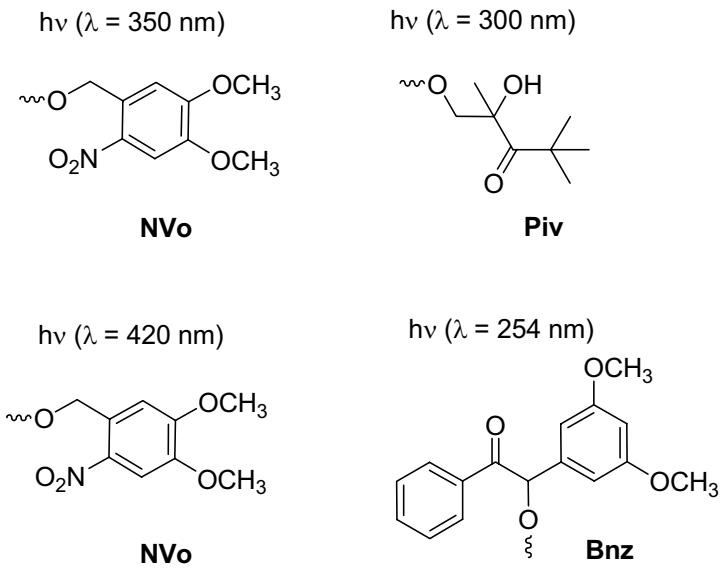

Figure 4.1: Photoremovable groups that show wavelength-selective cleavage.

Both the **Piv** and **Bnz** need irradiation wavelengths below 320 nm for selective cleavage. This fact limits their application to biological issues, since many biomolecules show appreciable absorption at $\lambda < 320$ nm and would interfere with the photocleavage process. The development of additional orthogonal photocleavable groups with sensitivity to longer wavelengths is, therefore, a challenging task. However, the majority of organic chromophores absorbs light in the same wavelength rage (i.e. between 250 and 420 nm), and absorption spectra frequently overlap. In addition, even if energy can be locally delivered using monochromatic light, rapid energy transfer can redistribute the excitation throughout the molecule and the initial location may be lost.[172] This means that not only the absorption spectrum needs to be considered when seeking for wavelength sensitivity, but also the kinetics of the photolytic process needs to be taken into account (the groups must show highly differential photolysis rates).[172]

Amongst the known photocleavable groups, the coumarin-4-ylmethyl family seems to be a suitable choice. The different members (Figure 4.2) show large extinction coefficients at wavelengths > 350 nm, high photolytic efficiency, fast photolysis kinetics and acceptable stability in the dark. The position of the absorption maximum can be shifted by introducing substituents in the ring. While bare coumarin-4-ylmethanol (CM) has its absorption maximum at 310 nm, electron-donating substitution in C6 or C7 shifts the absorption maximum to longer wavelengths (Figure 4.3). In

particular, dialkylaminosubstitution on C7 produces a strong red shift of more than 80 nm and extends the absorption range of the chromophore up to 470 nm. These properties make (7-dimethylaminocoumarin-4-yl)methyl (DMACM) and (7-diethylaminocoumarin-4-yl)methyl (DEACM) suitable alternatives to the pivaloyl and 3,5-dimethoxybenzoin groups as wavelength selective cages (see Figure 4.4).

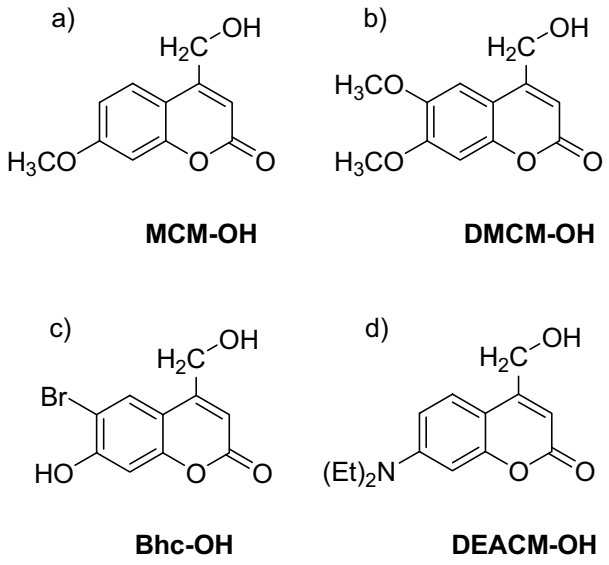

Figure 4.2: Members of the four subclasses of coumarin-4-ylmethyls (CM): a) 7-methoxy coumarin-4-ylmethanol (MCM-OH), b) 6,7-dimethoxy coumarin-4-ylmethanol (DMCM-OH), c) 6-bromo-7-hydroxy coumarin-4-ylmethanol (Bhc-OH), d) 7-diethylamino coumarin-4-ylmethanol (DEACM-OH).

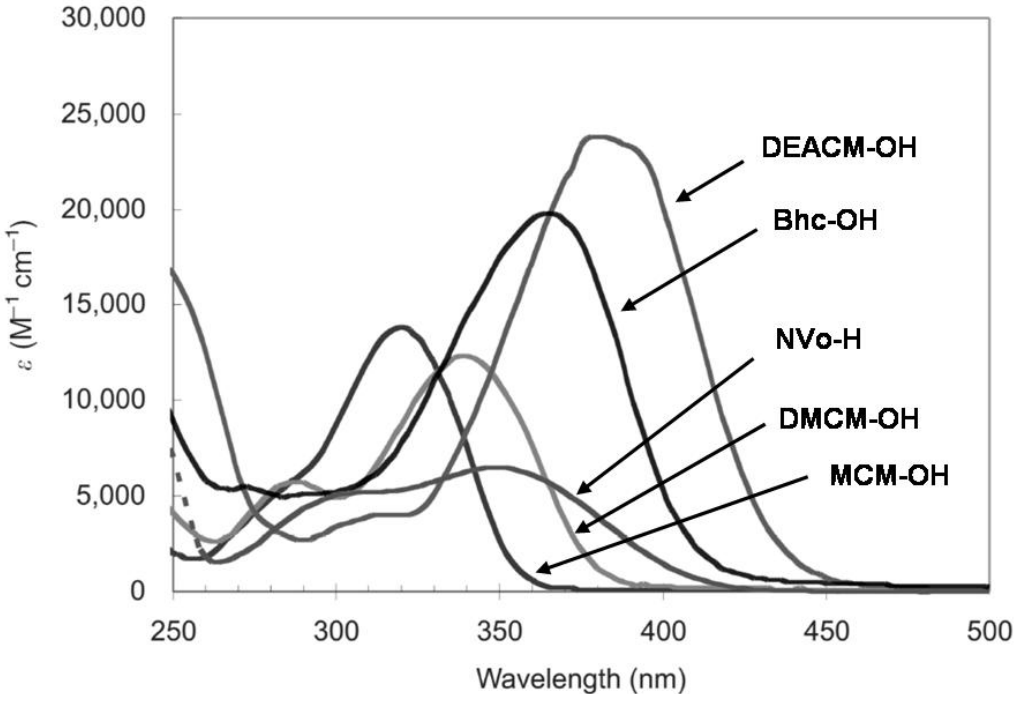

Figure 4.3 UV/vis spectra of different coumarin-4-yl-methanols and NVo-H in KMOPS, pH 7.2. Their molecular structures are given in Figure 4.2. Furuta/ Goeldner, Givens: Dynamic Studies in Biology, page 31, 2005. Copyright Wiley-VCH Verlag GmbH & Co. KGaA. Reproduced with permission.[175]

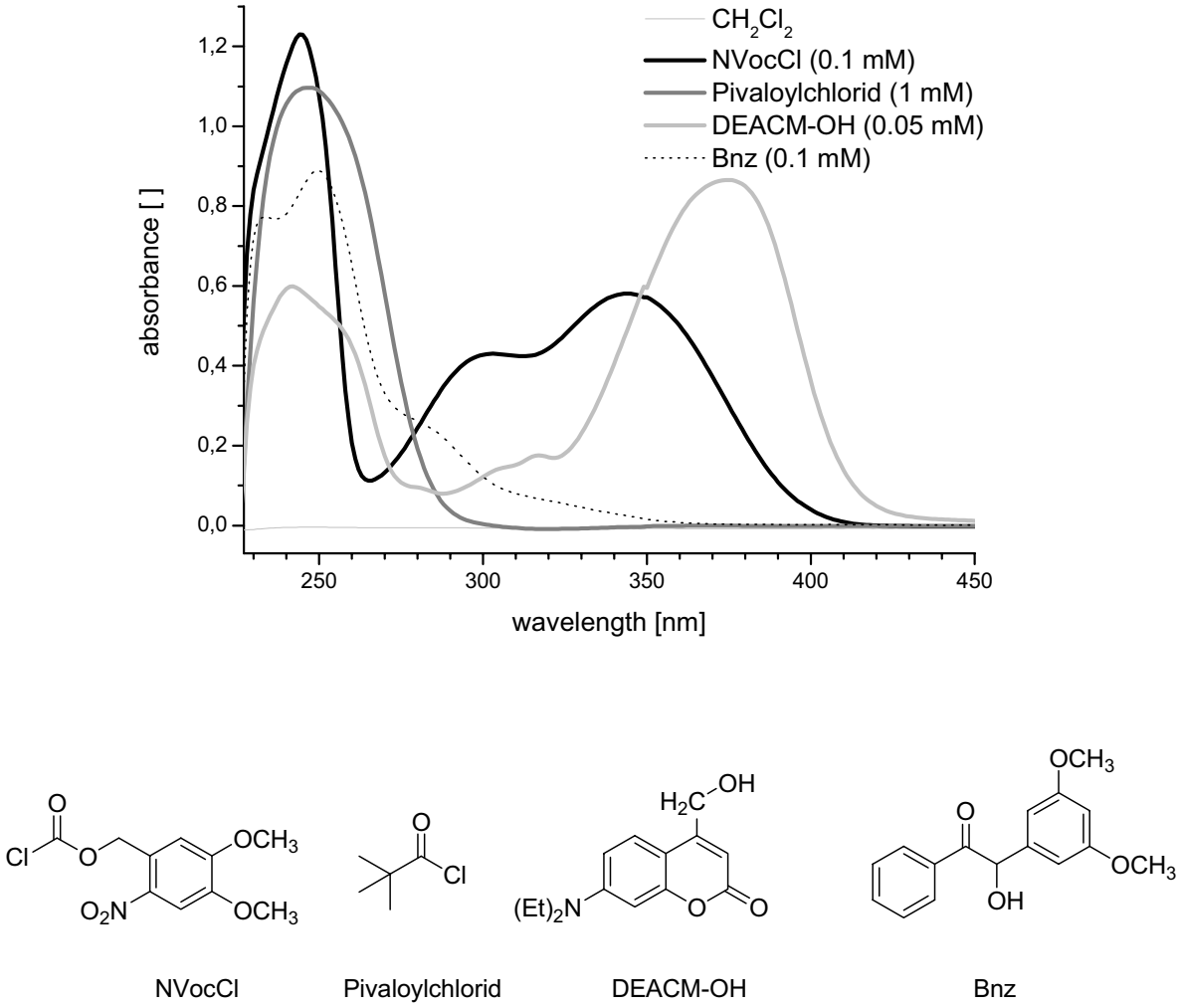

Figure 4.4: UV absorbance spectra of 6-nitroveratryloxycarbonyl chloride (NVocCl), Pivaloyl chloride, 3,5-dimethoxybenzoine (Bnz) and 7-diethylamino coumarin-4-ylmethanol (DEACM-OH) in dichloromethane. Note the different concentrations.

The photolytic process of coumarin-4-ylmethyl units has been studied and is represented in Figure 4.5. Upon irradiation, the C-O bond between C-4 methylene and X (leaving group) is cleaved to produce an anion of the leaving group and a solvent trapped coumarin as photo by-product.

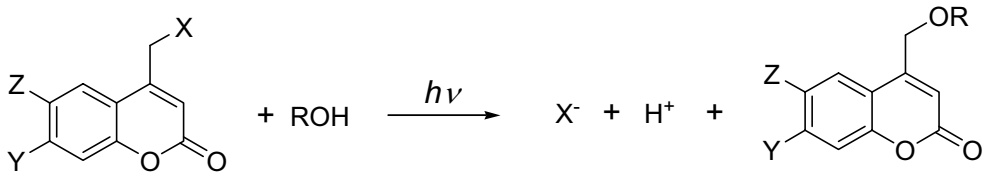

Figure 4.5: Photolysis of coumarin-4-ylmethyls.

Coumarins have been used as protecting groups for phosphates, carboxylates, amines, alcohols, phenols and carbonyl groups and have been widely applied to many fields such as fluorescent materials and laser dyes, nonlinear optical materials, photorefractive materials, photoresist, intermediates for medicine synthesis, luminescent materials.[176] A possible limitation for their application as photocleavable groups in biological applications is that they are strongly fluorescent. Their fluorescence may overlap with the emission spectra of fluorescent labels, and this may cause difficulties in monitoring specific effects by fluorescence imaging after activation.

4.2 Objectives and strategy

In this chapter, two photolabile groups working at irradiation wavelengths and intensities in the UV range suitable for applications in biology laboratory ($\lambda > 320$ nm) will be identified and tested for wavelength selective deprotection. The two groups will be coupled to an alkoxysilane unit and the resulting silanes will be reacted with silica surfaces. The photolytic properties of the photosensitive layers will be characterized in order to identify the suitable wavelengths and intensities for a selective response. Sequential irradiation of the photosensitive layers using masks of different geometries will allow us to generate a bifunctional pattern which will be revealed using fluorescent labels of different colours.

6-Nitroveratryloxycarbonyl (NVoc) and the 7-diethylamino coumarin-4-yl (DEACM) groups were selected as photocleavable groups. The NVoc group is a robust, versatile and efficient cage with one absorption maximum at 356 nm ($\varepsilon \sim 4500$) which tales up to 420 nm. It shows slow photolysis rates (~18 s^{-1}) and a moderate quantum yield (0.023). The DEACM group has absorption maxima at 390 - 400 nm with a molar absorptivity

of 20 000 M^{-1} cm^{-1}. This band extends up to 460 nm. Photolysis quantum yields are as high as 0.3, which is the highest among the reported coumarin cages and it has high deprotection rates (~10^9 s^{-1}). It has been used to protect phosphates,[177-181] alcohols,[182] and carboxylic groups[183] and could be extended to carbonyl and amine functionalities, as it has been already demonstrated with other members of the coumarin family.[184]

Given that the λ_{max} of NVoc and DEACM differ in 50 nm, that they do not overlap in the absorption range between 430 and 460 nm, and that they show very different kinetics of the photolytic process, we expect to be able to address both groups independently by using appropriate irradiation wavelength and intensity. In order to test the selective photoreactivity, these groups were attached to the amine group of aminopropyltriethoxysilane (Figure 4.6). Quartz substrates were modified with these silanes and the photolytic process at the surface was followed by UV spectroscopy. Once the adequate irradiation conditions were identified, the wavelength photosensitive silanes were used to generate chemical patterns onto substrates by masked irradiation which could be revealed by fluorescent staining.

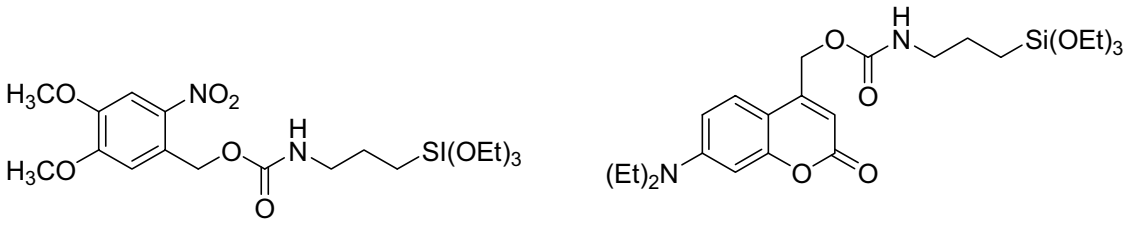

36
NVoc-APTS

41
DEACM-APTS

Figure 4.6: Structures of aminopropyltriethoxysilanes with photoremovable amine functionalities, using NVoc or DEACM as caging groups.

4.3 Experimental

Synthesis

The detailed synthetic procedure for the synthesis of compounds **36** and **41** can be found in Appendix A.3.1.

Surface modification of silica surfaces

Silanization of the substrates with silanes **36** and **41** and a 1:1 molar mixture of them was performed in THF solution using catalytic amounts of 1N NaOH and 0.2 to 1% (w/V) silane concentration. Silanization conditions (reaction time and catalyst concentration) were optimized in order to obtain maximum and homogeneous surface coverage.

Characterization of the surface layers

The surface modification process was monitored by UV spectroscopy on quartz substrates by detecting the absorbance bands of the chromophore. With this method, it was possible to identify the optimal silanization time (maximum absorption) for each silane. Static water contact angles were used to determine the change in the hydrophilicity of the surface reflecting the presence of the silane layer. The layer thickness was determined by ellipsometry (the refractive index was assumed to be 1.4571 in the deposited layers in a three phase model silicon substrate/ silica+organic layer/ air). Surface loadings, $\Delta\Gamma$, in terms of molecules mm^{-2}, were estimated from the ellipsometric thickness assuming a refractive index of 1.4571 for the silane layer, a typical density ρ of 1.0 g cm^{-3} for an organic layer with a refractive index *n* of 1.43, and an increment $dn/d\rho$ of 0.24g cm^{-3}.[43, 139]

Irradiation of the substrates for photodeprotection

Activation of the surface functionality by photocleavage of the NVoc or DEACM groups was carried out using a Xe-lamp coupled to a monochromator. The deprotection was monitored by the decay in the UV/vis spectrum (as a consequence of the cleavage of the chromophore). The minimum irradiation time for full deprotection was obtained from different experiments at various irradiation times. For testing the wavelength dependent deprotection, irradiation experiments were performed at 345 and at 412 nm. For laterally structured deprotection, quartz slides with chrome patterned fields containing micrometric stripes were placed on top of the substrate during irradiation. Additional details are given in the Appendix (A.3.3).

Fluorescence labeling

The generation of free surface amine groups after irradiation was verified by fluorescence staining of patterned substrates using Alexa Fluor dyes (Alexa Fluor® 647 and Alexa Fluor® 488 carboxylic acid succinimidyl esters). Amine coupling with the succinimidyl ester results in the formation of an amide bond between the fluorophore and the surface. To ascertain wavelength-selective deprotection of NVoc and DEACM, two different fluorescence labels were successively coupled to the free amine groups after a two-step irradiation process. Coupling conditions can be found in Appendix (A.3.4).

4.4 Results

4.4.1 Synthesis

NVoc-APTS was synthesized following a reported protocol represented in Figure 4.7. A condensation reaction of commercial 6-nitroveratryloxycarbonyl chloride with allylamine using sodium hydrogencarbonate was followed by a hydrosilylation reaction. The silane NVoc-APTS (**36**) could be isolated in a yield of 58% after chromatographic purification using HMDS passivated silica gel as chromatographic support.

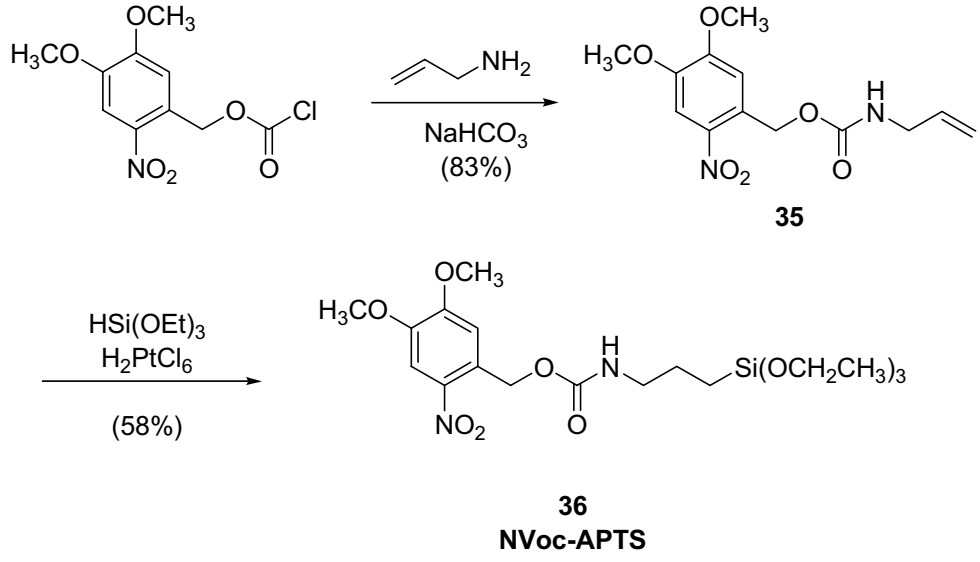

Figure 4.7: Synthesis of NVoc-APTS, **36**.

The synthesis of DEACM-APTS starts with the preparation of 7-diethylamino-4-hydroxymethylcoumarin (**38**), by first oxidating commercially available 7-(diethylamino)-4-methylcoumarin to the corresponding coumarin-4-carbaldehyde **37**,[185] followed by reduction of **37** to the desired hydroxymethylcoumarin **38** (Figure 4.8).[179, 183, 186] The reaction is a one-pot process and does not require isolation of the intermediate **37**. The product **38** could be obtained purified with a yield of 44%. Activation of the hydroxyl functionality of **38** with 4-nitrophenyl chloroformate allows subsequent coupling of allylamine.[184] Separation of **40** from the nitrophenol byproduct could not be achieved by chromatography and the product was purified by crystallization from a 3:1 mixture of ethylacetate and petroleumether with a yield of 22%. Hydrosilylation of **40** yielded mixture of the desired product DEACM-APTS, **41,** and the saturated byproduct **42** after 2 hours of reaction time (molar ratio of **41** was 0.45 according to the integration of the NMR signals). The basic character of the tertiary aromatic amine in **40** did not neutralize the catalyst (a Lewis acid). The mixture of both products was used for surface modification without chromatographic isolation to avoid product loss. The saturated compound **42** is not expected to react with the silica surface.

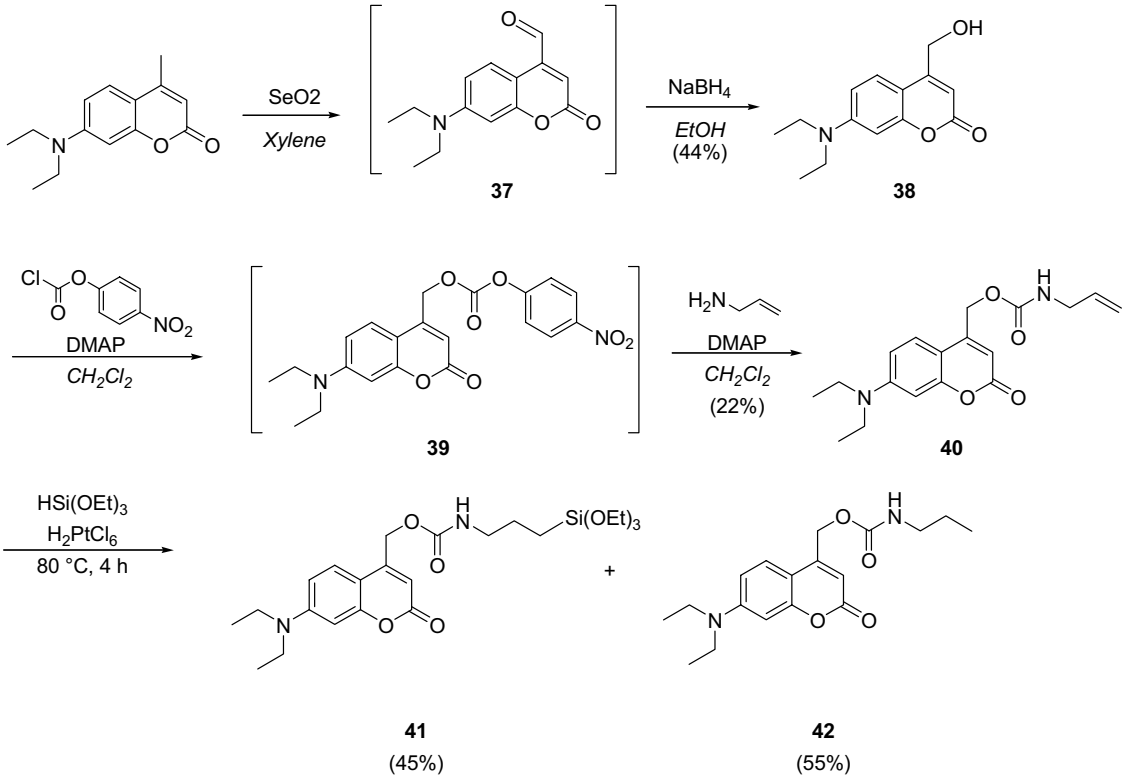

Figure 4.8: Synthesis of DEACM-APTS, **41**.

4.4.2 Properties of the surface layers

Monocomponent layers of silanes **36** and **41** were obtained by silanization in solution. Anchoring of the molecule to the silica surface occurs through the triethoxysilyl functionality. Trivalent alkoxysilanes are expected to favor the formation of denser surface layers than di- or monovalent alkoxysilanes. However, multivalence complicates the surface reaction scenario, since the highly reactive silanol species may condensate not only with the free OH groups of the silica surface, but also with each other forming oligomers. These may lead to larger 3D aggregates and consequently in substantial surface roughness. The progression of these reactions and consequently the characteristics of the final surface layer critically depend on experimental variables such as type of solvent, temperature, and reaction time, as well as on the catalyst and the concentration of the organosilane.[149-153] All these parameters were optimized in our case in order to obtain dense but smooth surface layers. For this purpose, the course and extent of the surface modification reaction was followed by ellipsometry and UV/vis spectroscopy. The silanization conditions were first varied to maximize the layer thickness and UV/vis absorbance. Typically maximum absorbance was obtained after 18 hours reaction time for NVoc-APTS, 70 hours reaction time for DEACM-APTS and 45 hours reaction time for mixed layers, at room temperature using THF as solvent and 1×10^{-3} M NaOH as catalyst. Representative UV spectra of quartz substrates modified with NVoc-APTS and DEACM-APTS under optimized conditions are shown in Figure 4.9 and were found to be in good accordance to the spectra of the precursor silanes in solution.

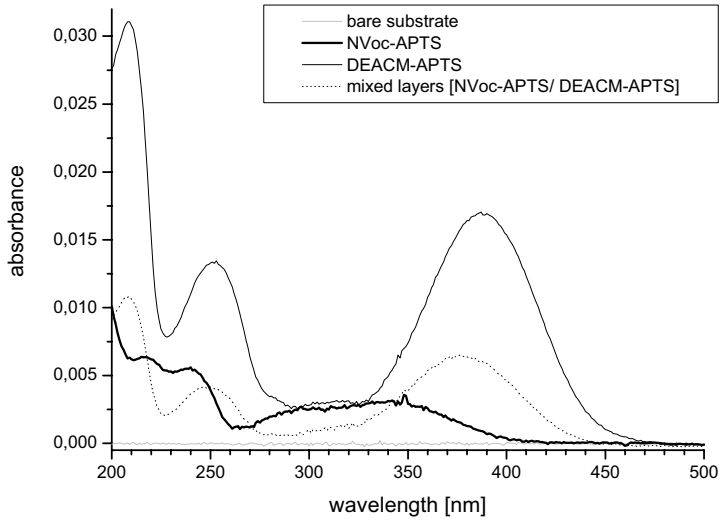

Figure 4.9: UV/ vis spectra of quartz substrates modified with NVoc-APTS (__), DEACM-APTS (__) and a 1:1 molar mixture of both silanes NVoc-APTS and DEACM-APTS (…).

Substrates obtained under optimized conditions revealed formation of silane layers with thickness around 0.55 nm for NVoc-APTS and 1.5 nm for DEACM-APTS and a static water contact angle of 65° and for both layers (Table 4-1). The layer thickness (0.54 and 1.5 nm) is smaller than the molecular length of the silanes (1.6 for Nvoc-APTS and 1.9 nm for DEACM-APTS) and indicates the formation of submonolayers. Assuming a refractive index of 1.4571 for the silane layer, a layer density of 1.11 g cm^{-3} was estimated (a typical density ρ of 1.0 g cm^{-3} is assumed for an organic layer with a refractive index *n* of 1.43, and an increment d*n*/dρ of 0.24 g cm^{-3}).[43, 139] From this density value and the experimental layer thickness, the molar surface loading and surface coverage were calculated (Table 4-1).[43, 139]

Table 4-1: Properties of the monocomponent layers. Ellipsometric layer thickness and water contact angle were measured on substrates obtained under optimized silanization conditions. The molar surface loading and surface coverage were calculated from the experimental layer thickness.

Surface modification	Layer thickness, [nm]	Water contact angle, [°]	molar surface loading $\Delta\Gamma$ [ng mm^{-2}]	Surface coverage [molecs mm^{-2}]	Water contact angle after irradiation, [°]
NVoc-APTS	0.54±0.05	65±5	0.60±0.08	9.7×10^{11}	59±2
DEACM-APTS	1.5±0.1*	65±5	1.67±0.16	2.6×10^{12}	60±5
MIXED LAYERS	1.4±0.1	68±1	1.55±0.16	?	63±3

*estimated from UV spectra.

Mixed layers were prepared by competitive chemisorption from an equimolar mixture of silanes **36** and **41**. The kinetics of the surface reaction was followed by UV spectroscopy and Figure 4.10a shows representative spectra recorded after increasing silanization times. The UV absorption, and therefore the amount of silane attached to the surface, increases with increasing silanization time and reaches a saturation level after about 45 hours (Figure 4.10b).

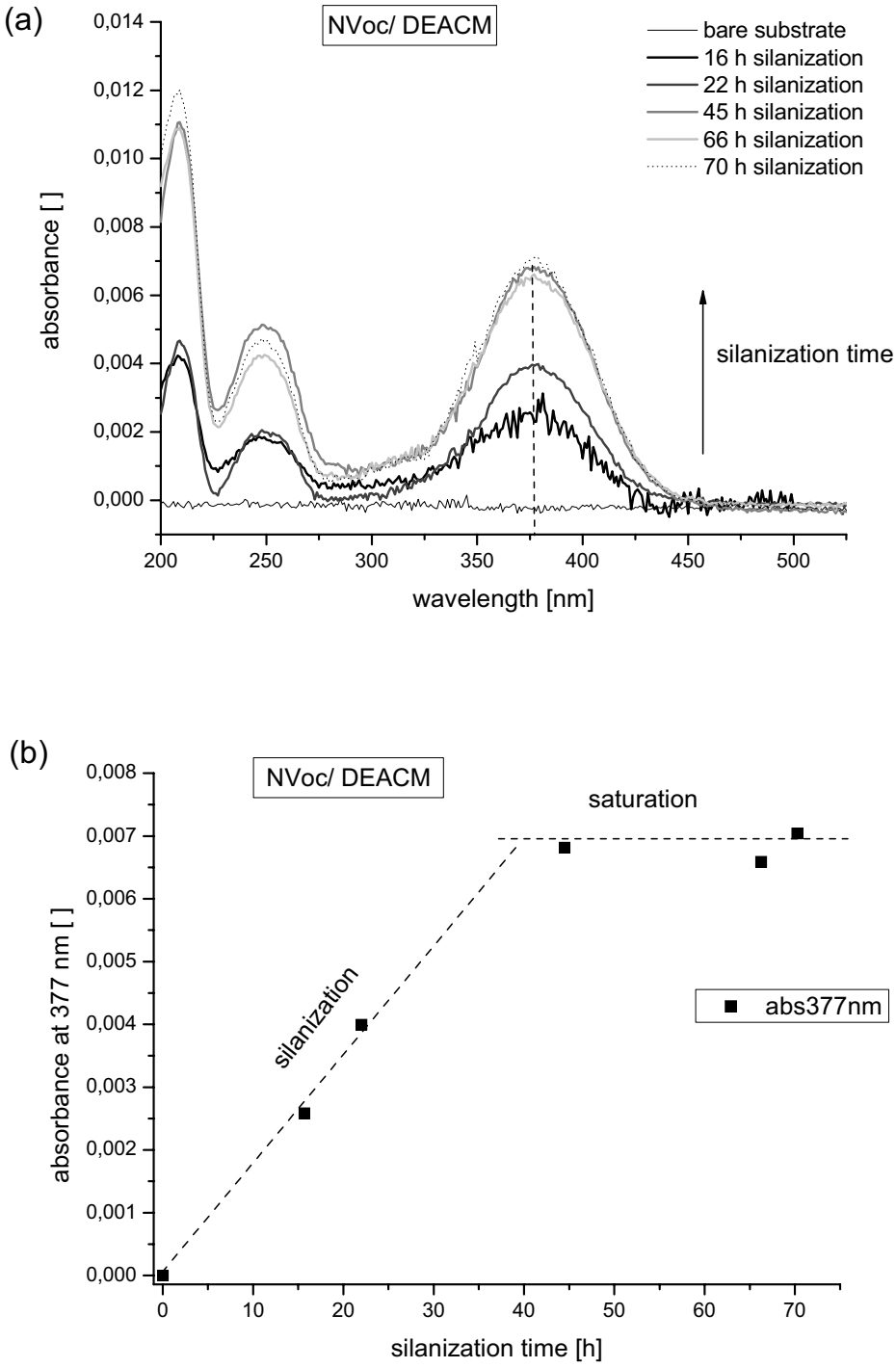

Figure 4.10: Kinetics of the silanization process as followed by UV spectroscopy. Measurements were performed on quartz substrates during silanization from an equimolar mixture of silanes **36** and **41**. Graphic (a) shows the raw UV/vis data and graphic (b) shows the obtained increase in the UV signal at 377 nm with the silanization time.

The molar ratio of the silanes at the surface can be determined by deconvoluting the UV spectrum of the mixed layers as the sum of the spectra of the two individual silanes. This analysis revealed a 3:7 molar ratio of silanes **36**:**41** and indicates higher reactivity of silane **41** with the surface. The contact angle of the mixed layers was found to be 68°, similar to those of the monocomponent layers, and the obtained layer thickness was 1.4±0.1 nm (Table 4-1).

4.4.3 Photoactivation of the surface by irradiation: wavelength selective deprotection

Substrates modified with the photosensitive silanes **36** and **41** were irradiated at different wavelengths. Irradiation is expected to cleave the photoactive groups and release free amine groups (Figure 4.11). The photolytic reaction can be followed by the decay of the UV absorbance of the substrates after washing because the chromophore is lost from the surface.

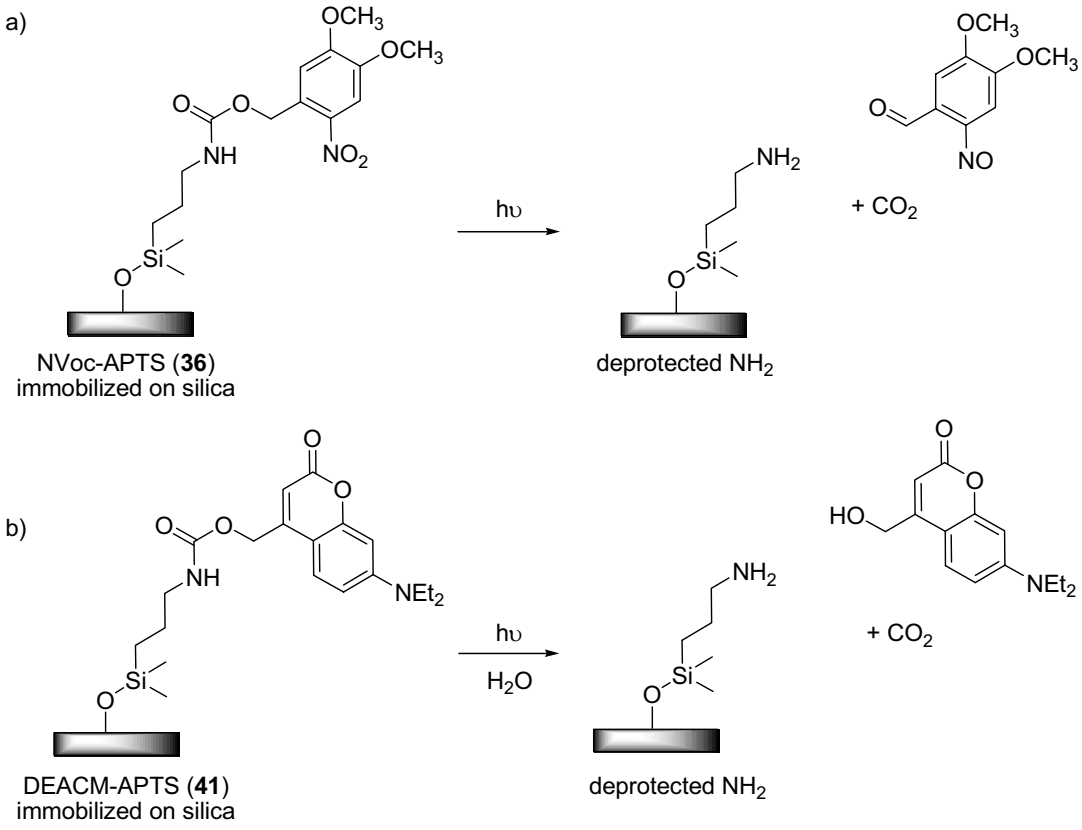

Figure 4.11: Photochemical deprotection at the surface of (a) immobilized NVoc-APTS (b) immobilized DEACM-APTS.

The selection of the irradiation wavelengths for wavelength selective deprotection of the NVoc and DEACM groups was made taking into account the values of λ_{max} of the chromophores for maximizing photolytic efficiency (345 nm and 389 nm), and also reported data on the photosensitivity of the NVoc group to different wavelengths. NVoc has been successfully cleaved in solution at 350 nm and at 419 nm[111, 171] and at the surface at 365 nm with 3 $mWcm^{-2}$ and at 411 nm with 200 $mWcm^{-2}$.[87] We selected the wavelengths 345 and 412 nm for our experiments. Figure 4.12a shows the UV spectra of substrates modified with silane **36** after different irradiation times at 345 nm. A clear drop in the absorbance corresponding to the NVoc group is noticed already after 30 seconds irradiation time. These results are in agreement with published data on similar substrates.[87, 108] The absorbance drops up to 70% after 40 minutes irradiation (Figure 4.12b), but it does not decrease further with longer irradiation times. This is presumably due to imine formation between the benzaldehyde photofragment and the primary amino group at the surface.[87] This side reaction reattaches the chromophore to the surface, causing a residual absorbance and decreasing the final density of amine groups. The photolytic reaction also reduces the water contact angle of the surface by 5°, indicating the liberation of the more polar amine group (Table 4-1). No significant change in the ellipsometric thickness could be observed after irradiation.

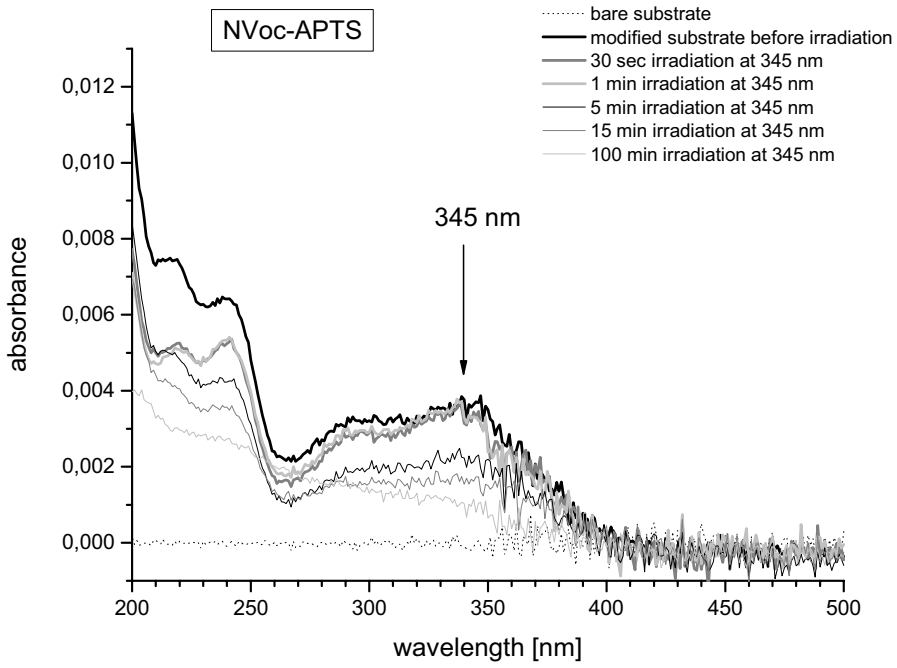

Figure 4.12: UV spectra of substrates modified with NVoc-APTS after irradiation at 345 nm for different times.

The UV spectra of substrates modified with silane **41** after irradiation at 412 nm are shown in Figure 4.13. Almost all DEACM seems to be cleaved off from the surface after 80 minutes of irradiation. This long irradiation time required for full deprotection contrasts with the expected higher photosensitivity of DEACM compared to NVoc and was initially attributed to the low absorption of DEACM at that wavelength. However, comparative irradiation experiments performed at λ_{max}=389 nm showed similar rates of the photolysis reaction (data not shown).

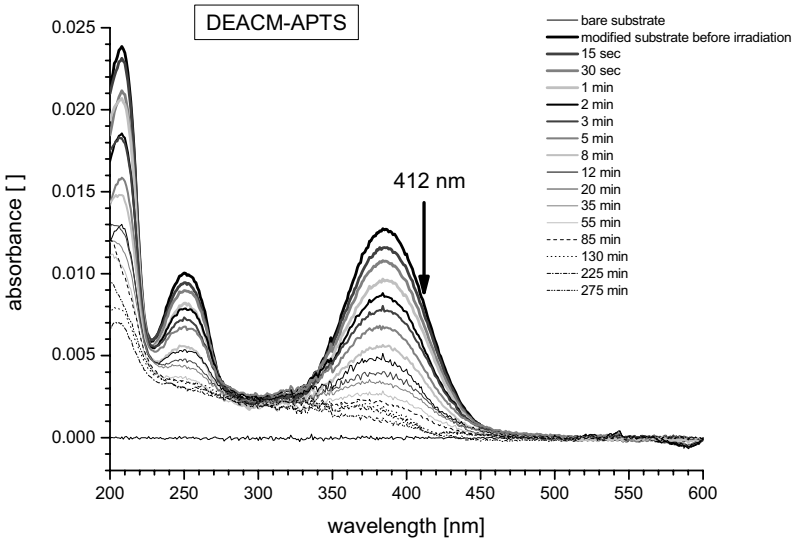

Figure 4.13: UV spectra of substrates modified with DEACM-APTS after irradiation at 412 nm for different times

The wavelength selectivity between NVoc and DEACM was then checked. Irradiation of NVoc-APTS modified substrates at 412 nm for 40 minutes did not change the UV spectrum of the subtrate significantly (Figure 4.14). This result was expected given the low extinction coefficient of NVoc at this wavelength, and corroborates the possibility of selective cleave of the DEACM group in the presence of NVoc groups at 412 nm. Irradiation of DEACM-APTS modified substrates at 345 nm caused a significant decrease in the absorbance values (Figure 4.15b), even at short irradiation times. The kinetics of the photolysis is even faster than the cleavage of NVoc at the same wavelength due to the higher efficiency of the photolytic process of the Coumarin moiety. These results indicate that the NVoc and DEACM chromophores can be used as wavelength sensitive photoremovable groups, but their deprotection is not orthogonal. Figure 4.16 summarizes the deprotection data.

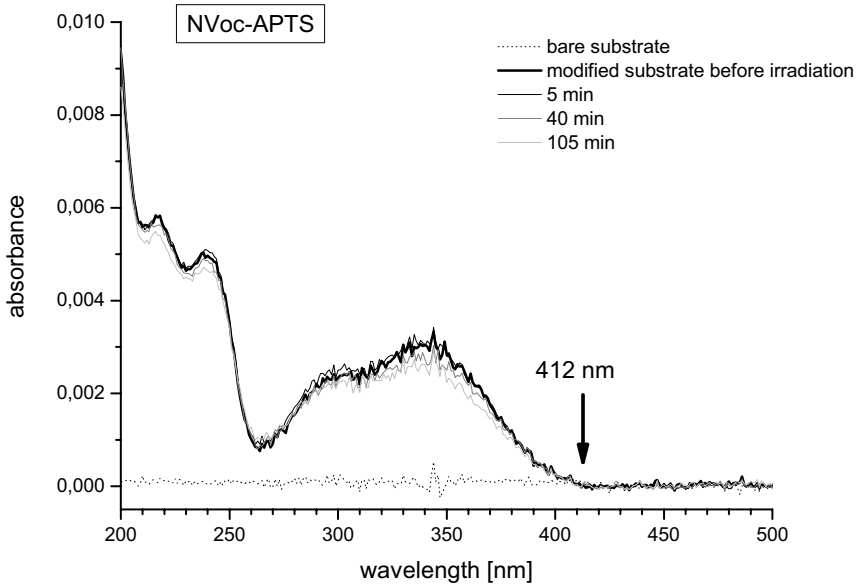

Figure 4.14: UV spectra of substrates modified with Nvoc-APTS after irradiation at 412 nm for different times.

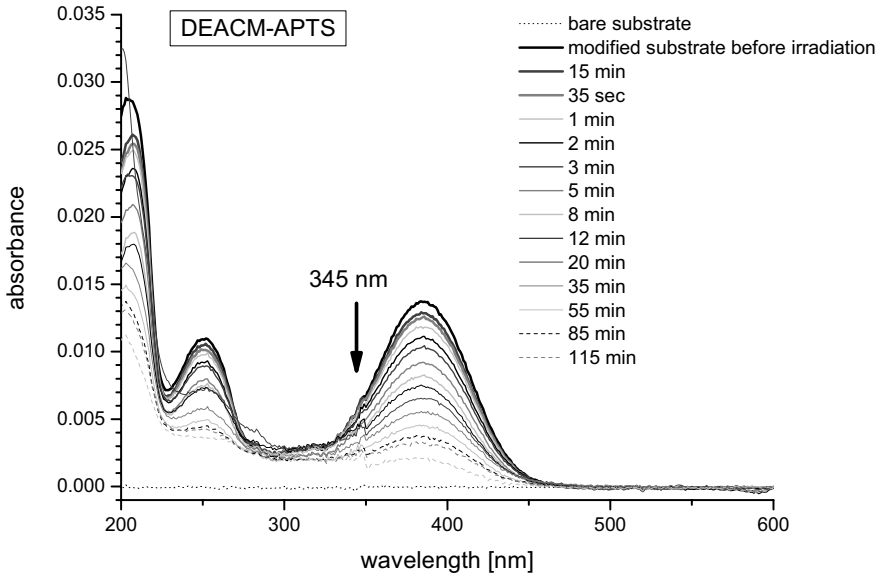

Figure 4.15: UV spectra of substrates modified with DEACM-APTS after irradiation at 345 nm for different times.

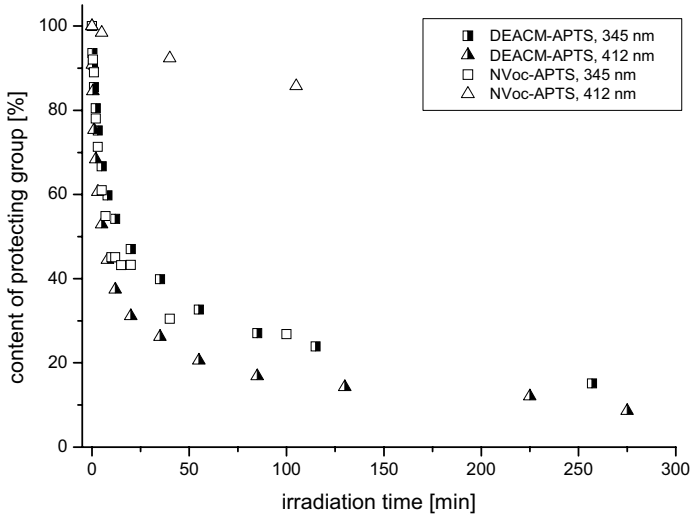

Figure 4.16: Summarized values of irradiation kinetics of NVoc-APTS and DEACM-APTS modified substrates at 345 nm and 412 nm. Data were extracted from the absorbance values at the corresponding λ_{max} (345 nm for NVoc and 389 nm for DEACM) and normalized with respect to the initial value.

4.4.4 Generating bi-functional patterned surfaces after two -step wavelength selective irradiation

The capability of NVoc- and DEACM-APTS mixed surfaces for generating complex lateral chemical patterns was explored by irradiating substrates through a mask in a two-step process using the selected wavelengths. When the substrates are irradiated through a mask, a pattern of activated and nonactivated areas reflecting the shape of the mask is generated. The resulting chemical contrast between exposed and nonirradiated regions can be used to direct the assembly process of specific targets onto the activated areas, like fluorescence dyes. If the different dyes are site-selectively assembled onto the desired active areas of a multifunctional surface, the underlying chemical pattern will be reflected in form of different colors under the fluorescent microscope. Figure 4.17 shows a schematic representation of the irradiation and surface coupling steps. The expected fluorescence pattern is shown in Figure 4.18.

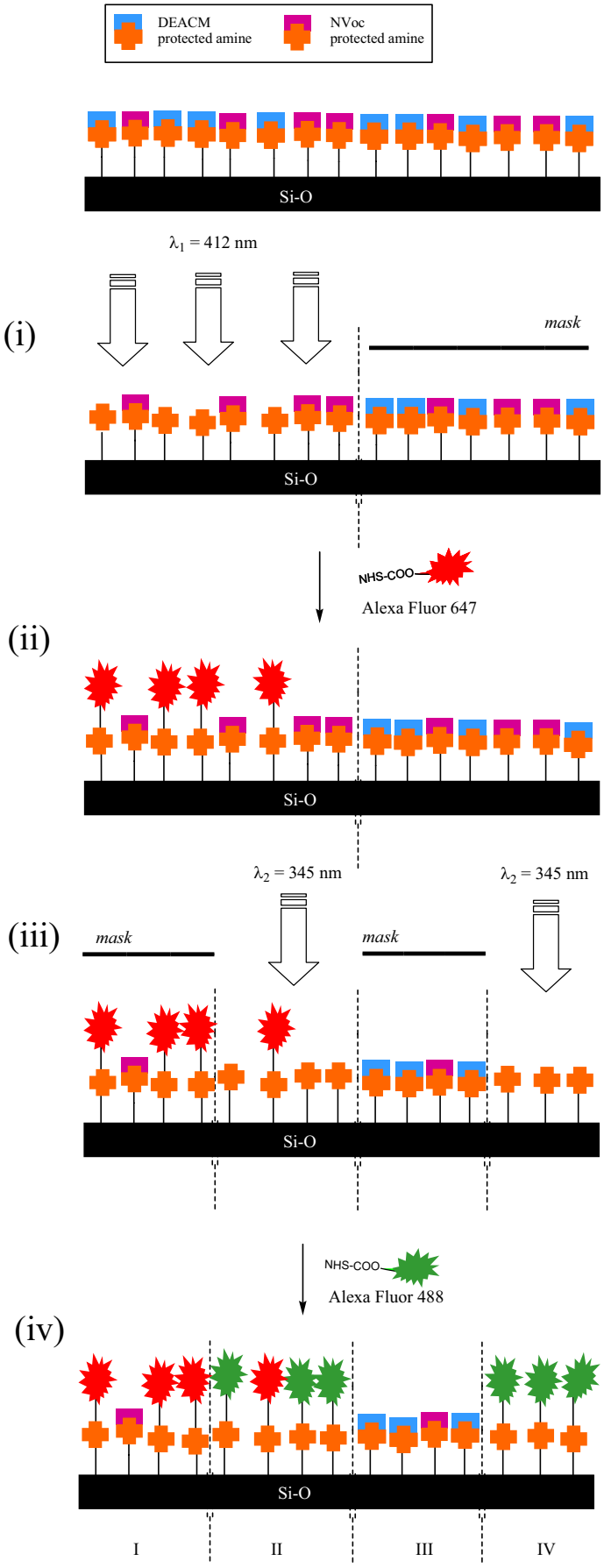

Figure 4.17: Surface patterning after two-step masked irradiation of mixed surfaces of NVoc- and DEACM-APTS and subsequent dye coupling. (i) Masked deprotection of DEACM-APTS at 412 nm, (ii) coupling of Alexa Fluor® 647 to released amine groups, (iii) Masked deprotection of NVoc-APTS at 345 nm, (iv) Coupling of Alexa Fluor® 488. After this process, four regions with different chemistries have been defined at the surface.

Initially, the NVoc- and DEACM-APTS mixed surface was irradiated at 412 nm through a quartz mask consisting of vertical 50 μm thick chrome stripes separated by 10 μm thick spaces. Surface regions with free amine groups were generated as a consequence of the cleavage of DEACM from the exposed (quartz) areas. These groups were then reacted with the dye Alexa Fluor® 647 succinimidyl ester, and the resulting fluorescent pattern was then visualized by fluorescence microscopy. Bright fluorescent stripes with a width of 10 μm on a non-fluorescent background could be clearly observed and proved selective binding of the dye to the free amine groups after deprotection (Figure 4.19a). A second irradiation step at 345 nm through a quartz mask with horizontal 50 μm chrome stripes separated by 10 μm cleaved the DEACM and NVoc groups at the exposed areas. These were reacted with Alexa Fluor® 488 succinimidyl ester. A pattern with fluorescent 10 μm horizontal stripes could be observed (Figure 4.19b). The fluorescence contrast at the horizontal pattern is lower than at the vertical pattern. This results were attributed to two reasons: (a) the lower extinction coefficient of Alexa Fluor® 488, and (b) background fluorescence as a consequence of the presence of DEACM (fluorescence maximum at 491 nm).[187] The fluorescence spectrum of DEACM overlaps with the emission spectra of Alexa Fluor® 488, thus causing difficulties in monitoring. This was confirmed by taking fluorescence images of DEACM with an appropriate filter (Figure 4.19d).

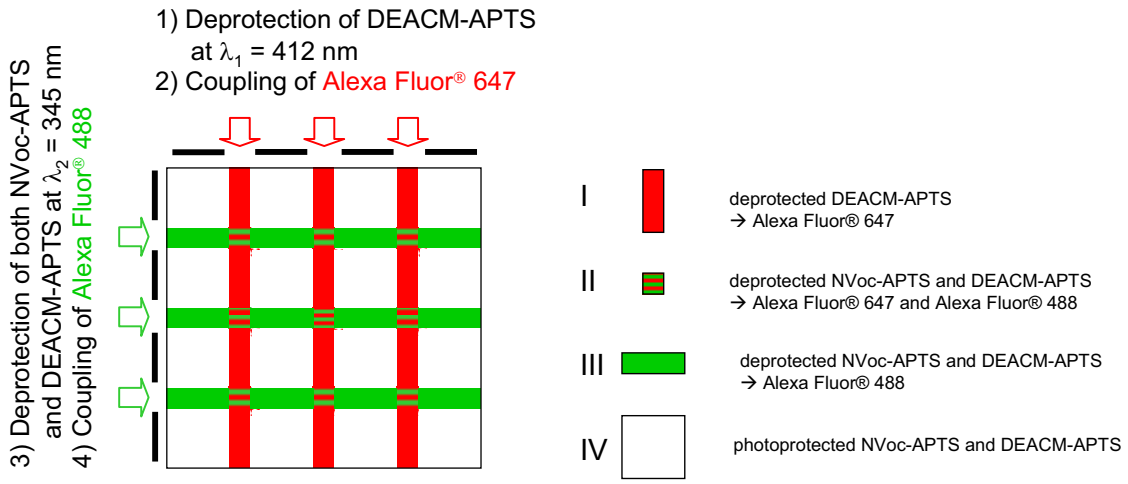

Figure 4.18: Fluorescence pattern expected for NVoc/ DEACM modified substrates after running through the process of wavelength-selective deprotection and subsequent fluorescence dye labeling. Four regions with different fluorescence properties are expected. The regions are also marked in Figure 4.17.

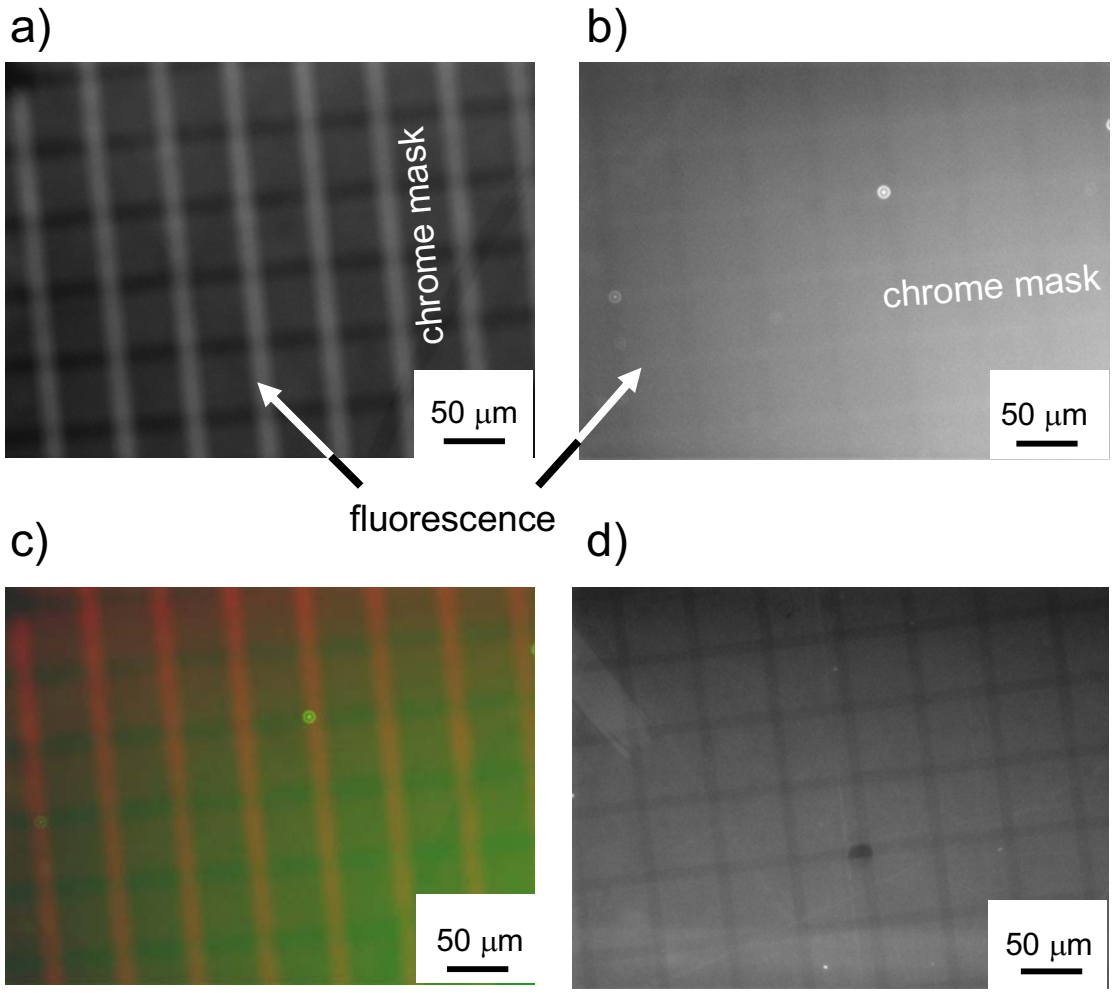

Figure 4.19: Fluorescence microscope images of NVoc- and DEACM-APTS modified substrates that were processed as indicated in Figure 4.17. (a) Fluorescence pattern of Alexa Fluor® 647, (b) fluorescence pattern of Alexa Fluor® 488, (c) overlap of images (a) and (b), (d) fluorescence pattern of DEACM.

4.5 Discussion

The hydrophobic or hydrophilic character of surface layers is determined by the chemical structure of the constituting molecules. Surface layers of silanes **36** and **41** showed similar hydrophobicity, as determined by the contact angle measurements, due to the small differences in their chemical composition. The methylenic spacer and aromatic head-groups causes the increase in the contact angle from 0-10° of bare silica up to 68° measured on mixed layers.

Silanes **36** and **41** seem to have different affinity for the silica surface, as denoted by the obtained values of the surface coverage. Under optimized silanization conditions, silane **41** builds more dense layers, presumably as a consequence of stronger π–interactions between the head groups leading to higher packing densities.[188, 189] The obtained value of the surface coverage for NVoc-APTS is smaller than those reported from silane layers with similar head groups and longer ethyleneglycol spacers ($\sim 3 \times 10^{12}$ molecs mm^{-2}, see Table 3-2).[154] This result agrees with the known tendency of alkyl thiols with long chains to build more compact SAMs than short-chain thiols as a consequence of the strong lateral interaction between the methylenic chains,[190] which seems to be favored also by the ethyleneglycol chain. The obtained surface loadings are smaller than the typical surface density of a SAM of thiols on gold with maximum coverage (4.5×10^{12} molecs mm^{-2}).

Mixed layers obtained by competitive chemisorption from equimolar mixtures of silanes **36** and **41** showed preferential adsorption of silane **41.** This result agrees with the higher surface loading observed in monocomponent layers of **41**.

The relationship between solution and surface compositions is not a trivial question in mixed silane layers. Considering that the silanization reaction is complex and highly sensitive to small variations in the reaction conditions (temperature, solvent, water content and nature of the substrate), predictability of the final composition of mixed layers is difficult. Another factor to take into account is that each silane, depending on its structure, presents different solubility and hydrolysis/ condensation properties which may affect the surface deposition process as in our case. Our optimized experimental

conditions seem to yield mixed surface layers which do not reflect the solution composition but are enriched in DEACM-APTS.

Previous works have demonstrated the potential of wavelength selective photoremovable groups to trigger chemical processes, either in solution of at surfaces, with predefined spatiotemporal resolution.[87, 173, 174] Exploitation of this principle in the biological arena requires the development of photoremovable groups compatible with the special needs of the biological systems. Sensitivity of the photolytic process to wavelengths which do not interfere with the bioactive species is an important requirement. For this purpose, photoactive groups need to be activatable at wavelengths longer than 320 nm. This special need strongly limits the number of suitable candidates. In fact, none of the reported combinations of photoremovable groups which show wavelength sensitivity up to now fulfill this requirement.

Photosensitivity at wavelengths longer than 320 nm means that the chromophore must possess strong UV absorption bands in that spectral range. If two groups with wavelength sensitivity are to be developed, both of them must have non-overlapping absorption maxima in this range. This is the case for NVoc and DEACM groups. NVoc shows an absorption maximum at ~350 nm which tails up to 420 nm. DEACM shows absorption maximum at 389 nm which tails up to 460 nm. Irradiation within the spectral range from 420 to 460 nm should allow cleavage of DEACM without changing NVoc. In fact, we have demonstrated that this is even possible at shorter wavelengths, e.g. 412 nm, at which NVoc absorption is almost negligible and DEACM sensitivity is higher (closeness to λ_{max}).

DEACM possess much higher photosensitivity than NVoc and adsorbs across the whole adsorption spectral range of the NVoc group. This means that DEACM will be more easily cleaved than NVoc within that range and this inhibits the deprotection process to be orthogonal. If a sequential deprotection is desired, DEACM must always be the first group to be addressed. If both groups are present at a surface, it is possible to selectively remove first DEACM by irradiation at 412 nm and then the remaining NVoc by subsequent irradiation at 345 nm.

Having demonstrated the possibility of generating bifunctional patterns, one necessarily

desires to extend the principle to higher levels of functionality. For this purpose, the photoactivity of a Bzn protected silane (Figure 4.20) at the 412 nm was tested in a final experiment. Irradiation for 60 minutes did not change the UV spectrum of the substrate, indicating that the Bnz group is stable under the conditions by which the DEACM photoprotecting group is completely removed (Figure 4.21).

Considering the demonstrated chromatic orthogonality of NVoc and Bzn,[87, 171, 191] and our obtained results with NVoc and DEACM, sophisticated patterned surfaces with up to three sites with different chemistries can be envisioned. Starting with the cleavage of DEACM (at 412 nm), the sequence for the removal of NVoc (at 345 nm) and Bnz (at 254 nm) is variable due to their chromatic orthogonality.

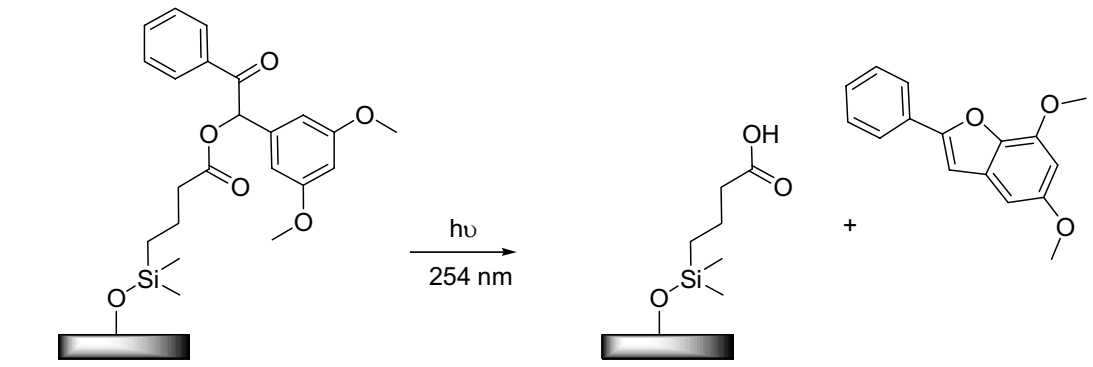

Figure 4.20: Photochemical deprotection reaction of immobilized Bnz-CPTS on the surface yielding a free carboxylic acid. Substrates were kindly provided by Dr. J. M. Alonso (MPI for Metals Research, Stuttgart).

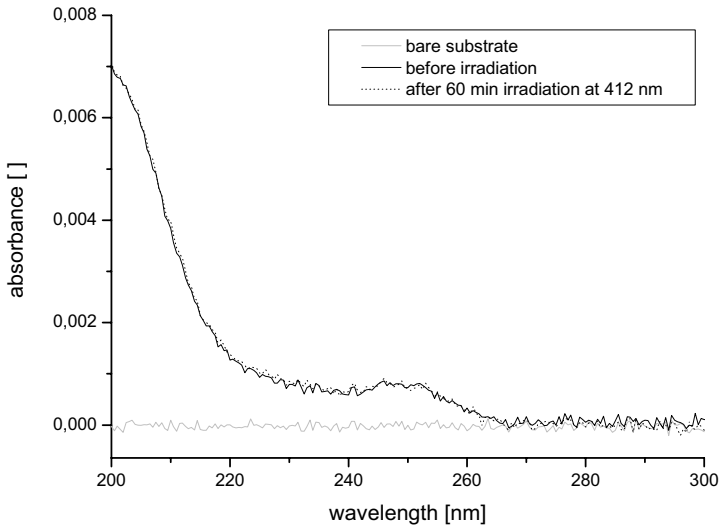

Figure 4.21: UV absorbance spectra of Bnz-CPTS modified quartz substrate before irradiation and after irradiation at 412 nm for 60 min.

.

Chapter 5

Surface tailored magnetite nanoparticles for functional protein anchoring via mixed alkoxysilane layers

5.1 Introduction

Magnetic nanoparticles have been extensively studied in biomedicine because of their potential applications as contrast enhancement agents for magnetic resonance imaging; careers for therapeutic drug, gene and radionucleide delivery; in radio frequency methods for the catabolism of tumours via hyperthermia, or in magnetic separation of biological entities.[3, 12, 192, 193] Magnetic separation *via* magnetic nanoparticles offers fast, gentle, scaleable and easily automated capture and isolation of targets (proteins, nucleic acids, cells etc.) from solution, and has demonstrated credibility not only in cell sorting or clinical diagnostics, but also in food analysis,[7, 8] minerals processing or wastewater treatment. For this purpose, super paramagnetic iron oxide nanoparticles (SPIONs) are typically used. Superparamagnetic materials are easily magnetized in the presence of a magnetic field, but show no remanent magnetization once the field is removed, i.e. they

are free from magnetic memory. When a field is applied to a suspension of SPIONs, they become magnetized and tend to agglomerate readily under the influence of inter-particle forces, allowing separation of the particles from the supernatant. When the field is removed, the absence of magnetic memory allows their easy re-dispersion in a different solvent to allow sorption and desorption processes to occur, as well as the release of agglomerate entrained targets. The very high surface area to volume ratio of the nanoparticles results in high loading capacity, rapid adsorption/ desorption kinetics and, consequently, in high efficiency of the separation process.

The affinity of the magnetic carier for the target in a biomagnetic separation process is usually controlled by coating the particle surface with organic layers containing functional units such as recognition sites, catalytic elements, or bioactive components. This can be achieved by either introducing functional surface agents in the solution during nanoparticle synthesis and precipitation,[194] or by adsorbing or reacting molecules on the magnetite particle surface after synthesis. In the latter case, diverse strategies have been used to coat SPIONs, including layer-by-layer deposition of electrolytes,[195] grafting polymers,[196] adsorption of surfactant molecules (eg. phospholipids,[1, 197] alkylphosphates,[198] fatty acids,[199] or dopamine or catechol based anchors[200]), or reaction with organofunctional silane coupling agents.[74, 201-203] In all cases, a single molecular entity has been used for coating and the resulting monofunctional layers show important limitations in terms of efficiency and selectivity of the separation process.[204]

Advances in the application and efficiency of SPIONs for bioseparations require advanced coatings. This is especially important when the application involves delicate biomolecular targets like proteins. The surface layer needs to be engineered to present high affinity and specificity for the targeted protein, and to retain protein function in its surface immobilized state. This requires the use of protein-repellent layers decorated with an optimized number of receptors in order to maximize the target binding capacity, but avoid loss of function by non-specific interactions or steric crowding, or irreversible protein attachment to the surface. Different methods have been used to avoid non-specific interactions of proteins with organic layers including blocking non-specific binding sites with BSA, or modifying the protein surface or the substrate surface with protein-repellent agents like oligo- and poly(ethyleneglycol) (OEG or PEG) or

dextranes.[46, 117] Incorporation of PEG chains into the functional surface seems to be the best method, since it allows flexibility in the compositional design of the layer by mixing the EG with other functionalities in desired proportions, and to adjust the surface properties precisely. This can be performed by direct coupling of the surface active functionality through OEG linkers, by coadsorption from solution of OEG and functional molecules (either in parallel[125-127] or sequential[128] surface reactions), or the use of branched surface coupling agents containing protein repellent and protein attractive arms.[67, 121-124]

5.2 Objectives

In this work, we demonstrate how SPIONs can be successfully coated with mixed layers of PEG chains and reactive amine functionalities by treating the surface with mixtures of silanes bearing the corresponding functional groups. Mixtures of amine-terminated and OEG silanes with different chain lengths and OH or OMe terminal groups have been tested to identify the optimum surface composition for the highest specificity and efficiency of the binding event. The structures of the silanes are represented in Figure 5.1. In general, they are -OH, -OMe and -NH_2 terminated silanes with OEG spacers with different lengths. Only silane **S1** has a short trimethylene spacer instead of an OEG chain. Issues like the correlation between solution composition and surface composition have been carefully studied, since different silanes may present different hydrolysis and condensation kinetics in solution under identical experimental conditions, and this can lead to different deposition rates of the components on the surface layer. The influence of the reaction conditions (temperature, solvent, water content of the system and nature of substrate) in the final surface composition has also being analyzed, as well as the stability of the final coatings. We demonstrate how this simple and cheap strategy renders biocompatible coatings with good performance in protein separation processes.

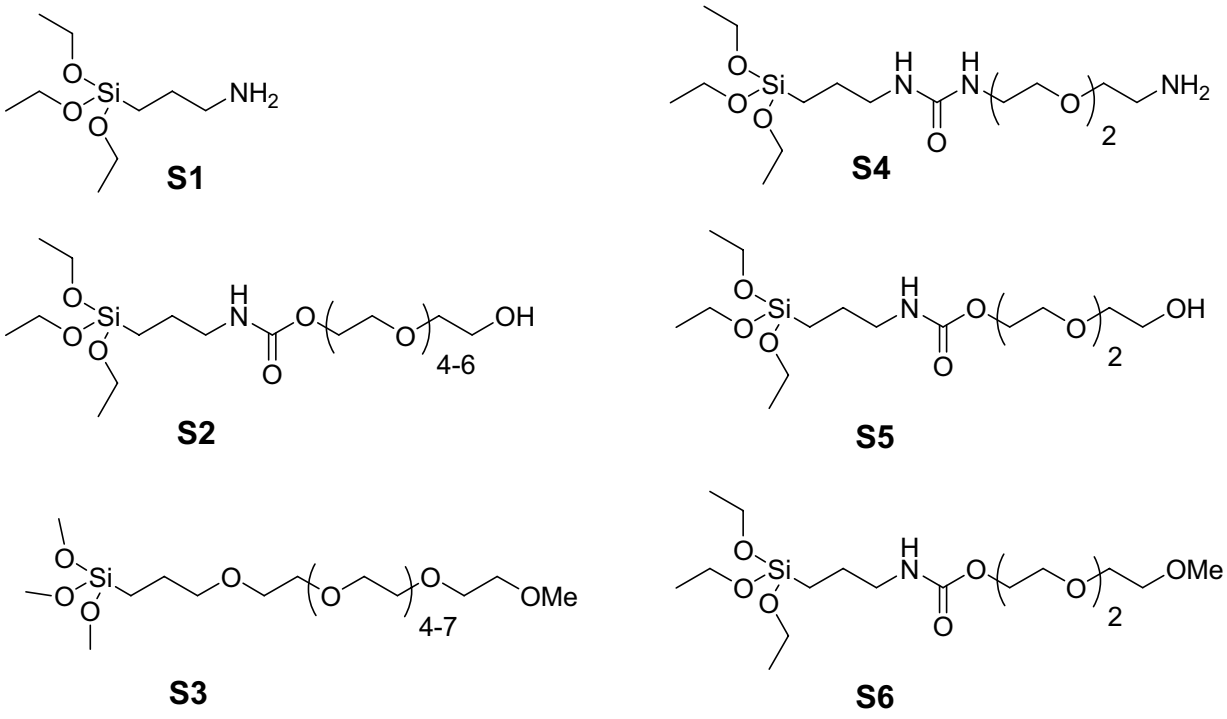

Figure 5.1: Structure of commercial (**S1**, **S2**, **S3**) and synthesized (**S4**, **S5**, **S6**) functional alkoxysilanes.

5.3 Experimental

Synthesis

Silanes **S1** to **S3** are commercial and silanes **S4** to **S6** were successfully synthesized and characterized as described in Appendix section A.4.1.

Surface modification of magnetic nanoparticles and characterization

Plain magnetic iron oxide particles (200 nm) in acqueous suspension were modified with mixtures of aminosilanes **S1** or **S4** with silanes **S2**, **S3**, **S5** or **S6** in different molar ratios. The reaction conditions for the surface modification were obtained from the literature.[87] THF as solvent, silane concentrations of 2% w/V, temperatures of 70 °C and reaction times of 17.5 hours were kept constant for all solution phase silanizations. Only one batch of particles modified with silane **S1** was prepared in water solution (instead of THF) for the storage stability measurements.

The particle concentration of the suspensions was determined by dry weight estimation of a sample of known volume. After the modification process and washing procedures, the particles were partitioned into aliquots of 2 mg in aqueous suspension and stored at -20°C.

Colorimetric assay of the amine density

The number of amine groups on the surface was determined in a colorimetric assay as represented in Figure 5.2. The procedure involves their reaction with an UV sensitive coupling reagent (4-nitrobenzaldehyde).[205] Under anhydrous conditions, imine formation occurs between the surface amine groups and nitrobenzaldehyde. Excess of nitrobenzaldehyde is removed by anhydrous washing, not affecting the nitrobenzaldehyde coupled to the surface. Hydrolyzation in the presence of water removes the nitrobenzaldehyde from the surface and allows quantification by UV spectroscopy. The amount of nitrobenzaldehyde coupled to the surface is directly proportional to the number of surface amine groups.

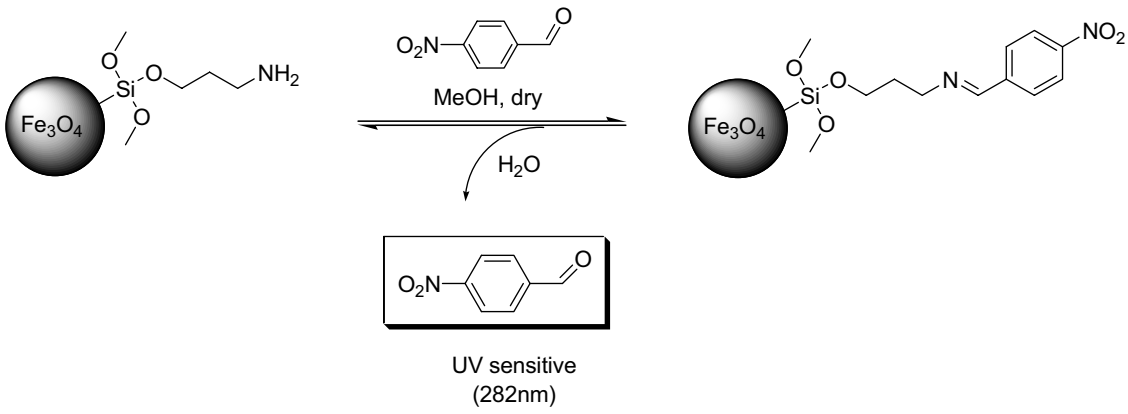

Figure 5.2: Colorimetric assay to determine the surface amine density.

Determination of DNA and proteins in adsorption and binding experiments

The amount of DNA/ protein adsorbed onto the particles can be calculated from the difference between initial amount and the quantity remaining in the supernatant after the adsorption process.

DNA amounts in solution were quantified by UV spectroscopy (absorbance at 260 nm).

Protein concentrations were determined by BCA assay. The BCA (bicinchoninic acid) detection method is based on the capability of proteins to reduce Cu^{2+} to Cu^{1+} in alkaline medium, followed by highly sensitive and selective colorimetric detection of the cuprous cation by complexation with bicinchoninic acid (Figure 5.3).

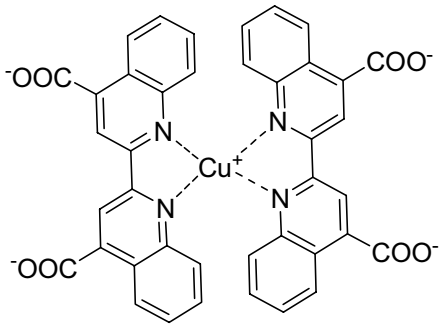

BCA-Cu^{+}
complex
(λ_{max} = 570 nm)

Figure 5.3: Colorimetric detection of cuprous cation by formation of a colored complex with two bichinchoninic acid molecules (BCA assay).

5.4 Results and discussion

5.4.1 Synthesis of silanes

Silanes **S4**, **S5** and **S6** were synthesized by reaction of 3-isocyanato propyltriethoxysilane with 2,2-ethylendioxy-bis-ethylamine, triethylene glycol and triethyleneglycol monomethylether, respectively (Figure 5.4). Quantitative carbamide (urea) formation (to **S4**) was obtained after 1 hour reaction time. The reaction with the hydroxyl groups yielding urethane bonds (in **S5** and **S6**) required addition of dibutyltin dilaurate as catalyst.

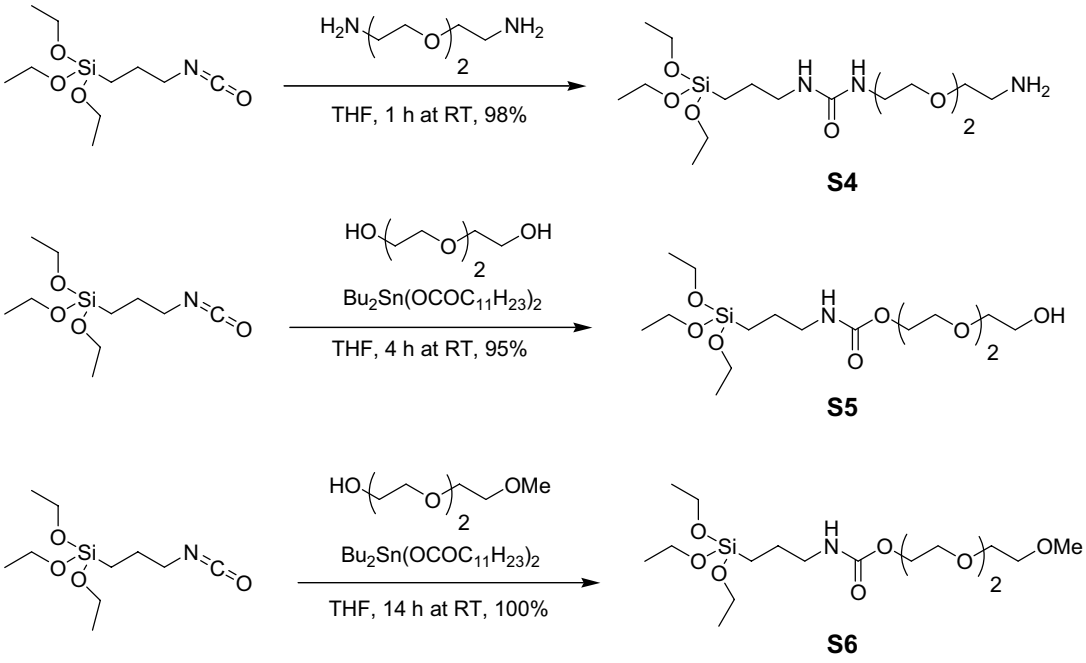

Figure 5.4: Synthesis of silanes **S4** to **S6**.

Since 2,2-ethylendioxy-bis-ethylamine and triethylene glycol possess two equivalent endgroups which could react likewise with the isocyanate, triethylene glycol based reactants were used in twofold molar excess with respect to the amount of silane. After complete consumption of these components, the solvent was removed under reduced pressure and the crude product used for surface modification without further purification. The excess of triethyleneglycol based starting material present in the crude product (1:1 molar ratio with respect to the desired silane) is not expected to react with the particles' surface.

5.4.2 Surface modification

Surface modification reaction

Silanes **S1** to **S6** and mixtures of them in different molar ratios were used to modify the magnetite nanoparticles. First, the silanization conditions were optimized in order to maximize the density of surface functional groups. Silanization of magnetite nanoparticles in solution has been reported to depend on the temperature, solvent and time selected for reaction.[201] According to published results, dense and stable surface layers of silane **S1** can be obtained using water or THF/ water as solvent, reaction temperatures above 50°C, and reaction times around 24 hours.[201] Our first experiments using silane **S1** confirmed these results, as shown in Figure 5.5. Surface amine density (analyzed by a colorimetric assay) after silanization with **S1** at 70°C for 24 hours in water (140 $\mu mol_{NH2}\ g^{-1}$) was 3 times higher than in THF (44 $\mu mol_{NH2}\ g^{-1}$), and almost 5 times higher than at 50°C (25 $\mu mol_{NH2}\ g^{-1}$).[201] However, silanes **S2** to **S6** (containing OEG spacers) and their condensation products showed limited solubility in water. Precipitation of, presumably, condensation products was detected already after short reaction times. For this reason, we performed all silanization reactions in THF at 70°C. In these conditions, the silanes and their hydrolysis and condensation products showed excellent solubility and no sign of insoluble aggregate formation during the 24 hours of reaction time was observed in any of the experiments. In general, no sign of particle aggregation phenomena due to formation of interparticle cross-linking through siloxane 'bridges' as a consequence of uncontrolled reaction conditions was detected by visualization. No significant differences in the sedimentation times or magnetic response times between unmodified and modified particles could be detected either.

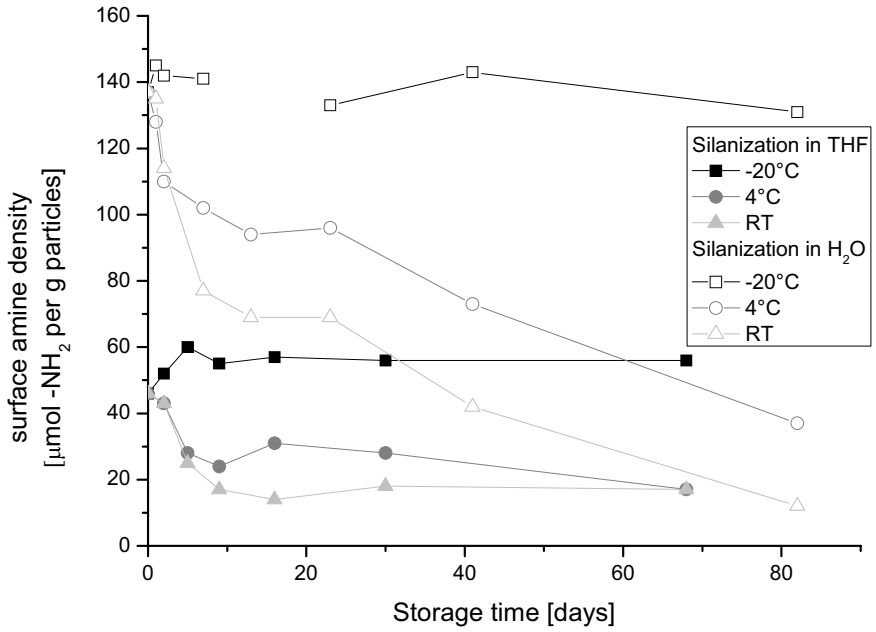

Figure 5.5: Density of surface amine groups of nanoparticles modified with silane **S1** after silanization in water and in THF at 70°C, and stability of the silane layer during storage in water at three different temperatures: room temperature, 4°C and -20°C (frozen state). Higher surface amine densities are obtained when performing the silanization reaction in water. Storage of the particles at -20°C does not seem to affect the silane layer.

Stability of the silane layer

The stability of silane coatings in water is always a concern. Hydrolysis of the Si-O-Si bonds, and consequently loss of the functional silane layer, could occur and would affect the performance of the silanized particles in the biological application. The kinetic of this process is expected to be accelerated by the temperature. We checked the stability of water suspensions of the surface modified magnetite nanoparticles at different temperatures (20 °C, 4 °C, -20 °C) after different silanization conditions (in water and THF) and storage times between 1 and 82 days. The progress of the detrimental hydrolysis reaction was followed by determining the surface amine density and Figure 5.5 shows the results. A significant decrease in the surface amine density was detected already after 2 days of storage at temperatures 20 °C or 4 °C. This process seems to be faster during the first 8 days. Storage of the suspension in frozen state (-20 °C) does not seem to affect the silane layer, at least during 3 months. This tendency could be observed in the particles modified with silane **S1** in water and in THF, and also

in the case of mixed silane layers (data not shown). For this reason, particles were immediately stored in frozen state once modified.

Surface density of amine groups in mixed layers

The surface composition of the mixed silane layers was analyzed by determining the surface amine density *via* a colorimetric method (see A.4.2 for details). Results are given in Figure 5.6. Monofunctionalized nanoparticles with aminosilanes **S1** or **S4** showed similar values of the amine density. It seems that the differences in the nature and length of the spacers do not lead to significant differences in the surface modification process. Similarly, mixed layers of aminosilanes **S1** or **S4** with the OMe or OH terminated silanes **S2**, **S3**, **S5** or **S6** gave also equivalent surface densities of amine groups. These results indicate that all silanes used have similar affinities for the magnetite surface, independently of their terminal functionality (-NH_2, -OH or -OMe), or their EG chain length. This result is non trivial, since surface modification by competitive chemisorption from a feeding solution may yield different ratios of the intervening components at the surface depending on their molecular structure. In fact, surface modification by grafting polymer chains of different lengths has rendered surfaces compositions enriched in the short chain component as a consequence of long chains already attached to the surface sterically shielding the remaining surface reactive sites.[206] On the other hand, long chain alkyl thiols usually form denser SAMs than short chain thiols as a consequence of stronger lateral attraction between the alkyl spacers.[190] In our case, the surface composition does not seem to be determined by the length of the spacer, but seems to reflect the solution composition. In fact, the surface amine density correlates linearly with the molar fraction of aminosilane used in the surface modification process in all mixed layers, as demonstrated in Figure 5.6. Better correlation was found when the molar fractions of aminosilanes **S1** or **S4** in solution was < 0.4. At higher molar fractions of aminosilane in solution significant scattering of data was observed in all mixtures. We do not have an explanation for this fact at this moment.

Considering that the silanization reaction is complex and highly sensitive to small variations in the reaction conditions (temperature, solvent, water content and nature of the substrate), the correlation between the surface composition and solution composition

of mixed layers is not trivial. Another factor to take into account is that each silane, depending on its structure, presents different solubility and hydrolysis/ condensation properties which may affect the surface deposition process. In spite of these issues, the optimized experimental conditions seem to yield mixed surface layers which reflect the solution composition.

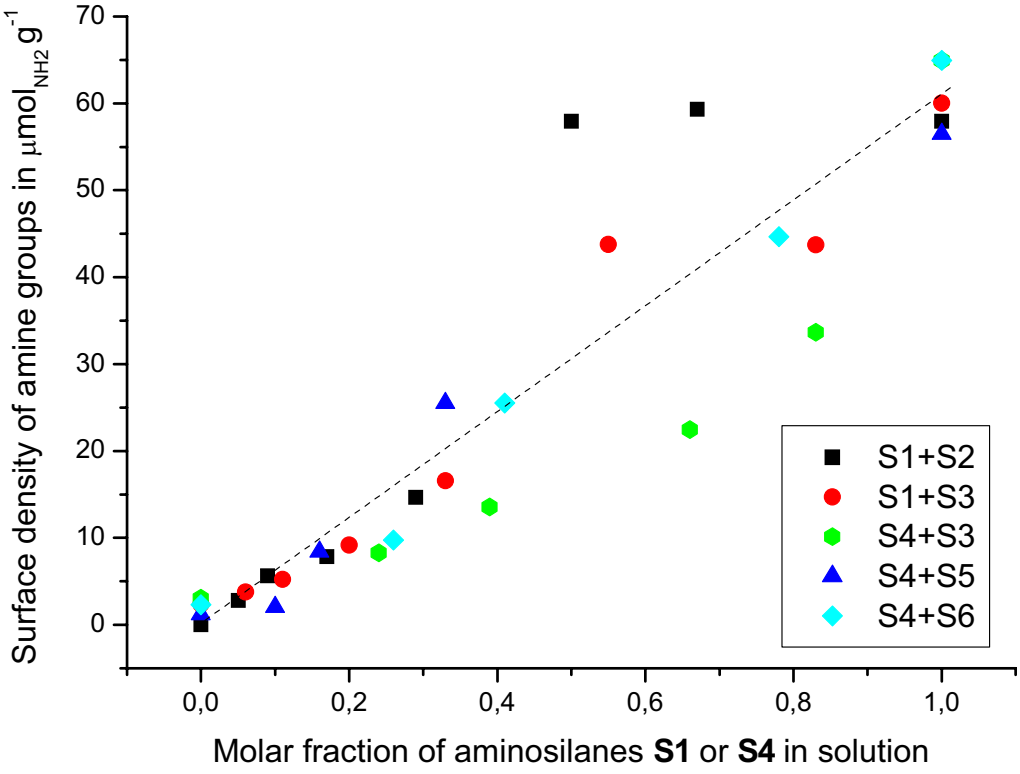

Figure 5.6: Density of amine groups of different mixtures **S1+ S2, S1+ S3, S4+ S3, S4+ S5** and **S4+ S6**.

5.4.3 Surface charge dependent adsorption of polyanions (DNA) onto $-NH_2$ modified nanoparticles

Amine modified surfaces are positively charged at pH below 9 due to the protonation of the amine group and are likely to adsorb negatively charged targets like DNA (phosphate groups of the DNA chain are fully deprotonated at pH < 8). Adsorption is expected to be driven by electrostatic interactions, and to be affected by the surface charge density (determined by the surface amine density and the pH) and the ionic strength of the medium.[207-209] The results of the adsorption of salmon sperm DNA on our amine modified nanoparticles with different surface compositions under chaotropic conditions at pH 8 are shown in Figure 5.7 and Figure 5.8. First, the adsorption capacity of the supports was identified by performing adsorption experiments using ~50 μg DNA and different particle concentrations. Figure 5.7 shows that 0.01 mg nanoparticles modified with aminosilane **S1** represented enough surface charge to adsorb ~40 μg DNA. The results of the adsorption of ~20 μg DNA onto 0.005 mg nanoparticles modified with mixtures of silanes **S1** and **S2** is shown in Figure 5.8. A clear decrease in the adsorbed amount of DNA was observed when the surface amine groups are diluted with the uncharged (OH terminated) silane **S2**. The reduction in the adsorbed DNA quantity does not correlate linearly with the density of amine groups. This could be a consequence of the different molecular lengths of silanes **S1** and **S2** which allows only partial exposure of the charged amine groups of the shorter silane **S1** at the particle surface.

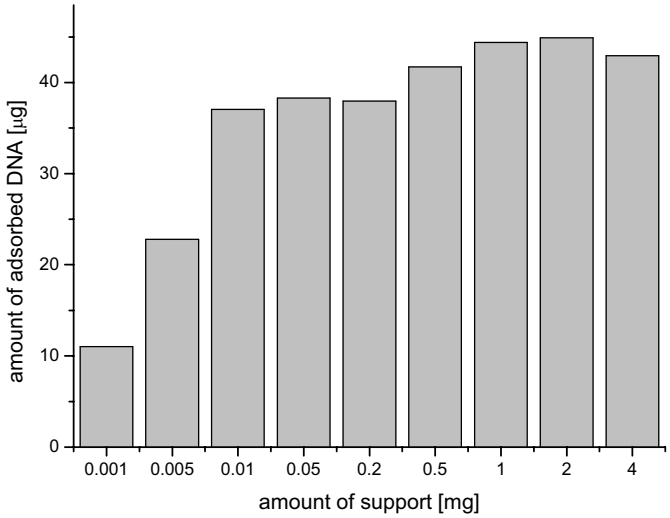

Figure 5.7: Adsorption of salmon sperm DNA onto different amounts of magnetite nanoparticles modified with silane **S1**. The initial amount of salmon sperm DNA in solution was 50 µg.

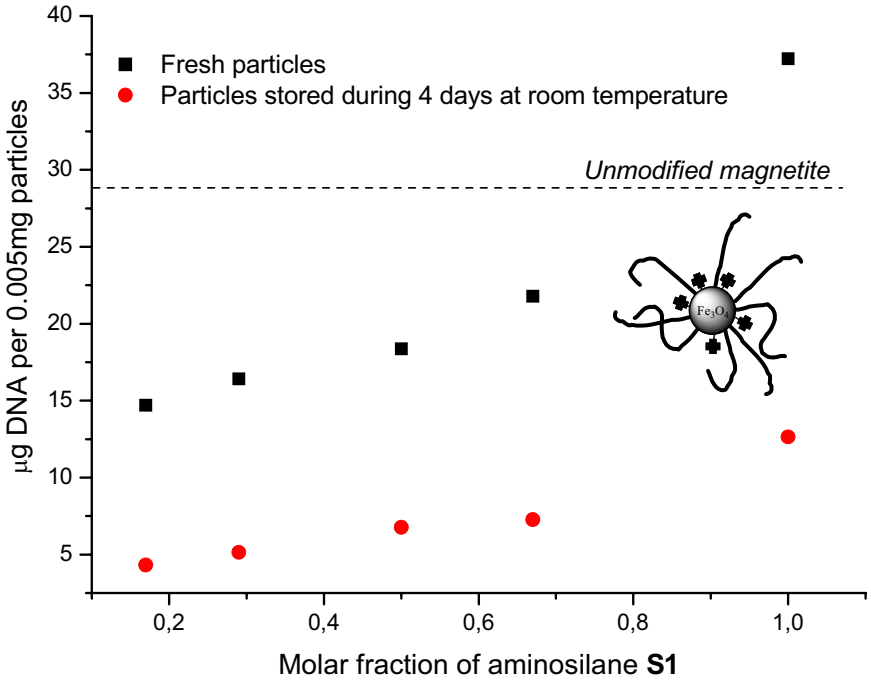

Figure 5.8: Adsorption of salmon sperm DNA onto magnetite nanoparticles modified with different mixtures of silanes **S1** and **S2**. Dilution of surface charge (either by lowering the molar fraction of silane **S1**, or after hydrolysis of the silane layer during storage at 20°C) results in a lower adsorption capacity of the supports.

The loss in the surface amine density during storage at temperatures above 4°C also affects the DNA adsorption capacity of the particles. In Figure 5.8 the results of a DNA adsorption experiment performed with nanoparticles which have been stored at 20°C during 4 days is presented. It can be seen that the amount of adsorbed DNA is dramatically reduced. Surprisingly, the adsorption capacity of the aged particles does not reach that of pure magnetite (~30 μg_{DNA} on 0.005 mg support). This result indicates that the ageing process may not only be due to hydrolysis and loss of the silane from the surface, but to degradation process concerning only the amine groups.

Immobilization of proteins onto OEG modified surfaces with different densities of surface amine groups

The optimum layer composition for protein immobilization was determined by studying the capture of proteins from solution using nanoparticles modified with layers containing different molar ratios of $-NH_2$ and -OMe terminated silanes. Different coupling protocols were tested, and the efficiency and selectivity of the subsequent immobilization process were analyzed and compared. Initially, Bovine Serum Albumin (BSA) was covalently coupled to particles modified with silanes **S1+S3, S4+S3** and **S4+S6** *via* glutaraldehyde activation, and the results were compared to non-specific adsorption of the protein onto the aminofunctionalized surface. Results are shown in Figure 5.9 in terms of the amount of immobilized protein (in μg) per mg of support. High amounts of protein (~40 μg mg^{-1}) could be covalently immobilized onto particles modified with monocomponent layers of the aminosilane **S1** after glutaraldehyde modification. In absence of the glutaraldehyde linker, significant amounts of BSA were also adsorbed onto the amino surface (~25 μg mg^{-1}) due to undesired non-specific electrostatic interaction of negatively charged regions of the protein with the positively charged amino surface. Particles modified with the aminosilane **S4,** with the incorporated TEG spacer, show much lower non-specific adsorption of the protein (~4 μg mg^{-1}) and were able to covalent immobilize ~13 μg mg^{-1} BSA *via* glutaraldehyde coupling. It is important to notice that silane **S4** contains only three EG units in the spacer which seem to be enough to significantly suppress non-specific adsorption of the BSA protein on our surface layers. Particles modified with –OMe terminated silanes **S3** and **S6** did not show significant affinity for the protein

(0 - 2 μg mg^{-1}) either with our without the glutaraldehyde activation step, as expected from their inertness and protein repellent properties of the EG layer.

Mixed layers of silanes **S1+S3** and **S4+S3** show very reduced affinity for the protein either as amine- or as aldehyde functionalized surfaces across the whole compositional range (Figure 5.9). We attribute the reduced immobilization potential of these mixed layers to the differences in length between the short aminosilanes **S1** (0.6 nm) and **S4** (1.9 nm) and the longer silane **S3** (3.4 nm in average), which leaves the amine groups buried in the EG layer and unable to reach the reactive groups at the protein surface, even after elongation with the glutaraldehyde linker (0.6 nm). In fact, mixed layers with silanes **S4+S6**, which have similar molecular lengths, were able to covalently immobilize increasing amounts of BSA as the ratio of aminosilane **S4** in the layer increased.

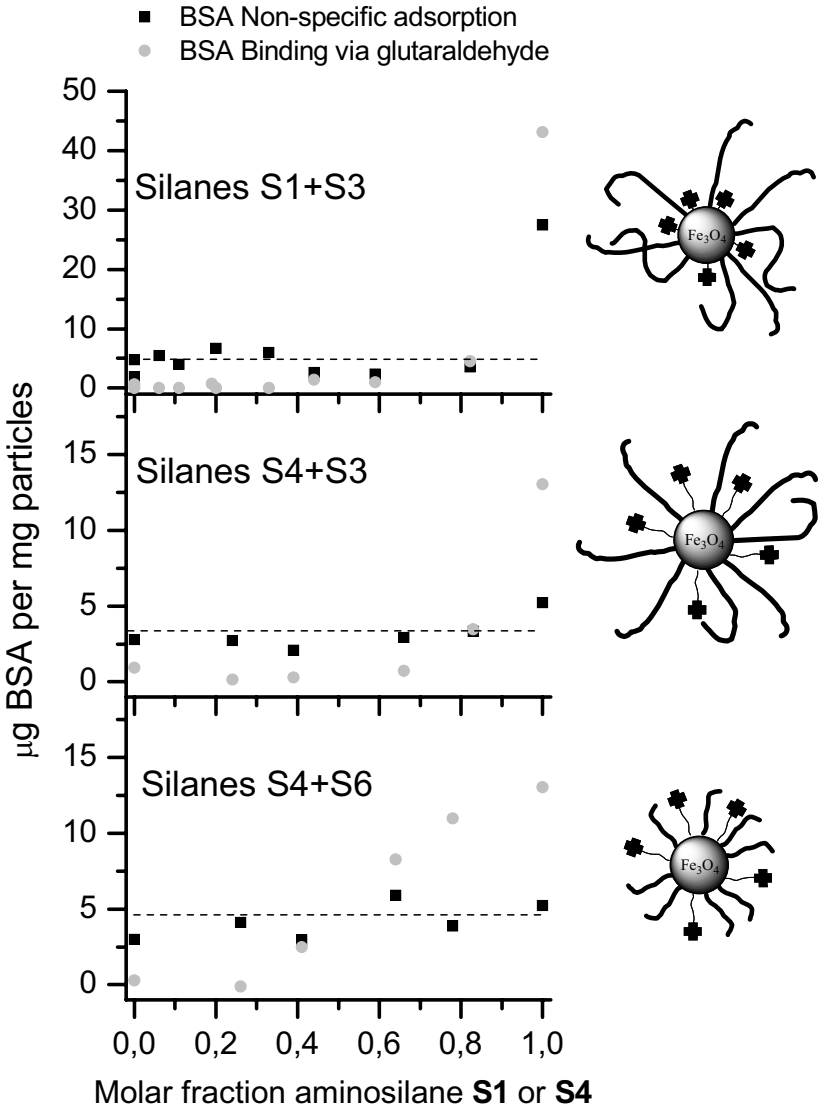

Figure 5.9: BSA adsorption and binding onto nanoparticles with different compositions. Note the different scales in the y axes.

In a second protein coupling experiment, the binding of streptavidin to biotinylated particles was tested. For this purpose, nanoparticles modified with silanes **S1**+**S3**, **S4**+**S3** and **S4**+**S6** in different ratios were first reacted with (+)-Biotin N-hydroxysuccinimidyl ester and then loaded with streptavidin. Results are shown in Figure 5.10. Biotinylated nanoparticles modified with silanes **S1+S3** showed increasing binding capacity of the protein with increasing surface content of the aminosilane **S1**. This increase was not linear and reached a saturation value of ~8 μg mg^{-1} at an amino

molar ratio of 0.6. Incorporation of additional reactive groups to the surface layer does not improve the binding performance any further. Nanoparticles modified with silanes **S4+S3** showed a similar tendency but reached higher saturation levels (22 μg mg^{-1}) at lower molar fractions of aminosilane (0.4). These results contrast with those obtained in the covalent immobilization of BSA, where incorporation of the non-reactive silane **S3** to the surface layer almost completely inhibited protein binding within the whole range of concentration. Coupling (+)-Biotin N-hydroxysuccinimidyl ester to the amino groups elongates the reactive sites at the surface about 0.9 nm, and this seems to be enough for streptavidin binding. In fact, binding was found to be more efficient onto particles modified with silanes **S4+S3**, presumably because of the smaller difference in their molecular lengths (1.9 and 3.4 nm respectively). Streptavidin binding on nanoparticles modified with silanes **S4+S6**, with similar molecular lengths, reached the saturation level already at 0.2 molar fraction of the aminosilane, presumably as a consequence of the full exposure of the attached biotin groups. The value of streptavidin loading at the saturation level is analogous to the saturation value achieved with silanes **S4+S3** (23 μg mg^{-1}). It is important to note that higher protein loadings were achieved with streptavidin, *via* recognition of biotins at the surface of the nanoparticles, than with BSA *via* glutaraldehyde mediated covalent coupling.

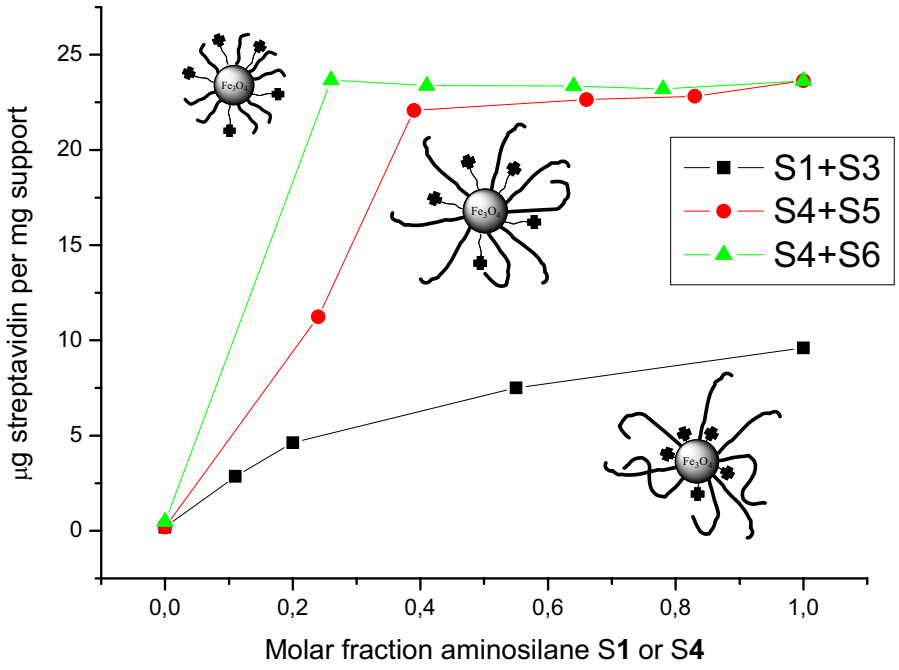

Figure 5.10: Coupling streptavidin to biotinylated particles with different surface concentration of active groups.

Proteins are big molecules which block large areas of the nanoparticle surface when they get immobilized. Typically, proteins attach to surface through 2 to 4 binding sites. This means that only a small fraction of the available surface reactive groups are usually required for protein immobilization. Surface modification with higher density of reactive sites does not necessarily improve the immobilization performance any further because the reactive groups are blocked underneath the adsorbed protein. Moreover, loss of immobilization potential may also occur as a consequence of steric crowding of immobilized receptors, or of non-specific interactions with the protein. Dilution of surface reactive groups by coadsorption of non-reactive chains into the surface layers is then necessary and has been already demonstrated in SAMs of thiols on gold as a method to optimize surface coverage and protein loading capacity. A 0.1 molar concentration of reactive thiol in the SAM has been proposed as optimum surface composition for functional and specific protein binding.[190] Our results with silane layers show that the optimum dilution of reactive groups for maximum binding depends on several factors, like the packing density of reactive groups at the surface, the access of

the reactive groups to the binding site at the protein (determined by the molecular length of the surface coupling agents), and the efficiency of the coupling method. In the following, we will discuss these issues.

SAMs of thiols are easily obtained as highly ordered and tightly packed surface layers with high density of surface groups. Trifunctional silanes, as a consequence of their ability to condensate and form aggregates, do not easily form such regular monolayers, if at all, and usually present lower densities of surface functional groups.[154] Assuming the formation of submonolayers, molar silane solution fractions higher than 0.1 are required to achieve the theoretically optimum of a 0.1 molar concentration of reactive silane at the surface. This hypothesis agrees with our experimental observations.

Good accessibility of the reactive sites at the surface for protein binding allows achievement of the maximum protein loading at lower surface density of reactive sites. Surface layers of silanes **S4+S6**, where the reactive sites point out of the EG layer achieve maximum streptavidin loading at 0.2 molar fraction of the aminosilane, whereas molar fractions of 0.4 or 0.6 are required in surface layers of silanes **S4+S3** and **S1+S3** respectively, where the reactive sites are embedded into the EG layer.

Finally, protein surface loading depends on the efficiency of the coupling method in term of stability of the binding process. The high affinity of the streptavidin-biotin complex ensures that almost all exposed biotin sites will immediately bind to the protein. On the contrary, covalent binding of BSA to aldehyde modified surfaces involve the formation of labile imine bonds which can easily be hydrolyzed. This explains why smaller quantities of BSA were immobilized on the nanoparticles, and no saturation level was achieved.

Summary and conclusions

Photoremovable caging groups attached to surface layers can be used to generate chemical patterns on planar substrates. If the caged functionality can interact with a complementary species, such substrates can be used for capturing and site-selective immobilizing specific biomolecular targets from solution.

Different wavelength-sensitive cages have been identified to protect different surface active groups to render surfaces with several latent and independently addressable functional states. In particular, the possibility of generating trifunctional surfaces based on DEACM, NVoc and Bzn cages has been demonstrated. Sequential irradiation of such surfaces through different masks generates surface patterns with complex compositions which can be used for immobilizing different proteins onto selected microregions of the surface. Additional application of these surfaces for the study and activation of cellular processes at surfaces are envisioned.

The protein immobilization efficiency and selectivity depends not only on the nature of the photoactivated ligand, but also on the surface design. Protein resistant coatings (eg. long EG chains) are required to suppress non-specific attachment of the target and to retain its biological activity in the surface immobilized state. Different molecular architectures of the EG chain can be selected and render different surface properties.

The following tendencies were observed in this study when using EG chains coupled to silica surfaces through triethoxysilanes:

(i) Surface layers containing linear EG chains form more dense layers (higher ligand density) than branched molecules.

(ii) In spite of a general lower ligand density, surface layers of branched silanes are able to immobilize higher amounts of proteins. The branched structure seems to improve the accessibility of the ligand for binding.

(iii) Hydrophobic interactions between alkyl spacers in branched silanes do not promote more dense packing, as expected from results reported on SAMs of long chain alkyl thiols. The presence of hydrophobic units in the layer increases non-specific adsorption of targets.

(iv) In mixed layers, ligand density can be varied by modifying the molar ratio of the active and inert component of the feeding solution, or by using components of different molecular length. If the inert component is longer than the active one, the ligand will be “buried” in a non-reactive layer and binding will be hindered.

Appendix (Experimental Part)

A.1 General

A.1.1 Chemicals and materials

Chemicals and solvents were purchased from Fluka Chemie AG (Taufkirchen, Germany), Fisher Scientific UK Ltd. (Loughborough, Leics. GB), Merck KGaA (Darmstadt, Germany), Sigma-Aldrich Chemie GmbH (Steinheim, Germany), and ABCR (Karlsruhe, Germany). Alkoxysilanes **S1**, **S2, S3** and 3-isocyanato propyltriethoxysilane were purchased from ABCR (Karlsruhe, Germany), BSA and IgGs were purchased from Sigma-Aldrich Chemie GmbH (Steinheim, Germany), streptavidin from Promega (Madison, Wisconsin, USA), the ONDs from Proligo France SAS (Paris, France), NHS-biotin from CALBIOCHEM® (San Diego, California, USA) and the BCA Protein Assay Kit from Pierce (Rockford, Illinois, USA). Solvents had p.a. purity and were used as received or dried over molecular sieves (4Å) for anhydrous reactions. Dry THF was obtained by distillation over sodium with benzophenone as indicator.

Ultrapure Milli-Q water (deionized water, filtered through 0.2 μm pores using a Milli-Q sytem from Millipore Corporation; resistivity: 18.2 MΩ cm at 25 °C) was used for buffer preparation, in the magnetic particle experiments and the surface modifications.

Fluorescent dyes

The fluorescent dyes Alexa Fluor® 647 carboxylic acid succinimidyl ester and Alexa Fluor® 488 carboxylic acid succinimidyl ester were purchased from invitrogen (Eugene, Oregon USA). Their spectral characteristics are given in Table 5-1.

Table 5-1: Spectral characteristics of used fluorescent dyes.

dye	Absorbance	Emission	
	$\lambda_{max, abs}$, [nm]	$\lambda_{max, em}$, [nm]	molecular extinction coefficient ε, [$cm^{-1}M^{-1}$]
Alexa Fluor® 647	650 nm	665 nm	239.000
Alexa Fluor® 488	495 nm	519 nm	71.000

Magnetic particles

Plain magnetic iron oxide particles (200 nm, spheric aggregates of 6-18 nm sized subparticles) were purchased in aqueous suspension from micromod Partikeltechnologie GmbH (Rostock-Warnemuende, Germany).

Solid substrates

Quartz slides (SUPRASIL®1) with a thickness of 1 mm were purchased from Heraeus Quarzglas (Hanau, Germany). Silicon wafers in (100) orientations were provided by Crystec (Berlin, Germany). For the experiments, pieces of 2.5 × 1 cm of both substrates were used.

Buffer composition

PBS buffer (pH 7.2): 136 mM NaCl, 3 mM KCl, 10 mM Na_2HPO_4, 2 mM KH_2PO_4;
PBS-0.01% Triton X-100: PBS (pH 7.2), 0.01% w/V Triton X-100;
10× TEN buffer (pH 8.0): 0.1 M Tris-Cl, 0.01 M EDTA, 1 M NaCl;
Tris-Cl: Tris base in H_20, adjusted to the desired pH.

20× SSC buffer: 3.0 M NaCl, 0.3 M sodium citrate; 1×SSC buffer was prepared from this stock solution by dilution with Milli-Q-water.

Buffers were sterilized by autoclaving (20 minutes at 121 °C).

A.1.2 Purification methods

Chromatography

Analytical thin layer chromatography was performed in TLC plates (ALUGRAM® SIL G/ UV_{254}) from Macherey-Nagel (Düren, Germany). Preparative thin layer chromatography was carried out using pre-coated TLC plates (SIL G-200 UV_{254}) from Macherey-Nagel (Düren, Germany). Preparative column chromatography and flash column chromatography were carried out using silica gel (60Å pore size, 63-200 μm particle size) from Merck KGaA (Darmstadt, Germany). The components were visualized on TLC plates using a UV lamp, iodine or potassium permangate solution.

Preparation of $KMnO_4$ developer: 40 g K_2CO_3 are dissolved in 100 ml distilled water. After addition of 10 ml NaOH solution (5% w/ V) and 6 g $KMnO_4$, distilled water is added to a final volume of 1 l.

Passivation of silica gel

The silica gel used as solid support for chromatographic purification of the triethoxysilane derivatives (Y-EG-NVoc, EG-OMe, APTS-NVoc, **S5**) was previously passivated with HMDS. Before packing the column, the silica gel was stirred for 10 min in a solution of 2% w/V HMDS in the corresponding eluent. By this treatment, the most reactive hydroxyl groups of the silica gel are partly converted into hydrophobic methyl groups. After packing the column with this mixture, immediate washing with pure eluent is necessary in order to completely remove excess of HMDS. A passivation time of 10 min has only a slight effect on the polarity of the silica and thus does not significantly alter the separation performance with respect to unmodified silica (as revealed by TLC analysis on passivated and unpassivated silica plates).

Kugelrohr distillations

Distillations of compounds were performed in a glass oven Kugelrohr apparatus from BÜCHI Labortechnik AG (Flawil, Switzerland).

A.1.3 Measurement equipment

Nuclear magnetic resonance spectroscopy

Solution ^{1}H (250 MHz or 300 MHz) and ^{13}C (65 MHz) spectra were recorded on either a BRUKER Ultra Shield 250 MHz or a BRUKER Spectrospin 300 Spectrometer (Bruker BioSpin GmbH, Rheinstetten, Germany). All measurements were performed at room temperature in $CDCl_3$ using chloroform as an internal reference with a chemical shift of 7.26 ppm and 77.16 ppm in the ^{1}H and ^{13}C spectra, respectively.[210] Chemical shifts (δ) are given in parts per million (ppm) and the coupling constants (*J*) in Hertz (Hz). The following abbreviations are used to indicate the multiplicities: s (singlet), s br (broad singlet), d (doublet), dd (double-doublet), dt (triple-doublet), tt (triple-triplet), q (quadruplet), qui (quintet) or m (multiplet).

Numerations of the compounds are exclusively for the assignation of the NMR signals and do not have any chemical relevance.

Water contact angle

The static water contact angles were measured on an OCA 30 Contact Angle System using SCA 202 Software (DataPhysics Instruments GmbH, Filderstadt, Germany). The equipment was combined with a CCD camera for image capturing.

Substrates were washed with water and dried in the oven before use. A 5 µl droplet of Milli-Q water was suspended on four different sites on the substrate. Presented values are the averaged values from the measurements; the error corresponds to the standard deviation.

Ellipsometric layer thickness determination

Layer thickness was measured on modified silicon wafers using an ELX-02C ellipsometer (DRE-Dr. Riss Ellipsometerbau GmbH, Ratzeburg, Germany).

UV/ vis spectrosocopy

UV spectra were recorded on a Varian Cary 4000 Uv-Vis Spectrometer (Varian Inc. Palo Alto, USA).

Single wavelength UV absorbance measurements were recorded on a BIORAD smart spec™3000 spectrometer using a 100 µl cuvette (irradiation pathway 10 mm).

Single wavelength UV measurements for determination of the protein content in solutions by BCA assay were recorded on an infinite™200 microplate reader (Tecan Deutschland GmbH, 74564 Crailsheim, Germany) in 96 well flat bottom tissue culture plates (Greiner Bio-One GmbH, Frickenhausen, Germany).

Optical microscopy

Optical microscopy images were recorded on a ZEISS Axioscope with attached digital camera (Zeiss AxioCam).

Fluorescence microscopy

Fluorescence microscopy was accomplished using an Axio Imager Z1 with software Axio Vision Rel. 4.6 (Carl Zeiss GmbH, Göttingen, Germany).

The filters used for detection of different fluorescent dyes are given in Table 5-2.

Table 5-2: Filter characteristics used for detection of different fluorescent dyes.

dye	filter		filter characteristics	
	name	*manufac.*	λ_{ex}	λ_{em}
Alexa Fluor® 647	HQ filterset for Cy5 (F41-008)	AHF	620 nm/ 60 nm	700 nm/ 75 nm
Alexa Fluor® 488	EGFP HC filter set (F36-525)	AHF	472 nm/ 30 nm	520 nm/ 30 nm
DEACM	Filter set 49	ZEISS	365 nm/ 30 nm	445 nm/ 50 nm
Fluorescein/ FITC	EGFP HC filter set (F36-525)	AHF	472 nm/ 30 nm	520 nm/ 30 nm

Reflectance Interference Spectroscopy (RIFS)

Measurements were performed with a BIAffinity equipment (Analytik Jena AG, Jena, Germany), in a flow chamber under continuous flow with a data acquisition rate of 1 s^{-1}. The sensor chips (glass substrates with a 10 nm Ta_2O_5 and 325 nm silica coating, 1 cm × 1 cm) were purchased from Analytik Jena and surface modified as described in section A.2.3.

A.1.4 Surface modification

UV irradiation

Irradiation experiments with monochromatic light were carried out using a Xe lamp coupled to a polychrome V Monochromator (TILL Photonics GmbH, Gräfelfing, Germany).

For site-selective irradiation, substrates were irradiates through a mask applied on top of the substrates. Masks in quartz with chrome patterned fields containing micrometric stripes (in different sizes and with different spacing) were provided by ML&C (Jena, Germany).

Substrates were irradiated (through a chrome mask or not) with monochromatic light for selected times and then washed with THF and rinsed with Milli-Q water to remove the photolysis products.

Passivation of glassware

Glass reaction vessels used for silanization were previously passivated either by leaving them overnight in a dessicator under vacuum and in the presence of HMDS, or by wetting the glass surface with pure HMDS. Posterior washing with THF and water is needed for complete removal of the excess of HMDS.

Substrate cleaning

Quarz slides, silicon wafers and transducer slides (for RIFS measurements) were cleaned by soaking into Piranha solution (a 5:1 V/V mixture of conc. H_2SO_4 and 30% H_2O_2) overnight and subsequent rising with Milli-Q water and drying in vacuum at 90 °C for one hour.

A.2 Experimental Part: Photoactive branched silanes for functional and patterned immobilization of proteins

A.2.1 Synthesis of Y-EG-NVoc (22) and Y-alkyl-NVoc (33)

3,6,9,12-tetraoxapentadec-14-en-1-ol

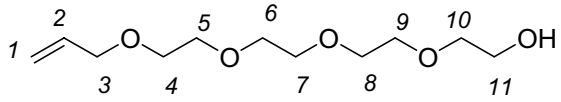

1

$C_{11}H_{22}O_5$

[234.29]

Method A

Tetraethylene glycol (10 g, 51 mmol), an equimolar amount of allyl chloride (3.9 g, 51 mmol) and tetrabutyl ammonium hydrogen sulfate (1.1 g, 3 mmol) were dissolved in dichloromethane (40 ml). A 50% (w/V) NaOH solution (0.5 mol NaOH, 40 ml) was slowly added under vigorous stirring. The reaction was allowed to proceed for further 17 hours at room temperature. The organic phase was removed using a separator funnel, the aqueous phase washed three times with water. The combined organic extracts were dried over sodium sulphate and filtered. After evaporation of the solvent under reduced pressure 38.6 g of a mixture of unreacted tetraethylene glycol, monoallyl ether and diallyl ether was obtained. The monoallyl ether was isolated by column chromatography on silica using ethyl acetate/ ethanol (9:1) as eluent to give a colorless oil (4.64 g, 20 mmol, 39% yield).

Method B[131]

A mixture of tetraethylene glycol (10 g, 51.5 mmol) and 50% aqueous solution of NaOH (0.7 ml, 8.8 mmol) was stirred at 50 °C for 4.75 hours. Allyl chloride (0.68 g, 8.8 mmol) was added drop wise. The mixture was stirred at 60 °C for 2 hours and at 80-85 °C for 21 hours. After cooling to room temperature the mixture was diluted with ethyl acetate (15 ml), filtered, and concentrated under reduced pressure. The orange-red

residue was subjected to column chromatography on silica using dichloromethane/ methanol (gradient 95:5 to 9:1) as eluent.

The pure product was obtained as pale yellow oil (1.19 g, 5 mmol, 60-65% with respect to the used amount of allyl chloride, 10% with respect to tetraethylene glycol).

^{1}H NMR (300.1 MHz, $CDCl_3$): δ/ ppm = 5.76-5.89 (m, 1H, H^2), 5.07-5.22 (m, 2H, H^1), 3.94 (dt, *J* = 7.0 Hz, *J* = 1.4 Hz, 2H, H^3), 3.50-3.65 (m, 16H, $H^{4,5,6,7,8,9,10,11}$), 2.11 (t, 1H, *J* = 5.8 Hz, -O**H**).

^{13}C NMR (75.5 MHz, $CDCl_3$): δ/ ppm = 134.7 (C^2), 117.0 (C^1), {72.5, 72.1} ($C^{3,7}$), {70.6, 70.5, 70.5, 70.3, 69.4} ($C^{4,5,6,7,8,9}$), 61.6 (C^{11}).

3,6,9,12-tetraoxapentadec-14-enyl 4-methylbenzenesulfonate

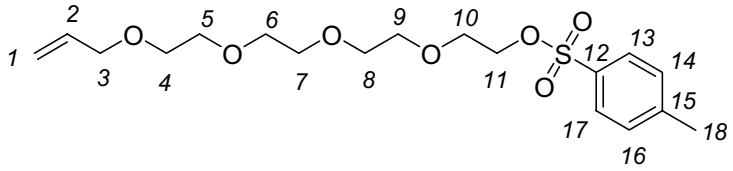

2

$C_{18}H_{28}O_7S$

[388.48]

1 (4.00 g, 17.0 mmol) and *p*-toluene sulfonyl chloride (4.75 g, 24.9 mmol) were dissolved in chloroform (16 ml). At 0-4 °C, pyridine (4.0 g, 50.6 mmol, 4.1 ml) was added drop wise under vigorous stirring. After complete addition the reaction mixture was stirred at this temperature for further 30 minutes and subsequently at room temperature overnight. The reaction mixture was then added to a mixture of crushed ice (16 g) and concentrated hydrochloric acid (4.5 ml). After phase separation the aqueous layer was washed with dichloromethane (3 × 50 ml), and the combined organic layers were dried over anhydrous sodium sulphate. Removal of the solvent yielded 8.2 g of a pale yellow liquid that was subjected to column chromatography using ethylacetate/ petroleum (2.5:1) as eluent. The pure product **2** was obtained as a colorless oil (5.95 g, 15.3 mmol, 90%, $R_f = 0.6$).

^{1}H NMR (300.1 MHz, $CDCl_3$): δ/ ppm = 7.74 (d, $J = 8.2$ Hz, 2H, $H^{13,17}$), 7.29 (d, $J = 8.2$ Hz, 2H, $H^{14,16}$), 5.92-5.79 (m, 1H, H^2), 5.25-5.09 (m, 2H, H^1), 4.10 (t, $J = 4.9$ Hz, 2H, H^{11}), 3.96 (dt, $J = 5.7$ Hz, $J = 1.3$ Hz, 2H, H^3), 3.65-3.53 (m, 14H, $H^{4,5,6,7,8,9,10}$), 2.39 (s, 3H, H^{18}).

^{13}C NMR (75.5 MHz, $CDCl_3$): δ/ ppm = 144.6 (C^{15}), 134.7 (C^2), 132.9 (C^{12}), {129.7, 127.8} ($C^{13,14,16,17}$), 116.8 (C^1), 72.0 (C^3), {70.5, 70.4, 70.4, 69.3, 69.2, 68.5} ($C^{4,5,6,7,8,9,10,11}$), 21.4 (C^{18}).

2-(2-(2-(2-(tetrahydro-2H-pyran-2-yloxy)ethoxy)ethoxy)ethoxy)ethanol

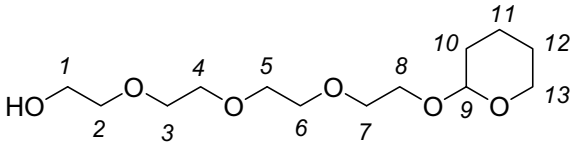

3

$C_{13}H_{26}O_6$

[278.34]

Method A:

A solution of TEG (10 g, 51.5 mmol) and 3,4-dihydro-2H-pyran (4.3 g, 51.5 mmol) in dichloromethane (10 ml) was added to a suspension of Amberlyst H-15 (1.25 g) in hexane (10 ml). The mixture was stirred for 2.5 hours. The resin was then filtered off and the solvent removed in the vacuum to give a yellow oil. Column chromatography using ethyl acetate/ hexane/ MeOH (36:60:5) as eluent gave **3** as a colorless liquid (3.77 g, 13.5 mmol, 26% yield).

Method B:

A solution of TEG (15.3 g, 79 mmol) and 3,4-dihydro-2H-pyran (1.32 g, 16 mmol) in dry dichloromethane (45 ml) was cooled in an ice bath. TsOH*H_2O (0.029 g, 0.15 mmol) was added, and the solution solution was stirred at 0 °C for further 10 minutes and then allowed to warm up to room temperature. After stirring for 5 hours at room temperature, a mixture of diethyl ether (100 ml), brine (25 ml), saturated aqueous $NaHCO_3$ solution (25 ml) and H_2O (50 ml) was added. The organic layer was separated, washed with brine (2 × 50 ml) and dried over $MgSO_4$/ K_2CO_3 (1:1). A colorless liquid was obtained after rotary evaporation of the solvent (2.9 g). TLC analysis of this crude product gave intense spots for the disubstituted compound as well (analogous to method A).

^{1}H NMR (300.1 MHz, $CDCl_3$): δ/ ppm = 4.54 (t, J = 3.4 Hz, 1H, H^9), 3.81-3.73 (m, 2H, H^1), 3.64-3.37 (m, 16H, $H^{2,3,4,5,6,7,8,13}$), 2.97 (s, 1H, -O**H**), 1.76-1.40 (m, 6H, $H^{10,11,12}$).

2-(2-(2-(2-(tetrahydro-2H-pyran-2-yloxy)ethoxy)ethoxy)ethoxy)ethyl 4-methylbenzene-sulfonate

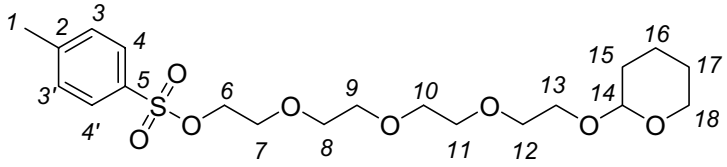

4

$C_{20}H_{32}O_8S$

[432.53]

A solution of **3** (1.9 g, 6.8 mmol) and *p*-toluene sulfonyl chloride (1.9 g, 10 mmol) in chloroform (10 ml) was cooled in an ice bath. Pyridine (1.6 g, 20 mmol) was added drop wise under vigorous stirring. After complete addition, the reaction mixture was stirred at 0-4 °C for further 30 minutes, then at room temperature for 4 hours. The reaction mixture was poured into a mixture of crushed ice (6.3 g) and concentrated hydrochloric acid (1.1 ml). The phases were separated and the organic layer was washed quickly with water, twice with saturated $NaHCO_3$ solution and dried over anhydrous Na_2SO_4/ K_2CO_3 (1:1). Removal of the solvent gave a colorless liquid (3.08 g) which was subjected to column chromatography using ethylacetate/ petroleum ether (2.5:1) as eluent to give **4** as colorless oil (1.68 g, 3.9 mmol, 57%).

^{1}H NMR (300.1 MHz, $CDCl_3$): δ/ ppm = 7.73 (d, J = 8.3 Hz, 2H, $H^{4,4'}$), 7.28 (d, J = 8.3 Hz, 2H, $H^{3,3'}$), 4.56 (t, J = 3.4 Hz, 1H, H^{14}), 4.09 (t, J = 4.7 Hz, 2H, H^6), {3.84-3.76 (m, 2H), 3.63-3.39 (m, 14H)} ($H^{7,8,9,10,11,12,13,18}$), 2.38 (s, 3H, H^1), 1.80-1.44 (m, 6H, $H^{15,16,17}$).

^{13}C NMR (75.5 MHz, $CDCl_3$): δ/ ppm = 144.7 (C^2), {129.8, 127.9} ($C^{3,3',4,4'}$), 98.9 (C^{13}), {70.7, 70.6, 70.5, 69.2, 68.6, 66.6} ($C^{6,7,8,9,10,11,12,13}$), 62.1 (C^{17}), {30.5, 25.4, 21.5, 19.4} ($C^{1,14,15,16}$).

1-bromo-2-(2-(2-(2-bromoethoxy)ethoxy)ethoxy)ethane[142]

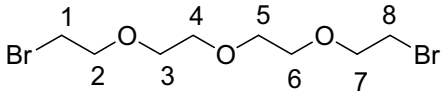

5

$C_8H_{16}Br_2O_3$

[320.02]

Tetraethylene glycol (10 g, 51.5 mmol) was dissolved in diethyl ether (150 ml, dried over molecular sieves 4Å) in a dry three-necked round-bottomed flask fitted with a septum cap, a reflux condenser and a gas inlet tube, under argon and with stirring. The resulting solution was cooled in an ice bath. Phosphorous tribromide (10 ml, 55 mmol) was added via a syringe and the mixture refluxed over night (18 hours). The mixture was then allowed to cool to RT, stirred for further 24 hours at RT and then poured into ice (75 g). The phases were separated, and the aqueous layer was extracted with ethyl acetate. The combined organic layers were shaken with saturated sodium hydrogen carbonate, separated, and dried over sodium sulfate. Removal of the solvent under reduced pressure yielded **5** as colorless oil (8.90 g, 27.8 mmol, 54%).

The ^{1}H and ^{13}C NMR spectra taken from the crude product did not show any additional peaks than those attributed to **5**. Purification by column chromatography using dichloromethane/ methanol as eluent yielded in a loss of product of about about 50%. The crude product was therefore directly used without purfification.

^{1}H NMR (300.1 MHz, $CDCl_3$): δ/ ppm = 3.76 (t, J = 6.3 Hz, 4H, $H^{2,7}$), 3.60-3.64 (m, 8H, $H^{3,4,5,6}$), 3.42 (t, J = 6.3 Hz, 4H, $H^{1,8}$).

^{13}C NMR (75.5 MHz, $CDCl_3$): δ/ ppm = {71.2, 70.6, 70.5} ($C^{2,3,4,5,6,7}$), 30.4 ($C^{1,8}$).

2-(2-(2-(2-(2-bromoethoxy)ethoxy)ethoxy)ethyl)isoindoline-1,3-dione[143]

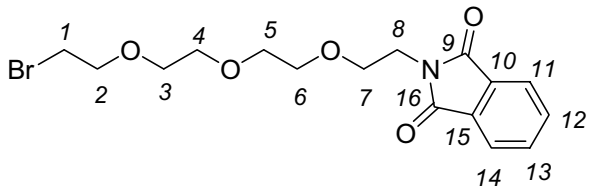

6

$C_{16}H_{20}BrNO_5$

[386.24]

A mixture of **5** (2.4 g, 7.5 mmol), phthalimide (0.54 g, 3.8 mmol), potassium carbonate (0.52 g, 3.8 mmol) and dimethyl sulfoxide (8 ml) were stirred at room temperature in the dark for 9 days. After addition of distilled water (6 ml), the aqueous phase was separated and extracted with dichloromethane. The combined organic layers were dried over anhydrous sodium sulphate. Removal of the solvent under reduced pressure yielded a yellow oil (2.48 g). The crude product was purified by column chromatography using a mixture of dichloromethane and ethyl acetate (9:1) as eluent. **6** was obtained as colorless oil that crystallized to colorless needles after standing for several days (0.87 g, 2.2 mmol, 30% with respect to **6**, 60% with respect to phthalimide; yield reported in ref[143]: 54% with respect to phthalimide).

^{1}H NMR (300.1 MHz, $CDCl_3$): δ/ ppm = 7.84-7.80 (m, 2H, $H^{11,14}$), 7.73-7.69 (m, 2H, $H^{12,13}$), {3.88 (t, J = 5.8 Hz, 2H), 3.77-3.70 (m, 4H)} ($H^{2,7,8}$), 3.65-3.57 (m, 8H, $H^{3,4,5,6}$), 3.43 (t, J = 6.3 Hz, 2H, H^1).

^{13}C NMR (300.1 MHz, $CDCl_3$): δ/ ppm = 168.3 ($C^{9,16}$), {134.0, 132.3, 123.3} ($C^{10,11,12,13,14,15}$), {71.3, 70.7, 70.6, 70.2, 68.0} ($C^{2,3,4,5,6,7}$), 37.4 (C^8), 30.4 (C^1).

1-phenyl-2,6,9,12,15,18-hexaoxahenicos-20-en-4-ol

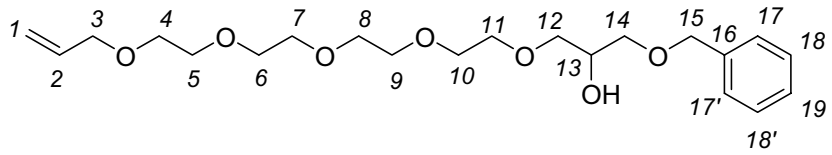

7

$C_{21}H_{34}O_7$

[398.49]

NaH (0.33 g suspension in paraffine, 60%, equivalent to 0.2 g NaH, 8.3 mmol) was washed with dry toluene (2 × 8 ml). (+/-)-3-benzyloxa-1,2-propanediol (1.44 g, 7.7 mmol) in toluene (6 ml) was added at room temperature. The white reaction mixture was heated to reflux for 30 minutes. **2** (2.8 g, 7 mmol) in toluene (5 ml) was added in the heat. The reaction was kept under reflux for 20 hours and then allowed to cool to room temperature. Distilled water (10 ml) was added. The phases were separated, and the aqueous phase was extracted with dichloromethane (3 × 40 ml). The combined organic layers were dried over anhydrous sodium sulphate. Removal of the solvent gave an orange liquid (3.1 g). **7** was obtained as colorless oil by twice column chromatography, using first ethylacetate then ethylacetate/ petroleumether (2.5:1) as eluent (0.89 g, 2.1 mmol, 31%).

^{1}H NMR (300.1 MHz, $CDCl_3$): δ/ ppm = 7.37-7.28 (m, 5H, $H^{17,17',18,18',19}$), 5.96-5.83 (m, 1H, H^2), 5.29-5.14 (m, 2H, H^1), 4.53 (d, J = 4.5 Hz, 2H, H^{15}), 4.00 (dt, J = 5.6 Hz, J = 1.4 Hz, 2H, H^3), 3.91-3.81 (m, 1H, H^{13}), 3.76-3.46 (m, 20H, $H^{4,5,6,7,8,9,10,11,12,14}$).

2-(13-(benzyloxymethyl)-3,6,9,12,15,18,21,24,27-nonaoxatriacont-29-enyloxy)tetrahydro-2H-pyran

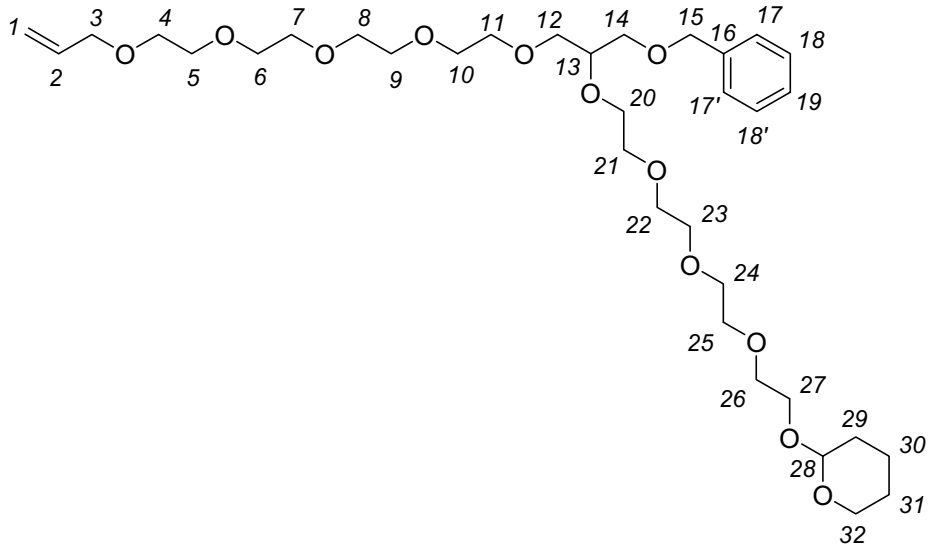

8

$C_{34}H_{58}O_{12}$

[658.82]

NaH (0.07 g suspension in paraffine, 60%, equivalent to 0.04 g NaH, 1.75 mmol) was washed with dry toluene (2 × 6 ml). A solution of **7** (0.54 g, 1.3 mmol) in dry toluene (5 ml) was added at room temperature. The reaction mixture was heated to reflux for 1 hour. A solution of **4** (0.57 g, 1.3 mmol) in dry toluene (8 ml) was added to the hot solution. The reaction was kept under reflux for 20 hours and then allowed to cool to room temperature. Distilled water (4 ml) was added. The phases were separated, and the aqueous phase was extracted with dichloromethane (3 × 20 ml). The combined organic layers were dried over anhydrous sodium sulphate and concentrated under reduced pressure. The orange crude product (1.12 g) was subjected to column chromatography using ethylacetate/ petroleum ether/ ethanol (10:6:1.5) as eluent. **8** was obtained as 50% mixture with the starting compound **7** by twice column chromatography (0.48 g, equivalent to 0.5 mmol pure 8, 35%).

^{1}H NMR (300.1 MHz, $CDCl_3$): δ/ ppm = 7.30-7.21 (m, 5H, $H^{17,17',18,18',19}$), 5.94-5.81 (m, 1H, H^2), 5.27-5.11 (m, 2H, H^1), 4.60-4.58 (m, 1H, H^{28}), 4.50 (s, 2H, H^{15}), 3.98 (dt, J = 5.7 Hz, J = 1.3 Hz, 2H, H^3), 3.85-3.44 (m, 39H, $H^{4,5,6,7,8,9,10,11,12,13,14,20,21,22,23,24,25,26,27,32}$), 1.83-1.45 (m, 6H, $H^{29,30,31}$).

2,5,8,11-tetraoxatridecan-13-yl 4-methylbenzenesulfonate

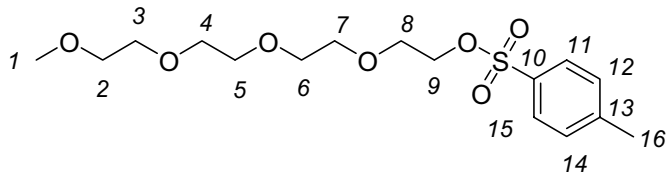

10

$C_{16}H_{26}O_7S$

[362.44]

Tetraethylene glycol monomethylether (5 g, 24 mmol) and *p*-toluene sulfonyl chloride (6.67 g, 35 mmol) were dissolved in chloroform (25 ml). At 0-4 °C pyridine (5.6 g, 71 mmol, 5.7 ml) was added drop wise under vigorous stirring. After complete addition the reaction mixture was stirred at this temperature for further 30 minutes and subsequently at room temperature overnight. Subsequently the reaction mixture was added to a mixture of crushed ice (23 g) and concentrated hydrochloric acid (6.3 ml). After phase separation the acqueous layer was extracted with dichloromethane. The combined organic layers were dried over anhydrous sodium sulphate. After removal of the solvent 10.3 g of colorless liquid were obtained. Column chromatography using ethylacetate/ petroleum (2.5:1) as eluent gave the pure product **10** as a colorless oil (8.0 g, 22.1 mmol, 92%).

^{1}H NMR (300.1 MHz, $CDCl_3$): δ/ ppm = 7.71 (d, J = 8.2 Hz, 2H, $H^{11,12}$), 7.27 (d, J = 8.2 Hz, 2H, $H^{12,14}$), 4.07 (t, J = 4.8 Hz, 2H, H^{9}), 3.61-3.44 (m, 14H, $H^{2,3,4,5,6,7,8}$), 3.28 (s, 3H, H^{1}), 3.26 (s, 3H, H^{16}).

^{13}C NMR (75.5 MHz, $CDCl_3$): δ/ ppm = 144.7 (C^{13}), 133.0 (C^{10}), {129.7, 127.8} ($C^{11,12,14,15}$), {71.8, 70.6, 70.5, 70.4, 70.4, 70.4, 69.2, 68.5} ($C^{2,3,4,5,6,7,8,9}$), 58.8 (C^{1}), 21.5 (C^{16}).

2,2'-(2,2'-oxybis(ethane-2,1-diyl)bis(oxy))bis(ethane-2,1-diyl) bis(4-methylbenzenesulfonate)

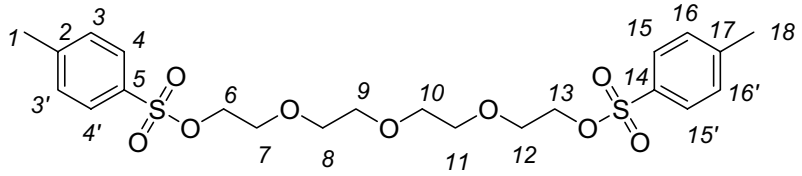

11

$C_{22}H_{30}O_9S_2$

[502.60]

Tetraethylene glycol (10 g, 51.5 mmol) and *p*-toluene sulfonyl chloride (28.95 g, 151.8 mmol) were dissolved in chloroform (70 ml). At 0-4°C pyridine (24.4 g, 24.9 ml, 308.5 mmol) was added drop wise under vigorous stirring. After complete addition the reaction mixture was stirred at this temperature for further 30 minutes and subsequently at room temperature for 22 hours. Then the reaction mixture was added to a mixture of crushed ice (100 g) and concentrated hydrochloric acid (25 ml). After phase separation the aqueous layer was washed extracted with chloroform (2 × 100 ml). The organic extracts were dried over anhydrous sodium sulphate. After removal of the solvent at reduced pressure 32 g of a pale yellow oil were obtained. Column chromatography using ethylacetate/ petroleum (2.5:1) gave the pure product **11** as colorless oil (16.13 g, 32 mmol, 63%).

^{1}H NMR (300.1 MHz, $CDCl_3$): δ/ ppm = 7.70 (d, J = 8.2 Hz, 4H, $H^{4,4',15,15'}$), 7.27 (d, J = 8.2 Hz, 4H, $H^{3,3',16,16'}$), 4.07 (t, J = 4.7 Hz, 4H, $H^{6,13}$), 3.59 (t, J = 4.7 Hz, 4H, $H^{7,12}$), 3.47 (s br, 8H, $H^{8,9,10,11}$), 2.36 (s, 3H, $H^{1,18}$).

^{13}C NMR (75.5 MHz, $CDCl_3$): δ/ ppm = 144.7 ($C^{2,17}$), 132.8 ($C^{5,14}$), 129.7 ($C^{3,3',16,16'}$), 127.8 ($C^{4,4',15,15'}$), {70.5, 70.4, 69.3, 68.5} ($C^{6,7,8,9,10,11,12,13}$), 21.5 ($C^{1,18}$).

2-(2-(2-(2-(1,3-dioxoisoindolin-2-yl)ethoxy)ethoxy)ethoxy)ethyl 4-methylbenzenesulfonate

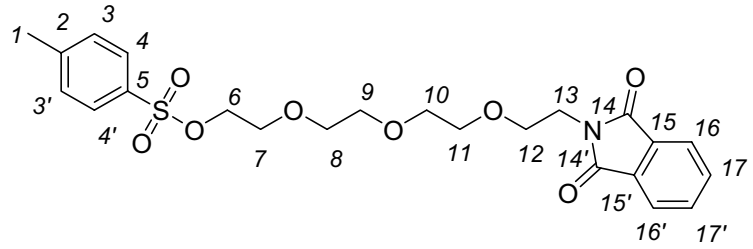

12

$C_{23}H_{27}NO_8S$

[477.5]

Procedure 1[143]: **11** (10 g, 19.9 mmol), phthalimide (1.44 g, 9.8 mmol) and potassium carbonate (1.37 g, 9.8 mmol) were suspended in DMSO (25 ml) and stirred under argon atmosphere for 7-10 days. Water (30 ml) was then added to the reaction mixture. After extraction with dichloromethane (2 × 50 ml), the aqueous phase was neutralized with diluted sulphuric acid and extracted again with dichloromethane (2 × 50 ml). The combined organic extracts were dried over anhydrous sodium sulphate. After removal of the solvent at reduced pressure (up to 3×10^{-3} mbar) a pale yellow oil (12.6 g) was obained.

Column chromatography using dichloromethane/ ethylacetate (9:1) as eluent gave the pure product **12** as a pale yellow oil (2.15 g, 4.5 mmol, 46% with respect to phthalimide, 23% with respect to **11**).

Procedure 2: **14** (1.6 g, 4.9 mmol) and *p*-toluene sulfonyl chloride (1.2 g, 6.3 mmol, 1.3 mol-eq.) were dissolved in chloroform (8 ml) and cooled to 0-4 °C. Pyridine (0.1 g, 1 ml, 12.6 mmol) was added dropwise under vigorous stirring. After complete addition the reaction mixture was stirred at this low temperature, then at room temperature over night. The reaction mixture was added to a mixture of crushed ice (5 g) and concentrated hydrochloric acid (1 ml). After phase separation the aqueous layer was washed three times with dichloromethane and dried over anhydrous sodium sulphate. Column chromatography using ethylacetate as eluent gave the pure product **12** as colorless oil (1.3 g, 2.8 mmol, 56%).

^{1}H NMR (300.1 MHz, $CDCl_3$): δ/ ppm = 7.84-7.82 (m, 2H, $H^{16,16'}$), 7.78 (d, *J* = 8.3 Hz, 2H, $H^{4,4'}$), 7.72-7.69 (m, 2H, $H^{17,17'}$), 7.33 (d, *J* = 8.3 Hz, 2H, $H^{3,3'}$), 4.13 (t, *J* = 4.8 Hz, 2H, H^{13}), {3.88-3.86 (m, 2H,) 3.75-3.70 (m, 2H)} ($H^{6,12}$), 3.66-3.49 (m, 12H, $H^{7,8,9,10,11,12}$), 2.43 (s, 3H, H^{1}).

^{13}C NMR (75.5 MHz, $CDCl_3$): δ/ ppm = 168.3 ($C^{14,14'}$), {144.9, 134.1, 132.3, 129.9, 128.1, 123.3} ($C^{3,3',4,4',5,14,14',15,15',16,16',17,17'}$), {70.8, 70.7, 70.7, 70.2} ($C^{8,9,10,11}$), 69.4 (C^{12}), {68.8, 68.0} ($C^{6,7}$), 37.4 (C^{13}), 21.7 (C^{1}).

2-(2-(2-(2-hydroxyethoxy)ethoxy)ethoxy)ethyl 4-methylbenzenesulfonate

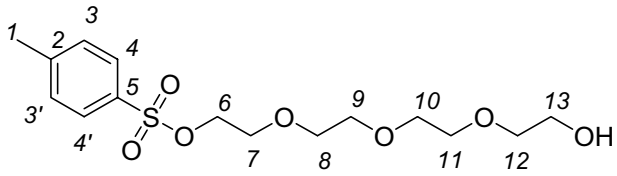

13

$C_{15}H_{24}O_7S$

[348.41]

Tetraethylene glycol (30 g, 154 mmol) and *p*-toluene sulfonyl chloride (17.66 g, 93 mmol, 0.6 mol-eq.) were dissolved in chloroform (120 ml) and cooled to 0-4 °C. Pyridine (14.7 g, 15 ml, 123.9 mmol) was added dropwise under vigorous stirring. After complete addition the reaction mixture was stirred at this low temperature, then further 4 hours at room temperature (or over night). The reaction mixture was added to a mixture of crushed ice (60 g) and concentrated hydrochloric acid (15 ml). After phase separation the aqueous layer was washed three times with dichloromethane and dried over anhydrous sodium sulphate. After removal of the solvent 31.4 g of a colorless liquid were obtained. Column chromatography using ethylacetate as eluent gave the pure product **13** as colorless oil (17.6 g, 50.5 mmol, 54% with respect to tosyl chloride, 33% with respect to tetraethylene glycol)

^{1}H NMR (300.1 MHz, CD_2Cl_2): δ/ ppm = 7.75 (d, *J* = 8.3 Hz, 2H, $H^{4,4'}$), 7.35 (d, *J* = 8.3 Hz, 2H, $H^{3,3'}$), 4.11 (t, *J* = 4.6 Hz, 2H, H^{6}), 3.50-3.64 (m, 14H, $H^{7,8,9,10,11,12,13}$), 2.54 (s br, 1H, -O**H**), 2.42 (s, 3H, H^{1}).

^{13}C NMR (75.5 MHz, CD_2Cl_2): δ/ ppm = 145.2 (C^{2}), 133.1 (C^{5}), {127.9, 129.9} ($C^{3,3',4,4'}$), {68.7, 69.6, 70.4, 70.4, 70.6, 70.7, 72.6} ($C^{6,7,8,9,10,11,12}$), 61.7 (C^{13}), 21.4 (C^{1}).

2-(2-(2-(2-(2-hydroxyethoxy)ethoxy)ethoxy)ethyl)isoindoline-1,3-dione[145]

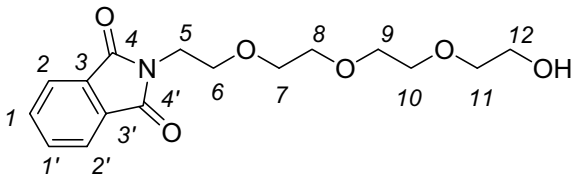

14

$C_{16}H_{21}NO_6$

[323.34]

13 (6.6 g, 18.9 mmol) and phthalimide potassium salt (6.3 g, 19.5 mmol) were placed in a dry flask. DMF (60 ml) was added. The reaction mixture was heated to about 80 °C and kept for 18 hours at this temperature. DMF was distilled off (at 5×10^{-2} mbar). The residue was taken up in ethyl acetate (125 ml), subsequently washed with 1 N hydrochloric acid (2×50 ml) and saturated sodium hydrogen carbonate solution (2×30 ml) and dried over anhydrous sodium sulphate. After removal of the solvent 3.8 g of a light white solid was obtained.

Column chromatography using ethylacetate/ ethanol (99:1) as eluent gave **14** as colorless oil (1.65 g, 5.1 mmol, 27%, crystallizes to a white solid).

^{1}H NMR (300.1 MHz, $CDCl_3$): δ/ ppm = 7.80-7.85 (m, 2H, $H^{2,2'}$), 7.68-7.73 (m, 2H, $H^{1,1'}$), 3.89 (t, J = 5.7 Hz, 2H, H^5), 3.54-3.75 (m, 14H, $H^{6,7,8,9,10,11,12}$), 2.55 (s br, 1H, -O**H**).

^{13}C NMR (75.5 MHz, $CDCl_3$): δ/ ppm = 168.4 ($C^{4,4'}$), {134.0, 132.3, 123.4} ($C^{1,1',2,2',3,3'}$), {72.6, 70.8, 70.7, 70.5, 70.3, 68.1} ($C^{6,7,8,9,10,11}$), 61.9 (C^{12}), 37.4 (C^5).

4-(2,5,8,11,14-pentaoxaheptadec-16-enyl)-2,2-dimethyl-1,3-dioxolane

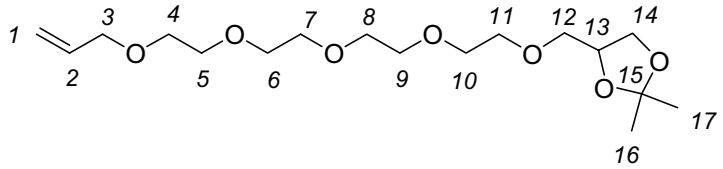

15

$C_{17}H_{32}O_7$

[348.43]

Procedure 1 (using KOH as base):[134]

Solketal (0.185 g, 1.4 mmol) was dissolved in toluene (5 ml). Finely powdered KOH (0.03 g, 0.5 mmol) was added, and the reaction mixture heated under reflux for one hour. After cooling to room temperature **2** (0.6 g, 1.5 mmol) was added and the reaction mixture again heated and kept under reflux for 65 hours. Any water produced was *in-situ* removed by azeotropic distillation. The reaction mixture was allowed to cool down to room temperature and filtered. Evaporation of the solvent under reduced pressure yielded a yellow oil (0.63 g).

TLC analysis of the crude product in ethyl acetate gave three spots with $R_f = 0.16$ (solketal), 0.77 (**2**), 0.94 (attributed to TosCl) and 0.45. The substance with $R_f = 0.36 – 0.5$ was isolated by preparative thin layer chromatography as pale yellow residue (0.03 g, 0.09 mmol, 6%) and identified (by ^{1}H NMR spectroscopy) to be **15** with some impurities.

Procedure 2 (using Na as base):

Sodium (1.6 g, 69.6 mmol) was placed in a dry, argon fluted three-necked flask with reflux condenser and drop funnel. The five fold amount of solketal (30.4 g, 230.0 mmol, 28.6 ml) was added dropwise under stirring. Gas formation was observed. The yellowish reaction mixture was heated to about 50 °C to complete dissolving of sodium. **2** (15 g, 38.6 mmol) in dry toluene (80 ml) was added. The dark reaction mixture was heated under reflux, kept at this temperature for 18 hours and was then allowed to cool down to room temperature. After addition of water (100 ml), the phases were separated and the aqueous phase extracted with ethylacetate and dichloromethane. All combined

organic phases were dried over sodium sulphate. Removal of the solvent under reduced pressure yielded an orange oil (38.1 g).

Excess of solketal was removed by distillation (37 °C, 3.3×10^{-2} mbar) and the residue subjected to column chromatography using ethylacetate as eluent. **15** was obtained as pale, nearly colorless, yellow oil (8.7 g, 24.9 mmol, 64.5%).

^{1}H NMR (300.1 MHz, $CDCl_3$): δ/ ppm = 5.88-5.75 (m, 1H, H^{2}), 5.21-5.05 (m, 2H, H^{1}), 4.17 (quintet, J = 6.0 Hz, 1H, H^{13}), {3.97-3.91 (m, 3H), 3.65-3.37 (m, 19H)} ($H^{3,4,5,6,7,8,9,10,11,12,14}$), {1.33 (s, 3H), 1.25 (s, 3H)} ($H^{16,17}$).

^{13}C NMR (75.5 MHz, $CDCl_3$): δ/ ppm = 135.2 (C^{2}), 116.4 (C^{1}), 109.2 (C^{15}), 74.9 (C^{3}), {72.4, 72.0, 71.0, 70.6, 70.6, 70.5, 69.6} ($C^{4,5,6,7,8,9,10,11,12,13}$), 66.8 ($C^{14}$), {26.6, 26.3} ($C^{16,17}$).

4,7,10,13,16-pentaoxanonadec-18-ene-1,2-diol[146]

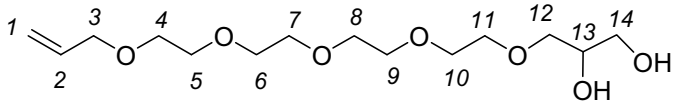

16

$C_{14}H_{28}O_7$

[308.37]

15 (6.0 g, 17.2 mmol) and Dowex 50WX8 H^{+}-Form (20 g, previously washed with THF) were suspended in THF (150 ml). The suspension was stirred at room temperature for 66 hours. The catalyst was filtered off and the filtrate concentrated under reduced pressure. The obtained pale yellow oil was attributed to be the desired product **16** with less than 5% remaining **15** (4.75 g, 15.4 mmol, 90%). Purification by column chromatography using ethylacetate/ ethanol (2:1) as eluent yielded pure **16** as colorless oil (3.85 g, 12.5 mmol, 73%).

^{1}H NMR (300.1 MHz, $CDCl_3$): δ/ ppm = 5.95-5.82 (m, 1H, H^{2}), 5.28-5.13 (m, 2H, H^{1}), 4.00 (dt, J = 5.7 Hz, J = 1.3 Hz, 2H, H^{3}), {3.86-3.80 (m, 1H), 3.70-3.49 (m, 20H)} ($H^{4,5,6,7,8,9,10,11,12,13,14}$), 3.45 (s br, 1H, -O**H**), 2.84 (s br, 1H, -O**H**).

^{13}C NMR (75.5 MHz, $CDCl_3$): δ/ ppm = 134.9 (C^{2}), 117.1 (C^{1}), {73.0, 72.3, 70.8, 70.7, 70.7, 70.7, 70.6, 70.6, 70.6, 69.5} ($C^{3,4,5,6,7,8,9,10,11,12,13}$), 64.0 ($C^{14}$).

2,5,8,11,14,18,21,24,27,30-decaoxatritriacont-32-en-16-ol

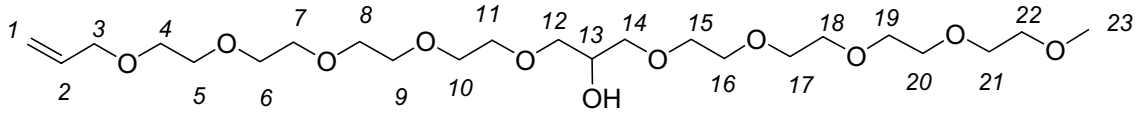

18

$C_{23}H_{46}O_{11}$

[498.60]

NaH (0.08 g, 3.3 mmol) was placed in a dry three-necked round bottom flask. Under argon atmosphere tetraethyleneglycol monomethylether (5.15 g, 24.7 mmol) in dry THF (20 ml) was added. The formation of bubbles could be observed (due to H_2 formation). The solution was heated to reflux. **24** (5 g, 17.2 mmol) in dry THF (40 ml) was then added in the heat. The reaction was kept under reflux for 2 days. After complete conversion of the epoxide (analyzing a small sample by ^{1}H NMR spectroscopy) the reaction mixture was allowed to cool down to room temperature. Water (60 ml) was added and the mixture was extracted with dichloromethane. After neutralization with a few drops of diluted H_2SO_4, the aqueous phase was extracted again with dichloromethane. The combined organic extracts were dried over sodium sulphate and concentrated on a rotatory evaporator.

Excess of tetraethyleneglycol monomethylether was removed by distillation (150 °C, 2.8×10^{-2} mbar). The brown residual oil was used for further reactions without any further purification (6.97 g, 14 mmol, 82%). The absence of **15** was confirmed by gaschromatographic analysis (GC-MS).

^{1}H NMR (300.1 MHz, $CDCl_3$): δ/ ppm = 5.83-5.96 (m, 1H, H^2), 5.14-5.29 (m, 2H, H^1), 4.00 (dt, J = 5.7 Hz, $J \approx$ 1.4 Hz, 2H, H^3), 3.91-3.96 (m, 1H, H^{13}), 3.45-3.69 (m, 36H, $H^{4,5,6,7,8,9,10,11,12,14,15,16,17,18,19,20,21,22}$), 3.36 (s, 3H, H^{23}), 2.91 (m, 1H, -O**H**).

^{13}C NMR (75.5 MHz, $CDCl_3$): δ/ ppm = 134.8 (C^2), 117.0 (C^1), {72.6, 72.2, 72.0, 70.8, 70.6, 70.6, 70.6, 70.5, 69.5} ($C^{3,4,5,6,7,8,9,10,11,12,13,14,15,16,17,18,19,20,21,22}$), 59.0 ($C^{23}$).

2-(13-2,5,8,11,14-pentaoxapentadecyl-3,6,9,12,15,18,21,24,27-nonaoxatriacont-29-enyl)isoindoline-1,3-dione

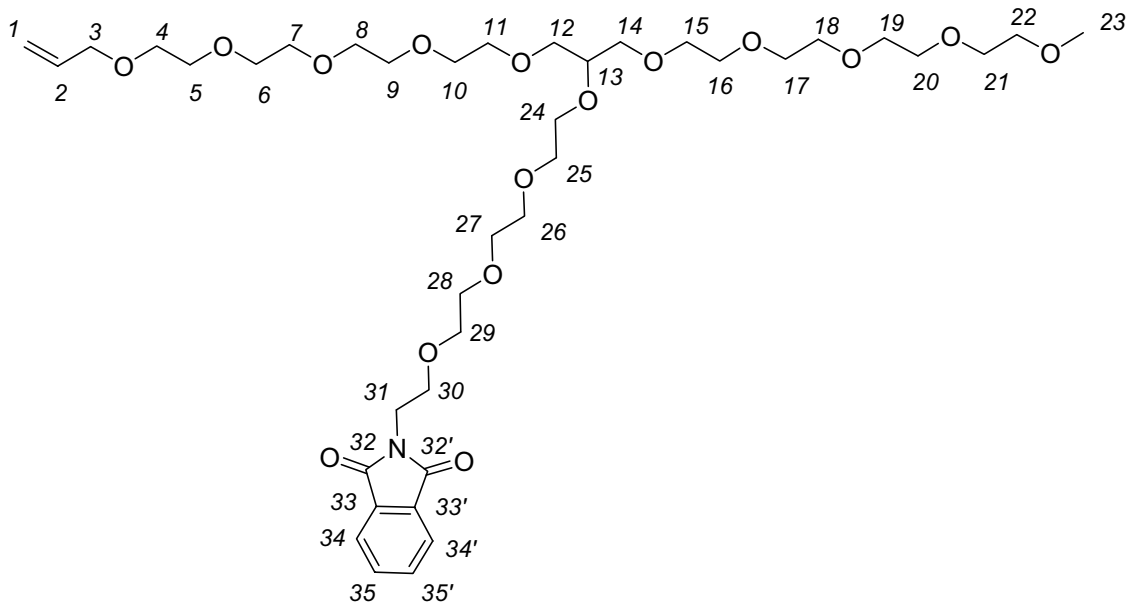

19

$C_{39}H_{65}NO_{16}$

[803.93]

NaH (0.12 g, 5 mmol) was placed in a dry three-necked round bottom flask. Under argon atmosphere **18** (2.5 g, 5 mmol) in 15 ml dry THF was added. There was some gas development (due to H_2 formation), but the NaH was not dissolved completely. The reaction mixture was heated up to 80 °C and stirred for about 30 minutes, until it became clear. Then **12** (2.4 g, 5 mmol) in dry THF (10 ml) was added to this clear brown solution. The reaction mixture was kept under reflux for at least 4 hours (or overnight). After cooling to room temperature, distilled water (30 ml) was added. The mixture was extracted with dichloromethane (2 × 50 ml), neutralized with diluted H_2SO_4 and then extracted again twice with dichloromethane. The combined organic extracts were dried over sodium sulphate and concentrated on a rotatory evaporator.

Low molecular-weight molecules were distilled off in the vacuum (up to 200 °C at 8×10^{-3} mbar). The residual orange-brown oil could be determined to be **19** and was used without any further purification. (3.6 g, 4.5 mmol, 90%).

^{1}H NMR (300.1 MHz, $CDCl_3$): δ/ ppm = 7.85-7.80 (m, 2H, $H^{34,34'}$), 7.73-7.68 (m, 2H, $H^{35,35'}$), 5.96-5.83 (m, 1H, H^{2}), 5.28-5.14 (m, 2H, H^{1}), 4.00 (dt, J = 5.7 Hz, $J \approx$ 1.4 Hz, 2H, H^{3}), 3.90-3.86 (t, J = 5.8 Hz, 2H, H^{31}), 3.36 (s, 3H, H^{23}), {3.65-3.45 (m, 47H), 3.69-3.75 (m, 4H)} ($H^{4,5,6,7,8,9,10,11,12,13,14,15,16,17,18,19,20,21,22,24,25,26,27,28,29,30}$).

^{13}C NMR (75.5 MHz, $CDCl_3$): δ/ ppm = 168.3 ($C^{32,32'}$), {134.9, 134.0, 132.3, 123.3} ($C^{2,33,33',34,34'}$), 117.1 (C^{1}), 78.5 (C^{13}), {72.7, 72.3, 72.1, 71.4, 71.0, 70.9, 70.9, 70.8, 70.7, 70.7, 70.7, 70.7, 70.7, 70.6, 70.6, 70.2, 69.9, 69.6, 68.0, 61.9} ($C^{3,4,5,6,7,8,9,10,11,12,14,15,16,17,18,19,20,21,22,24,25,26,27,28,29,30}$), 59.1 ($C^{23}$), 37.4 ($C^{31}$).

13-2,5,8,11,14-pentaoxapentadecyl-3,6,9,12,15,18,21,24,27-nonaoxatriacont-29-en-1-amine

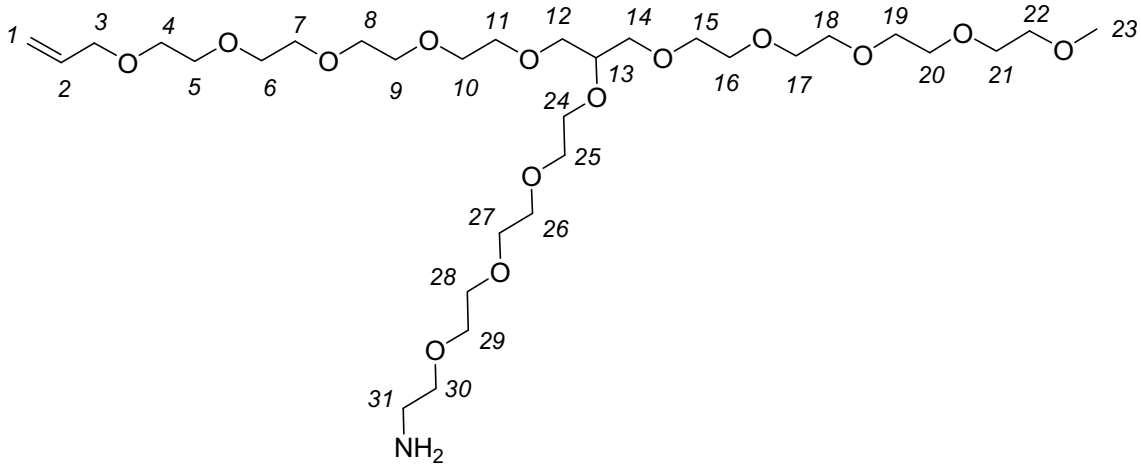

20

$C_{31}H_{63}NO_{14}$

[673.83]

19 (3.4 g, 4.2 mmol) and hydrazine monohydrate (0.65 g, 0.65 ml, 13 mmol, equal to 0.42 g) were dissolved in ethanol (40 ml). The solution was heated to reflux and for about 11 hours. Then the mixture was allowed to cool to room temperature and filtered. The solid residue was washed with ethanol. The combined filtrates were concentrated on a rotatory evaporator. Excess of hydrazine was removed by distillation (100 °C, 9×10^{-3} mbar). ^{1}H NMR spectroscopic analysis approved the presence of the reduced compound as byproduct in 25 mol-%. The residual brown liquid **20** (2.75 g, equivalent to 3.1 mmol pure **20**, 73%) was used as obtained for further reactions.

^{1}H NMR (300.1 MHz, $CDCl_3$): δ/ ppm = 5.96-5.83 (m, 1H, H^{2}), 5.29-5.15 (m, 2H, H^{1}), 4.00 (dt, J = 5.7 Hz, $J \approx$ 1.2 Hz, 2H, H^{3}), 3.76-3.45 (m, 51H, $H^{4,5,6,7,8,9,10,11,12,13,14,15,16,17,18,19,20,21,22,24,25,26,27,28,29,30}$), 3.36 (s, 3H, H^{23}), 2.87 (t, J = 5.3 Hz, H^{31}), 2.40 (s br, 2H, -N**H**$_2$).

^{13}C NMR (75.5 MHz, $CDCl_3$): δ/ ppm = 135.0 (C^{2}), 117.1 C^{1}), 78.5 (C^{13}), {73.2, 72.7, 72.3, 72.1, 71.4, 71.0, 70.9, 70.9, 70.8, 70.7, 70.7, 70.7, 70.4, 69.9, 69.6} ($C^{3,4,5,6,7,8,9,10,11,12,14,15,16,17,18,19,20,21,22,24,25,26,27,28,29,30}$), 59.1 ($C^{23}$), 41.9 ($C^{31}$).

13-2,5,8,11,14-pentaoxapentadecyl-3,6,9,12,15,18,21,24,27-nonaoxatriacontan-1-amine

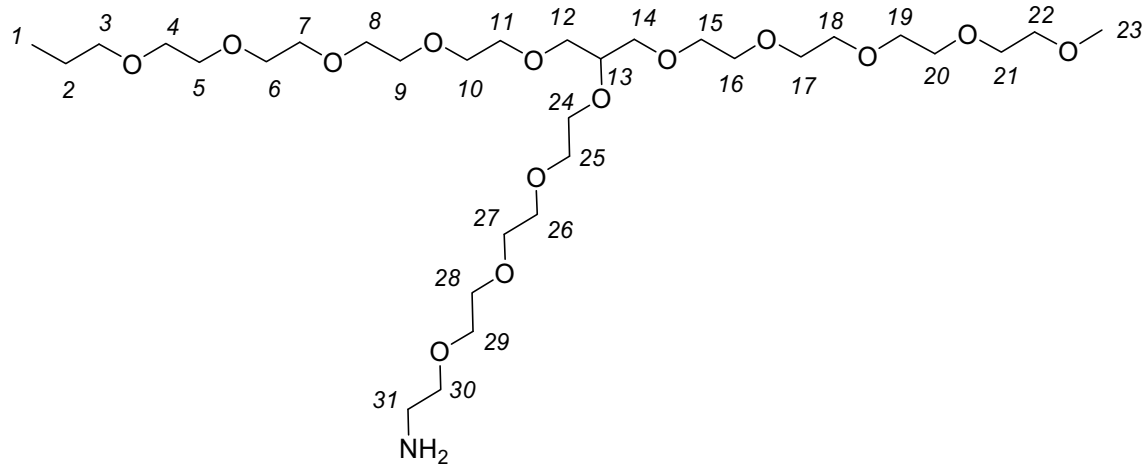

reduced compound

$C_{31}H_{65}NO_{14}$

[675.83]

The reduced compound was obtained as byproduct in the synthesis of **20**. The ^{1}H NMR signals attributed to H^1 and H^2 show different positions and multiplicity with respect to the signals of **20**: δ/ ppm = 0.87 (t, J = 7.4 Hz) for H^1 and 1.62-1.50 (m) for H^2. The signals in the ^{13}C NMR spectrum attributed to C^1 and C^2 are shifted with respect to the signals of **22**: δ/ ppm = 10.6 for C^1 and 22.9 for C^2.

4,5-dimethoxy-2-nitrobenzyl 13-2,5,8,11,14-pentaoxapentadecyl-3,6,9,12,15,18,21,24,27-nonaoxatriacont-29-enylcarbamate

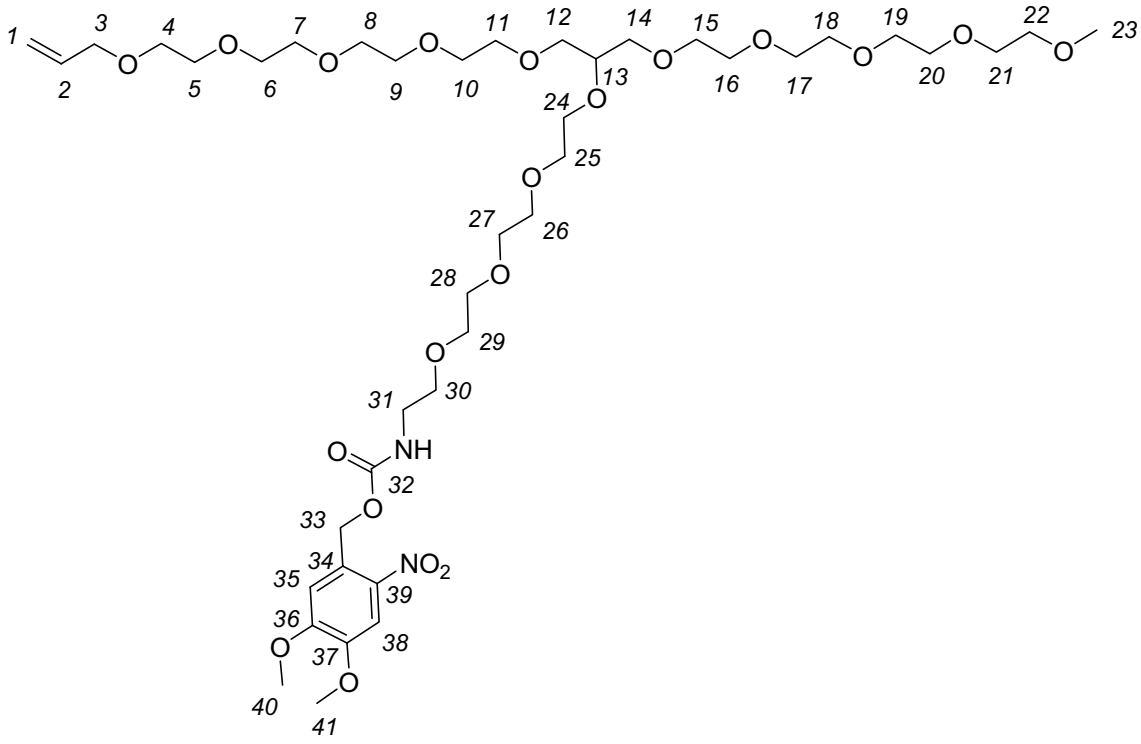

21

$C_{41}H_{72}N_2O_{20}$

[913.01]

A solution of **20** (2.75 g, contains 25 mol-% reduced compound, equivalent to 3.1 mmol pure **20**) and sodium hydrogen carbonate (0.97 g, 11.6 mmol) in 25 ml water was cooled to 0-4 °C in an ice-bath. Under stirring a solution of 6-nitroveratryloxycarbonyl chloride (1.49 g, 5.4 mmol) in dioxan (105 ml) was slowly added. After complete addition, the reaction mixture was kept at this temperature under stirring for further 15 min, then at room temperature for at least 3 hours. After neutralization with aqueous hydrochloric acid solution (1N HCl, 2.4 ml) the mixture was extracted with dichloromethane. The organic extracts were dried over sodium sulphate, and the solvents removed at reduced pressure. The obtained brown oil (5.4 g) was subjected to column chromatography using a mixture of ethylacetate and ethanol (1:1) as eluent. **21** could be obtained only in an 80 mol-% mixture with the reduced compound **23** (2.34 g, equivalent to 2.1 mmol pure **21**, 69% with respect to initial amount of **20**).

^{1}H NMR (300.1 MHz, $CDCl_3$): δ/ ppm = 7.69 (s, 1H, H^{38}), 7.02 (s, 1H, H^{35}), 5.96-5.83 (m, 1H, H^{2}), 5.50 (s br, 2H, H^{33}), 5.29-5.14 (m, 1.6H, H^{1}), 4.01 (dt, J = 5.6 Hz, J = 1.3 Hz, 2H, H^{3}), {3.96 (s, 3H), 3.93 (s, 3H)} ($H^{40,41}$), 3.75-3.38 (m, 53H, $H^{4,5,6,7,8,9,10,11,12,13,14,15,16,17,18,19,20,21,22,24,25,26,27,28,29,30,31}$), 3.36 (s, 3H, H^{23}).

^{13}C NMR (75.5 MHz, $CDCl_3$): δ/ ppm = 153.7 ($C^{32,36}$), 148.3 (C^{37}), 135.0 (C^{2}), 117.0 (C^{1}), {110.5, 108.4} ($C^{35,38}$), {78.8, 78.6, 73.2, 72.3, 72.1, 71.5, 71.0, 70.9, 70.9, 70.8, 70.7, 70.7, 70.7, 70.6, 70.5, 70.2, 70.1, 69.9, 69.6, 67.2} ($C^{3,4,5,6,7,8,9,10,11,12,13,14,15,16,17,18,19,20,21,22,24,25,26,27,28,29,30}$), {63.6, 59.1, 56.6, 56.5} ($C^{23,33,40,41}$), 41.2 (C^{31}), 22.9.

4,5-dimethoxy-2-nitrobenzyl 4,4-diethoxy-22-2,5,8,11,14-pentaoxapentadecyl-3,8,11,14,17,20,23,26,29,32-decaoxa-4-silatetratriacontan-34-ylcarbamate

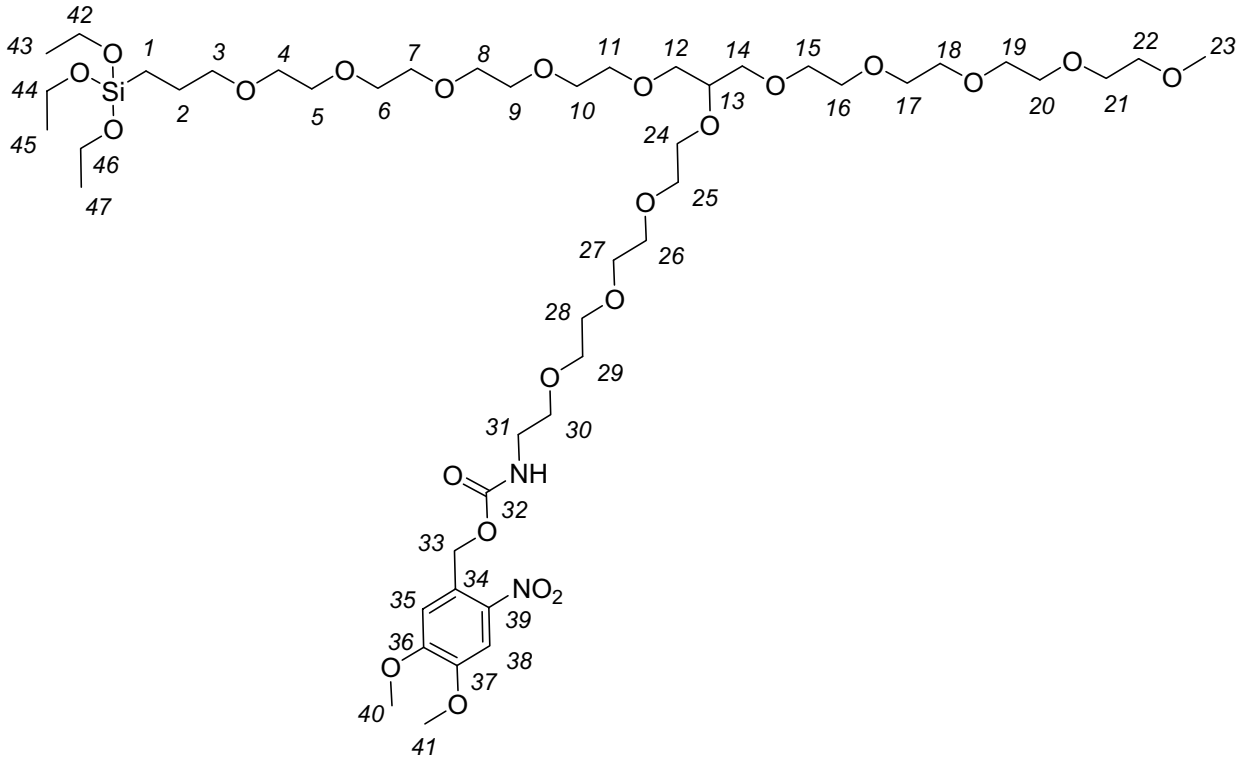

22

$C_{47}H_{88}N_2O_{23}Si$

[1077.29]

In a previously with HMDS passivated, dry reaction flask with attached distillation apparatus **21** (1.26 g of an 80 mol-% mixture with **23**, equivalent to 1.1 mmol pure **22**) and triethoxysilane (2.27 g, 13.8 mmol, 10 mol-equivalent) were heated to 80 °C, under

argon. Isopropanolic H_2PtCl_6 solution (60 µl, c = 0.027 mg/µl) were added. The reaction was followed by ^{1}H NMR spectroscopy. Eventually more catalyst had to be added. After about 5 hours, the excess of triethoxysilane was removed by distillation (up to 100 °C, 8×10^{-3} mbar). The crude product was subjected to column chromatography on a passivated silica support (treatment with HMDS (2% w/V) for 10 min, see A.1.2). The desired silane **22** could be obtained in a 70% mixture with the reduced compound **23** (0.78 g, equivalent to 0.5 mmol pure **21**, 42% with respect to the initial amount of **21**).

^{1}H NMR (300.1 MHz, $CDCl_3$): δ/ ppm = 7.70 (s, 1H, H^{38}), 7.03 (s, 1H, H^{35}), 5.55 (s br, 1H, -N**H**-), 5.51 (s, 2H, H^{33}), {3.95 (s, 3H), 3.98 (s, 3H)} ($H^{40,41}$), 3.81 (q, *J* = 6.9 Hz, 6H, $H^{42,44,46}$), 3.65-3.39 (m, 61H, $H^{3,4,5,6,7,8,9,10,11,12,13,14,15,16,17,18,19,20,21,22,24,25,26,27,28,29,30,31}$), 3.37 (s, 3H, H^{23}), 1.75-1.64 (m, 2H, H^2), 1.21 (t, *J* = 6.9 Hz, 9H, $H^{43,45,47}$), 0.65-0.59 (m, 2H, H^1).

^{13}C NMR (75.5 MHz, $CDCl_3$): δ/ ppm = {126.0, 110.5, 108.4, 106.8, 106.8} ($C^{34,35,36,37,38,39}$), {78.8, 78.6, 73.6, 73.2, 72.1, 71.5, 71.0, 70.9, 70.8, 70.8, 70.7, 70.7, 70.5, 70.2, 70.1, 69.9} ($C^{3,4,5,6,7,8,9,10,11,12,13,14,15,16,17,18,19,20,21,22,24,25,26,27,28,29,30}$), {63.6, 59.2, 58.5, 56.6, 56.6} ($C^{23,33,42,44,46}$), 41.2 (C^{31}), 18.4 ($C^{43,45,47}$), 13.1 (C^2), 6.6 (C^1).

4,5-dimethoxy-2-nitrobenzyl 13-2,5,8,11,14-pentaoxapentadecyl-3,6,9,12,15,18,21,24,27-nonaoxatriacontylcarbamate

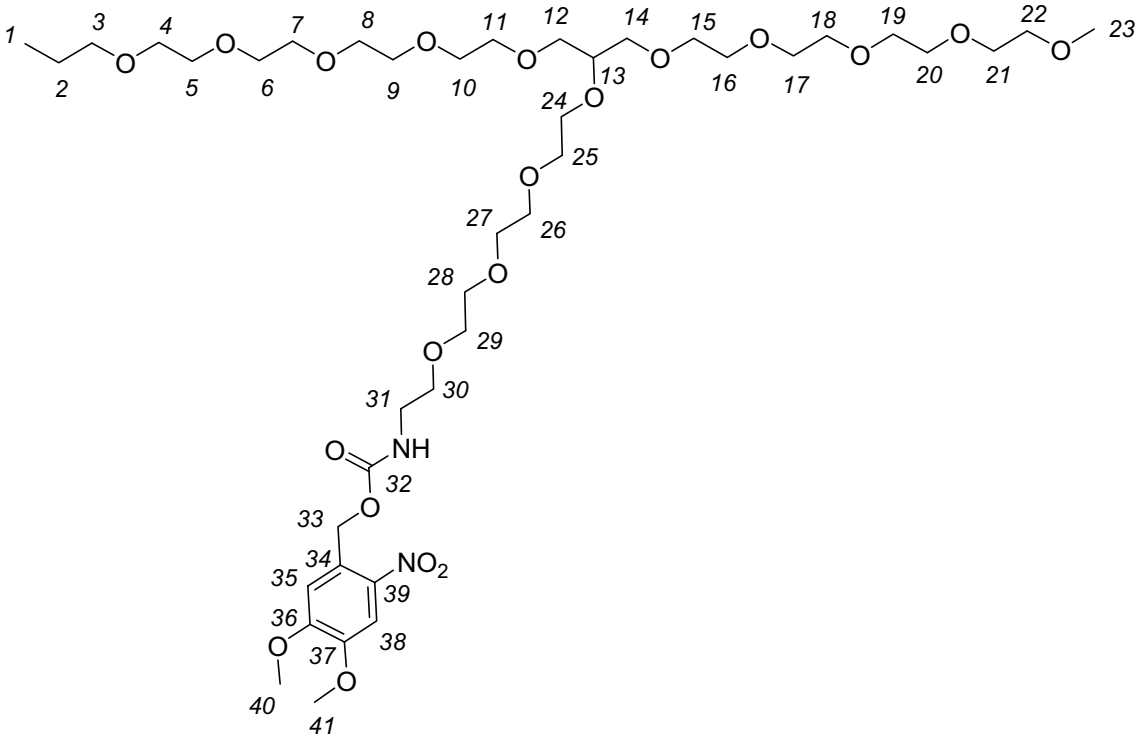

23

$C_{41}H_{74}N_2O_{20}$

[915.03]

23, the reduced compound of **21**, was obtained as byproduct in the synthesis of **21** and **22**. The ^{1}H NMR signals attributed to H^1 and H^2 show different positions and multiplicity with respect to the signals of **22**: δ/ ppm = 0.9 (t, J = 7.4 Hz) for H^1 and 1.59 (m) for H^2. The signals in the ^{13}C NMR spectrum attributed to C^1 and C^2 are shifted with respect to the signals of **22**: δ/ ppm = 10.6 for C^1 and 23.1 for C^2.

2-(2,5,8,11,14-pentaoxaheptadec-16-enyl)oxirane[147]

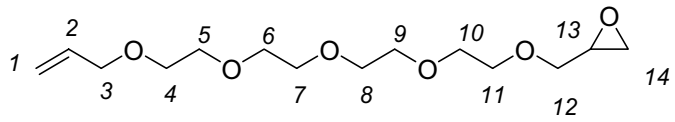

24

$C_{14}H_{26}O_6$

[290.35]

1 (7.5 g, 32 mmol), tetrabutyl ammonium hydrogen sulphate (11.6 g, 34 mmol) and 50% aqueous sodium hydroxide solution (13 ml) were mixed and cooled in an ice bath to 0–4 °C. (+/-)-Epichlorhydrin was slowly added under vigorous stirring. After complete addition the reaction mixture was kept stirring at this temperature for further 20 min, then at room temperature for 12 hours. The solution was then poured onto crushed ice (6 g) and mixed well. The upper organic layer was isolated, and the aqueous layer extracted with ether and dichloromethane. The combined organic extracts were then dried over sodium sulphate. The solvent was then removed under reduced pressure. The excess of epichlorhydrin was distilled off (30 °C, 2.2×10^{-2} mbar). Unreacted **1** was then removed by column chromatography using ethylacetate/ ethanol (99:1) as eluent. The desired product **24** was obtained as colorless oil (5.05 g, 17.4 mmol, 54%).

(literature yield: 50%)

^{1}H NMR (300.1 MHz, $CDCl_3$): δ/ ppm = 5.80-5.94 (m, 1H, H^2), 5.09-5.26 (m, 2H, H^1), 3.98 (d, J = 5.9 Hz, 2H, H^3), 3.76-3.53 (m, 17H, $H^{4,5,6,7,8,9,10,11,12}$), {3.42-3.36 (m, 1H,), 3.14-3.08 (m, 1H), 2.76-2.73 (m, 1H), 2.55-2.58 (m, 1H)} ($H^{12,13,14}$).

^{13}C NMR (75.5 MHz, $CDCl_3$): δ/ ppm = 134.9 (C^2), 117.0 (C^1), 72.2, 72.0 ($C^{3,12}$), {70.8, 70.7, 70.7, 69.5 }($C^{4,5,6,7,8,9,10,11}$), 50.8 (C^{13}), 44.3 (C^{14}).

2-(2-(2-(2-aminoethoxy)ethoxy)ethoxy)ethanol

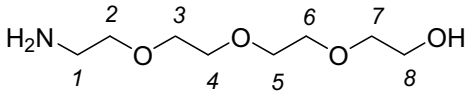

25

$C_8H_{19}NO_4$

[193.24]

A solution of **14** (1.3 g, 4.0 mmol) and hydrazine monohydrate (0.59 g, 11.7 mmol, 0.57 ml) in ethanol (25 ml) was heated under reflux for 16 hours and then allowed to cool to room temperature. The formed white precipitate was removed by filtration (washing with ethanol and dichloromethane). The filtrates were dried over anhydrous sodium sulphate and concentrated under reduced pressure. Excess of hydrazine was removed by distillation (5×10^{-3} mbar, 40 °C), to yield a yellow oil that was identified to be **25** in quantitative yield (0.52 mmol, 4 mmol).

^{1}H NMR (300.1 MHz, $CDCl_3$): δ/ ppm = 4.32 (s br, 3H, -O**H**, -N**H**$_2$), 3.69-3.50 (m, 14H, $H^{2,3,4,5,6,7,8}$), 2.86 (t, J = 5.1 Hz, 2H, H^1).

^{13}C NMR (75.5 MHz, $CDCl_3$): δ/ ppm {72.9, 72.0} ($C^{2,7}$), {70.5, 70.4, 70.2, 70.1} ($C^{3,4,5,6}$), 61.3 (C^3), 41.1 (C^1).

4,5-dimethoxy-2-nitrobenzyl 2-(2-(2-(2-hydroxyethoxy)ethoxy)ethoxy)ethylcarbamate

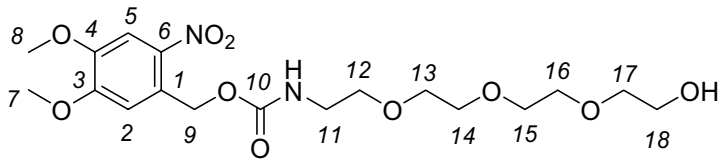

26

$C_{18}H_{28}N_2O_{10}$

[432.42]

A solution of **25** (0.83 g, 4.3 mmol) and sodium hydrogen carbonate (1.02 g, 12.1 mmol) in distilled water (20 ml) was cooled to 0-4 °C. 6-Nitroveratryloxycarbonyl chloride (1.4 g, 5.1 mmol) in dioxane (100 ml) was added dropwise over a period of 45 minutes, and the reaction mixture was allowed to stir at room temperature overnight.

After addition of diluted hydrochloric acid (1 N HCl, 3 ml), the aqueous phase was extacted with dichloromethane. The combined organic layers were dried over anhydrous sodium sulphate and concentrated under reduced pressure.

The crude product was purified by column chromatography using ethylacetate/ ethanol 9:1 as eluent to give **27** as pale yellow solid (1.48 g, 3.4 mmol, 79%).

^{1}H NMR (300.1 MHz, $CDCl_3$): δ/ ppm = 7.70 (s, 1H, H^5), 7.06 (s, 1H, H^2), 6.38 (s br, 1H, -N**H**), 5.51 (s, 2H, H^9), {3.97 (s, 3H), 3.94 (s, 3H)} ($H^{7,8}$), {3.71-3.55 (m, 14H, $H^{12,13,14,15,16,17,18}$), 3.43-3.38 (m, 2H, H^{11}), 1.73 (s br, 1H, -O**H**).

^{13}C NMR (75.5 MHz, $CDCl_3$): δ/ ppm = {156.5, 153.8} ($C^{3,10}$), {148.3, 128.9} ($C^{4,6,1}$), {110.5, 108.5} ($C^{2,5}$), {72.8, 70.9, 70.7, 70.5, 70.4, 70.3} ($C^{12,13,14,15,16,17}$), {63.5, 61.8} ($C^{9,18}$), {56.7, 56.6} ($C^{7,8}$), 41.3 (C^{11}).

1-(4,5-dimethoxy-2-nitrophenyl)-3-oxo-2,7,10,13-tetraoxa-4-azapentadecan-15-yl 4-methylbenzenesulfonate

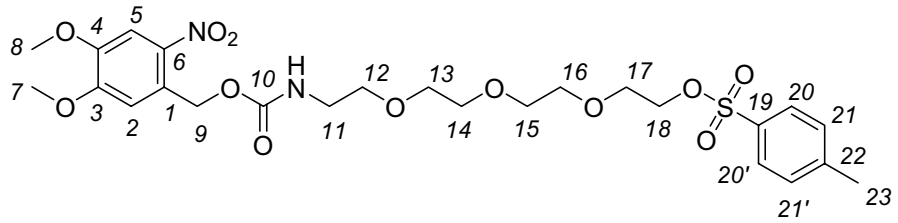

27

$C_{25}H_{34}N_2O_{12}S$

[586.61]

A solution of **26** (0.88 g, 2.0 mmol) and p-toluene sulfonyl chloride (0.67 g, 3.5 mmol, 1.75 mol-eq.) in chloroform (10 ml) was cooled to 0-4 °C. Pyridine (0.57 g, 7.0 mmol, 0.58 ml) was added drop wise. After complete addition of pyridine, the reaction mixture was stirred for further 30 minutes in the cold and then at room temperature overnight. The reaction mixture was then poored into a mixture of crushed ice (2.3 g) and concentrated hydrochloric acid (0.6 ml), and the phases were separated. The aqueous layer was extracted with dichloromethane (3 × 15 ml), and the combined organic layers were dried over anhydrous sodium sulphate. After removal of the solvent under reduced pressure, the crude product was obtained as viscous orange oil. Purification by column chromatography using ethylacetate as eluent yielded pure **27** as pale yellow oil (1.03 g, 1.76 mmol, 88%).

^{1}H NMR (300.1 MHz, $CDCl_3$): δ/ ppm = 7.78 (d, J = 8.2 Hz, 2H, $H^{21,21'}$), 7.70 (s, 1H, H^5), 7.32 (d, J = 8.2 Hz, 2H, $H^{20,20'}$), 7.02 (s, 1H, H^2), 5.48 (s br, 3H, H^9, -N**H**-), 4.13-4.20 (m, 2H, H^{18}), {3.96 (s, 3H), 3.94 (s, 3H)} ($H^{7,8}$), {3.68 (t, J = 4.8 Hz, 2H), 3.63-3.55 (m, 10H)} ($H^{12,13,14,15,16,17}$), 3.42-3.37 (m, 2H, H^{11}), 2.43 (s, 3H, H^{23}).

^{13}C NMR (75.5 MHz, $CDCl_3$): δ/ ppm = {153.7, 148.3, 144.9, 130.0, 128.1} ($C^{1,3,4,6,10,19,20,20',21,21',22}$), {110.6, 108.4} ($C^{2,5}$), {71.0, 70.8, 70.7, 70.5, 70.1,69.4, 68.9} ($C^{12,13,14,15,16,17,18}$), 63.6 (C^9), {56.6, 56,6} ($C^{7,8}$), 41.2 (C^{11}), 21.7 (C^{23}).

2-((dec-9-enyloxy)methyl)oxirane

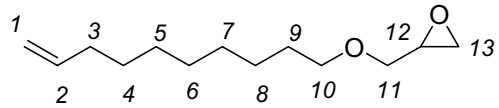

28

$C_{14}H_{26}O_6$

[290.35]

9-Decen-1-ol (3.88 g, 24.8 mmol), tetrabutyl ammonium hydrogen sulfate (6.47 g, 19.1 mmol) and 50% aqueous sodium hydroxide solution (7.3 ml) were mixed and cooled in an ice bath to 0–4 °C. (+/-)-Epichlorhydrin (10.9 g, 9.2 ml, 117.8 mmol) was slowly added under vigorous stirring. After complete addition the yellow reaction mixture was kept stirring at this temperature for further 30 min, then at room temperature for 20 hours. Crushed ice (5 g) was added and mixed well. The organic layer was isolated, and the aqueous layer extracted with dichloromethane and diethylether. The combined organic extracts were dried over sodium sulphate.

Excess of epichlorhydrin was removed by distillation under vacuum (60 °C, 1.2×10^{-2} mbar). The product was then separated from unreacted 9-decen-1-ol by distillation (110-150° C, 5×10^{-3} mbar). Still containing traces of unreacted 9-decen-1-ol were then removed by column chromatography using petroleum ether/ ethyl acetate (9:1) as eluent to give the pure product **28** as colorless oil (3.59 g, 16.9 mmol, 68%).

^{1}H NMR (300.1 MHz, $CDCl_3$): δ/ ppm = 5.88-5.72 (m, 1H, H^2), 5.02-4.89 (m, 2H, H^1), 3.73-3.67 (m, 1H, H^{11}), 3.55-3.33 (m, 3H, $H^{10,11}$), {2.62-2.58 (m, 1H), 2.81-2.77 (m, 1H), 3.17-3.11 (m, 1H)} ($H^{12,13}$), 2.07-1.99 (m, 2H, H^3), 1.64-1.52 (m, 2H, H^9), 1.42-1.28 (m, 10H, $H^{4,5,6,7,8}$).

^{13}C NMR (75.5 MHz, $CDCl_3$): δ/ ppm = 139.2 (C^2), 114.2 (C^1), {71.8, 71.5} ($C^{10,11}$), 51.0 (C^{12}), 44.4 (C^{13}), 33.9 (C^3), {29.8, 29.5, 29.1, 29.0, 26.1} ($C^{4,5,6,7,8,9}$).

2,5,8,11,14,18-hexaoxaoctacos-27-en-16-ol

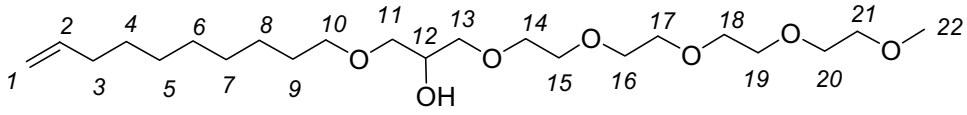

29

$C_{21}H_{42}O_7$

[420.58]

NaH (0.072 g, 3 mmol) was placed in a dry three-necked round bottom flask. Under argon atmosphere tetraethyleneglycol monomethylether (3.00 g, 14.4 mmol) in dry THF (20 ml) was added. The formation of bubbles could be observed (due to H_2 formation). The solution was heated to about 60 °C. **28** (3.00 g, 14.1 mmol) in dry THF (20 ml) was then added dropwise in the heat. The reaction mixture was heated under reflux and kept at this temperature for 2 days. After complete conversion of the epoxide (analyzing a small sample by ^{1}H NMR spectroscopy) the reaction mixture was allowed to cool down to room temperature. Water (6 ml) was added and the mixture was extracted with dichloromethane. After neutralization with a few drops of diluted H_2SO_4, the aqueous phase was extracted again with dichloromethane. The combined organic extracts were dried over sodium sulphate and concentrated on a rotatory evaporator.

Excess of tetraethyleneglycol monomethylether was removed by distillation (180 °C, 1.1×10^{-2} mbar, 1.64 g, 50% of the used amount). The pure product **29** was obtained by distillation (220-250 °C, 1.1×10^{-2} mbar) as a pale yellow oil (2.98 g, 7.1 mmol, 50%).

^{1}H NMR (300.1 MHz, $CDCl_3$): δ/ ppm = 5.73-5.60 (m, 1H, H^2), 4.88-4.76 (m, 2H, H^1), 3.85-3.77 (m, 1H, H^{12}), 3.53-3.26 (m, 22H, $H^{10,11,13,14,15,16,17,18,19,20,21}$), 3.24 (s, 3H, H^{22}), 2.70 (s br, 1H, -O**H**), 1.93-1.86 (m, 2H, H^3), 1.45-1.38 (m, 2H, H^9), 1.26-1.10 (m, 10H, $H^{4,5,6,7,8}$).

^{13}C NMR (75.5 MHz, $CDCl_3$): δ/ ppm = 139.1 (C^2), 114.1 (C^1), {72.7, 72.0, 71.8, 71.7, 70.8, 70.6, 70.6, 70.5, 70.5, 69.4} ($C^{10,11,12,13,14,15,16,17,18,19,20,21}$), 59.0 ($C^{22}$), 33.8 ($C^3$), {29.6, 29.4, 29.4, 28.9} ($C^{4,5,6,7,9}$), 26.1 (C^8).

2-(16-((dec-9-enyloxy)methyl)-2,5,8,11,14,17,20,23,26-nonaoxaoctacosan-28-yl)isoindoline-1,3-dione

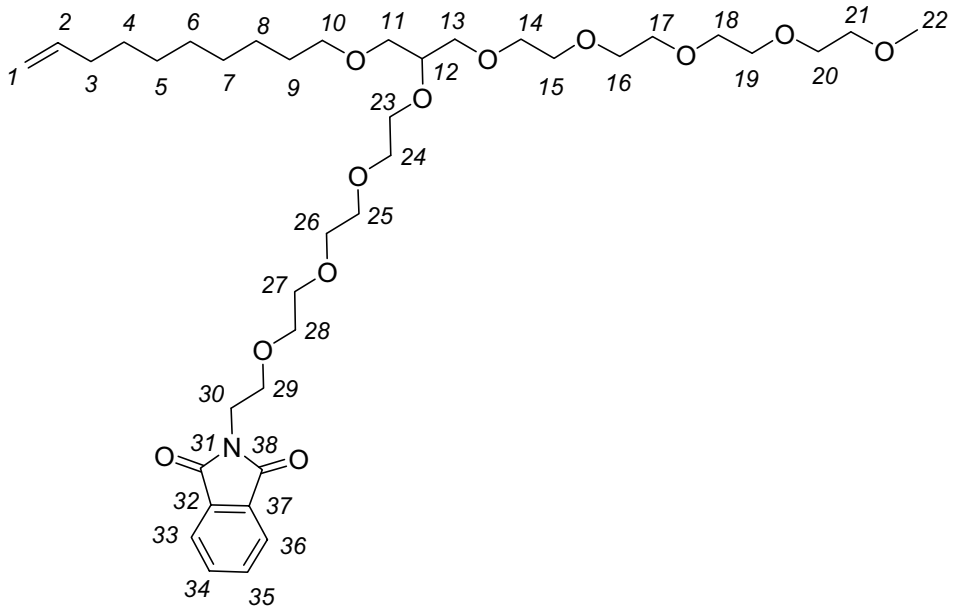

30

$C_{38}H_{63}NO_{12}$

[725.91]

NaH (0.1 g, 4.2 mmol) was placed in a dry three-necked round bottom flask. Under argon atmosphere **29** (1.76 g, 4.2 mmol) in dry THF (25 ml) was added. The reaction mixture was stirred under reflux for 2.5 hours until NaH was completely dissolved. Then **12** in dry THF (15 ml) was added, evocating sunny yellow coloration of the reaction mixture. The reaction mixture was kept under reflux for 15 hours. After cooling to room temperature, distilled water (30ml) was added. The mixture was extracted three times with dichloromethane, neutralized with diluted H_2SO_4 and then extracted again twice with dichloromethane. The combined organic extracts were dried over sodium sulphate and concentrated on a rotatory evaporator.

Low molecular-weight molecules were distilled off in the vacuum (up to 180 °C, 8×10^{-3} mbar). The residual orange oil could be determined to be **30** and was used without any further purification. (2.33 g, 3.2 mmol, 80%).

^{1}H NMR (300.1 MHz, $CDCl_3$): δ/ ppm = 7.85-7.80 (m, 2H, $H^{33,36}$), 7.73-7.67 (m, 2H, $H^{34,35}$), 5.86-5.72 (m, 1H, H^{1}), 5.00-4.89 (m, 2H, H^{2}), 3.88 (t, 2H, *J* = 5.7 Hz, H^{30}), {3.74-3.70 (m, 4H), 3.64-3.38 (m, 33H)} ($H^{10,11,12,13,14,15,16,17,18,19,20,21,23,24,25,26,27,28,29}$), 3.36 (s, 3H, H^{22}), 2.05-1.98 (m, 2H, H^{3}), 1.57-1.48 (m, 2H, H^{9}), 1.38-1.26 (m, 10H, $H^{4,5,6,7,8}$).

^{13}C NMR (75.5 MHz, $CDCl_3$): δ/ ppm = 134.1 (C^{2}), {139.4, 132.4, 123.4} ($C^{32,33,34,35,36,37}$), 78.6 (C^{12}), {72.2, 71.8, 71.7, 71.0, 70.9, 70.9, 70.8, 70.8, 70.8, 70.7, 70.7, 70.3, 69.9, 68.1} ($C^{10,11,13,14,15,16,17,18,19,20,21,23,24,25,26,27,28,29}$), 59.2 ($C^{22}$), 37.5 ($C^{30}$), 34.0 ($C^{3}$), {29.9, 29.6, 29.6, 29.3, 29.1, 26.3} ($C^{4,5,6,7,8,9}$).

16-((dec-9-enyloxy)methyl)-2,5,8,11,14,17,20,23,26-nonaoxaoctacosan-28-amine

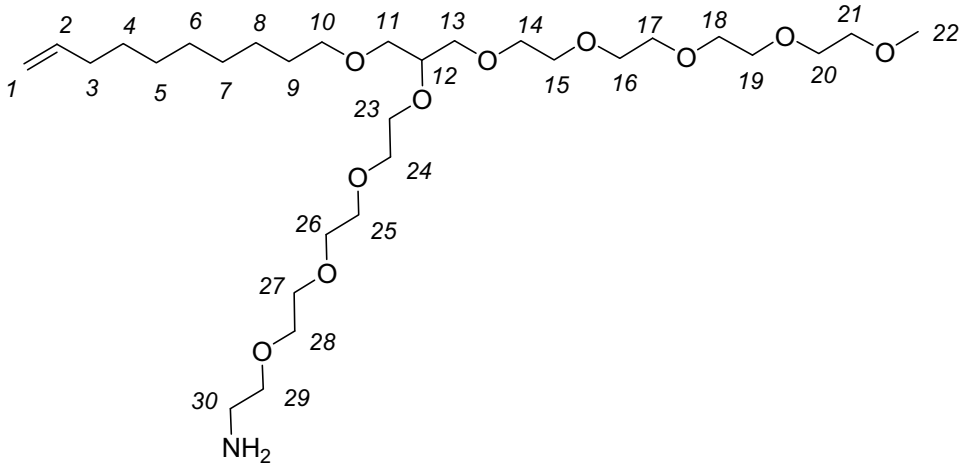

31

$C_{30}H_{61}NO_{10}$

[595.81]

30 (2.3 g, 3.3 mmol) and hydrazine monohydrate (0.5 g, 0.5 ml, 10 mmol) were dissolved in ethanol (30 ml). The solution was heated to reflux and for 18 hours. Then the mixture was allowed to cool to room temperature and filtered. The solid residue was washed with ethanol. The combined filtrates were concentrated on a rotatory evaporator. Excess of hydrazine was removed by distillation (100 °C, 9×10^{-3} mbar).

The residual brown liquid **31** (2 g, 3.3 mmol, quantitative) was used as obtained for further reactions.

^{1}H NMR (300.1 MHz, $CDCl_3$): δ/ ppm = 5.82-5.69 (m, 1H, H^{2}), 4.97-4.85 (m, 2H, H^{1}), {3.73-3.69 (m, 2H), (3.60-3.34 (m, 35H)} ($H^{10,11,12,13,14,15,16,17,18,19,20,21,23,24,25,26,27,28,29}$), 3.32 (s, 3H, H^{22}), 2.82 (t, J = 5.2 Hz, 2H, H^{30}), 2.09 (s br, 2H, -N**H**$_2$), 2.02-1.95 (m, 2H, H^{3}), 1.51-1.45 (m, 2H, H^{9}), 1.34-1.21 (m, 10H, $H^{4,5,6,7,8}$).

^{13}C NMR (75.5 MHz, $CDCl_3$): δ/ ppm = {78.4, 73.2, 72.0, 71.6, 71.4, 70.8, 70.8, 70.8, 70.6, 70.6, 70.6, 70.6, 70.5, 70.3, 69.8} ($C^{10,11,13,14,15,16,17,18,19,20,21,23,24,25,26,27,28,29}$), 59.0 ($C^{22}$), 41.8 ($C^{3}$), 33.8 ($C^{3}$), {29.6, 29.4, 29.4, 29.1, 28.9} ($C^{4,5,6,7,9}$), 26.1 (C^{8}).

4,5-dimethoxy-2-nitrobenzyl 16-((dec-9-enyloxy)methyl)-2,5,8,11,14,17,20,23,26-nonaoxaoctacosan-28-ylcarbamate

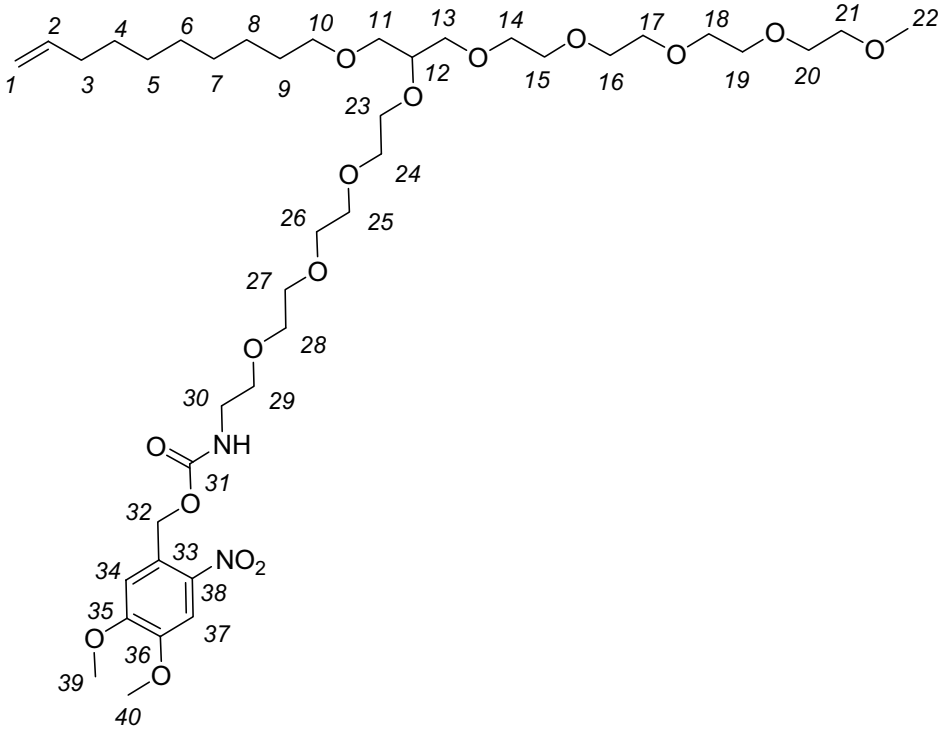

32

$C_{40}H_{70}N_2O_{16}$

[834.99]

A solution of **31** (1.54 g, 2.6 mmol) and sodium hydrogen carbonate (0.59 g, 7.0 mmol) in 25 ml water was cooled to 0-4 °C in an ice-bath. Under stirring a solution of 6-nitroveratryloxycarbonyl chloride (0.95 g, 3.4 mmol) in dioxan (70 ml) was slowly added. After complete addition, the reaction mixture was kept at this temperature under stirring for further 15 min, then at room temperature for at least 3 hours (or overnight). After neutralization with aqueous hydrochloric acid solution (1 N HCl, 1.5 ml) the mixture was extracted with dichloromethane. The organic extracts were dried over sodium sulphate, and the solvents removed under reduced pressure. The obtained brown oil (3.2 g) was subjected to column chromatography using a mixture of ethylacetate and ethanol (14:1) as eluent. **32** was obtained in a 70 mol-% mixture with the reduced compound **34** (1.5 g, equivalent to 1.3 mmol pure **32**, 48%).

^{1}H NMR (300.1 MHz, $CDCl_3$): δ/ ppm = 7.70 (s, 1H, H^{37}), 7.02 (s, 1H, H^{34}), 5.87-5.74 (m, 1H, H^{2}), 5.51 (s and s br, 3H, H^{32}, -N**H**-), 5.01-4.90 (m, 2H, H^{1}), {3.98 (s, 3H), 3.95 (s, 3H)} ($H^{39,40}$), {3.77-3.73 (m, 2H), 3.68-3.38 (m, 35H)} ($H^{10,11,12,13,14,15,16,17,18,19,20,21,23,24,25,26,27,28,29}$), 3.37 (s, 3H, H^{22}), 2.06-1.99 (m, 2H, H^{3}), 1.55-1.49 (m, 2H, H^{9}), 1.39-1.21 (m, 10H, $H^{4,5,6,7,8}$).

^{13}C NMR (75.5 MHz, $CDCl_3$): δ/ ppm = 139.3 (C^{2}), 114.2 (C^{1}), {110.4, 108.3} ($C^{34,37}$), 78.5 (C^{12}), {72.0, 71.7, 71.5, 70.9, 70.8, 70.8, 70.7, 70.7, 70.6, 70.6, 70.6, 70.4, 70.1, 69.8} ($C^{10,11,12,13,14,15,16,17,18,19,20,21,23,24,25,26,27,28,29}$), 59.1 ($C^{22}$), {56.5, 56.5, 55.9} ($C^{32,39,40}$), 43.8 ($C^{30}$), 33.9 ($C^{3}$), {29.7, 29.5, 29.5, 29.1, 29.0} ($C^{4,5,6,7,9}$), 26.2 (C^{8}).

4,5-dimethoxy-2-nitrobenzyl 4,4-diethoxy-17-2,5,8,11,14-pentaoxapentadecyl-3,15,18,21,24,27-hexaoxa-4-silanonacosan-29-ylcarbamate

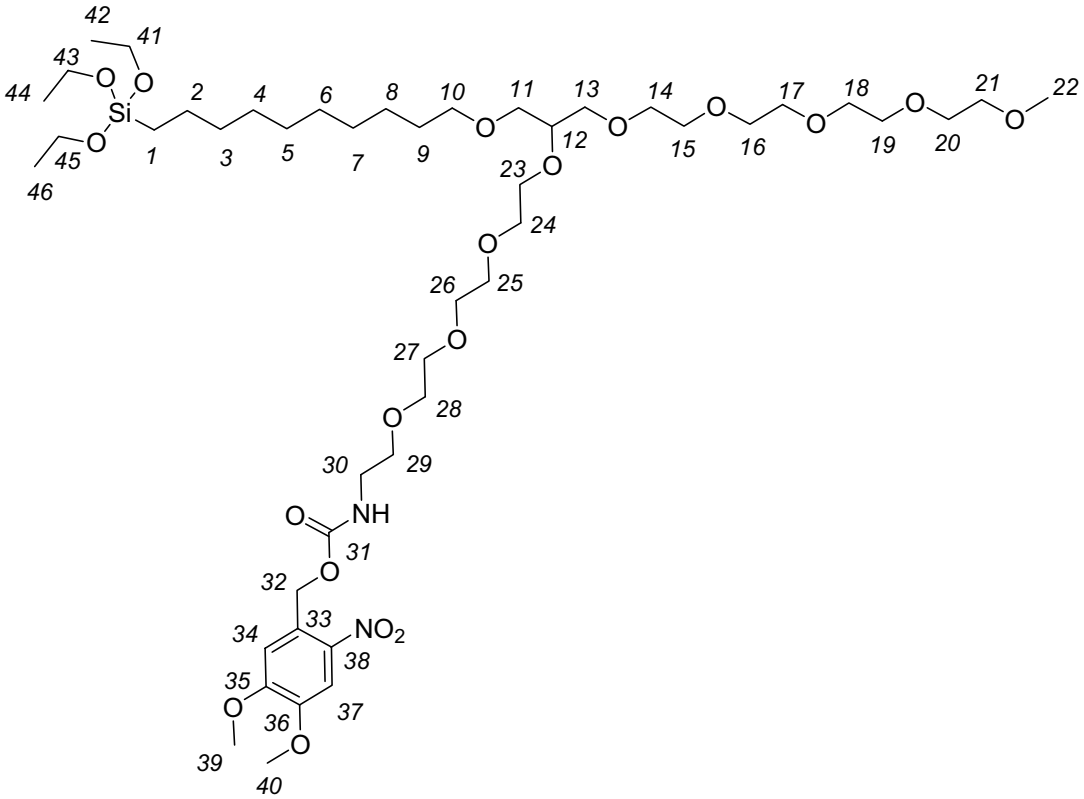

33

$C_{43}H_{80}N_2O_{19}Si$

[957.18]

32 (0.89 g, 1 mmol) and triethoxysilane (1.78 g, 10.8 mmol, 2 ml) were placed into a previously passivated, dry reaction flask with attached distillation apparatus and heated

to 80 °C, under argon. After homogeneous mixture of both reactants, isopropanolic H_2PtCl_6 solution (60 µl, c = 0.027 mg/ µl) was added. The reaction was followed by ^{1}H NMR spectroscopy. Eventually more catalyst had to be added. After about 4 hours, the excess of triethoxysilane was removed by distillation (up to 80 °C, 8×10^{-3} mbar). The crude product was dissolved in dichloromethane and filtered through Celite®500. After removal of the solvent under reduced pressure, **33** was obtained as yellow oil in a 60 mol-% mixture with the reduced compound **34** (0.75 g, equivalent to 0.5 mmol pure **33**, 47%).

^{1}H NMR (300.1 MHz, $CDCl_3$): δ/ ppm = 7.70 (s, 1H, H^{37}), 7.03 (s, 1H, H^{34}), 5.62 (s br, 1H, -N**H**-), 5.51 (s, 2H, H^{32}), {3.95 (s, 3H), 3.40 (s, 3H)} ($H^{39,40}$), 3.81 (q, J = 7.1 Hz, 6H, $H^{41,43,45}$), 3.76-3.40 (m, 39H)} ($H^{10,11,12,13,14,15,16,17,18,19,20,21,23,24,25,26,27,28,29,30}$), 3.37 (s, 3H, H^{22}), 1.58-1.50 (m, 2H, H^2), 1.36-1.20 (m (t underneath with *J* = 7.1 Hz, 23H, $H^{3,4,5,6,7,8,9,42,44,46}$), 0.64-0.59 (m, 2H, H^1).

^{13}C NMR (75.5 MHz, $CDCl_3$): δ/ ppm = {110.4, 108.4} ($C^{34,37}$), 78.6 (C^{12}), {72.1, 71.8, 71.8, 71.6, 71.0, 70.9, 70.9, 70.8, 70.7, 70.7, 70.7, 70.7, 70.5, 70.2, 69.9, 63.6} ($C^{10,11,12,13,14,15,16,17,18,19,20,21,23,24,25,26,27,28,29}$), {63.6, 59.2, 58.4, 56.6, 56.5} ($C^{22,32,39,40,41,43,45}$), 41.2 (C^{30}), {33.4, 29.8, 29.8, 29.7, 29.7, 29.4, 26.3} ($C^{3,4,5,6,7,8,9}$), 18.4 ($C^{42,44,46}$), 14.2 (C^2), 10.6 (C1).

4,5-dimethoxy-2-nitrobenzyl 16-(decyloxymethyl)-2,5,8,11,14,17,20,23,26-nonaoxaoctacosan-28-ylcarbamate

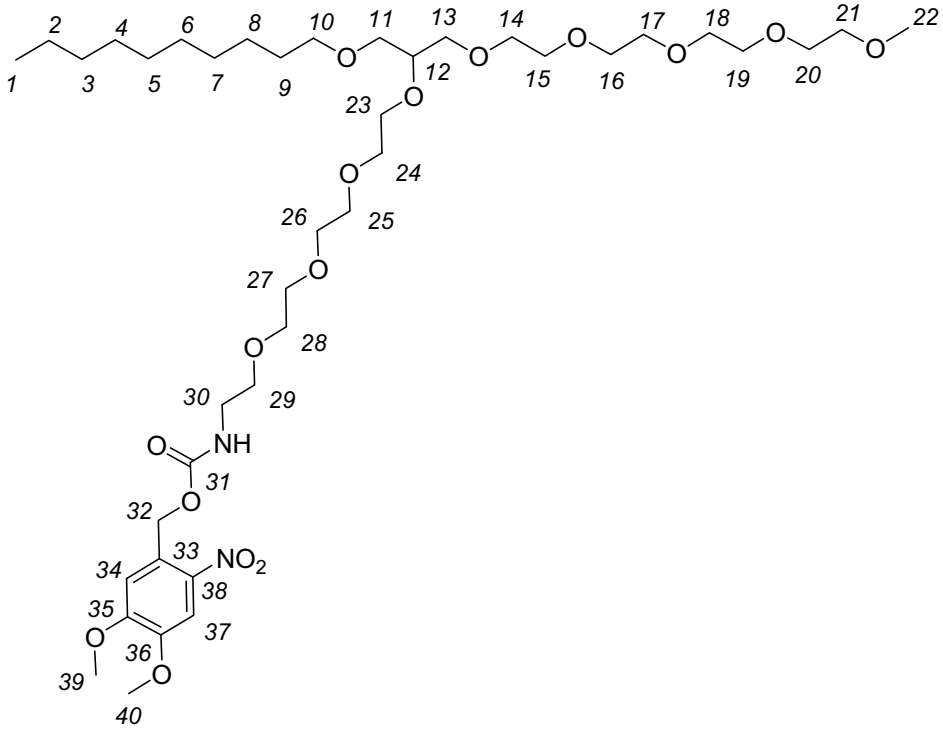

34

$C_{40}H_{72}N_2O_{16}$

[836.99]

34, the reduced compound of **32**, was obtained as byproduct in the synthesis of **33.** The ^{1}H NMR signals attributed to H^1 and H^2 show different positions and multiplicity with respect to the signals of **32**: δ/ ppm = 0.87 (t, J = 7.0 Hz) for H^1 and ≈1.3 for H^2 (below the signals arising from $H^{4,5,6,7,8}$). The signals in the ^{13}C NMR spectrum attributed to C^1 and C^2 are shifted with respect to the signals of **32**: δ/ ppm = 14.2 for C^1 and 22.9 for C^2.

A.2.2 Synthesis of EG-OMe

2,5,8,11,14-pentaoxaheptadec-16-ene[145]

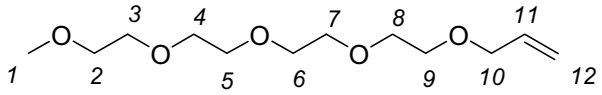

allylic precursor to EG-OMe

$C_{12}H_{24}O_5$

[248.32]

Tetraethylene glycol monomethylether (5 g, 24 mmol) and *p*-toluene sulfonyl chloride (6.67 g, 35 mmol) were dissolved in chloroform (25 ml). At 0-4 °C pyridine (5.6 g, 71 mmol, 5.7 ml) was added drop wise under vigorous stirring. After complete addition the reaction mixture was stirred at this temperature for further 30 minutes and subsequently at room temperature overnight. Subsequently the reaction mixture was added to a mixture of crushed ice (23 g) and concentrated hydrochloric acid (6.3 ml). After phase separation the acqueous layer was extracted with dichloromethane. The combined organic layers were dried over anhydrous sodium sulphate. After removal of the solvent 10.3 g of colorless liquid were obtained. Column chromatography using ethylacetate/ petroleum (2.5:1) as eluent gave the pure product as a colorless oil (8.0 g, 22.1 mmol, 92%).

^{1}H NMR (300.1 MHz, $CDCl_3$): δ/ ppm = 5.90-5.74 (m, 1H, H^{11}), 5.24-5.08 (m, 2H, H^{12}), 3.95 (dt, 2H, J = 5.6 Hz, J = 1.3 Hz, H^{10}), 3.61-3.46 (m, 16H, $H^{2,3,4,5,6,7,8,9}$), 3.30 (s, 3H, H^1).

^{13}C NMR (75.5 MHz, $CDCl_3$): δ/ ppm = 134.8 (C^{11}), 116.9 (C^{12}), {72.1, 71.9, 70.6, 70.6, 70.6, 70.6, 70.5, 69.4} ($C^{2,3,4,5,6,7,8,9,10}$), 58.9 (C^1).

18,18-diethoxy-2,5,8,11,14,19-hexaoxa-18-silahenicosane

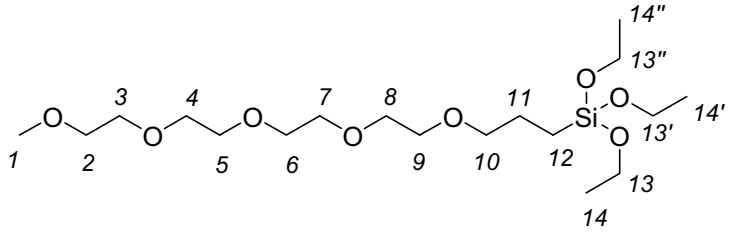

EG-OMe

$C_{18}H_{40}O_8Si$

[412.59]

The previously synthesized allylic precursor (2,5,8,11,14-pentaoxaheptadec-16-ene) (2.0 g, 8.0 mmol) and triethoxysilane (13.2 g, 80.0 mmol, 14.8 ml, 10 mol-equivalent) were heated to 80 °C under argon, in a previously HMDS passivated reaction flask connected to a distillation apparatus. Isopropanolic hexachloroplatinic acid solution (401 µl, c = 0.027 mg/ µl, 26.4 µmol, 3.3×10^{-3} mol-equivalent) was added to the hot solution. The reaction was monitored by ^{1}H NMR spectroscopy. ^{1}H NMR analysis of the reaction mixture indicated a composition of silane/ reduced compound of 0.7:0.3 after 7 hours reaction time. The excess of triethoxysilane was removed by distillation (38 °C, 40×10^{-3} mbar). The crude product was subjected to column chromatography with a passivated silica support (treatment with HMDS (2% w/ V) for 10 min). The desired silane **EG-OMe** could be obtained as colorless oil in a 60% mixture with the reduced compound (0.99 g).

^{1}H NMR (300.1 MHz, $CDCl_3$): δ/ ppm = 3.73 (q, *J* = 7.0 Hz, 6H, $H^{13,13',13''}$), 3.59-3.31 (m, 18H, $H^{2,3,4,5,6,7,8,9,10}$), 3.29 (s, 3H, H^1), 1.66-1.56 (m, 2H, H^{11}), 1.14 (t, *J* = 7.0 Hz, 9H, $H^{14,14',14''}$), 0.52-0.57 (m, 2H, H^{12}).

^{13}C NMR (75.5 MHz, $CDCl_3$): δ/ ppm = {73.6, 73.0, 71.9, 70.6, 70.5, 70.5, 70.0, 70.0} ($C^{2,3,4,5,6,7,8,9,10}$), {58.9, 58.3} ($C^{1,13,13'}$), 22.8 (C^{11}), 18.2 ($C^{14,14',14''}$), 6.4 (C^{12}).

Signals attributed to the reduced compound are shifted with respect to the allylic compound and show different multiplicity: δ/ ppm = 1.51 ppm (q, *J* = 7.3 Hz) for H^{11} and 0.83 ppm (t, *J* = 7.3 Hz) for H^{12} in the ^{1}H NMR spectrum; δ/ ppm = 14.2 for C^1 and 22.9 for C^2 in the ^{13}C NMR spectrum.

A.2.3 Surface modification

Surface Reaction

The surface modification process was performed following a published protocol.[87, 97] Experiments with increasing catalyst concentration and deposition times were performed in order to obtain smooth and homogeneous surface layers with maximum density of functional groups (as revealed by UV spectroscopy). In an optimized procedure, the silane (Y-EG-NVoc or Y-alkyl-NVoc) was prehydrolyzed as a 1% w/ V solution in THF with catalytic amounts of NaOH (55 µl 1N aqu. NaOH in 17 ml THF) in a passivated reaction vessel for 4 h. After filtration through a micropore-sized filter (0.2 µm PTFE filter), clean substrates were immersed into this prehydrolyzed solution for 63 h/ 163 h. After deposition, the substrates were thoroughly washed with THF to remove any unspecifically adsorbed silane, then with Milli-Q-water and baked for 1 hour in the vacuum oven at 90°C.

In the case of the 1:1 molar ratio mixture of silanes EG-NVoc and EG-OMe, a 1% w/ V solution of the silanes in THF was used and the silanization time was 45 hours.
Surface modification with APTS were performed in Milli-Q-water using the same conditions as described in literature,[87] an APTS concentration of 2% w/ V, a hydrolysis time of 30 min and a silanization time of 1 h.

Prior to further applications, the substrates were sonicated in an ultrasound THF bath for 3 minutes, washed with Milli-Q-water and dried with a N_2 stream.

Irradiation

Activation of the surface functionalities by photocleavage of the NVoc group was achieved by irradiation at 355 nm for 10 min. The substrates were thoroughly washed with THF and Milli-Q-water after the irradiation process to remove the photolysis side products. The deprotection was monitored by the decay in the UV-vis spectrum (as a consequence of the cleavage of the chromophore). The minimum irradiation time of for full deprotection (10 min) was obtained from different experiments at various irradiation times.

A.2.4 Adsorption and binding experiments

Non-specific adsorption of BSA

In a BIAffinity flow chamber, a solution of BSA (1 mg ml^{-1}) in PBS was injected onto different modified sensor chips (bare sensor chip, modified with APTS, Y-EG-NVoc, Y-EG-NH_2, Y-alkyl-NVoc, Y-alkyl-NH_2). The optical thickness during incubation with a flow rate of 10 µl/ min was measured.

Immobilization of streptavidin onto biotin modified substrates

Blocking surfaces with acetic anhydride[154]

The surface free silanol groups might possibly undergo etherification reaction with the NHS-active ester as well, resulting in high amounts of immobilized biotin on all substrates, independently of the presence of amine groups. To block all reactive sites capable to react with the biotin NHS ester, all substrates were incubated in acetic anhydride for 15 minutes after silanization and then washed with THF.

Coupling of biotin-NHS ester

After blocking with acetic anhydride and eventually irradiation, the modified sensor chips were covered with a solution of biotin-NHS (0.2 mg ml^{-1}) in dry DMF. After incubation at room temperature for 1.5 hours, the substrates were washed with DMF, THF, Milli-Q water, dried in a N_2 stream and directly used for the streptavidin binding experiments in the BIAffinity flow chamber.

Binding of streptavidin to biotin-modified surfaces

In a BIAffinity flow chamber, a solution of streptavidin (10 µg ml^{-1}, 152 nM) in PBS was injected onto biotinylated surfaces with a flow rate of 10 µl min^{-1}.

Site-selective irradiation

Quartz substrates modified with Y-EG-NVoc were irradiated applying a quartz mask patterned with chrome lines. The mask was applied on top of the substrate with the chrome patterned side towards the substrate in order to avoid scattering.

After the irradiation, the substrates were subsequently washed with THF, Milli-Q-water and then sonictated in THF for 3 min.

Binding of Alexa Fluor® dye to masked irradiated substrates

Mask irradiated Y-EG-NVoc substrates (quartz mask with 50 µm wide chrome lines, spaced with 10 µm) were dried in the vacuum at 90 °C for 15 minutes. 100 µl of a solution of Alexa Fluor®647 succinimidyl ester in dry DMSO (0.14 mg ml^{-1}, corresponding to 110 µg ml^{-1}) were deposited on the quartz substrate (on the side that was situated next to the mask during irradiation) and left at room temperature overnight (preserved from light). After removal of the solution with a pipette, the substrate was subsequently washed with DMSO, THF and Milli-Q-water and dried in the vacuum at 90° C prior analysis under the fluorescence microscope.

OND immobilization onto masked irradiated substrates and hybrid capturing

Masked irradiated Y-EG-NVoc substrates (quartz mask with 50 µm wide chrome lines, spaced with 10 µm) were dried in the vacuum at 90 °C for 15 minutes. The surface was covered with 50 µl of a 1% glutaraldehyde solution in 1×SSC for 3 hours. After washing 5 times with 1×SSC buffer, 150 µl of ss-5'-NH_2-$(CH_2)_6$-$_dT_{25}$-3' in 1×SSC (5.03 M) were spotted on the surface and left for 15 hours at room temperature to allow formation of an imine bond with the primary amine on the surface. After washing again twice with 1×SSC buffer, the substrate was covered with 150 µl of $NaBH_3CN$ in 1×SSC (0.25 g/ ml) for 30 minutes in order to reduce the imine bond to a more stable amine bond. After washing with Milli-Q-water the substrate was left for 1 minute in water at 80 °C to denaturalize any non-specifically bound oligonucleotide base pair. The fluorescein-labeled complementary OND (f-5'-dA_{25}-3') was added to the surface in 1×SSC solution (250 µl, 5.03 M) at room temperature and left for 3 hours in order to

hybridize. After washing with 1×SSC buffer and Milli-Q-water, the substrate dried with a N_2 stream and analyzed by fluorescence microscopy.

Antigen immobilization onto masked irradiated substrates and detection by the corresponding fluorescent labeled antibody

Mask irradiated Y-EG-NVoc substrates (50 µm wide chrome lines and spaced with 10 µm) were dried in the vacuum at 90 °C for 15 minutes. The surface was covered with 50 µl of a 1% glutaraldehyde solution in 1×SSC for 3 hours at RT. After washing 5 times with 1×SSC buffer and 2 times with PBS-0.01% Triton X-100 buffer, 150 µl of goat IgG in PBS-0.01% Triton X-100 (0.095 mg ml^{-1}) were spotted on the surface and left for 13 hours at 4 °C to allow formation of an imine bond with the primary amine on the surface. After washing again twice with PBS-0.01% Triton X-100, the substrate was dried with a N_2 stream and covered with 150 µl of $NaBH_3CN$ in PBS-0.01% Triton X-100 (0.25 g ml^{-1}) for 35 minutes at RT in order to reduce the imine bond to a more stable amine bond. After washing 3 times with PBS-0.01% Triton X-100, 250 µl FITC-labeled anti-goat IgG (developed in rabbit) in PBS-0.01% Triton X-100 (0.15 mg ml^{-1}) were added to the surface and left at room temperature for 2.5 hours. After washing 3 times with PBS-0.01% Triton X-100, sonification in PBS-0.01% Triton X-100 for 3 min., washing with PBS and Milli-Q-water, the substrate was dried with a N_2 stream and analyzed by fluorescence microscopy.

Steptavidin immobilization onto masked irradiated substrates via biotin and detection by molecular recognition using fluorescein-labeled biotin

Mask irradiated Y-EG-NVoc substrates (50 µm wide chrome lines and spaced with 10 µm) were washed with THF and dried in the vacuum at 90 °C for 10 minutes. The surface was covered with 150 µl of a solution of biotin-NHS in dry DMF (100 mg ml^{-1}) for 30 min. at room temperature. After removal of the solution with a pipette, the substrates were washed 3 times with DMF and sonicated for 3 min in DMF to remove unbinded biotin-NHS. The substrates were washed twice with PBS-0.01% Triton X-100, dried in a N_2 stream and covered with 200 µl of a streptavidin solution (100 µg ml^{-1}) in PBS-0.01% Triton X-100 for 2 hours at room temperature. After

washing with PBS-0.01% Triton X-100 and PBS, 200 µl of a solution of biotin-4-fluoresceine (150 µg ml^{-1}) in PBS-0.01% Triton X-100 were added to the surface and left for 1.25 hours. The substrate was then washed twice with PBS-0.01% Triton X-100 and Milli-Q water, dried with a N_2 stream and analyzed under the fluorescence microscope.

Peptide immobilization

Y-EG-NVoc substrates and mask irradiated Y-EG-NVoc substrates (200 µm wide chrome lines and spaced with 100 µm) were dried with a N_2 stream. The surfaces were covered with each 100 µl of a 1% glutaraldehyde solution in 1×SSC for 3 hours at RT. After washing thoroughly with 1×SSC buffer and subsequently with PBS buffer, 150 µl of cyclo[RG(DMNPB)-DfK] in PBS (2 mg ml^{-1}) were spotted on each surface and left for 2 hours at RT in the dark. The substrates were then washed with PBS and Milli-Q water and dried with a N_2 stream.

Activation of the cyclo[RGDfK] occurred upon mask irradiation (200 µm wide chrome lines and spaced with 100 µm) at 351 nm (0.8 mW cm^{-2}) for 10 min. After washing with acetonitrile, Milli-Q water and dryng with a N_2 stream, the substrates were used for the cell experiments.

A.2.5 Cell experiments

Mouse fibroblasts (NIH/ 3T3) were cultured in DMEM medium (Invitrogen, Karlsruhe, Germany) supplemented with 10% fetal bovine serum (FBS), 1% L-glutamine (Invitrogen) at 37 °C and at 10% CO_2. Before plating on the quartz substrates, cells were trypsinized using 0.25% trypsin and 1mM EDTA in Hanks' buffered salt solution.

The modified quartz slides were sterilized in 70% ethanol and washed with 70% PBS at RT.

Procedure to obtain images shown in Figure 3.39:

150 µl of DMEM culture medium containing 3.3×10^5 cells/ml (corresponding to 50.000 cells/ substrate) were plated on the substrate. After 4 hours incubation at 37 °C (5% CO_2), new medium was added to the substrates. The culture was maintained for further 15 hours. Cells were counted in one field of the substrate, acquired through a 10× objective after 4 and 19 hours.

Procedure to obtain images shown in Figure 3.41:

150 µl of DMEM culture medium containing 2×10^5 cells/ml (corresponding to 30.000 cells/ substrate) were plated on the substrate. After 1 hour incubation at 37 °C, (5% CO_2) new medium was added to the substrates and the culture maintained for further 2 hours. After adding further 30.000 cells/ substrate, the culture was maintained fro further 18 hours. Cells were counted in one field of the substrate, acquired through a 10× objective after 3, 6 and 21 hours.

A.3 Experimental Part: New Coumarin-4-ylmethyl silanes for wavelength-selective photoactivation

A.3.1 Synthesis

N-[4,5-dimethoxy-2-nitrobenzyloxycarbonyl]allylamine[87, 101]

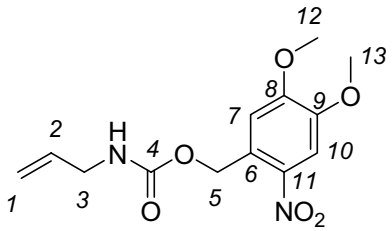

35

$C_{13}H_{16}N_2O_6$

[296.28]

Allylamine (0.5 g, 8.8 mmol), sodium hydrogencarbonate (1.75 g, 20.8 mmol) and water (25 ml) were placed into a dry round-bottom flask and cooled in an ice-bath. A solution of 6-nitroveratryloxycarbonyl chloride (2.5 g, 9 mmol) in dioxane (150 ml) was added dropwise under vigorous stirring (over a period of 30 min). A white precipitate forms instantaneously. The mixture was allowed to stir overnight at room temperature, preserved from light. After addition of 5 ml 1 N HCl, the mixture was extracted three times with dichloromethane. The combined organic extracts were dried over sodium sulphate. After removal of the solvent under reduced pressure, the solid residue was purified by column chromatography using a mixture of dichloromethane and ethyl acetate (9:1) as eluent. **35** was obtained as yellow powder (2.16 g, 7.3 mmol, 83%).

^{1}H NMR (300.1 MHz, $CDCl_3$): δ/ ppm = 7.69 (s, 1H, H^{10}), 6.99 (s, 1H, H^7), 5.92-5.79 (m, 1H, H^2), 5.51 (s, 2H, H^5), 5.24-5.12 (m, 2H, H^1), 4.98 (s br, 1H, -N**H**-), {3.96 (s, 3H), 3.94 (s, 3H)} ($H^{12,13}$), 3.84 (dt, *J* = 9.0 Hz, 1.5Hz, H^3).

^{13}C NMR (75.5 MHz, $CDCl_3$): δ/ ppm = {155.9, 153.6} ($C^{4,8}$), 148.3 (C^9), 140.1 (C^{11}), 134.4 (C^2), 128.2 (C^6), 116.4 (C^1), {110.5, 108.4} ($C^{7,10}$), 63.8 (C^5), {56.5, 56.5} ($C^{12,13}$), 43.7 (C^3).

3-triethoxsilylpropyl-N-[4,5-dimethoxy-2-nitrobenzyloxycarbonyl]amine[87, 211]

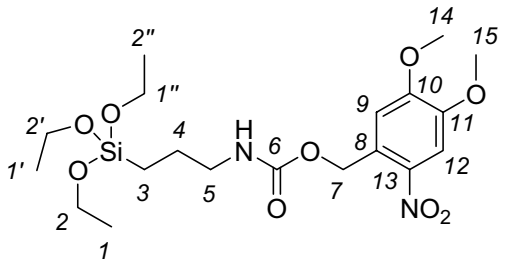

36

$C_{19}H_{32}N_2O_9Si$

[460.55]

35 (1 g, 3.4 mmol) and triethoxysilane (13.3 g, 93 mmol) were placed into a previously passivated dry round-bottom flask and heated under Ar atmosphere to about 80 °C until both reagents mix homogeneously. After addition of 190 µl of a 1.6% w /V solution of H_2PtCl_6 in *iso*-PrOH, the mixture was allowed to react for 3.5 hours. The excess of triethoxysilane was removed by distillation under reduced pressure and the solid residue purified by column chromatography on passivated silica gel (see A.1.2) to give **36** as yellow solid (0.91 g, 2 mmol, 58%).

^{1}H NMR (300.1 MHz, $CDCl_3$): δ/ ppm = 7.70 (s, 1H, H^{12}), 7.01 (s, 1H, H^9), 5.50 (s, 2H, H^7), 5.14 (s br, -N**H**-), {3.97 (s, 3H), 3.95 (s, 3H)} ($H^{14,15}$), 3.82 (q, *J* = 7.0 Hz, 6H, $H^{2,2',2''}$), 3.23 (m, 2H, H^5), 1.70-1.60 (m, 2H, H^4), 1.22 (t, *J* = 7.0 Hz, 9H, $H^{1,1',1''}$), 0.67-0.61 (m, 2H, H^3).9.0 Hz, 1.5Hz, H^3).

^{13}C NMR (75.5 MHz, $CDCl_3$): δ/ ppm = {156.0, 153.7} ($C^{6,10}$), 148.3 (C^{11}), 140.1 (C^{13}), 128.5 (C^8), {110.5, 108.4} ($C^{9,12}$), 58.6 ($C^{2,2',2''}$), {56.6, 56.5} ($C^{14,15}$), 43.7 (C^5), 23.4 (C^4), 18.4 ($C^{1,1',1''}$), 7.9 (C^3).

7-(diethylamino)-4-(hydroxymethyl)-2H-chromen-2-one[183]

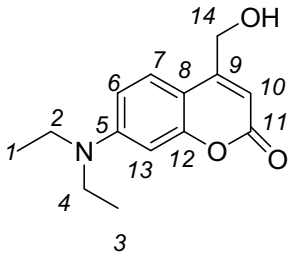

38

$C_{14}H_{17}NO_3$

[247.29]

Selenium(IV) dioxide (3.32 g, 30 mmol) was added to a solution of 7-diethylamino-4-methylcoumarin (4.64 g, 20 mmol) in xylene (120 ml, mixture of isomers). The reaction mixture was heated under reflux with vigorous stirring. After 24 hours, the brown mixture was allowed to cool to room temperature, filtered and concentrated under reduced pressure. The dark brown residual oil was dissolved in ethanol (130 ml). Sodium borohydride (0.38 g, 10 mmol) was added, and the solution stirred for 3.5 hours at room temperature. Hydrochloric acid (1N, 20 ml) was carefully added. After dilution with water, the red solution was extracted three times with dichloromethane. The combined organic extracts were washed with water and brine (saturated sodium hydrogen carbonate solution) and dried over anhydrous sodium sulphate. Removal of the solvent under reduced pressure gave a dark-brown oil (7.39 g). Column chromatography using dichloromethane/ acetone (5:1) as eluent afforded the desired alcohol **38** (2.19 g, 8.9 mmol, 29.5% yield).

^{1}H NMR (300.1 MHz, $CDCl_3$): δ/ ppm = 7.32 (d, J = 9.0 Hz, 1H, H^7), 6.55-6.58 (m, 1H, H^6), 6.51-6.52 (m, 1H, H^{13}), 6.25 (t, $J \approx$ 1.2 Hz, 1H, H^{10}), 4.84 (s br, 2H, H^{14}), 3.41 (q, J = 7.1 Hz, 4H, $H^{2,4}$), 1.55 (s breit, 1H, -O**H**), 1.20 (t, J = 7.1 Hz, 6H, $H^{1,3}$).

(7-(diethylamino)-2-oxochroman-4-yl)methyl allylcarbamate[184]

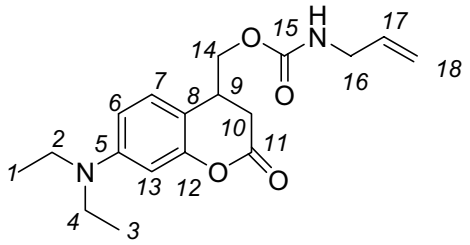

40

$C_{18}H_{22}N_2O_4$

[330.38]

38 (0.3 g, 1.1 mmol) was dissolved in dry dichloromethane (30 ml). 4-Dimethylaminopryridine (DMAP, 0.28 g, 2.3 mmol) and 4-Nitrophenylchloroformate (0.26 g, 1.3 mmol) were added simultaneously. The dark-brown-yellow solution was stirred at room temperature. A small sample was taken for analysis after 17.5 hours. The formation of the carbamate **39** could be confirmed by ^{1}H NMR spectroscopy, observing a shift of the signals attributed to H^{14} from 4.83/4.84 ppm in the alcohol **38** to 5.22 ppm in the carbamate. The carbamate **39** was not isolated.

4-Dimethylaminopyridine (DMAP, 0.29 g, 2.4 mmol) and allylamine (0.1 g, 1.75 mmol) were added to the stirring solution. After 23.5 hours at room temperature, the reaction mixture was quenched with citric acid (15% w/V, 15 ml) and diluted with dichloromethane. After phase separation the aqueous phase was extracted with dichloromethane. The combined organic extracts were dried over anhydrous sodium sulphate and concentrated under reduced pressure. The obtained dark-orange oil (0.69 g) was subjected to column chromatography using ethylacetate/ petroleum ether (3:1) as eluent. Fractions containing compounds with an R_f of 0.9 were combined and concentrated. The desired product **40** was allowed to crystallize from the obtained orange oil. The mixture was then taken up in ethylacetate/ petroleum ether (3:1) and filtered. The residual yellow solid (0.08 g, 0.2 mmol, 22% yield) was determined to be the desired product **40**.

^{1}H NMR (300.1 MHz, $CDCl_3$): δ/ ppm = 1.17-1.22 (t, J = 7.1 Hz, 1H, -O**H**), 3.40 (q, 4H, $H^{2,41}$), 3.86 (tt, J = 5.7 Hz, $J \approx$ 1.4 Hz, 2H, H^{16}), 5.04 (s, 1H, -N**H**-), 5.14-5.26 (m, 4H, $H^{14,18}$), 5.80-5.93 (m, 1H, H^{17}), {6.12 (s br, 1H), 6.50-6.51 (m, 1H), 6.54-6.58 (m, 1H)} ($H^{6,10,13}$), 7.29 (d, J = 8.7 Hz, 1H, H^{7}).

^{13}C NMR (75.5 MHz, $CDCl_3$): δ/ ppm = {162.1, 156.4, 155.5, 150.8, 150.4} ($C^{5,9,11,12,15}$) 134.2 (C^{17}), 124.5 (C^{7}), 116.6 (C^{18}), {108.8, 106.4, 98.0} ($C^{6,8,10,13}$), 62.0 (C^{14}), 44.9 ($C^{2,4}$), 43.8 (C^{16}), 12.6 ($C^{1,3}$).

(7-(diethylamino)-2-oxo-2H-chromen-4-yl)methyl 3-(triethoxysilyl)propylcarbamate

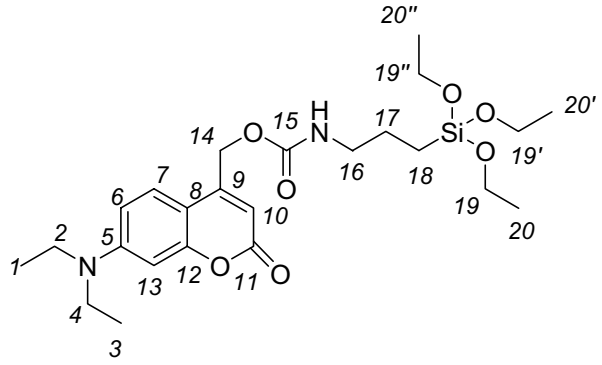

41

$C_{24}H_{36}N_2O_7Si$

[494.65]

40 (0.07 g, 0.21 mmol) and triethoxysilane (1.8 g, 10.8 mmol) were placed into a previously with HMDS passivated dry round-bottom flask and heated under Argon atmosphere to about 80 °C. After addition of isopropanolic H_2PtCl_6 solution (50 µl, 0.027 mg/ µl), the mixture was allowed to react for 4 hours at 80 °C and then to cool down. Excess of triethoxysilane was removed in the vacuum, and the solid residue was taken up in dichloromethane and filtered through Celite500. The filtrate was concentrated under reduced pressure and determined to be **41** in a 45% mixture with the reduced compound **42** (0.12 g, equivalent to 0.13 mmol of pure **41**, 63%).

^{1}H NMR (300.1 MHz, $CDCl_3$): δ/ ppm = 7.30 (d, J = 8.9 Hz, 1H, H^7), {6.58 (dd, J = 8.9 Hz, J = 2.5 Hz, 1H), 6.51 (d, J = 2.5 Hz, 1H), 6.12 (s br, 1H} ($H^{6,10,13}$), 5.22 (s br, 2H, H^{14}), 4.91 (s br, 1H, -N**H**-), 3.91-3.79 (q, J = 7.2 Hz, 6H, $H^{19,19',19''}$), 3.41 (q, J = 7.2 Hz, 4H, $H^{2,4}$), 3.27-3.17 (m, 2H, H^{16}), 1.72-1.62 (m, 2H, H^{17}), 1.26-1.18 (m, 15H, $H^{1,3,20,20',20''}$), 0.63-0.68 (m, 1H, H^{18}).

^{13}C NMR (75.5 MHz, $CDCl_3$): δ/ ppm = {98.1, 106.4, 108.9, 124.6, 124.6, 150.5, 150.7, 155.7, 156.4, 162.1} ($C^{5,6,7,8,9,10,11,12,13,15}$), 61.8 ($C^{14}$),. 58.7 ($C^{19,19',19''}$), 45.0 ($C^{2,4}$), 43.1 ($C^{16}$), 12.6 ($C^{1,3}$), 7.9 ($C^{18}$).

(7-(diethylamino)-2-oxochroman-4-yl)methyl propylcarbamate

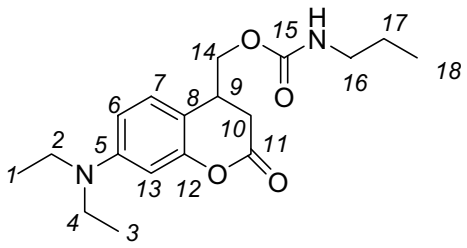

42

$C_{20}H_{24}N_2O_4$

[332.38]

42, the reduced compound of **40**, was obtained as byproduct in the synthesis of **41.** The ^{1}H NMR signals attributed to H^{17} and H^{18} show different positions and multiplicity with respect to the signals of **40**: δ/ ppm = 0.87 (t, *J* = 7.0 Hz) for H^{18} and 1.61-1.50 (m) for H^{17}. The signals in the ^{13}C NMR spectrum attributed to C^{17} and C^{18} are shifted with respect to the signals of **40**: δ/ ppm = 11.3 for C^{18} and 23.3 for C^{17}.

A.3.2 Surface modification

Surface Reaction: NVoc-APTS

In an optimized procedure, a 1% w/ V solution of NVoc-APTS in THF was prehydrolyzed in a passivated reaction vessel using catalytic amounts of aqueous NaOH (17 µl 1N NaOH in 17 ml THF) for 1 h. Eventually formed polymeric aggregates were removed by filtration through a 0.2 µm pore sized PTFE filter, and clean substrates were immersed into this filtered solution for 18 h. Out of the solution, the substrates were successively rinsed with THF and Milli-Q water to remove physisorbed molecules. The chemisorbed silane molecules were fixed with baking 1 hour at 90-95 °C.

Surface Reaction: DEACM-APTS

In an optimized procedure, a 0.2% w/ V solution of the DEACM-APTS in THF was prehydrolyzed in a passivated reaction vessel using catalytic amounts of aqueous NaOH

(13.5 µl 1N NaOH/ 17 ml THF) for 1 h. Eventually formed polymeric aggregates were removed by filtration through a 0.2 µm pore sized PTFE filter, and clean substrates were immersed into this filtered solution for 70 h. Out of the solution, the substrates were successively rinsed with THF and Milli-Q water to remove physisorbed molecules. The chemisorbed silane molecules were fixed with baking 1 hour at 90-95 °C.

Surface Reaction: mixed layers of NVoc-APTS and DEACM-APTS

A solution of each 0.1% w/ V NVoc-APTS and DEACM-APTS in THF was prehydrolyzed in a passivated reaction vessel using catalytic amounts of aqueous NaOH (13.5 µl 1N NaOH/ 17 ml THF) for 1.5 h. Eventually formed polymeric aggregates were removed by filtration through a 0.2 µm pore sized PTFE filter, and clean substrates were immersed into this filtered solution for 45 h. Out of the solution, the substrates were successively rinsed with THF and Milli-Q water to remove physisorbed molecules. The chemisorbed silane molecules were fixed with baking 1 hour at 90-95 °C.

Before further application, all substrates were sonicated in THF for 3 minutes, washed with Milli-Q-water and dried with a N_2 stream. For determination of the ellipsometric thickness and contact angle, substrates were dried under vacuum at 90 °C for 30 minutes.

A.3.3 Irradiation

NVoc-APTS and DEACM-APTS modified quartz substrates were irradiated at 345 and 412 nm during different exposure times. After thoroughful washing with THF and Milli-Q-water to remove the photolysis side products, the substrates were analyzed by UV spectroscopy. The deprotection was monitored by the decay in the UV-vis spectrum (as a consequence of the cleavage of the chromophore). The minimum irradiation times for full deprotection were: 20 min for DEACM-APTS at 412 nm and 20 min for NVoc-APTS at 345 nm.

A.3.4 Site-selective patterning by masked irradiation

A substrate containing mixed layers of NVoc-APTS and DEACM-APTS was mask irradiated (quartz mask with 50 µm wide chrome lines, spaced with 10 µm) for 20 min at 412 nm.

A.3.5 Fluorescence labelling

After thoroughful washing with THF and Milli-Q water, 150 µl of a solution of Alexa Fluor®647 succinimidyl ester in dry DMSO (0.14 mg/ ml) were deposited on the quartz substrate and left at RT for 12 hours, preserved from light. The droplet was then removed with a pipette, and unbounded dye was removed by washing with DMSO, THF (sonification for 3 min) and Milli-Q. After drying with a N_2 stream, the substrate was again masked irradiated for 20 min at 345 nm (quartz mask bearing the same pattern rotated around 90° with respect to the first mask). The photolysis products were washed off and the dried substrate was covered with 150 µl of a solution of Alexa Fluor®647 succinimidyl ester in dry DMSO (0.1 mg/ ml) and incubated at RT for 8.5 hours. Unbounded dye was again washed off and the dried substrate was analyzed with a fluorescence microscope using different filters (see A.1.3).

A.4 Experimental Part: Surface tailored magnetite nanoparticles

A.4.1 Synthesis of silanes

1-(2-(2-(2-aminoethoxy)ethoxy)ethyl)-3-(3-(triethoxysilyl)propyl)urea

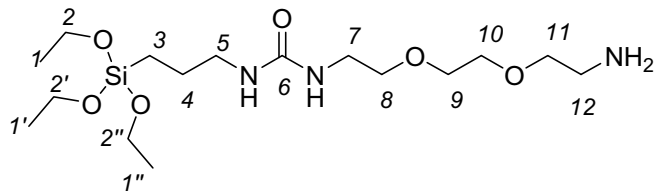

S4

$C_{16}H_{37}N_3O_6Si$

[395.57]

3-Isocyanato propyltriethoxysilane (2.47 g, 10 mmol) was added dropwise under argon atmosphere to a stirring solution of 2,2 ethylendioxy-bis-ethylamine (2.96 g, 20 mmol, 2 mol-equivalent) in dry THF (25 ml). The mixture was allowed to react at room temperature. The reaction was followed by proton NMR analysis. After 1 hour the reaction was complete and the solvent was removed under reduced pressure. The reaction crude was used for the surface modification process without further purification (5.31 g, 9.8 mmol **S4**, 98%).

^{1}H NMR (250.1 MHz, $CDCl_3$): δ/ ppm = 5.39 (m, 1H, -N**H**-), 5.18 (m, 1H, -N**H**-), 3.76 (q, 6H, *J* = 7.0 Hz, $H^{2,2',2''}$), 3.59-3.47 (m, 8H, $H^{8,9,10,11}$), {3.36-3.27 (m, 2H), 3.15-3.07 (m, 2H)} ($H^{5,7}$), 2.83 (t, 2H, *J* = 5.3 Hz, H^{12}), 1.60-1.48 (m, 2H, H^4), 1.23 (s br, 2H, -N**H**$_2$), 1.17 (t, 2H, *J* = 7.0 Hz, $H^{1,1',1''}$), 0.61-0.55 (m, 2H, H^3).

2-(2-(2-hydroxyethoxy)ethoxy)ethyl 3-(triethoxysilyl)propylcarbamate

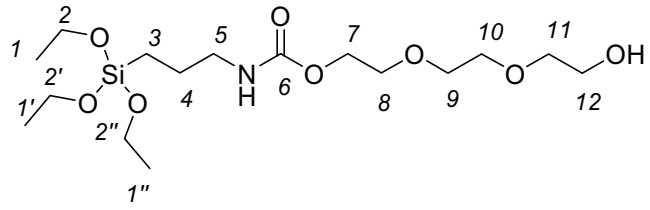

S5

$C_{16}H_{35}NO_8Si$

[397.54]

3-Isocyanato propyltriethoxysilane (1.05 g, 4 mmol) was added dropwise under argon atmosphere to a stirring solution of triethylene glycol (1.2 g, 8 mmol) in dry THF (20 ml). After additon of 2 drops of dibutyltin dilaureate, the mixture was allowed to react at room temperature for 4 hours. The solvent was removed under reduced pressure, and the crude was used for surface modification without further purification (2.07 g, 2.9 mmol **S5**, 95%).

Purification by column chromatography on passivated silica using ethylacetate/ ethanol (95:5) as eluent gave the pure product **S5** (0.34 g, 0.9 mmol, 21%).

^{1}H NMR (250.1 MHz, $CDCl_3$): δ/ ppm = 5.14 (s br, 1H, -N**H**-), 4.23-4.19 (m, 2H, H^7), 3.81 (q, 6H, J = 7.0 Hz, $H^{2,2',2''}$), 3.74-3.59 (m, 10H, $H^{8,9,10,11,12}$)} ($H^{5,7}$), 3.16 (q, J = 6.7 Hz, 2H, H^5), 2.28 (s br,1H, -O**H**), 1.66-1.54 (m, 2H, H^4), 1.21 (t, J = 7.0 Hz, 2H, $H^{1,1',1''}$), 0.67-0.58 (m, 2H, H^3).

2-(2-(2-methoxyethoxy)ethoxy)ethyl 3-(triethoxysilyl)propylcarbamate

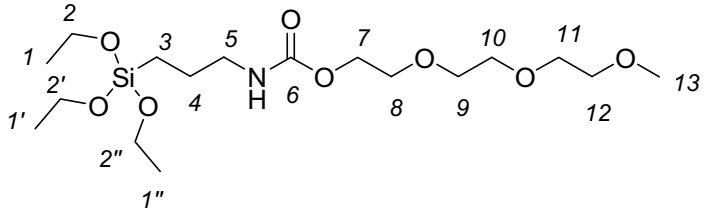

S6

$C_{17}H_{37}NO_8Si$

[411.56]

3-Isocyanato propyltriethoxysilane (2.47 g, 10 mmol) was added dropwise under argon atmosphere to a stirring solution of triethyleneglycol monomethylether (3.28 g, 20 mmol) in dry THF (25 ml). After additon of dibutyltin dilaureate (20 µl), the mixture was allowed to react at room temperature for 14 hours. The solvent was removed under reduced pressure, and the crude was used for surface modification without further purification (5.74 g, 9.7 mmol **S6**, 100%).

^{1}H NMR (250.1 MHz, $CDCl_3$): δ/ ppm = 5.01 (s br, 1H, -N**H**-), 4.17-4.13 (t br, 2H, H^7), 3.76 (q, *J* = 7.0 Hz, 6H, $H^{2,2',2''}$), 3.67-3.48 (m, 10H, $H^{8,9,10,11,12}$)} 3.33 (m, 3H, H^{13}), ($H^{5,7}$), 3.15-3.07 (m, 2H, H^5), 1.62-1.49 (m, 2H, H^4), 1.17 (t, *J* = 7.0 Hz, 2H, $H^{1,1',1''}$), 0.60-0.53 (m, 2H, H^3).

A.4.2 Surface modification of magnetite nanoparticles

75 mg of iron oxide particles in aqueous suspension were washed three times with mixtures of THF/water (1/1), three times with THF and then resuspended in 3 ml THF. The particle suspension was added to 3 ml of a freshly prepared solution of the silane (or silane mixture) under vigorous stirring. The final concentration of silane in the particle suspension was 2% w/V. After stirring for 17.5 hours at 70 °C, the supernatant was removed by magnetic immobilization, the particles were washed several times with THF and water, and finally they were resuspended in water. The suspension was partitioned into aliquots of 2 mg and stored at -20 °C.

Particles were modified with a mixture of aminosilanes **S1** or **S4** with silanes **S2**, **S3**, **S5** or **S6** in different molar ratios.

For the storage stability measurements, one batch of particles modified with silane **S1** in water solution (instead of THF) was prepared following the same method.

Determination of the solid content of the particle suspensions

200 µl of the particle suspension were dried at 95 °C in vacuum for three hours. Particle content was determined by dry weight estimation (duplicate determination).

Colorimetric assay of the amine density

2 mg of nanoparticles were washed four times with 600 µl coupling solution (0.8% V/ V glacial acetic acid in dry methanol). Subsequently, 400 µl of 4-nitrobenzaldehyde solution (0.7 mg/ ml in coupling solution) were added to the particles and the suspension allowed to react for 3-4 hours in a microcentrifuge tube with end-over-end rotation After removal of the supernatant and washing (4 × 400 µl coupling solution), 400 µl of hydrolysis solution (0.13% V/ V glacial acetic acid in methanol/ water 1:1) was added to the particles and the tube shaken for a further hour. The supernatant was then removed and its absorbance measured at 282 nm.

The amount of 4-nitrobenzaldehyde in the hydrolysis solution was calculated by interpolation using a calibration curve constructed from a range of standard solutions of

4-nitrobenzaldehyde in hydrolysis solution prepared separately.

A.4.3 Adsorption and binding experiments

Adsorption of DNA onto modified nanoparticles

50 µg of sheared, salmon sperm DNA was diluted in 400 µl of 10xTEN at pH 8. 400 µl of 4 M NaCl containing 20% w/ V PEG (M_w8000) were added to give a final DNA concentration of 0.0625 µg/ µl. This DNA solution was mixed with 2 mg of nanoparticles (previously washed twice with sterile water) in a sterile Eppendorf tube. The mixture was incubated with gentle agitation for 5 minutes at room temperature after which the support material was immobilised and the supernatant was retained for determination of its DNA content.

Determination of DNA content from supernatants by UV spectroscopy

The DNA solutions were analyzed by UV spectroscopy at 260 nm (sample volume: 120 µl). The DNA concentrations were calculated using a calibration curve constructed from a series of salmon sperm DNA solutions of known concentration (between 0.0025 mg/ ml and 0.125 mg/ ml).

Adsorption of BSA onto amino modified nanoparticles

2 mg of amine modified nanoparticles were washed twice with 600 µl PBS buffer. 0.03 mg BSA (0.2 mg ml^{-1} in PBS) were added to the beads and the suspension incubated for two hours at RT in a microcentrifugue tube with end-over-end rotation. The supernatant was separated and its protein content was determined with BCA assay.

Synthesis of glutaraldehyde modified nanoparticles

2 mg of nanoparticles were washed twice with 1000 µl 1×SSC buffer. 600 µl glutaraldeyde solution (5% V/ V in 1×SSC) were added and allowed to react at room temperature for 2 hours in a microcentrifuge tube with end-over-end rotation. The supernatant was then removed and the particles washed three times with 1000 µl 1×SSC

to remove the excess of glutaraldehyde.

Binding BSA to glutaraldehyde modified nanoparticles

2 mg of glutaraldehyde modified nanoparticles were washed twice with 600 µl PBS buffer. 0.03 mg BSA (0.2 mg ml^{-1} in PBS) were added to the beads and the suspension incubated for two hours at RT in a microcentrifuge tube with end-over-end rotation. The supernatant was separated and its protein content was determined with BCA assay.

Binding biotin to amino modified nanoparticles

2 mg of nanopartilces were washed three times with 1000 µl dry DMF. 0.075 mg NHS-biotin (0.3 mg ml^{-1} in dry DMF) were added to the beads and the suspension incubated for two hours at room temperature in a microcentrifuge tube with end-over-end rotation. After removal of the supernatant, the particles were washed with 1000 µl DMF to remove the excess of NHS-biotin.

Binding streptavidin to biotin modified nanoparticles

2 mg of biotin modified nanoparticles were washed three times with 600 µl PBS buffer to remove DMF. 0.05 mg streptavidin (0.2 mg ml^{-1} in PBS) were added to the beads and the suspension incubated for two hours at room temperature in a microcentrifuge tube with end-over-end rotation. The supernatant was separated and its protein content was determined with BCA assay.

Determination of protein content from supernatants by BCA assay

50 µl of the protein solutions to be analyzed were placed in a 96 well flat bottom microplate (duplicate determination). 50 µl of BCA working solution was added. After incubation at 60 °C for 40 minutes the optical density at 570 nm was read out. The protein concentrations were calculated using a calibration curve constructed from a range of standard solutions of the corresponding protein in PBS or elution solution contemporaneously analyzed at the same microtiter plate.

Deutsche Zusammenfassung

Einleitung

Biologisch aktive Oberflächen spielen eine wichtige Rolle in vielen Bereichen der Biotechnologie und klinischen Diagnostik, wie z. B. in Form von aktivierten Nanopartikeln als Trägermaterial für die Affinitätschromatographie zur Isolierung von Proteinen. Der Aufbau der Oberflächenschicht entscheidet maßgeblich über Empfindlichkeit und Exaktheit des jeweiligen Nachweis- oder Trennsystemes. Bei einigen Anwendungen, wie z. B. in Protein-Chips, ist eine biologische Aktiviät nur ortsspezifisch erwünscht. Silane mit photoaktivierbarer, geschützter Funktionalität bieten in diesem Kontext eine interessante Alternative zu gängigen Strukturierungsmethoden[76, 77, 84, 85,78-83], konnten bisher aber nur in der ortsselektiven Immobilisierung von kleinen Molekülen, kolloidalen Partikeln und Oligonukleotiden (OND) angewendet werden.[87, 97, 108]. Die vorliegende Dissertation stellt eine Weiterentwicklung dieses Ansatzes zur Herstellung bioaktiver und photoansprechbarer Silica-Oberflächen für die ortsselektive Immobilisierung von Proteinen dar.

Im Literaturteil *(Kapitel 1)* wurde ein Überblick über Methoden zur Immobilisierung von Proteinen und über Strategien zur Oberflächenstrukturierung gegeben. Nach einer kurzen Beschreibung der verwendeten Oberflächencharakterisierungstechniken (*Kapitel 2*) schließen sich weitere drei Kapitel an.

In *Kapitel 3* wurde ein neuer Typ von verzweigten photosensitiven Silanen, der inerte Oligoethylenglykol (OEG)-Arme enthält, vorgestellt und nach erfolgreicher Synthese

zur Oberflächenmodifizierung von Silica in der ortsselektiven Immobilisierung von Proteinen angewendet. Die Untersuchungen an zwei Schutzgruppen zur wellenlängenselektiven Oberflächenaktivierung (*Kapitel 4*) legen den Grundstein für die Herstellung anspruchsvollerer strukturierter Oberflächen mit zwei verschiedenen ortsselektiv immobilisierten Proteinen. Darüberhinaus wurde die spezifische Immobilisierung von Proteinen an gemischten Silanschichten untersucht und zur Herstellung bioaktiver magnetischer Nanopartikel mit hoher Bindungseffizienz eingesetzt (*Kapitel 5).*

Im Folgenden werden die Hauptinhalte der Kapitel 3 bis 6 kurz abgehandelt.

I Photoaktivierbare verzweigte Silane

Eine neue Klasse von photosensitiven Silanen mit einer aus Tetraethylenglykol (TEG)-Armen aufgebauten, verzweigten Struktur, die an einem Ende eine Aminofunktionalität in photolabiler geschützter Form und am anderen eine inerte Methoxygruppe trägt, wurde vorgestellt. Die photosensitive NVoc-Schutzgruppe für die Aminofunktion, die bei Bestrahlung im UV-Bereich abgespalten werden kann, bietet das Instrument zur chemischen Strukturierung von mit diesem Silan modifizierten Oberflächen. Die bei der Photolyse freigesetzten reaktiven Aminogruppen bilden die Basis für eine Vielzahl von bekannten Immobilisierungsstrategien, wie z. B. die spezifische Anbindung von Streptavidin an mit Biotin modifizierte Substrate, die exemplarisch untersucht wurde.

Drei verschiedene Syntheserouten wurden zur Synthese von verzweigten Silanen aufgestellt. Ausgehend von Epichlorhydrin als dreifunktionalem Bindeglied, das die TEG-Arme zusammenhält, konnten schließlich zwei verschiedene Verbindungen, (Y-EG-NVoc) und (Y-alkyl-NVoc), deren Struktur in (Abb. I) dargestellt ist, synthetisiert werden. Die Trennung der Vorstufen erfolgte säulenchromatographisch und stellte das Hauptproblem in der Synthese dar. Es scheint, dass die polaren TEG-Ketten die Wechselwirkungen mit dem zur Trennung verwendeten Kieselgel-Trägermaterial dominieren, was zu breiten Verteilungen der Profukte auf der Säule und damit hohen Produktverlusten führte.

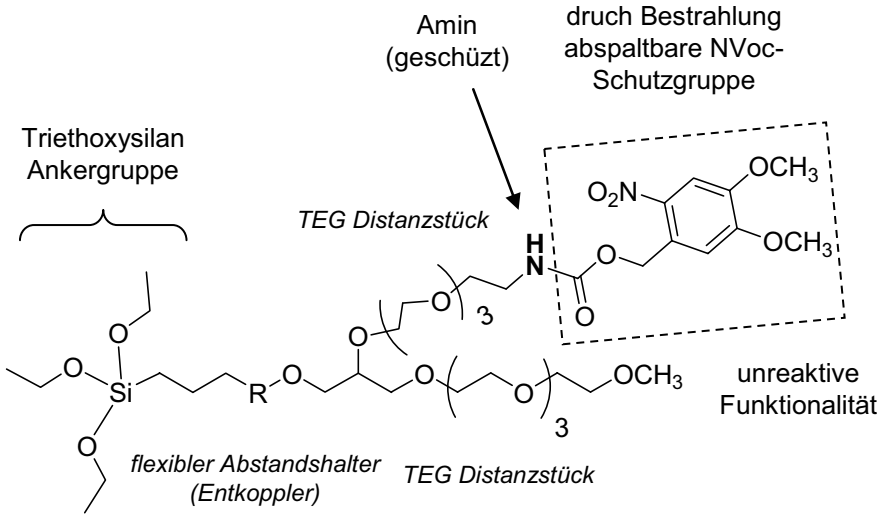

Y-EG-NVoc (R = $(OCH_2CH_2)_4$),

Y-alkyl-NVoc (R = C_7H_{14})

Abb. I: Strukturformeln der synthetisierten verzweigten Silane Y-EG-NVoc und Y-alkyl-NVoc.

Nach optimierten Silanisierungsbedingungen wurden Schichten von Y-EG-NVoc mit einem Kontaktwinkel von 51° und von Y-alkyl-NVoc mit einem Kontakwinkel von 63° erhalten. Die ellipsometrisch bestimmten Schichtdicken lassen auf Submonolagen schließen, die mit Oberflächenbedeckungen von 2,4 ng mm^{-2} für Y-EG-NVoc und 1,6 ng mm^{-2} für Y-alkyl-NVoc, unter denen von selbstorganisierten Thiol-Monoschichten (SAM) auf Gold liegen.

Die Abspaltung der photolabilen NVoc-Schutzgruppe wurde auf modifizierten Quarzsubstraten durch UV-Bestrahlung im Absorptionsmaximum bei 355 nm untersucht. Bei einer Bestrahlungszeit von 10 min wird eine maximale Entschützung von 50-60 % erreicht. Durch UV-Bestrahlung durch eine Maske konnten chemisch-strukturierte Oberflächen mit Strukturen im Mikrometerbereich hergestellt werden. Die Existenz der Aminogruppen in den bestrahlten Bereichen konnte durch Anbindung eines Fluoreszenzfarbstoffes belegt werden. Weitere Experimente mit haben verdeutlicht, dass diese photochemisch strukturierten Oberflächen nach geeigneter Biofunktionalisierung erfolgreich in der ortsselektiven Immobilisierung von ONDs, Antikörpern und Zellen eingesetzt werden können (Abb. II).

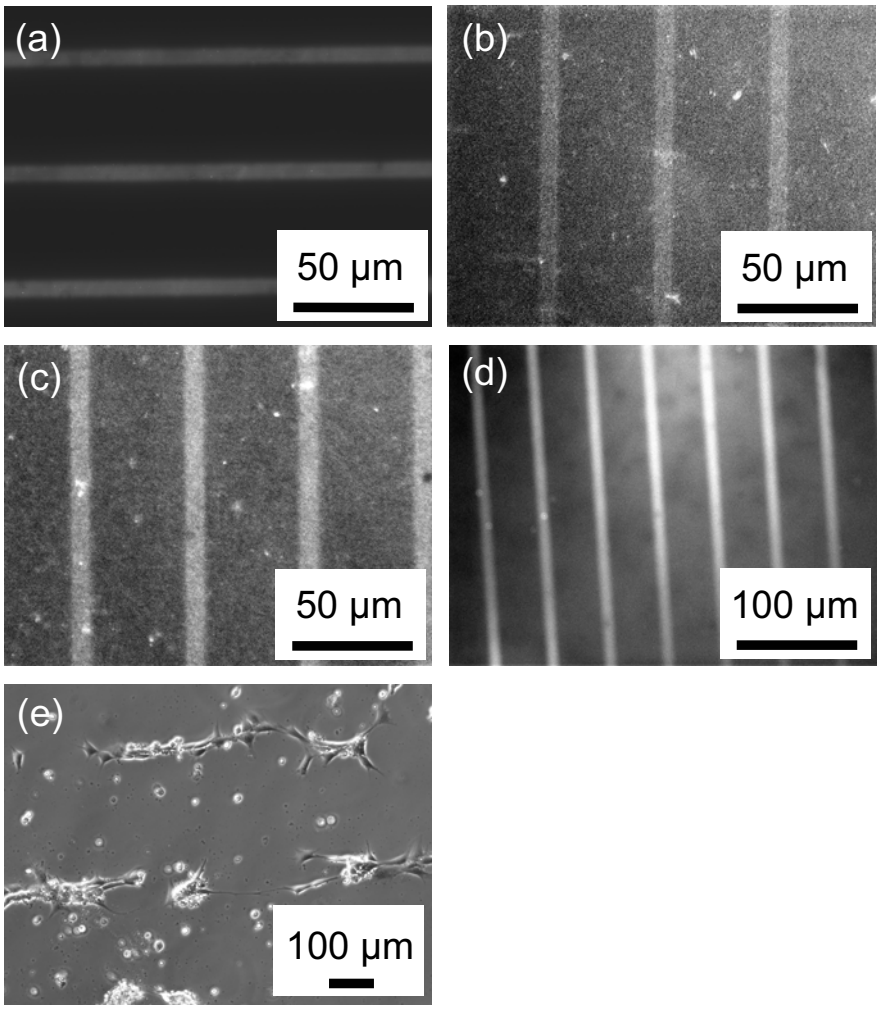

Abb. II: Fluoreszenzmikroskopaufnahmen von mit Y-EG-NVoc modifizierten Substraten, an die Alexa Fluor®647 Farbstoff angebunden wurde (a) sowie verschiedene mit Fluoreszenzfarbstoffen markierte Biomoleküle, ein mit Fluorescein markiertes OND nach Immobilisierung des komplimentären OND-Stranges (b), ein mit FITC markierter IgG-Antikörper nach Immobilisierung von IgG (c), Fluorescein-markiertes Biotin an immobilisiertes Streptavidin (d). Bild (e) zeigt eine Lichtmikroskopaufnahme von NIH/ 3T3-Fibroblasten, die auf diese Oberfläche gesetzt wurden. Genauere Informationen können dem *Kapitel 4* der Arbeit entnommen werden.

Die selektive Immobilisierung von Streptavidin an die im Entschützungsprozeß freigesetzten Aminogruppen wurde mithilfe von reflektometrischer Interferenzspektroskopie (RIFS) verfolgt und quantifiziet (Abb. III). Während die unspezifische Adsorption an geschützte Substrate aufgrund der vorhandenen OEG Ketten (wie erwartet) vernachlässigbar klein war, korrelierte die Bindungfähigkeit von Streptavidin an photochemisch aktivierte Y-EG-NVoc und Y-alkyl-NVoc mit der Packungsdichte der beiden Schichten, was ebenso für lineare EG-Ketten zutraf

(EG-NVoc). Im Vergleich mit linearen EG-Ketten zeigte die verzweigte Struktur Y-EG-NVoc eine höhere Bindungsfähigkeit und eignet sich somit besser für empfindliche Anwendungen.

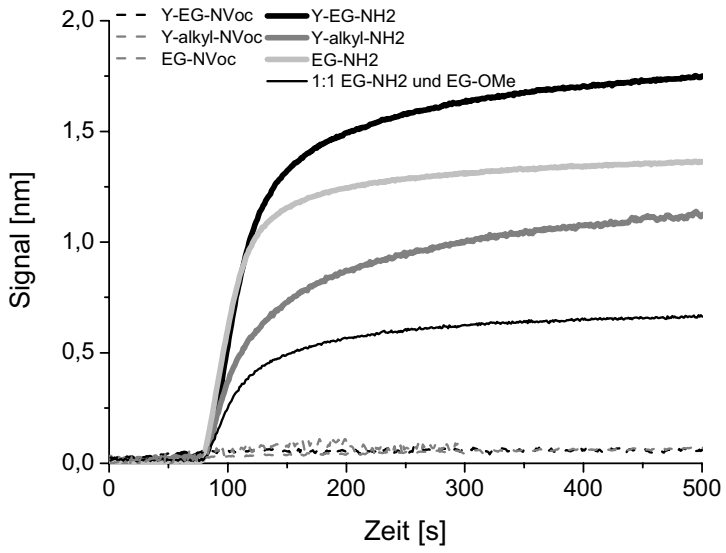

Abb. III: Mit RIFS verfolgte Bindung von Streptavidin an biotin-gekuppelte Oberflächen.

II Wellenlängen-selektive Photoaktivierung

Zwei photosensitive Schutzgruppen, (1) die bereits in *Kapitel 4* erwähnte, erfolgreich verwendete 6-Nitroveratryloxycarbonyl (NVoc)-Schutzgruppe und (2) Diethylamin-coumarin-4-yl (DEACM), wurden auf wellenlängenselektive Abspaltung getestet. Dazu wurden Siliziumdioxidsubstrate mit den entsprechenden beiden zuvor synthetisierten geschützten Aminopropyltriethoxysilanen (NVoc-APTS und DEACM-APTS, Abb. IV) modifiziert. Nach optimierten Silanisierungsbedingungen wurden Schichten mit unterschiedlichen Oberflächenbedeckungen von $9{,}7 \times 10^{11}$ für NVoc-APTS und $2{,}4 \times 10^{12}$ für DEACM-APTS erhalten, die auf eine unterschiedliche Neigung beider Silane zur Siliziumdioxid-Oberfläche deuten. Die höhere Packungsdichte der DEACM-APTS Schichten ist vermutlich auf höhere π-Wechselwirkungen zwischen den einzelnen aromatischen Gruppenzu zurückzuführen. Konsequenterweise wurde auch für gemischte Schichten aus 1:1 Mischungen beider Silane ein höherer Anteil an DEACM-

APTS gefunden.

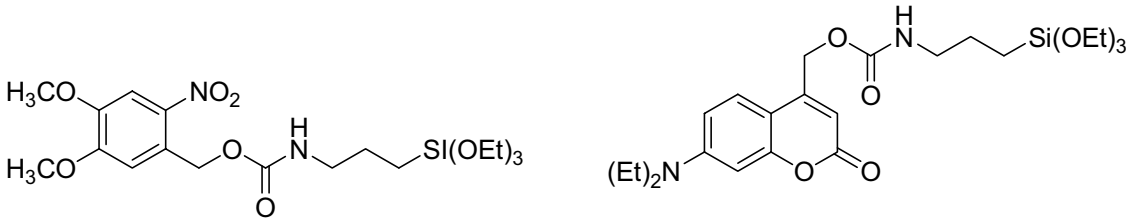

NVoc-APTS **DEACM-APTS**

Abb. IV: Strukturformeln der beiden synthetisierten geschützten Aminopropyltriethoxysilane, NVoc-APTS und DEACM-APTS.

Spektroskopische Untersuchungen der Entschützungen beider photolabilen Gruppen bei unterschiedlichen Wellenlängen ergaben, dass DEACM bei 412 nm fast vollständig abgespalten wird, während NVoc bei dieser Wellenlänge relativ wenig beeindrächtigt wird. Da DEACM höhere Photosensitivität besitzt als NVoc und außerdem im gesamten Absorptionsbereich von NVoc absorbiert, ist eine Orthogonalität beider Gruppen ausgeschlossen. Bei Anwesenheit beider photosensitiven Gruppen kann jedoch DEACM zunächst selektiv abgespalten werden und anschließend NVoc bei 345 nm, wenn DEACM in den entsprechenden Bereichen nicht mehr vorliegt (Abb. V) Gemischte Schichten beider Silane wurden in einem zwei-stufigen Bestrahlungsprozess nacheinander ortsselektiv entschützt und mit zwei verschiedenen Fluoreszenfarbstoffen gekuppelt. Das erhaltene Fluoreszenz-Muster bestätigte die Möglichkeit, mit diesen beiden Schutzgruppen gezielt komplexe chemisch strukturierte Oberflächen zu erzeugen.

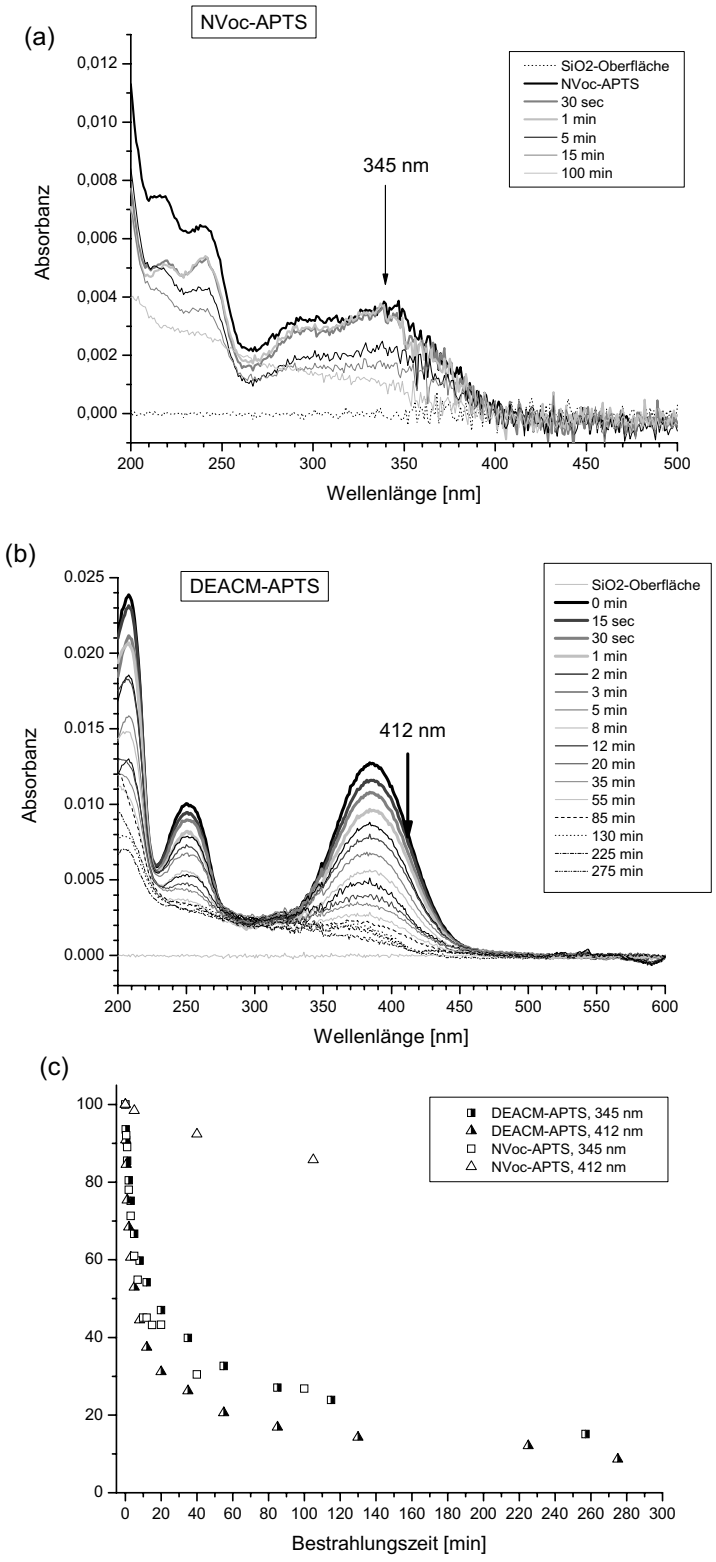

Abb. V: Entschützung auf der Oberfläche von (a) NVoc-APTS durch Bestrahlung bei 345 nm und (b) DEACM-APTS durch Bestrahlung bei 412 nm, (c) Zusammenfassung der Entschützungskinetiken.

III Maßgeschneiderte magnetische Nanopartikel für die funktionale Immobilisierung von Proteinen

Superparamagnetische Eisenoxid-Nanopartikel wurden mit gemischten Silanschichten von Amin- und OH/ OMe-terminierten Silanen in unterschiedlichen Zusammensetzungen modifiziert. Silane mit unterschiedlich langen EG-Armen analog Abb. VI wurden verwendet, um den Einfluss der Kettenlänge zwischen den beiden co-adsorbierten Silanen innerhalb einer Schicht auf das Ergebnis der spezifischen Immobilisierung zu beleuchten..

Wie aus der ermittelten Anzahl der Aminogruppen in den gemischten Oberflächenschichten hervorgeht, spiegelt die Zusammensetzung der Silane auf der Oberfläche diejenige der zur Silanisierung verwendeten Lösung wieder, unabhängig von Längenunterschieden der jeweils miteinander co-adsorbierten Silane (Abb. VII). Sie und deutet darauf hin, dass die verwendeten Silane -unabhängig von ihrer Kopfgruppenfunktionalität- die gleiche Neigung zur Anbindung an Eisenoxid besitzen.

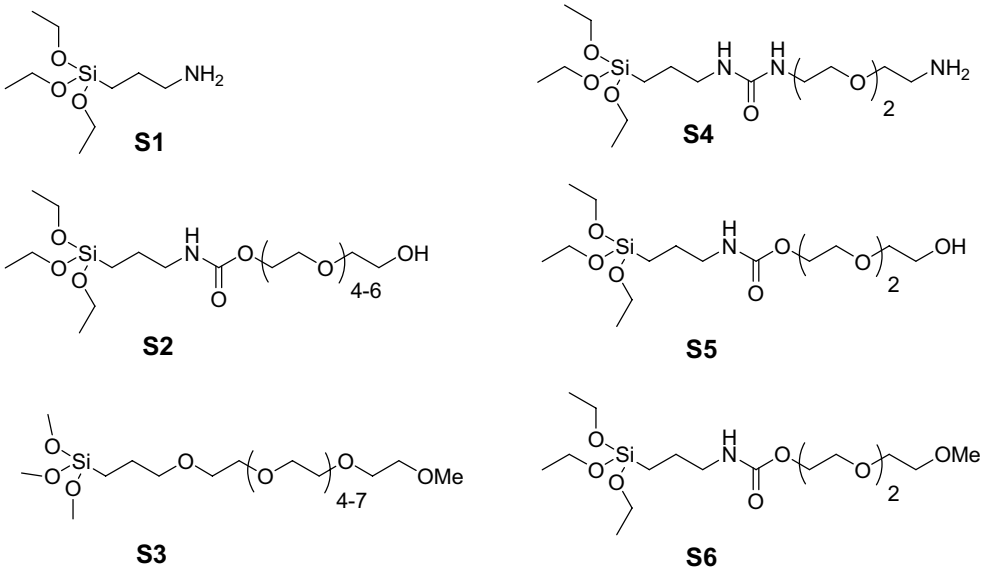

Abb. VI: Strukturformeln der Silane, die für die Oberflächenmodifizierung von SPIONs verwendet wurden. Silane **S1** bis **S3** sind kommerziell erhältlich (ABCR, Karlsruhe, Germany). Silane **S4** bis **S6** wurden jeweils ausgehend von 3-Isocyanatpropyltriethoxysilan synthetisiert.

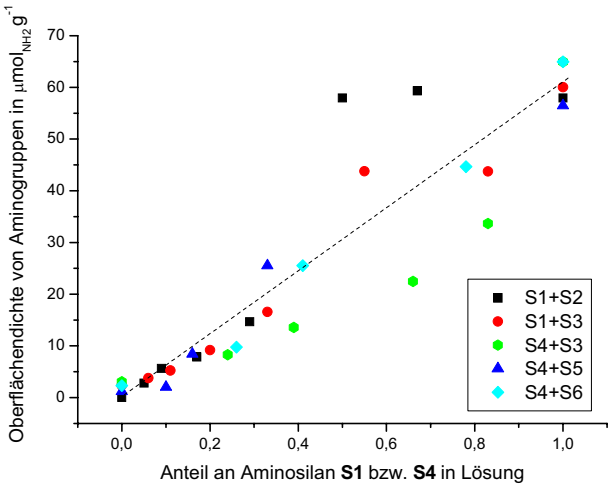

Abb. VII: Graphische Darstellung der Anzahl von Aminogruppen auf der Oberfläche in Abhängigkeit von der Zusammensetzung der Lösung.

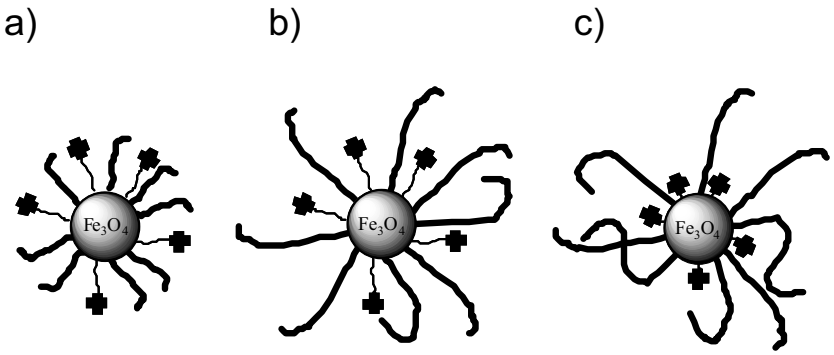

Abb. VIII: Untersuchte Systeme: a) Mischungen aus Silanen gleicher Kettenlänge (**S4+S6**), b) und c) Mischungen aus Silanen unterschiedlicher Kettenlänge; (**S3+S4**) mit geringem Längenunterschied, (**S1+S3**) mit großem Längenunterschied Unterschied.

Eine optimale Oberflächenkomposition für eine gezielte Immobilisierung von Proteinen wurde mithilfe der spezifischen Bindung von Streptavidin an mit Biotin modifizierte Partikel untersucht. Die Immobilisierung resultierte für alle untersuchten Systeme in einem Sättigungsplateau (Abb. IX). Eine Oberflächenkonzentration von 20 % bei gleichlangen Ketten ist nötig, um maximale Streptavidinbedeckung zu erreichen, was im Bereich von 10 % liegt, die für SAM von Thiolen auf Gold für gewöhnlich berichtet werden. Die höheren Werte für die Oberflächenkonzentrationen, die für Schichten mit längeren OEG-Ketten gefunden werden, lassen sich durch Abschirmung der

Amingruppen erklären. Ein Teil der Amingruppen wird durch die langen OEG-Ketten „versteckt“ und steht dem Protein nicht mehr als Bindungsstelle zur Verfügung. Somit ist die effektive Konzentration an Amingruppen kleiner.

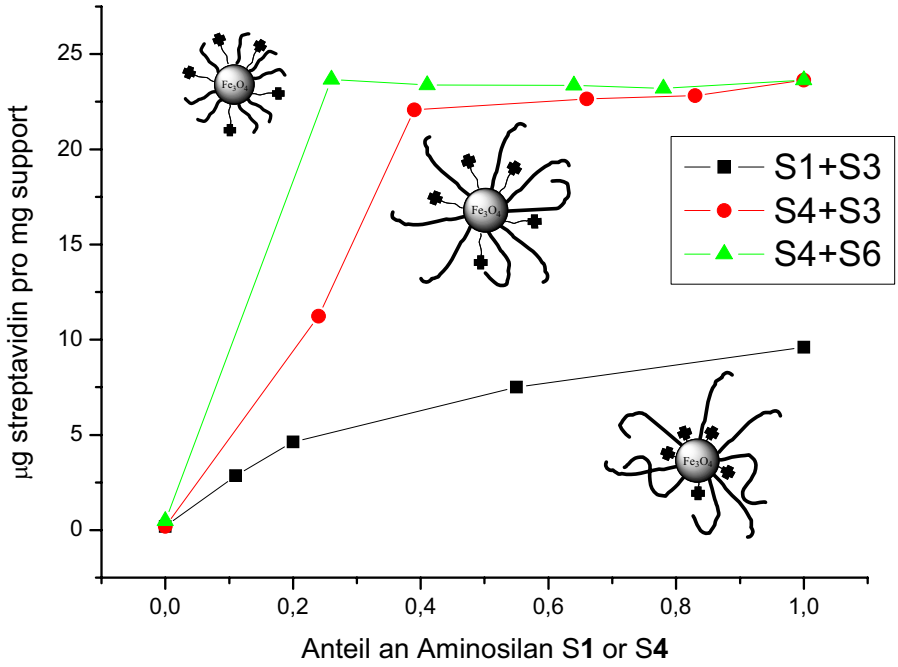

Abb. IX: Bindung von Streptavidin an biotin-modifizierte Nanopartikel mit unterschiedlichen Anteilen an Aminogruppen.

Schlussfolgerungen

Die Ergebnisse der vorliegenden Arbeit sind relevant in Anbetracht der Möglichkeiten, die sich daraus im Hinblick auf die Entwicklung von komplexen Oberflächen für die Anwendung in biotechnologischen Fragestellungen ergeben.

Es konnte gezeigt werden, dass die Gestaltung der Oberfläche eine tragende Rolle in der spezifischen und funktionalen Immobilisierung von Proteinen einnimmt und dass die Bioaktivität einer Oberfläche durch die molekulare Gestaltung der proteinabweisenden OEG-Kette gezielt gesteuert werden kann.

-
-
-

References

1. Bucak, S.; Jones, D. A.; Laibinis, P. E.; Hatton, T. A., Protein separations using colloidal magnetic nanoparticles. *Biotechnology Progress* **2003,** 19, (2), 477-484.

2. Karumanchi, R.; Doddamane, S. N.; Sampangi, C.; Todd, P. W., Field-assisted extraction of cells, particles and macromolecules. *Trends in Biotechnology* **2002,** 20, (2), 72-78.

3. Saiyed, Z. M.; Telang, S. D.; Ramchand, C. N., Application of magnetic techniques in the field of drug discovery and biomedicine. *BioMagnetic Research and Technology* **2003,** 1:2.

4. Cutler, P., Protein arrays: The current state-of-the-art. *Proteomics* **2003,** 3, (1), 3-18.

5. Templin, M. F.; Stoll, D.; Schwenk, J. M.; Potz, O.; Kramer, S.; Joos, T. O., Protein microarrays: Promising tools for proteomic research. *Proteomics* **2003,** 3, (11), 2155-2166.

6. del Campo, A.; Bruce, I. J., Diagnostics and High Throughput Screening. *Biomedical Nanotechnology* **2005,** edited by I. Malsch, (CRC Taylor & Francis), 75-112.

7. Amagliani, G.; Omiccioli, E.; del Campo, A.; Bruce, I. J.; Brandi, G.; Magnani, M., Development of a magnetic capture hybridization-PCR assay for Listeria monocytogenes direct detection in milk samples. *Journal of Applied Microbiology* **2006,** 100, (2), 375-383.

8. Galluzzi, L.; Bertozzini, E.; del Campo, A.; Penna, A.; Bruce, I. J.; Magnani, M., Capture probe conjugated to paramagnetic nanoparticles for purification of Alexandrium species (Dinophyceae) DNA froml environmental samples. *Journal of Applied Microbiology* **2006,** 101, (1), 36-43.

9. Widder, K. J.; Senyei, A. E.; Scarpelli, D. G., Magnetic Microspheres - Model System for Site Specific Drug Delivery Invivo. *Proceedings of the Society for Experimental Biology and Medicine* **1978,** 158, (2), 141-146.

10. Senyei, A.; Widder, K.; Czerlinski, G., Magnetic Guidance of Drug-Carrying Microspheres. *Journal of Applied Physics* **1978,** 49, (6), 3578-3583.

11. Alexiou, C.; Arnold, W.; Klein, R. J.; Parak, F. G.; Hulin, P.; Bergemann, C.; Erhardt, W.; Wagenpfeil, S.; Lubbe, A. S., Locoregional cancer treatment with magnetic drug targeting. *Cancer Research* **2000,** 60, (23), 6641-6648.

12. Pankhurst, Q. A.; Connolly, J.; Jones, S. K.; Dobson, J., Applications of magnetic nanoparticles in biomedicine. *Journal of Physics D: Applied Physics* **2003,** 36, R167-R181.

13. Whitford, D., *Proteins - Structure and Function*. Wiley & Sons, West Sussex, UK: 2005; p 13-84.

14. Lee, Y. S.; Mrksich, M., Protein chips: from concept to practice. *Trends in Biotechnology* **2002,** 20, (12), S14-S18.

15. Houseman, B. T.; Huh, J. H.; Kron, S. J.; Mrksich, M., Peptide chips for the quantitative evaluation of protein kinase activity. *Nature Biotechnology* **2002,** 20, (3), 270-274.

16. Doyon, J. B.; Snyder, T. M.; Liu, D. R., Highly sensitive in vitro selections for DNA-linked synthetic small molecules with protein binding affinity and specificity. *Journal of the American Chemical Society* **2003,** 125, (41), 12372-12373.

17. Hodneland, C. D.; Lee, Y. S.; Min, D. H.; Mrksich, M., Selective immobilization of proteins to self-assembled monolayers presenting active site-directed capture ligands. *Proceedings of the National Academy of Sciences of the United States of America* **2002,** 99, (8), 5048-5052.

18. McGall, G.; Labadie, J.; Brock, P.; Wallraff, G.; Nguyen, T.; Hinsberg, W., Light-directed synthesis of high-density oligonucleotide arrays using semiconductor photoresists. *Proceedings of the National Academy of Sciences of the United States of America* **1996,** 93, (24), 13555-13560.

19. Hyun, J.; Lee, W. K.; Nath, N.; Chilkoti, A.; Zauscher, S., Capture and release of proteins on the nanoscale by stimuli-responsive elastin-like polypeptide "switches". *Journal of the American Chemical Society* **2004,** 126, (23), 7330-7335.

20. Klueh, U.; Seery, T.; Castner, D. G.; Bryers, J. D.; Kreutzer, D. L., Binding and orientation of fibronectin to silanated glass surfaces using immobilized bacterial adhesin-related peptides. *Biomaterials* **2003,** 24, (22), 3877-3884.

21. Sorribas, H.; Braun, D.; Leder, L.; Sonderegger, P.; Tiefenauer, L., Adhesion proteins for a tight neuron-electrode contact. *Journal of Neuroscience Methods* **2001,** 104, (2), 133-141.

22. Xiao, S. J.; Textor, M.; Spencer, N. D.; Sigrist, H., Covalent attachment of cell-adhesive, (Arg-Gly-Asp)-containing peptides to titanium surfaces. *Langmuir* **1998,** 14, (19), 5507-5516.

23. Gamsjaeger, R.; Wimmer, B.; Kahr, H.; Tinazli, A.; Picuric, S.; Lata, S.; Tampe, R.; Maulet, Y.; Gruber, H. J.; Hinterdorfer, P.; Romanin, C., Oriented binding of the His(6)-tagged carboxyl-tail of the L-type Ca2+ channel alpha(1)-subunit to a new NTA-functionalized self-assembled monolayer. *Langmuir* **2004,** 20, (14), 5885-5890.

24. Hutschenreiter, S.; Neumann, L.; Radler, U.; Schmitt, L.; Tampe, R., Metal-chelating amino acids as building blocks for synthetic receptors sensing metal ions and histidine-tagged proteins. *Chembiochem* **2003,** 4, (12), 1340-1344.

25. Madoz-Gurpide, J.; Abad, J. M.; Fernandez-Recio, J.; Velez, M.; Vazquez, L.; Gomez-Moreno, C.; Fernandez, V. M., Modulation of electroenzymatic NADPH oxidation through oriented immobilization of ferredoxin : NADP(+) reductase onto modified gold electrodes. *Journal of the American Chemical Society* **2000,** 122, (40), 9808-9817.

26. Nam, J. M.; Han, S. W.; Lee, K. B.; Liu, X. G.; Ratner, M. A.; Mirkin, C. A., Bioactive protein nanoarrays on nickel oxide surfaces formed by dip-pen nanolithography. *Angewandte Chemie-International Edition* **2004,** 43, (10), 1246-1249.

27. Smith, B. M.; Lappi, S. E.; Brewer, S. H.; Dembowy, S.; Belyea, J.; Franzen, S., Covalent attachment of a nickel nitrilotriacetic acid group to a germanium attenuated total reflectance element. *Langmuir* **2004,** 20, (4), 1184-1188.

28. Thess, A.; Hutschenreiter, S.; Hofmann, M.; Tampe, R.; Baumeister, W.; Guckenberger, R., Specific orientation and two-dimensional crystallization of the proteasome at metal-chelating lipid interfaces. *Journal of Biological Chemistry* **2002,** 277, (39), 36321-36328.

29. del Campo, A.; Bruce, I. J., Novel solid supports and efficient surface chemistries for the manufacture of DNA arrays. *Topics in current Chemistry* **2005,** 260, 77-111.

30. Emoto, K.; Harris, J. M.; VanAlstine, J. M., Grafting poly(ethylene glycol) epoxide to amino-derivatized quartz: Effect of temperature and pH on grafting density. *Analytical Chemistry* **1996,** 68, (21), 3751-3757.

31. Kamath, K. R.; Danilich, M. J.; Marchant, R. E.; Park, K., Platelet interactions with plasma-polymerized ethylene oxide and N-vinyl-2-pyrrolidone films and linear poly(ethylene oxide) layer. *Journal of Biomaterials Science-Polymer Edition* **1996,** 7, (11), 977-988.

32. Popat, K. C.; Mor, G.; Grimes, C. A.; Desai, T. A., Surface modification of nanoporous alumina surfaces with poly(ethylene glycol). *Langmuir* **2004,** 20, (19), 8035-8041.

33. Lee, S. W.; Laibinis, P. E., Protein-resistant coatings for glass and metal oxide surfaces derived from oligo(ethylene glycol)-terminated alkyltrichlorosilanes. *Biomaterials* **1998,** 19, (18), 1669-1675.

34. Kohler, N.; Fryxell, G. E.; Zhang, M. Q., A bifunctional poly(ethylene glycol) silane immobilized on metallic oxide-based nanoparticles for conjugation with cell targeting agents. *Journal of the American Chemical Society* **2004,** 126, (23), 7206-7211.

35. Jon, S. Y.; Seong, J. H.; Khademhosseini, A.; Tran, T. N. T.; Laibinis, P. E.; Langer, R., Construction of nonbiofouling surfaces by polymeric self-assembled monolayers. *Langmuir* **2003,** 19, (24), 9989-9993.

36. Sharma, S.; Popat, K. C.; Desai, T. A., Controlling nonspecific protein interactions in silicon biomicrosystems with nanostructured poly(ethylene glycol) films. *Langmuir* **2002,** 18, (23), 8728-8731.

37. Stark, M. B.; Holmberg, K., Covalent Immobilization of Lipase in Organic-Solvents. *Biotechnology and Bioengineering* **1989,** 34, (7), 942-950.

38. Y.-C. Tseng, K. P., Synthesis of photoreactive poly(ethylene glycol) and its application to the prevention of surface-induced platelet activation. *Journal of Biomedical Materials Research* **1992,** 26, (3), 373-391.

39. Tseng, Y.-C.; McPherson, T.; Yuan, C. S.; Park, K., Grafting of ethylene glycol-butadiene block copolymers onto dimethyl-dichlorosilane-coated glass by [gamma]-irradiation. *Biomaterials* **1995,** 16, (13), 963-972.

40. Lee, S.-W.; Laibinis, P. E., Protein-resistant coatings for glass and metal oxide surfaces derived from oligo(ethylene glycol)-terminated alkyltrichlorosilanes. *Biomaterials* **1998,** 19, (18), 1669-1675.

41. Sharma, S.; Johnson, R. W.; Desai, T. A., Ultrathin poly(ethylene glycol) films for silicon-based microdevices. *Applied Surface Science* **2003,** 206, (1-4), 218-229.

42. Popat, K. C.; Johnson, R. W.; Desai, T. A., Characterization of vapor deposited poly (ethylene glycol) films on silicon surfaces for surface modification of microfluidic systems. *Journal of Vacuum Science & Technology B* **2003,** 21, (2), 645-654.

43. Piehler, J.; Brecht, A.; Valiokas, R.; Liedberg, B.; Gauglitz, G., A high-density poly(ethylene glycol) polymer brush for immobilization on glass-type surfaces. *Biosensors & Bioelectronics* **2000,** 15, (9-10), 473-481.

44. Groll, J.; Amirgoulova, E. V.; Ameringer, T.; Heyes, C. D.; Rocker, C.; Nienhaus, G. U.; Moller, M., Biofunctionalized, Ultrathin Coatings of Cross-Linked Star-Shaped Poly(ethylene oxide) Allow Reversible Folding of Immobilized Proteins. *J. Am. Chem. Soc.* **2004,** 126, (13), 4234-4239.

45. Martwiset, S.; Koh, A. E.; Chen, W., Nonfouling characteristics of dextran-containing surfaces. *Langmuir* **2006,** 22, (19), 8192-8196.

46. Morra, M., On the molecular basis of fouling resistance. *Journal of Biomaterials Science-Polymer Edition* **2000,** 11, (6), 547-569.

47. Alexander, S., Polymer Adsorption on Small Spheres - Scaling Approach. *Journal De Physique* **1977,** 38, (8), 977-981.

48. Degennes, P. G., Flexible Polymers at Solid Liquid Interfaces. *Annali Di Chimica* **1987,** 77, (3-4), 389-410.

49. De Gennes, P. G., *Scaling Concepts in Polymer Physics*. Cornell Universtity Press: Itaca, NY, 1987.

50. Jeon, S. I.; Andrade, J. D., Protein--surface interactions in the presence of polyethylene oxide : II. Effect of protein size. *Journal of Colloid and Interface Science* **1991,** 142, (1), 159-166.

51. Jeon, S. I.; Lee, J. H.; Andrade, J. D.; De Gennes, P. G., Protein--surface interactions in the presence of polyethylene oxide : I. Simplified theory. *Journal of Colloid and Interface Science* **1991,** 142, (1), 149-158.

52. Szleifer, I., Statistical thermodynamics of polymers near surfaces. *Current Opinion in Colloid & Interface Science* **1996,** 1, (3), 416-423.

53. Szleifer, I., Protein adsorption on surfaces with grafted polymers: A theoretical approach. *Biophysical Journal* **1997,** 72, (2), 595-612.

54. Szleifer, I., Protein adsorption on tethered polymer layers: effect of polymer chain architecture and composition. *Physica A* **1997,** 244, (1-4), 370-388.

55. Szleifer, I., Polymers and proteins: Interactions at interfaces. *Current Opinion in Solid State & Materials Science* **1997,** 2, (3), 337-344.

56. Besseling, N. A. M.; Scheutjens, J. M. H. M., Statistical Thermodynamics of Molecules with Orientation-Dependent Interactions in Homogeneous and Inhomogeneous Systems. *Journal of Physical Chemistry* **1994,** 98, (44), 11597-11609.

57. Besseling, N. A. M.; Lyklema, J., Equilibrium Properties of Water and Its Liquid-Vapor Interface. *Journal of Physical Chemistry* **1994,** 98, (44), 11610-11622.

58. Besseling, N. A. M.; Lyklema, J., Hydrophobic Hydration of Small Apolar Molecules and Extended Surfaces - a Molecular-Model. *Pure and Applied Chemistry* **1995,** 67, (6), 881-888.

59. Besseling, N. A. M., Theory of hydration forces between surfaces. *Langmuir* **1997,** 13, (7), 2113-2122.

60. Szleifer, I.; Carignano, M. A., Tethered polymer layers: phase transitions and reduction of protein adsorption. *Macromolecular Rapid Communications* **2000,** 21, (8), 423-448.

61. McPherson, T.; Kidane, A.; Szleifer, I.; Park, K., Prevention of protein adsorption by tethered poly(ethylene oxide) layers: Experiments and single-chain mean-field analysis. *Langmuir* **1998,** 14, (1), 176-186.

62. Carignano, M. A.; Szleifer, I., Prevention of protein adsorption by flexible and rigid chain molecules. *Colloids and Surfaces B-Biointerfaces* **2000,** 18, (3-4), 169-182.

63. Irvine, D. J.; Mayes, A. M.; GriffithCima, L., Self-consistent field analysis of grafted star polymers. *Macromolecules* **1996,** 29, (18), 6037-6043.

64. Irvine, D. J.; Mayes, A. M.; Satija, S. K.; Barker, J. G.; Sofia-Allgor, S. J.; Griffith, L. G., Comparison of tethered star and linear poly(ethylene oxide) for control of biomaterials surface properties. *Journal of Biomedical Materials Research* **1998,** 40, (3), 498-509.

65. Amirgoulova, E. V.; Groll, J.; Heyes, C. D.; Ameringer, T.; Rocker, C.; Moller, M.; Nienhaus, G. U., Biofunctionalized polymer surfaces exhibiting minimal interaction towards immobilized proteins. *Chemphyschem* **2004,** 5, (4), 552-555.

66. D. J. Irvine; Mayes, A. M.; Satija, S. K.; Barker, J. G.; Sofia-Allgor, S. J.; Griffith, L. G., Comparison of tethered star and linear poly(ethylene oxide) for control of biomaterials surface properties. *Journal of Biomedical Materials Research* **1998,** 40, (3), 498-509.

67. Groll, J.; Ademovic, Z.; Ameringer, T.; Klee, D.; Moeller, M., Comparison of coatings from reactive star shaped PEG-stat-PPG prepolymers and grafted linear PEG for biological and medical applications. *Biomacromolecules* **2005,** 6, (2), 956-962.

68. Sofia, S. J.; Premnath, V.; Merrill, E. W., Poly(ethylene oxide) grafted to silicon surfaces: Grafting density and protein adsorption. *Macromolecules* **1998,** 31, (15), 5059-5070.

69. Götz, H.; Beginn, U.; Bartelink, C. F.; Grünbauer, H. J. M.; Möller, M., Preparation of Isophorone Diisocyanate Terminated Star Polyethers. *Macromolecular Materials and Engineering* **2002,** 287, (4), 223-230.

70. Coradin, T.; Lopez, P. J., Biogenic silica patterning: Simple chemistry or subtle biology? *Chembiochem* **2003,** 4, (4), 251-259.

71. Behrens, S. H.; Grier, D. G., The charge of glass and silica surfaces. *Journal of Chemical Physics* **2001,** 115, (14), 6716-6721.

72. Schaeferling, M.; Schiller, S.; Paul, H.; Kruschina, M.; Pavlickova, P.; Meerkamp, M.; Giammasi, C.; Kambhampati, D., Application of self-assembly techniques in the design of biocompatible protein microarray surfaces. *Electrophoresis* **2002,** 23, (18), 3097-3105.

73. Grasset, F.; Saito, N.; Li, D.; Park, D.; Sakaguchi, I.; Ohashi, N.; Haneda, H.; Roisnel, T.; Mornet, S.; Duguet, E., Surface modification of zinc oxide nanoparticles by aminopropyltriethoxysilane. *Journal of Alloys and Compounds* **2003,** 360, (1-2), 298-311.

74. Liu, X. Q.; Ma, Z. Y.; Xing, J. M.; Liu, H. Z., Preparation and characterization of amino-silane modified superparamagnetic silica nanospheres. *Journal of Magnetism and Magnetic Materials* **2004,** 270, (1-2), 1-6.

75. Luscombe, C. K.; Li, H. W.; Huck, W. T. S.; Holmes, A. B., Fluorinated silane self-assembled monolayers as resists for patterning indium tin oxide. *Langmuir* **2003,** 19, (13), 5273-5278.

76. Wallraff, G. M.; Hinsberg, W. D., Lithographic Imaging Techniques for the Formation of Nanoscopic Features. *Chem. Rev.* **1999,** 99, (7), 1801-1822.

77. Mendes, P. M.; Preece, J. A., Precision chemical engineering: integrating nanolithography and nanoassembly. *Current Opinion in Colloid & Interface Science* **2004,** 9, (3-4), 236-248.

78. Younan Xia, G. M. W., Soft Lithography. *Angewandte Chemie International Edition* **1998,** 37, (5), 550-575.

79. Younan Xia, George M. W., Softlithographie. *Angewandte Chemie* **1998,** 110, (5), 568-594.

80. Tan, J. L.; Tien, J.; Chen, C. S., Microcontact Printing of Proteins on Mixed Self-Assembled Monolayers. *Langmuir* **2002,** 18, (2), 519-523.

81. Inerowicz, H. D.; Howell, S.; Regnier, F. E.; Reifenberger, R., Multiprotein Immunoassay Arrays Fabricated by Microcontact Printing. *Langmuir* **2002,** 18, (13), 5263-5268.

82. Hyun, J.; Zhu, Y.; Liebmann-Vinson, A.; Beebe, T. P.; Chilkoti, A., Microstamping on an Activated Polymer Surface: Patterning Biotin and Streptavidin onto Common Polymeric Biomaterials. *Langmuir* **2001,** 17, (20), 6358-6367.

83. Renault, J. P.; Bernard, A.; Bietsch, A.; Michel, B.; Bosshard, H. R.; Delamarche, E.; Kreiter, M.; Hecht, B.; Wild, U. P., Fabricating Arrays of Single Protein Molecules on Glass Using Microcontact Printing. *J. Phys. Chem. B* **2003,** 107, (3), 703-711.

84. MacBeath, G.; Schreiber, S. L., Printing proteins as microarrays for high-throughput function determination. *Science* **2000,** 289, (5485), 1760-1763.

85. Haab, B.; Dunham, M.; Brown, P., Protein microarrays for highly parallel detection and quantitation of specific proteins and antibodies in complex solutions. *Genome Biology* **2001,** 2, (2), research0004.1 - research0004.13.

86. Borchers, K.; Weber, A.; Brunner, H.; Tovar, G. E. M., Microstructured layers of spherical biofunctional core-shell nanoparticles provide enlarged reactive surfaces for protein microarrays. *Analytical and Bioanalytical Chemistry* **2005,** 383, (5), 738-746.

87. del Campo, A.; Boos, D.; Spiess, H. W.; Jonas, U., Surface modification with orthogonal photosensitive silanes for sequential chemical lithography and site-selective particle deposition. *Angewandte Chemie-International Edition* **2005,** 44, (30), 4707-4712.

88. Dulcey, C. S.; Georger, J. H.; Krauthamer, V.; Stenger, D. A.; Fare, T. L.; Calvert, J. M., Deep Uv Photochemistry of Chemisorbed Monolayers - Patterned Coplanar Molecular Assemblies. *Science* **1991,** 252, (5005), 551-554.

89. Tarlov, M. J.; Burgess, D. R. F.; Gillen, G., UV Photopatterning of Alkanethiolate Monolayers Self-Assembled on Gold and Silver. *Journal of the American Chemical Society* **1993,** 115, (12), 5305-5306.

90. Effenberger, F.; Gotz, G.; Bidlingmaier, B.; Wezstein, M., Photoactivated preparation and patterning of self-assembled monolayers with 1-alkenes and aldehydes on silicon hydride surfaces. *Angewandte Chemie-International Edition* **1998,** 37, (18), 2462-2464.

91. Prucker, O.; Naumann, C. A.; Ruhe, J.; Knoll, W.; Frank, C. W., Photochemical attachment of polymer films to solid surfaces via monolayers of benzophenone derivatives. *Journal of the American Chemical Society* **1999,** 121, (38), 8766-8770.

92. Blawas, A. S.; Reichert, W. M., Protein patterning. *Biomaterials* **1998,** 19, (7-9), 595-609.

93. Fodor, S. P. A.; Read, J. L.; Pirrung, M. C.; Stryer, L.; Lu, A. T.; Solas, D., Light-Directed, Spatially Addressable Parallel Chemical Synthesis. *Science* **1991,** 251, (4995), 767-773.

94. Elender, G.; Kuhner, M.; Sackmann, E., Functionalisation of Si/SiO2 and glass surfaces with ultrathin dextran films and deposition of lipid bilayers. *Biosensors & Bioelectronics* **1996,** 11, (6-7), 565-577.

95. McGall, G. H.; Barone, A. D.; Diggelmann, M.; Fodor, S. P. A.; Gentalen, E.; Ngo, N., The efficiency of light-directed synthesis of DNA arrays on glass substrates. *Journal of the American Chemical Society* **1997,** 119, (22), 5081-5090.

96. Vossmeyer, T.; Jia, S.; DeIonno, E.; Diehl, M. R.; Kim, S. H.; Peng, X.; Alivisatos, A. P.; Heath, J. R., Combinatorial approaches toward patterning nanocrystals. *Journal of Applied Physics* **1998,** 84, (7), 3664-3670.

97. Jonas, U.; del Campo, A.; Kruger, C.; Glasser, G.; Boos, D., Colloidal assemblies on patterned silane layers. *Proceedings of the National Academy of Sciences of the United States of America* **2002,** 99, (8), 5034-5039.

98. Zhao, B.; Moore, J. S.; Beebe, D. J., Pressure-Sensitive Microfluidic Gates Fabricated by Patterning Surface Free Energies Inside Microchannels. *Langmuir* **2003,** 19, (5), 1873-1879.

99. Lee, K.; Pan, F.; Carroll, G. T.; Turro, N. J.; Koberstein, J. T., Photolithographic Technique for Direct Photochemical Modification and Chemical Micropatterning of Surfaces. *Langmuir* **2004,** 20, (5), 1812-1818.

100. Ryan, D.; Parviz, B. A.; Linder, V.; Semetey, V.; Sia, S. K.; Su, J.; Mrksich, M.; Whitesides, G. M., Patterning Multiple Aligned Self-Assembled Monolayers Using Light. *Langmuir* **2004,** 20, (21), 9080-9088.

101. Pillai, V. N. R., Photoremovable protecting groups. *Synthesis* **1980**, 1-26.

102. Pirrung, M. C.; Bradley, J. C., Dimethoxybenzoin Carbonates - Photochemically-Removable Alcohol Protecting Groups Suitable for Phosphoramidite-Based DNA- Synthesis. *Abstracts of Papers of the American Chemical Society* **1994,** 208, 198-ORGN.

103. Pirrung, M. C.; Bradley, J. C., Comparison of Methods for Photochemical Phosphoramidite-Based DNA-Synthesis. *Journal of Organic Chemistry* **1995,** 60, (20), 6270-6276.

104. Pirrung, M. C.; Bradley, J. C., Dimethoxybenzoin Carbonates - Photochemically-Removable Alcohol Protecting Groups Suitable for Phosphoramidite-Based DNA- Synthesis. *Journal of Organic Chemistry* **1995,** 60, (5), 1116-1117.

105. Pirrung, M. C.; Shuey, S. W., Photoremovable Protecting Groups for Phosphorylation of Chiral Alcohols - Asymmetric-Synthesis of Phosphotriesters of (-)-3',5'-Dimethoxybenzoin. *Journal of Organic Chemistry* **1994,** 59, (14), 3890-3897.

106. Stowell, M. H. B.; Rock, R. S.; Rees, D. C.; Chan, S. I., Efficient synthesis of photolabile alkoxy benzoin protecting groups. *Tetrahedron Letters* **1996,** 37, (3), 307-310.

107. del Campo, A.; Boos, D.; Spiess, H. W.; Jonas, U., Oberflächenmodifikation mit orthogonalen photosensitiven Silanen zur sequenziellen chemischen Lithographie und ortsselektiven Partikelabscheidung. *Angewandte Chemie* **2005,** 117, (30), 4785-4791.

108. Boos, D., Synthesis and Characterisation of Photoreactive Silanes for the Self-Assembly on Functionalised Silica Surfaces. *Dissertation, Johannes Gutenberg-Universität Mainz, Germany* **2004**.

109. Kraus, G.; Gauglitz, G., Application and Comparison of Algorithms for the Evaluation of Interferograms. *Fresenius Journal of Analytical Chemistry* **1992,** 344, (4-5), 153-157.

110. Schmitt, H.-M.; Brecht, A.; Piehler, J.; Gauglitz, G., An integrated system for optical biomolecular interaction analysis. *Biosensors and Bioelectronics* **1997,** 12, (8), 809-816.

111. Bochet, C. G., Photolabile protecting groups and linkers. *Journal of the Chemical Society-Perkin Transactions 1* **2002**, (2), 125-142.

112. Mayer, G.; Heckel, A., Biologically active molecules with a "light switch". *Angewandte Chemie-International Edition* **2006,** 45, (30), 4900-4921.

113. Sundberg, S. A.; Barrett, R. W.; Pirrung, M.; Lu, A. L.; Kiangsoontra, B.; Holmes, C. P., Spatially-Addressable Immobilization of Macromolecules on Solid Supports. *Journal of the American Chemical Society* **1995,** 117, (49), 12050-12057.

114. Yan, F. N.; Chen, L. H.; Tang, Q. L.; Rong, W., Synthesis and characterization of a photocleavable cross-linker and its application on tunable surface modification and protein photodelivery. *Bioconjugate Chemistry* **2004,** 15, (5), 1030-1036.

115. Dendane, N.; Hoang, A.; Guillard, L.; Defrancq, E.; Vinet, F.; Dumy, P., Efficient Surface Patterning of Oligonucleotides Inside a Glass Capillary through Oxime Bond Formation. *Bioconjugate Chemistry* **2007,** 18, 671-676.

116. Critchley, K.; Jeyadevan, J. P.; Fukushima, H.; Ishida, M.; Shimoda, T.; Bushby, R. J.; Evans, S. D., A mild photoactivated hydrophilic/hydrophobic switch. *Langmuir* **2005,** 21, (10), 4554-4561.

117. Hower, J. C.; He, Y.; Bernards, M. T.; Jiang, S. Y., Understanding the nonfouling mechanism of surfaces through molecular simulations of sugar-based self-assembled monolayers. *Journal of Chemical Physics* **2006,** 125, (21), -.

118. Herrwerth, S.; Eck, W.; Reinhardt, S.; Grunze, M., Factors that determine the protein resistance of oligoether self-assembled monolayers - Internal hydrophilicity, terminal hydrophilicity, and lateral packing density. *Journal of the American Chemical Society* **2003,** 125, (31), 9359-9366.

119. Prime, K. L.; Whitesides, G. M., Adsorption of Proteins onto Surfaces Containing End-Attached Oligo(Ethylene Oxide) - a Model System Using Self-Assembled Monolayers. *Journal of the American Chemical Society* **1993,** 115, (23), 10714-10721.

120. Kingshott, P.; Thissen, H.; Griesser, H. J., Effects of cloud-point grafting, chain length, and density of PEG layers on competitive adsorption of ocular proteins. *Biomaterials* **2002,** 23, (9), 2043-2056.

121. Ameringer, T.; Hinz, M.; Mourran, C.; Seliger, H.; Groll, J.; Moeller, M., Ultrathin functional star PEG coatings for DNA microarrays. *Biomacromolecules* **2005,** 6, (4), 1819-1823.

122. Groll, J.; Ameringer, T.; Spatz, J. P.; Moeller, M., Ultrathin coatings from isocyanate-terminated star PEG prepolymers: Layer formation and characterization. *Langmuir* **2005,** 21, (5), 1991-1999.

123. Groll, J.; Fiedler, J.; Engelhard, E.; Ameringer, T.; Tugulu, S.; Klok, H. A.; Brenner, R. E.; Moeller, M., A novel star PEG-derived surface coating for specific cell adhesion. *Journal of Biomedical Materials Research Part A* **2005,** 74A, (4), 607-617.

124. Groll, J.; Haubensak, W.; Ameringer, T.; Moeller, M., Ultrathin coatings from isocyanate terminated star PEG prepolymers: Patterning of proteins on the layers. *Langmuir* **2005,** 21, (7), 3076-3083.

125. Oklejas, V.; Harris, J. M., In-situ investigation of binary-component self-assembled monolayers: A SERS-based spectroelectrochemical study of the effects of monolayer composition on interfacial structure. *Langmuir* **2003,** 19, (14), 5794-5801.

126. Folkers, J. P.; Laibinis, P. E.; Whitesides, G. M., Self-Assembled Monolayers of Alkanethiols on Gold - Comparisons of Monolayers Containing Mixtures of Short-Chain and Long-Chain Constituents with Ch3 and Ch2oh Terminal Groups. *Langmuir* **1992,** 8, (5), 1330-1341.

127. Tamada, K.; Hara, M.; Sasabe, H.; Knoll, W., Surface phase behavior of n-alkanethiol self-assembled monolayers adsorbed on Au(111): An atomic force microscope study. *Langmuir* **1997,** 13, (6), 1558-1566.

128. Fadeev, A. Y.; McCarthy, T. J., Binary monolayer mixtures: Modification of nanopores in silicon-supported tris(trimethylsiloxy)silyl monolayers. *Langmuir* **1999,** 15, (21), 7238-7243.

129. Groll, J.; Amirgoulova, E. V.; Ameringer, T.; Heyes, C. D.; Rocker, C.; Nienhaus, G. U.; Moller, M., Biofunctionalized, ultrathin coatings of cross-linked star-shaped poly(ethylene oxide) allow reversible folding of immobilized proteins. *Journal of the American Chemical Society* **2004,** 126, (13), 4234-4239.

130. Vanderah, D. J.; Arsenault, J.; La, H.; Gates, R. S.; Silin, V.; Meuse, C. W.; Valincius, G., Structural Variations and Ordering Conditions for the Self-Assembled Monolayers of HS(CH2CH2O)3-6CH3. *Langmuir* **2003,** 19, (9), 3752-3756.

131. Delamarche, E.; Donzel, C.; Kamounah, F. S.; Wolf, H.; Geissler, M.; Stutz, R.; Schmidt-Winkel, P.; Michel, B.; Mathieu, H. J.; Schaumburg, K., Microcontact printing using poly(dimethylsiloxane) stamps hydrophilized by poly(ethylene oxide) silanes. *Langmuir* **2003,** 19, (21), 8749-8758.

132. Schwabacher, A. W.; Lane, J. W.; Schiesher, M. W.; Leigh, K. M.; Johnson, C. W., Desymmetrization reactions: Efficient preparation of unsymmetrically substituted linker molecules. *Journal of Organic Chemistry* **1998,** 63, (5), 1727-1729.

133. Patchornik, A.; Amit, B.; Woodward, R. B., Photosensitive protecting groups. *J. Am. Chem. Soc.* **1970,** 92, (21), 6333-6335.

134. Lawrence, M. J.; Lawrence, S. M.; Chauhan, S.; Barlow, D. J., Synthesis and aggregation properties of dialkyl polyoxyethylene glycerol ethers. *Chemistry and Physics of Lipids* **1996,** 82, (2), 89-100.

135. Bhattacharya, S.; Dileep, P. V., Cationic oxyethylene lipids. Synthesis, aggregation, and transfection properties. *Bioconjugate Chemistry* **2004,** 15, (3), 508-519.

136. Jeong, K. S.; Park, E. J., Self-Assembly of Interlocked Supramolecular Dendrimers. *J. Org. Chem.* **2004,** 69, (7), 2618-2621.

137. Koulocheri, S. D.; Pitsinos, E. N.; Haroutounian, S. A., A convenient route to alkaloid lipids: application for the synthesis of a leptophylline A analogue. *Synthesis* **2002**, (1), 111-115.

138. Jungk, S. J.; Moore, J. A.; Gandour, R. D., Efficient synthesis of C-pivot lariat ethers. 2-(Alkoxymethyl)-1,4,7,10,13,16-hexaoxacyclooctadecanes. *J. Org. Chem.* **1983,** 48, (7), 1116-1120.

139. Piehler, J.; Brecht, A.; Hehl, K.; Gauglitz, G., Protein interactions in covalently attached dextran layers. *Colloids and Surfaces B-Biointerfaces* **1999,** 13, (6), 325-336.

140. Brecht, A.; Gauglitz, G., Optical probes and transducers. *Biosens Bioelectron* **1995,** 10, (9-10), 923-36.

141. Sakellariou, E. G.; Montalban, A. G.; Beall, S. L.; Henderson, D.; Meunier, H. G.; Phillips, D.; Suhling, K.; Barrett, A. G. M.; Hoffman, B. M., Novel peripherally functionalized seco-porphyrazines: synthesis, characterization and spectroscopic evaluation. *Tetrahedron* **2003,** 59, (46), 9083-9090.

142. Mills, O. S.; Mooney, N. J.; Robinson, P. M.; Watt, C. I. F.; Box, B. G., Preparation and Properties of Some Crown-Ethers Incorporating Stable Carbocations. *Journal of the Chemical Society-Perkin Transactions 2* **1995**, (4), 697-706.

143. Wada, M.; Nakai, H.; Sato, Y.; Hatanaka, Y.; Kanaoka, Y., Photochemistry of the Phthalimide System .30. Application of the Remote Photocyclization with a Pair System of Phthalimide and Methylthio Groups - a Photochemical-Synthesis of Crown Ether Analogs. *Chemical & Pharmaceutical Bulletin* **1983,** 31, (2), 429-435.

144. Kim, J. D.; Han, G.; Zee, O. P.; Jung, Y. H., Deprotection of benzyl and p-methoxybenzyl ethers by chlorosulfonyl isocyanate-sodium hydroxide. *Tetrahedron Letters* **2003,** 44, (4), 733-735.

145. Janssen, R. G.; Utley, J. H. P.; Carre, E.; Simon, E.; Schirmer, H., Electroorganic reactions. Part 55. Quinodimethane chemistry. Part 3. Transition metal complexes as inter- and intra-molecular redox catalysts for the electrosynthesis of poly(p-xylylene) (PPX) polymers and oligomers. *Journal of the Chemical Society, Perkin Transactions 2* **2001**, (9), 1573-1584.

146. Schiller, S. M.; Naumann, R.; Lovejoy, K.; Kunz, H.; Knoll, W., Archaea Analogue Thiolipids for Tethered Bilayer Lipid Membranes on Ultrasmooth Gold Surfaces. *Angewandte Chemie International Edition* **2003,** 42, (2), 208-211.

147. Sun, X. G.; Kerr, J. B., Synthesis and Characterization of Network Single Ion Conductors Based on Comb-Branched Polyepoxide Ethers and Lithium Bis(allylmalonato)borate. *Macromolecules* **2006,** 39, (1), 362-372.

148. del Campo, A., unpublished results.

149. Bunker, B. C.; Carpick, R. W.; Assink, R. A.; Thomas, M. L.; Hankins, M. G.; Voigt, J. A.; Sipola, D.; de Boer, M. P.; Gulley, G. L., The impact of solution agglomeration on the deposition of self-assembled monolayers. *Langmuir* **2000,** 16, (20), 7742-7751.

150. Kallury, K. M. R.; Macdonald, P. M.; Thompson, M., Effect of Surface-Water and Base Catalysis on the Silanization of Silica by (Aminopropyl)Alkoxysilanes Studied by X-Ray Photoelectron-Spectroscopy and C-13 Cross-Polarization Magic-Angle-Spinning Nuclear-Magnetic-Resonance. *Langmuir* **1994,** 10, (2), 492-499.

151. Bierbaum, K.; Kinzler, M.; Woll, C.; Grunze, M.; Hahner, G.; Heid, S.; Effenberger, F., A near-Edge X-Ray-Absorption Fine Structure Spectroscopy and X-Ray Photoelectron-Spectroscopy Study of the Film Properties of Self-Assembled Monolayers of Organosilanes on Oxidized Si(100). *Langmuir* **1995,** 11, (2), 512-518.

152. Britcher, L. G.; Kehoe, D. C.; Matisons, J. G.; Smart, R. S. C.; Swincer, A. G., Silicones on Glass Surfaces .2. Coupling Agent Analogs. *Langmuir* **1993,** 9, (7), 1609-1613.

153. Fadeev, A. Y.; McCarthy, T. J., Self-assembly is not the only reaction possible between alkyltrichlorosilanes and surfaces: Monomolecular and oligomeric covalently attached layers of dichloro- and trichloroalkylsilanes on silicon. *Langmuir* **2000,** 16, (18), 7268-7274.

154. Alonso, J. M.; Reichel, A.; Piehler, J.; del Campo, A., Photopatterned surfaces for site-specific and functional immobilization of proteins. *Langmuir* **in press**.

155. Piehler, J.; Schreiber, G., Fast transient cytokine-receptor interactions monitored in real time by reflectometric interference spectroscopy. *Analytical Biochemistry* **2001,** 289, (2), 173-186.

156. Haubner, R.; Gratias, R.; Diefenbach, B.; Goodman, S. L.; Jonczyk, A.; Kessler, H., Structural and functional aspects of RGD-containing cyclic pentapeptides as highly potent and selective integrin alpha(v)beta(3) antagonists. *Journal of the American Chemical Society* **1996,** 118, (32), 7461-7472.

157. Haubner, R.; Finsinger, D.; Kessler, H., Stereoisomeric peptide libraries and peptidomimetics for designing selective inhibitors of the alpha(V)beta(3) integrin for a new cancer therapy. *Angewandte Chemie-International Edition* **1997,** 36, (13-14), 1375-1389.

158. Petersen, S.; Alonso, J. M.; Specht, A.; Duodu, P.; Goeldner, M.; del Campo, A., Phototriggering cell adhesion by caged cyclic RGD peptides. *Angewandte Chemie-International Edition* **in press**.

159. Uttamchandani, M.; Walsh, D. P.; Yao, S. Q.; Chang, Y. T., Small molecule microarrays: recent advances and applications. *Current Opinion in Chemical Biology* **2005,** 9, (1), 4-13.

160. Monsathaporn, S.; Effenberger, F., Preparation and photoinduced patterning of azidoformate-terminated self-assembled monolayers. *Langmuir* **2004,** 20, (24), 10375-10378.

161. Ito, Y., Photoimmobilization for microarrays. *Biotechnology Progress* **2006,** 22, (4), 924-932.

162. Kado, Y.; Mitsuishi, M.; Miyashita, T., Fabrication of three-dimensional nanostructures using reactive polymer nanosheets. *Advanced Materials* **2005,** 17, (15), 1857-+.

163. Kanoh, N.; Kumashiro, S.; Simizu, S.; Kondoh, Y.; Hatakeyama, S.; Tashiro, H.; Osada, H., Immobilization of natural products on glass slides by using a photoaffinity reaction and the detection of protein-small-molecule interactions. *Angewandte Chemie-International Edition* **2003,** 42, (45), 5584-5587.

164. White, M. A.; Johnson, J. A.; Koberstein, J. T.; Turro, N. J., Toward the syntheses of universal ligands for metal oxide surfaces: Controlling surface functionality through click chemistry. *Journal of the American Chemical Society* **2006,** 128, (35), 11356-11357.

165. Pellois, J. P.; Wang, W.; Gao, X. L., Peptide synthesis based on t-Boc chemistry and solution photogenerated acids. *Journal of Combinatorial Chemistry* **2000,** 2, (4), 355-360.

166. Cho, C. Y.; Moran, E. J.; Cherry, S. R.; Stephans, J. C.; Fodor, S. P. A.; Adams, C. L.; Sundaram, A.; Jacobs, J. W.; Schultz, P. G., An Unnatural Biopolymer. *Science* **1993,** 261, (5126), 1303-1305.

167. Pease, A. C.; Solas, D.; Sullivan, E. J.; Cronin, M. T.; Holmes, C. P.; Fodor, S. P. A., Light-Generated Oligonucleotide Arrays for Rapid DNA-Sequence Analysis. *Proceedings of the National Academy of Sciences of the United States of America* **1994,** 91, (11), 5022-5026.

168. Gao, X. L.; Yu, P. L.; LeProust, E.; Sonigo, L.; Pellois, J. P.; Zhang, H., Oligonucleotide synthesis using solution photogenerated acids. *Journal of the American Chemical Society* **1998,** 120, (48), 12698-12699.

169. Singh-Gasson, S.; Green, R. D.; Yue, Y. J.; Nelson, C.; Blattner, F.; Sussman, M. R.; Cerrina, F., Maskless fabrication of light-directed oligonucleotide microarrays using a digital micromirror array. *Nature Biotechnology* **1999,** 17, (10), 974-978.

170. Li, S. W.; Bowerman, D.; Marthandan, N.; Klyza, S.; Luebke, K. J.; Garner, H. R.; Kodadek, T., Photolithographic synthesis of peptoids. *Journal of the American Chemical Society* **2004,** 126, (13), 4088-4089.

171. Bochet, C. G., Wavelength-selective cleavage of photolabile protecting groups. *Tetrahedron Letters* **2000,** 41, (33), 6341-6346.

172. Bochet, C. G., Chromatic orthogonality in organic synthesis. *Synlett* **2004**, (13), 2268-2274.

173. Bochet, C. G., Orthogonal photolysis of protecting groups. *Angewandte Chemie-International Edition* **2001,** 40, (11), 2071-2073.

174. Kessler, M.; Glatthar, R.; Giese, B.; Bochet, C. G., Sequentially photocleavable protecting groups in solid-phase synthesis. *Organic Letters* **2003,** 5, (8), 1179-1181.

175. Furuta, T., Coumarin-4-ylmethyl Phototriggers. In *Dynamic Studies in Biology*, Goeldner, M.; Givens, R., Eds. Wiley-VCH, Weinheim, Germany: 2005.

176. Trenor, S. R.; Shultz, A. R.; Love, B. J.; Long, T. E., Coumarins in polymers: From light harvesting to photo-cross-linkable tissue scaffolds. *Chemical Reviews* **2004,** 104, (6), 3059-3077.

177. Geißler, D.; Kresse, W.; Wiesner, B.; Bendig, J.; Kettenmann, H.; Hagen, V.; DMACM-Caged Adenosine Nucleotides: Ultrafast Phototriggers for ATP, ADP, and AMP Activated by Long-Wavelength Irradiation. *ChemBioChem* **2003,** 4, (2-3), 162-170.

178. Hagen, V.; Frings, S.; Wiesner, B.; Helm, S.; Kaupp, U. B.; Bendig, J., [7-(Dialkylamino)coumarin-4-yl]methyl-Caged Compounds as Ultrafast and Effective Long-Wavelength Phototriggers of 8-Bromo-Substituted Cyclic Nucleotides. *ChemBioChem* **2003,** 4, (5), 434-442.

179. Schonleber, R. O.; Bendig, J.; Hagen, V.; Giese, B., Rapid photolytic release of cytidine 5'-diphosphate from a coumarin derivative: a new tool for the investigation of ribonucleotide reductases. *Bioorganic & Medicinal Chemistry* **2002,** 10, (1), 97-101.

180. Hagen, V.; Bendig, J.; Frings, T.; Eckhardt, T.; Helm, S.; Reuter, D.; Kaupp, B., Highly Efficient and Ultrafast Phototriggers for cAMP and cGMP by Using Long-Wavelength UV/Vis-Activation. *Angewandte Chemie International Edition* **2001,** 40, (6), 1045-1048.

181. Eckardt, T.; Hagen, V.; Schade, B.; Schmidt, R.; Schweitzer, C.; Bendig, J., Deactivation Behavior and Excited-State Properties of (Coumarin-4-yl)methyl Derivatives. 2. Photocleavage of Selected (Coumarin-4-yl)methyl-Caged Adenosine Cyclic 3',5'-Monophosphates with Fluorescence Enhancement. *J. Org. Chem.* **2002,** 67, (3), 703-710.

182. Suzuki, A. Z.; Watanabe, T.; Kawamoto, M.; Nishiyama, K.; Yamashita, H.; Ishii, M.; Iwamura, M.; Furuta, T., Coumarin-4-ylmethoxycarbonyls as Phototriggers for Alcohols and Phenols. *Org. Lett.* **2003,** 5, (25), 4867-4870.

183. Shembekar, V. R.; Chen, Y.; Carpenter, B. K.; Hess, G. P., A Protecting Group for Carboxylic Acids That Can Be Photolyzed by Visible Light. *Biochemistry* **2005,** 44, (19), 7107-7114.

184. Furuta, T.; Wang, S. S. H.; Dantzker, J. L.; Dore, T. M.; Bybee, W. J.; Callaway, E. M.; Denk, W.; Tsien, R. Y., Brominated 7-hydroxycoumarin-4-ylmethyls: Photolabile protecting groups with biologically useful cross-sections for two photon photolysis. *Proceedings of the National Academy of Sciences* **1999,** 96, (4), 1193-1200.

185. Ito, K.; Maruyama, J., Studies on Stable Diazoalkanes as Potential Fluorogenic Reagents .1. 7-Substituted 4-Diazomethylcoumarins. *Chemical & Pharmaceutical Bulletin* **1983,** 31, (9), 3014-3023.

186. Schade, B.; Hagen, V.; Schmidt, R.; Herbrich, R.; Krause, E.; Eckardt, T.; Bendig, J., Deactivation Behavior and Excited-State Properties of (Coumarin-4-yl)methyl Derivatives. 1. Photocleavage of (7-Methoxycoumarin-4-yl)methyl-Caged Acids with Fluorescence Enhancement. *J. Org. Chem.* **1999,** 64, (25), 9109-9117.

187. Hagen, V.; Frings, S.; Wiesner, B.; Helm, S.; Kaupp, U. B.; Bendig, J., [7-(Dialkylamino)coumarin-4-yl]methyl-Caged Compounds as Ultrafast and Effective Long-Wavelength Phototriggers of 8-Bromo-Substituted Cyclic Nucleotides. *ChemBioChem* **2003,** 4, (5), 434-442.

188. Maisch, S.; Buckel, F.; Effenberger, F., Preparation of High Quality Electrical Insulator Self-Assembled Monolayers on gold. Experimental Investigation of the Conduction Mechanism through Organic Thin Films. *Journal of the American Chemical Society* **2005,** 127, 17315-17322.

189. Halik, M.; Klauk, H.; Zschieschang, U.; Schmid, G.; Dehm, c.; Schütz, M.; Maisch, S.; Effenberger, F.; Brunnbauer, M.; Stellacci, F., Low-voltage organic transistors wich an amorphous molecular gate dielectric. *Nature* **2004,** 431, 963-966.

190. Love, J. C.; Estroff, L. A.; Kriebel, J. K.; Nuzzo, R. G.; Whitesides, G. M., Self-assembled monolayers of thiolates on metals as a form of nanotechnology. *Chemical Reviews* **2005,** 105, (4), 1103-1169.

191. Blanc, A.; Bochet, C. G., Wavelength-Controlled Orthogonal Photolysis of Protecting Groups. *J. Org. Chem.* **2002,** 67, (16), 5567-5577.

192. Safarik, I.; Safarikova, M., Magnetic techniques for the solation and purification of proteins and peptides. *BioMagnetic Research and Technology* **2004,** 2, (7).

193. Franzreb, M.; Siemann-Herzberg, M.; Hobley, T. J.; Thomas, O. R. T., Protein purification using magnetic adsorbent particles. *Applied Microbiology and Biotechnology* **2006,** 70, 505-516.

194. Mohapatra, S.; Pramanik, N.; Mukherjee, S.; Ghosh, S. K.; Pramanik, P., A simple synthesis of amine-derivatised superparamagnetic iron oxide nanoparticles for bioapplications. *Journal of Materials Science* **2007,** 42, (17), 7566-7574.

195. Kekalo, K.; Agabekov, V.; Zhavnerko, G.; Shutava, T.; Kutavichus, V.; Kabanov, V.; Goroshko, N., Magnetic nanocomposites for sorbents and glue layers. *Journal of Magnetism and Magnetic Materials* **2007,** 311, (1), 63-67.

196. Zhang, J. L.; Srivastava, R. S.; Misra, R. D. K., Core-Shell Magnetite Nanoparticles Surface Encapsulated with Smart Stimuli-Responsive Polymer: Synthesis, Characterization, and LCST of Viable Drug-Targeting Delivery System. *Langmuir* **2007,** 23, 6342-6351.

197. Gonzales, M.; Krishnan, K. M., Synthesis of magnetoliposomes with monodisperse iron oxide nanocrystal cores for hyperthermia. *Journal of Magnetism and Magnetic Materials* **2005,** 293, (1), 265-270.

198. Sahoo, Y.; Pizem, H.; Fried, T.; Golodnitsky, D.; Burstein, L.; Sukenik, C. N.; Markovich, G., Alkyl Phosphonate/Phosphate Coating on Magnetite Nanoparticles: A Comparison with Fatty Acids. *Langmuir* **2001,** 17, 7907-7911.

199. Lattuada, M.; Hatton, A., Functionalization of Monodisperse Magnetic Nanoparticles. *Langmuir* **2007,** 23, 2158-2168.

200. Xu, C. J.; Xu, K. M.; Gu, H. W.; Zheng, R. K.; Liu, H.; Zhang, X. X.; Guo, Z. H.; Xu, B., Dopamine as a robust anchor to immobilize functional molecules on the iron oxide shell of magnetic nanoparticles. *Journal of the American Chemical Society* **2004,** 126, (32), 9938-9939.

201. Bruce, I. J.; Sen, T., Surface modification of magnetic nanoparticles with alkoxysilanes and their application in magnetic bioseparations. *Langmuir* **2005,** 21, (15), 7029-7035.

202. Ma, M.; Zhang, Y.; Yu, W.; Shen, H. Y.; Zhang, H. Q.; Gu, N., Preparation and characterization of magnetite nanoparticles coated by amino silane. *Colloids and Surfaces a-Physicochemical and Engineering Aspects* **2003,** 212, (2-3), 219-226.

203. del Campo, A.; Sen, T.; Lellouche, J. P.; Bruce, I. J., Multifunctional magnetite and silica-magnetite nanoparticles: Synthesis, surface activation and applications in life sciences. *Journal of Magnetism and Magnetic Materials* **2005,** 293, (1), 33-40.

204. Bonanno, L. M.; DeLouise, L. A., Crowding effects on target detection in an affinity biosensor. *Langmuir* **2007,** 23, 5817-5823.

205. Moon, J. H.; Kim, J. H.; Kim, K.; Kang, T. H.; Kim, B.; Kim, C. H.; Hahn, J. H.; Park, J. W., Absolute surface density of the amine group of the aminosilylated thin layers: Ultraviolet-visible spectroscopy, second harmonic generation, and synchrotron-radiation photoelectron spectroscopy study. *Langmuir* **1997,** 13, (16), 4305-4310.

206. Advincula, R. C.; Brittain, W.; Caster, A.; Ruhe, J., Polymer Brushes: Synthesis, Characterization, Applications. *Wiley-VCH* **2004**.

207. Carré, A.; Lacarrière, V.; Birch, W., Molecular interactions between DNA and an aminated glass substrate. *Journal of Colloid and Interface Science* **2003,** 260, 49-55.

208. Sundaram, S.; Viriyayuthakorn, S.; Roth, C. M., Oligonucleotide Structure Influences the Interactions between Cationic Polymers and Oligonucleotides. *Biomacromolecules* **2005,** 6, 2961-2968.

209. Rosa, M.; Dias, R.; da Graca Miguel, M.; Lindman, B., DNA-Cationic Surfactant Interaction are different for Double-and Single-Stranded DNA. *Biomacromolecules* **2005,** 6, 2164-2171.

210. Gottlieb, H. E.; Kotlyar, V.; Nudelman, A., NMR chemical shifts of common laboratory solvents as trace impurities. *Journal of Organic Chemistry* **1997,** 62, (21), 7512-7515.

211. Effenberger, F.; Heid, S., Synthesis of Model Compounds for the Formation of Self-Assembled Monolayers on a Silicon Surface. *Synthesis* **1995**, (09), 1126-1130.